Tensions Induites par une agression foudre dans les câbles de contrôle-mesure des centres de production d'énergie

Luis Gerardo Diaz Pulgar

Thèse de doctorat

UNIVERSITÉ DE LIMOGES

ED n°521: Sciences et Ingénierie pour l'Information, Mathématiques

Laboratoire XLIM

Thèse

pour obtenir le grade de

DOCTEUR DE L'UNIVERSITÉ DE LIMOGES

Spécialité : Electronique des Hautes Fréquences, Photonique et Systèmes

présentée et soutenue par

Luis Gerardo DIAZ PULGAR

le 29 Novembre 2016

Lightning Induced Voltages in Cables of Power Production Centers

Thèse dirigée par Alain REINEIX & Christophe GUIFFAUT

JURY :

Président

Bernard JECKO, professeur émérite, Université de Limoges

Rapporteurs

Francoise PALADIAN, professeur, Université Blaise Pascal - Clermont-Ferrand II.

Farhad RACHIDI, professeur, École Polytechnique Fédérale de Lausanne.

Examinateurs

Jean-Philippe PARMANTIER, ingénieur chargé de Mission CEM. ONERA

Christophe GUIFFAUT, chargé de recherche CNRS. Institut de Recherche XLIM

Alain REINEIX, directeur de recherche CNRS. Institut de Recherche XLIM

Encadrants

Céline MIRY, ingénieur. SEI - Électricité de France

Philippe BARATON, ingénieur chercheur. EDF-R& D

Invités

Charlotte TROUILLOUD, ingénieur chargé d'études en Électricité. SEPTEN-EDF

Pascal DUQUERROY, ingénieur chercheur. EDF-R& D

Université de Limoges

Acknowledgements

Cette thèse a été réalisée dans le cadre d'une convention CIFRE (Convention Industrielle de Formation par la Recherche en Entreprise) mise en place par l'ANRT (Association Nationale de la Recherche Technique). Elle a réuni EDF-R&D et le département OSA (Ondes et Systèmes Associés) de l'institut de recherche XLIM.

This whole project started as a combination of several fortunate events, that I like to think; construct a blessing. Right now, all I can feel is a deep gratitude for the group of persons that have accompanied me during this journey.

I must start with Céline Miry and Philippe Baraton, who from the beginning gave me their trust and liberty to carry on this project. Thank you for receiving me into your group at EDF-R&D, encouraging the good work, being an example of leadership, and specially accounting me as a colleague. All the time I spent with you, I've always felt appreciated and acknowledge. You have made this experience, happily unforgettable.

Right next to the EDF team, is the XLIM group: Alain Reineix and Christophe Guiffaut, you were charged with the mission of receiving a not-french-speaking Venezuelan into the peaceful Limoges, and the warmness of your team. Thank you very much for all your support, your patience with my limits, your guidance, and your respect and nourishment of my own ideas. I still I do not have clear what's bigger in you: your brains or your humanity. A thousand times thank you.

Alongside the road, I had the fortune of sharing with two different teams, at two different cities, and as a consequence; I gained two brothers-in-arms: Nassif Berrabah, and Nicolas Bui. My good friends, thank you very much for your company, the good scientific (and sometimes silly) discussions, for your patience with my terrible French, and supporting me while learning it. I had the grace of sharing with you inside and

outside the work, and be a witness of the terrific humans beings you are. I feel really lucky to have crossed path with you guys, my prayers are with you, and your families.

Then, there are those special angels between lines that make the whole system work, and in my case, explain how the whole system works: Fabien Colin, Nadine Aymard and Clarie Lemarchand. My special gratitude towards you, with your immense kindness and patience behind all the paperwork you had to make because of me. Thank you for being there, and moving all the strings to make the bureaucracy work in my favor.

Now a person that without him, the analyses of this work would have not happen in a similar manner: Pascal Duquerroy, with your particular and practical view of the lightning protections world, I could've benefit of a broader spectrum of the problems that really matters, and concentrate the energies around them. I'm looking forward to our next technical meetings, and hopefully continue the exchange of nutritious experiences.

Also I had the opportunity to cross by pleasure or business, some persons that made this journey enjoyable: Emanuel Amador, Emanuela Buccafuri, Adrien Resmond, Houssan Tanzeghti, Minh Nguyen Tuan, Jose Blancarte, Alberto Tejeda, Ricardo D'Angelo, Geraud Blatman, Ibrahim Kane, Jorge Avella. Thank you very much for your friendship.

Finally, but not last, a special sentiment of gratitude towards the person that held me by the hand during the most intense moments of this project: Cristina Pinto. Thank you very much for your sacrifice, your regard full of love, and you support trough the ups and downs. Without you, rising every morning to keep going, would've be senseless.

I'm convinced that all of you were part of something bigger than us, it can not be mere coincide for me to find such a marvelous company trough all this path. At the end, I feel deeply in gratitude with our God, for is through all of you men and women, that I could've experience a little of his preference for me. Once again, thank you all.

A Tulio y Mercedes,
A Maria y Euclides.

Contents

Acknowledgements 3

List of Figures 11

List of Tables 19

Acronyms 21

Introduction 23

1 Lightning transients in Power Production Centers 25
- 1.1 Introduction . . . 25
- 1.2 The lightning discharge . . . 26
  - 1.2.1 Parameters of a lightning strike useful to conceive protection measures . . . 28
- 1.3 Consequences of a lightning impact on a building . . . 30
- 1.4 Lightning induced voltages in IM cables in NPPs . . . 32
  - 1.4.1 Procedure recommended in the standard KTA-2206 to compute the Lightning Induced Voltages . . . 33
  - 1.4.2 Introduction of a new regulation for the lightning protection of Power Generation Centers in France . . . 43
  - 1.4.3 Numerical strategies to assess the lightning induced voltages in cables . . . 44
- 1.5 Proposal of a computational tool to assess lightning transients in Power Generation Centers. . . . 49
  - 1.5.1 General Objective . . . 50
  - 1.5.2 Specific Objectives . . . 50

2 FDTD Modeling of a Large Industrial Site 53
- 2.1 Introduction . . . 53
- 2.2 The thin wire formalism of Holland . . . 54
  - 2.2.1 A thin wire shifted in the FDTD cell . . . 55
  - 2.2.2 An insulated thin wire . . . 59

2.2.3 A coaxial thin wire . . . 60
2.3 The return stroke . . . 62
2.4 The building . . . 68
2.4.1 Perfectly metallic structure . . . 68
2.4.2 Lossy conductive plates . . . 69
2.4.3 A junction of lossy thin wires . . . 70
2.4.4 Validation of transients in a building . . . 71
2.5 The instrumentation and measurement cable . . . 74
2.5.1 A Transmission Line solution for the current propagation in a buried conductor . . . 75
2.5.2 Comparison of methods to compute the transients in a buried cable . . . 76
2.6 The grounding system . . . 78
2.6.1 Potential rise of a Hollands Thin Wire . . . 79
2.6.2 Validation of the formulation for the potential rise . . . 81
2.7 A first approach to a complete case . . . 89
2.7.1 Case Study: A large industrial site . . . 90
2.7.2 Validation of the FDTD Thin Wire Model . . . 91
2.7.3 Currents in the coaxial cable . . . 93
2.7.4 Voltages at the extremities of a coaxial cable . . . 94
2.8 Conclusions . . . 97

3 Parametric Study of a Lightning Impact to a Large Industrial Site 101
3.1 Introduction . . . 101
3.2 The reference case . . . 102
3.3 Effect of the current at the channel base . . . 104
3.4 Effect of the ground resistivity . . . 110
3.4.1 Transients in a IM cable for different soil resistivities . . . 110
3.4.2 Synthesis of the effect of the soil resistivity . . . 115
3.5 The building size. . . . 115
3.5.1 Transients in a IM cable connected to building of different sizes 117
3.6 The grounding connections of the concrete cable duct. . . . 119
3.6.1 Transients in the IM cable for different grounding connections of the cable duct . . . 119
3.6.2 Synthesis on the effect of the grounding of the cable duct in the transient voltages . . . 123
3.7 The connections to ground of the shield of the coaxial cable . . . 123
3.7.1 Transients in a IM cable for different connections of the shield . 123
3.7.2 Effect of the inclusion of the transfer admittance. . . . 126
3.7.3 Synthesis of the effect of the connection of the shield . . . 128
3.8 The external grounding system configuration. . . . 129

3.8.1 Transients in a IM cable for different configurations of grounding 131
3.8.2 Synthesis of the effect of the external grounding system configuration. 136
3.9 The length of the IM cable. 136
3.9.1 Transients in a IM cables of different lengths 136
3.9.2 Synthesis of the effect of the cable length in the transient voltages. 137
3.10 The connection point of the lightning channel to the building. 140
3.10.1 Transients in a IM cable for different lightning striking position . 140
3.10.2 Synthesis of the effect of the lightning striking position 143
3.11 The EM model for the building wall. 143
3.11.1 Transients in a IM cable for different EM models of building walls. 143
3.11.2 Synthesis of the effect of the model of the building wall 146
3.12 The inclusion of cable trays inside the concrete cable duct. 146
3.12.1 Effect of the cable trays in the transient voltages of an IM cable . 147
3.12.2 Synthesis of the effect of the cable trays 151
3.13 The inclusion of the expansion joints between concrete cable ducts. . . . 151
3.13.1 Transients in a control cable for different amount of expansion bridges 151
3.14 The type of canalization of the IM cable. 155
3.14.1 Equivalent model of a pipeline for a Holland thin wire 155
3.14.2 Transients of a IM cable for different canalizations 156
3.14.3 Synthesis of the effect of the cable route 157
3.15 Synthesis of the parametric study. 158

4 A meta-model for the lightning induced voltages in IM cables 165
4.1 Introduction 165
4.2 Overview of the Design of Experiments technique 166
4.2.1 The factors of a DoE 166
4.2.2 The response of a Design of Experiments 167
4.2.3 Types of Design of Experiments 168
4.2.4 Optimal Design of Experiments 170
4.3 The Design of Experiments adapted to the lightning induced voltages in IM cables 172
4.3.1 The factors for the problem of LIV in IM cables 172
4.3.2 The meta-model for the response of the LIV in IM cables 174
4.3.3 The Design Matrix for the problem of LIV in IM cables 175
4.3.4 Procedure to fit the model 176
4.4 A meta-model for the LIV of IM cables 178
4.4.1 Coefficients of the models 178
4.4.2 Adjustment of the prediction to the simulation data 181
4.4.3 Parameter's relevance 183
4.4.4 Errors of the models 188

4.5 Comparison with the KTA procedure 191
4.6 Conclusions 193

5 Conclusions and perspectives **197**
5.1 Conclusions 197
5.2 Perspectives 198

Communications **201**

List of Figures

1.1 Relation between lightning aggressions in French territory and electrical service outages during 2014. Adapted from [3] . . . 26
1.2 General process of a cloud to ground lightning discharge. Adopted from [1] . . . 26
1.3 Characteristic behavior of return strokes currents. Adopted from [Berger] 27
1.4 Cumulative frequency of the current peak. Adapted from the standard IEC-62305-1 [6] . . . 29
1.5 Transient behavior of a Heidler pulse. T_1 and T_2 stand for the rise and decay time. (Adapted from [6]) . . . 30
1.6 Damages caused by a lightning strike to a building in an industrial site 31
1.7 Problem of interest: Induced voltages at the termination of a buried IM cable leaving a building stroke by lightning. . . . 32
1.8 General scope of the problem treated in the standard Kerntechnischer Ausschuss (KTA) 2206 . . . 33
1.9 Geometry to calculate the induced voltage in a cable duct. . . . 34
1.10 Channel base currents as considered in the KTA-2206 . . . 35
1.11 Work-flow to compute the peak voltage at the terminations of a cable inside a cable duct according to the standard KTA-2206 . . . 38
1.12 Connections of terminations of cable used in [14]. . . . 39
1.13 Circuit distribution of electrical parameters in the Transmission Line (TL) model. . . . 45
1.14 Structure of ElectroMagnetic (EM) fields in the Transverse ElectroMagnetic (TEM) mode. . . . 46
1.15 Excitation in common mode and differential mode. Adapted from [12] 46
1.16 Detail of the phenomena interacting at the cable duct connection to the building. . . . 47

2.1 Bare wire in a FDTD cell according to Holland's formalism [6] . . . 54
2.2 Integration volume centered on the component $E_{z,1,m}$, to compute the inductance $L_{z,1,m}$. Taken from [7] . . . 56
2.3 Thin wire of radius a crossing a Yee cell, $(u,\ v,\ w)$ take any Cartesian direction $x,\ y$ or z in circular permutation. Taken from [7] . . . 56

2.4 TL equivalent circuit for a thin wire 58
2.5 Current weighting coefficient Pc_u of the cell node m resulting from the contribution of all wires in the vicinity. Adapted from [7] 59
2.6 TL equivalent circuit for an insulated single core thin wire. Adapted from [9]. 60
2.7 TL equivalent for the inner circuit of a shielded cable 61
2.8 Solution methods for each component in a cable 62
2.9 Generic EM model of a lightning channel 63
2.10 Characteristics of the electromagnetic environment of a return stroke. Adapted from [17] 64
2.11 EM models for the lightning channel 65
2.12 Current distribution for a perfectly conducting wire in air 66
2.13 Current distribution for a perfectly conducting wire embedded in a $4\,\mathrm{m}\times4\,\mathrm{m}$ dielectric of $\varepsilon_r = 9$ 66
2.14 Current distribution for a lossy wire with uniform distributed resistances, embedded in a material of $\varepsilon_r = 5$ and $\mu_r = 5$ with $20\,\mathrm{m}\times20\,\mathrm{m}$ of transversal area 66
2.15 Current distribution for a lossy wire with non uniform distributed resistance, embedded in a material of $\varepsilon_r = 5$ and $\mu_r = 5$. 67
2.16 Current propagation for two different return strike models 67
2.17 Fields radiated at 200 m for two different lightning channel numerical models 67
2.18 Boundary between a metallic volumetric structures and air cells in Finite Differences Time Domain (FDTD). 69
2.19 Thin lossy plate with BIBC in FDTD. 70
2.20 Junction of multiple wires. 71
2.21 Schematic of a building as proposed in [24] 72
2.22 Induced voltage in the junction of the electrical wiring and the building structure 73
2.23 Current in the junction of the electrical wiring and the building structure 73
2.24 Geometry of the case to validate the thin wire formalism to model an horizontal conductor. 74
2.25 FDTD implementation of the case study depicted in figure 2.24 77
2.26 Currents in the buried horizontal cable depicted in figure 2.24. "*Ref.*" are the results extracted from [28]. "*FDTD*" are the results obtained using the thin wire formalism of Holland, and "*TL*" are the results computed solving expression (2.27) 77
2.27 Electric field in a FDTD cell around a thin wire 78
2.28 Thin wire oriented along z-axis. Close radial components along x-axis. 79
2.29 Case study of a single vertical rod. 82
2.30 Current injected to the vertical rod.(Adapted from [29]) 83

2.31 Detailed view of the buried vertical rod in the FDTD scheme. 83
2.32 Transient potential rise of a vertical conductor. 84
2.33 Case study of a counterpoise. 85
2.34 Detailed view of the buried counterpoise in the FDTD scheme. 86
2.35 Current excitation of the buried counterpoise 86
2.36 Transient potential rise of a buried counterpoise. 87
2.37 Case study of a grounding grid 88
2.38 Current injected in the grid. 88
2.39 Potential rise of the point in the grounding grid depicted in 2.37b. . . . 89
2.40 Equivalent circuit for the junction of a coaxial cable and a bare conductor. 89
2.41 Study case of a buried cable connected to a building stroke by lightning 90
2.42 Geometry and material properties of the cable under study 91
2.43 Details of the terminations in the FDTD case 92
2.44 Normalized current in the single core cable for two computational tools, at three positions along the cable. 92
2.45 Normalized current in the single core cable at the building side. For two different computational tools. Comparison of lightning channel implementations. 93
2.46 Transient current in the single core cable for two computational tools, at three positions along the cable. 94
2.47 Transient current in the conductor of a single core cable (solid line) and in the shield of an equivalent coaxial cable (dotted line). 95
2.48 Transient current in the core conductor of the coaxial cable. 95
2.49 Variations on the connection of the termination impedance 96
2.50 Transient voltage at the 50 Ω load in the terminations. 97

3.1 Main case of study, a 50 m cubic building hit by lightning, with one 50 m IM cable inside a buried cable duct. 102
3.2 Transversal view of the cable duct under study. 103
3.3 Details of the terminations of the cable duct 104
3.4 Current flowing through the cable duct at the building side. For the case depicted in figure 3.1 105
3.5 Current flowing through the cable shield. For the case depicted in figure 3.1 107
3.6 Voltage at the 50 Ω load. For the case depicted in figure 3.1 109
3.7 Influence of the soil resistivity in the voltage at the 50 Ω load. For the case depicted in figure 3.1 111
3.8 Influence of the soil resistivity in the current entering to the cable duct from the building. For the case depicted in figure 3.1 112
3.9 Influence of the soil resistivity in the current flowing through the cable shield. For the case depicted in figure 3.1 114

3.10 Geometry of the cases for evaluate the effect of the building size. 116
3.11 Influence of the size of the building in the voltages at the terminations of the cable. 117
3.12 Influence of the size of the building in the current entering to the cable duct. 118
3.13 Influence of the building's size in the current of the cable shield. 118
3.14 Detail of the grounding connections considered for the cable duct. . . . 119
3.15 Effect of the grounding on the cable duct in the voltage at the 50 Ω load. For a negative subsequent stroke 120
3.16 Effect of the grounding on the cable duct in the voltage at the 50 Ω load. For a positive first stroke 120
3.17 Effect of the grounding on the cable duct in the shield current. For a negative subsequent stroke 121
3.18 Effect of the grounding on the cable duct in the shield current. For a positive first stroke 122
3.19 Effect of the grounding on the cable duct in the current entering from the building. 122
3.20 Voltage at the 50 Ω load for a subsequent stroke. 124
3.21 Voltage at the 50 Ω load for a first stroke. At the building side. *Note:* observe that the blue and green curves are amplified by 100 124
3.22 Current in the shield for a subsequent stroke. 125
3.23 Current in the shield for a first stroke. Solid line: At the building side. Dotted line: At 50 m from the building. *Note:* observe that the blue and green curves are amplified by 100 125
3.24 Current entering from the building to the cable duct. 126
3.25 Equivalent TL model for a coaxial cable considering the transfer impedance. 127
3.26 Transversal view of the cable duct and the points used to measure the electric field to compute the distributed source V_{si} 127
3.27 Voltage at the load 129
3.28 General view of the case studies that concerns the study of the grounding system 130
3.29 Voltage at the 50 Ω load for a negative subsequent stroke 130
3.30 Voltage at the 50 Ω load for a positive first stroke. 130
3.31 Frequency response of the voltage at the at the 50 Ω load for a subsequent stroke. Solid line: At the building side. Dotted line: at 50 m from the building 131
3.32 Shield current for a negative subsequent stroke 132
3.33 Shield current at the building side for a positive first stroke. 132
3.34 Current entering from the building to the cable duct. 132
3.35 Case study of two grounding rings connected. 133

3.36 Effect of connecting two grounding systems in the shield current for a negative subsequent stroke. 134
3.37 Effect of connecting two grounding systems in the shield current for a positive first stroke. 134
3.38 Effect of connecting two grounding systems in the voltage at the 50 Ω load for a negative subsequent stroke 135
3.39 Effect of connecting two grounding systems in the voltage at the 50 Ω load for a negative subsequent stroke 135
3.40 Effect of the length of the cable in the voltage at the 50 Ω load for a negative subsequent stroke 137
3.41 Effect of the length of the cable in the voltage at the 50 Ω load for a positive first stroke 138
3.42 Frequency response of the voltage at the at the 50 Ω load for a subsequent stroke. Solid line: At the building side. Dotted line: at 50 m from the building 138
3.43 Effect of the length of the cable in the current at the shield for a negative subsequent stroke 139
3.44 Effect of the length of the cable in the current at the shield for a positive first stroke 139
3.45 Effect of the length of the cable in the current entering at the cable duct from the building 140
3.46 Top view from the case study. Different lightning strike locations 141
3.47 Effect of the striking position in the voltage at the 50 Ω load for a negative subsequent stroke 142
3.48 Effect of the striking position in the voltage at the 50 Ω load for a positive first stroke 142
3.49 Effect of the EM model of the building in the voltage at the 50 Ω load for a negative subsequent stroke 144
3.50 Effect of the EM model of the building in the voltage at the 50 Ω load for a positive first stroke 144
3.51 Effect of the EM model of the building in the current entering to the cable duct from the building. 145
3.52 Effect of the EM model of the building in the shield current for a negative subsequent stroke 145
3.53 Effect of the EM model of the building in the shield current for a positive first stroke 146
3.54 Generic metallic closed cable duct. 147
3.55 Detail of the cable duct with trays at the remote end. 147
3.56 Effect of the presence of cable trays in the current entering to the cable duct from the building. 148

3.57 Effect of the presence of cable trays in the voltage at the 50 Ω load, at the building side. For an open cable duct and a connected shield. 149
3.58 Effect of the presence of cable trays in the voltage at the 50 Ω load, at the building side. For a grounded cable duct and an open shield. 149
3.59 Effect of the presence of cable trays in the voltage at the 50 Ω load, at the building side. For a grounded cable duct and a connected shield. . 150
3.60 Frequency response of the effect of the voltage at the 50 Ω load, at the building side. Evaluation of the presence of the cable trays for a negative subsequent stroke. Solid line: with cable trays. Dotted line: without cable trays. 150
3.61 Detail of the schematic of one expansion joint, with copper bridges uniformly distributed around the perimeter of the cable duct. 152
3.62 Effect of the presence of expansion joints in the voltage at the 50 Ω load, for a positive first stroke. 153
3.63 Effect of the presence of expansion joints in the voltage at the 50 Ω load, for a negative subsequent stroke. 153
3.64 Effect of the presence of expansion joints in the frequency response of the voltage at the 50 Ω load. Building side. For a negative subsequent stroke. 153
3.65 Effect of the presence of expansion joints in shield current. For a negative subsequent stroke. 154
3.66 Effect of the presence of expansion joints in shield current. For a positive first stroke. 154
3.67 A coaxial cable inside a dielectric pipeline 156
3.68 Effect of the presence of metallic trays in the voltage at the 50 Ω load, for a negative subsequent stroke. 157
3.69 Effect of the presence of metallic trays in the voltage at the 50 Ω load, for a positive first stroke. 157

4.1 Design cube for 2^3-factorial plan 169
4.2 Work-flow to find a model for each output variable. 178
4.3 Fit between simulated and predicted values. For a negative subsequent stroke excitation. 181
4.4 Fit between simulated and predicted values. For a negative first stroke excitation. 182
4.5 Fit between simulated and predicted values. For a positive first stroke excitation. 182
4.6 Pareto diagram for parameters estimates of cables inside a duct. 185
4.7 Pareto diagram for parameters estimates of cables in a dielectric pipe. . 186
4.8 Residual error of simulated values for each prediction. For a negative subsequent stroke excitation. 189

4.9 Residual error of simulated values for each prediction. For a negative first stroke excitation. 189
4.10 Residual error of simulated values for each prediction. For a positive first stroke excitation. 189
4.11 Peak induced voltages for all the scenarios in 4.3. For a cable inside a duct, and an excitation of a negative subsequent stroke. 192

List of Tables

1.1 Maximum values of the current parameters. Adapted from [9] 30
1.2 Transient characteristics of the return stroke current as suggested by the KTA-2206. 35
1.3 Parameters that characterize the current at the base of the lightning channel I_B. according to expression (1.1) 35
1.4 Weighting factors p_k to use in (1.2) 36
1.5 Lightning type factor K to use in (1.3) 36
1.6 Fictive extension of the expansion joints l_{DFv} (m) 37
1.7 Coupling impedance to use in (1.5). 37
1.8 Equivalent frequency of the impulses considered in the KTA-2206 [14] . 40

3.1 Ratio of current division from the channel base to the cable duct. 106
3.2 Rise time of the current at the channel base and at the entrance of the cable duct. 106
3.3 Coaxial cable parameters used to compute the transfer admittance (3.2a) 128
3.4 Synthesis of the effects considered on the voltages at the cable terminations. 159
3.4 Synthesis of the effects considered on the voltages at the cable terminations. 160
3.4 Synthesis of the effects considered on the voltages at the cable terminations. 161
3.4 Synthesis of the effects considered on the voltages at the cable terminations. 162

4.1 Design Matrix for 2^3-factorial plan. 170
4.2 Summary of the factors considered for the meta-model of LIV in IM cables. 174
4.3 Design points conceived with an I-optimal criterion. 176
4.4 Single parameters β_i and K_i for the maximum voltages in a cable. . . . 179
4.5 Crossed parameters β_{ij} and K_{ij} for the maximum voltages in a cable inside a duct. For a negative subsequent stroke excitation. 179
4.6 Crossed parameters β_{ij} and K_{ij} for the maximum voltages in a cable inside a duct. For a negative first stroke excitation. 179
4.7 Crossed parameters β_{ij} and K_{ij} for the maximum voltages in a cable inside a duct. For a positive first stroke excitation. 180

4.8 Crossed parameters β_{ij} and K_{ij} for the maximum voltages in a cable inside a pipe. For a negative subsequent stroke excitation. 180
4.9 Crossed parameters β_{ij} and K_{ij} for the maximum voltages in a cable inside a pipe. For a negative first stroke excitation. 180
4.10 Crossed parameters β_{ij} and K_{ij} for the maximum voltages in a cable inside a pipe. For a positive first stroke excitation. 181
4.11 Factors with a cumulative influence under 60 % according to the Pareto curves. 187
4.12 Average error of the models. 190
4.13 Design points with interesting errors for the maximum voltage of a cable inside a duct. Type of excitation: negative subsequent stroke. . . 190
4.14 Design points with interesting errors for the maximum voltage of a cable inside a duct. Type of excitation: negative first stroke. 190
4.15 Design points with interesting errors for the maximum voltage of a cable inside a duct. Type of excitation: positive first stroke. 191

Acronyms

DF	Degrees of Freedom.
DM	Design Matrix.
DoE	Design of Experiments.
DP	Design Point.
EM	ElectroMagnetic.
EMI	ElectroMagnetic Interference.
FD	Finite Difference.
FDR	False Discovery Rate.
FDTD	Finite Differences Time Domain.
FEM	Finite Element Method.
FFT	Fast Fourier Transform.
GM	Garlekin Method.
IE	Integral Equation.
IM	Instrumentation & Measurement.
KTA	Kerntechnischer Ausschuss.
LIV	Lightning Induced Voltage.
LPS	Lightning Protections System.
MoM	Method of Moments.
MPI	Message Passing Interface.
MTLE	Model of Transmission Line Modified Exponentially.
NPP	Nuclear Power Plant.
ODE	Ordinary Differential Equation.

PEC Perfect Electric Conductor.
PGC Power Generation Center.
PML Perfectly Matched Layers.

RMSE Root Mean Square Error.
RSM Response Surface Metamodels.

TE Transverse Electric.
TEM Transverse ElectroMagnetic.
TGPR Transient Ground Potential Rise.
TL Transmission Line.
TM Transverse Magnetic.

Introduction

A lightning strike to an industrial facility carries great risk to its operation. The dangerous amount of energy involved in a single hit might damage equipments, interrupt operations, or even hurt the personnel. Therefore, it is required to adopt measures to protect from the consequences of this unavoidable phenomenon.

In order to conceive protection measures, the consequences of a lightning impact must be assessed, i.e., the phenomenon must be studied with detail: from the nature of the formation of the lightning discharge, to the effects of different type of impacts, and the interactions of all the components exposed to the lightning energy.

In this work, the object of study are industrial sites in general, and particularly of the type of Power Generation Center (PGC). When lightning strikes a building inside an industrial site, currents propagates through the building and all the components connected to it: underground facilities, external and internal cables, and buried conductors.

Among all the consequences of this type of strike, the focus is made in the possible damage or malfunctioning of one of the most susceptible elements of an installation: the sensitive electronic equipment used in the Instrumentation & Measurement (IM) System. In general, these are integrated circuits that might have a relative low voltage withstand, and are usually connected to cable routes that are susceptible of carrying EM disturbances related to lightning.

In this work, the focus will be the transient surges in IM cables connected to a building directly hit by lightning. To do that, a numerical simulation approach is adopted. In a manner that, the whole industrial facility, is modeled and translated into equivalent and validated EM models.

The numerical solution of the models is based on the FDTD algorithm, and a method to consider wired structures: the thin wire formalism of Holland. This formalism is used to account for all the grid-like structures of an industrial site: the building steel grids of the walls and its foundations, the grounding systems, and the isolated or coaxial cables.

The FDTD numerical solution was implemented in the numerical code: Transient ElectroMagnetic SImulator - Finite Difference (TEMSI-FD), since it allows the use of an implementation of a versatile thin wire model based on Holland's formalism, with a fast computational time, and permits to perform even faster simulations using a Message Passing Interface (MPI) protocol to manage parallel computations.

Nevertheless, a complete EM model for a lightning impact in FDTD takes time to solve, even a couple of hours. This, although efficient in results, is not a practical application. Therefore, exist also the necessity to expand the validated results obtained with the FDTD simulations, to a more pragmatic and direct solution.

The proposal of this work is to elaborate a meta-model that describes the voltages developed in the IM cables when a lightning strikes a building. This meta-model is a mathematical expression that directly correlates the peak voltage at the cable terminations, with all the parameters that interact and drive the phenomenon.

In a manner that, an easy-to-implement tool, based on accurate FDTD simulation scenarios, serves to compute one of the most important variables to evaluate the lightning response of a IM cable: its maximum voltage.

To construct the meta-model, a wide set of scenarios of simulation are proposed using the technique of Design of Experiments (DoE). This technique also contributes to the analysis of the voltage response of the cable, since it correlates and weights the input parameters and their influence. This is, a frame of analysis of a complex system, is given in parallel with a response prediction expression.

The work is organized as follows:

- In chapter 1, the problem of lightning surges in cables of an industrial site is depicted, a standardized and simplified procedure of computation is analyzed, and different numerical strategies to assess the problem are briefly described. At the end of the chapter, the main proposal of the work is outlined.

- In chapter 2, the validation of the EMs models developed for each component of the industrial site is shown, including an implementation of all the components assembled.

- In chapter 3, a parameter variation is performed over a common reference case. In a manner that, the influence of each parameter is observed, evaluated and justified; in all the magnitudes affecting the response at the terminations of the cable duct.

- Finally, in chapter 4, the implementation of the DoE technique is described, with all the implications that a complex EM problem involves. At the end of the chapter the evaluation of the prediction of the meta-models is presented, and an application on a realistic case study is shown.

Chapter 1

Lightning transients in Power Production Centers

1.1 Introduction

Lightning is a natural phenomenon characterized by the rapid flow of high amounts of electrical charge in the atmosphere [1, 2]. It is a direct consequence of the inherent distribution of electrical charge in the planet, and it is though to be an important component in keeping the balance of the global electric field.

Been an unavoidable phenomenon, it has an impact on human activity, mostly with deleterious effects. Take for example the map depicted in figure 1.1, which depicts a direct correlation between lightning occurrences and Outages of Electric Service [3].

This kind of atmospheric discharge affects cities and villages, ground structures or aerospace vehicles, industrial or health facilities. In this work; the structure of interest is an industrial building, particularly; a Power Generation Center (PGC).

A lightning might affect the functioning of a PGC in a wide variety of ways, here only the effects over sensitive electronic equipment connected to Instrumentation & Measurement (IM) cables is treated. To do that, this chapter starts with a brief description of the lightning discharge, assessing the parameters useful to conceive and design protective measures.

Afterwards, some general aspects relating the consequences of a lightning strike to a building are assessed, in order to give a frame to the problem over electronic equipment, and the current propagation in IM cables.

Also, an important part of the chapter is dedicated to the analysis of the current methodology used to study the lightning effects on IM cables in a PGC. Finally, a proposal to assess this problem with a different approach is made alongside with the objectives of this work.

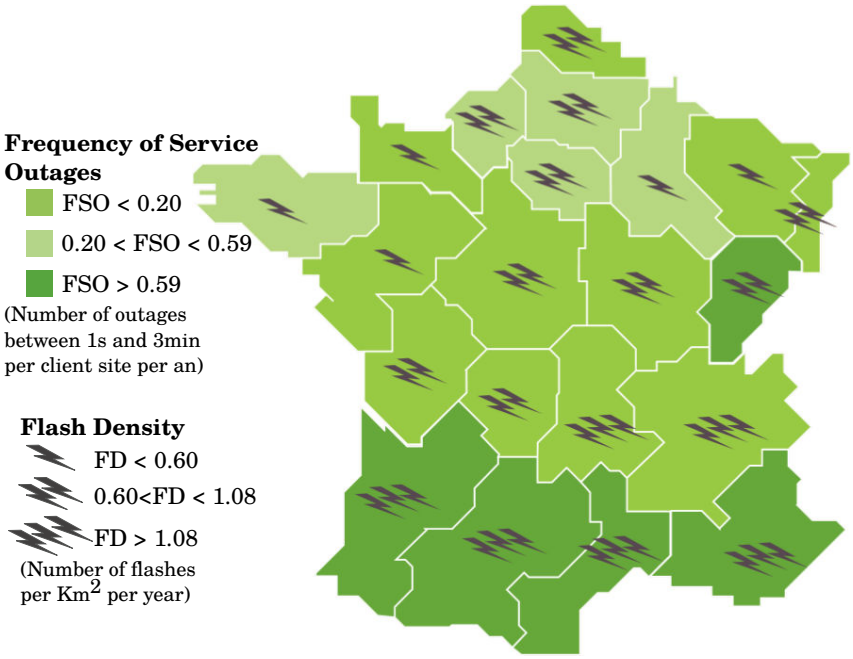

Figure 1.1: Relation between lightning aggressions in French territory and electrical service outages during 2014. Adapted from [3]

1.2 The lightning discharge

The uneven charge distribution in the clouds of a thunderstorm might give rise to atmospheric discharges. These discharges might be: intra-cloud, between different clouds, cloud to ground or cloud to ionosphere [1]. Among them, the cloud-to ground discharges are of special interest to the activity of a PGC.

A lightning strike to ground occurs when a particular charge density is reached in a section of the cloud; positive or negative, a process of electrical breakdown is initiated in the air, giving rise to a stepped leader. In figure 1.2, a negative descending leader is illustrated.

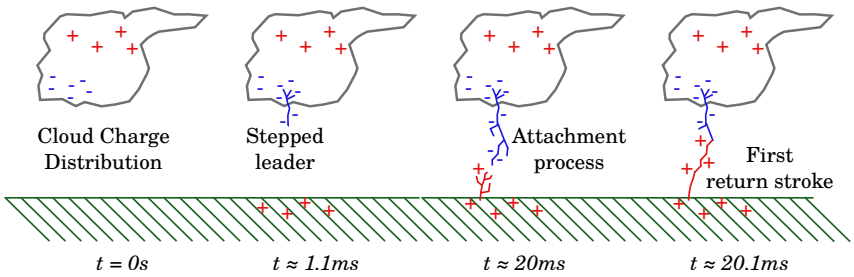

Figure 1.2: General process of a cloud to ground lightning discharge. Adopted from [1]

This leader descends to ground inducing opposite charge in its immediate vicinity, and when is sufficiently close to a grounded structure such as a soil, a tree, or a building; an opposite polarity leader rises, attaches, and forms the lightning channel.

Once the channel is formed, electric charge from the ground propagates to the

cloud in a current propagation phenomena known as a *first return stroke*. Finally, it is usual that *subsequents return strokes* continue to propagate through the lightning channel.

Upward discharges might also occur, they typically strike structures taller than 100 m, a size of no interest for this work [2].

Depending on the polarity of the downward leader, the return strokes might be positive or negative. Typical observations for these discharges are depicted in figure 1.3. In general, the behavior of both type of strokes have been characterized according to several measurements [4]:

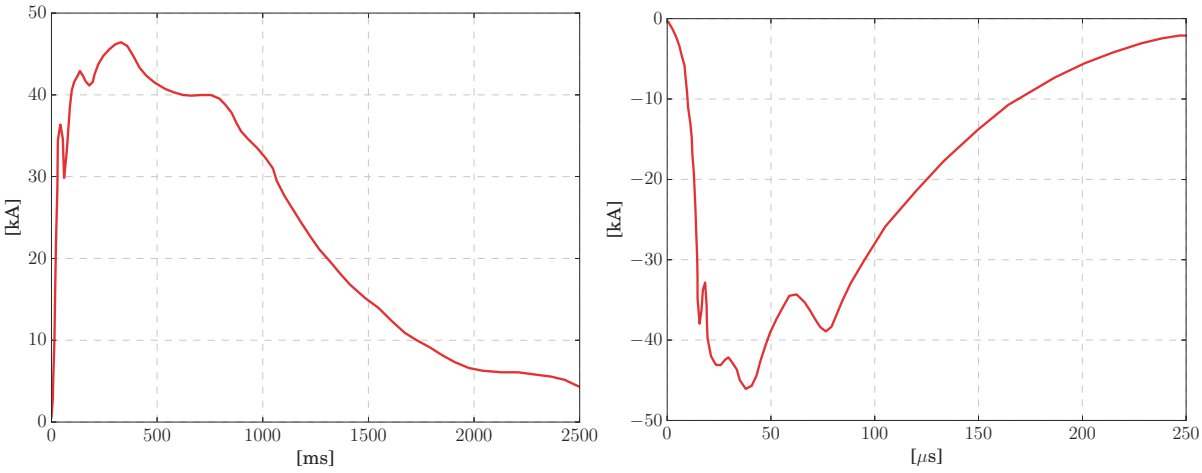

(a) Positive First Stroke **(b) Negative First Stroke**

Figure 1.3: Characteristic behavior of return strokes currents. Adopted from [Berger]

- **Regarding the current magnitude:** Both polarities of first strokes impulses might have amplitudes of tens of kilo-amperes, being the positive stroke usually higher, with recorded values over 100 kA.
- **Regarding the rise-time:** First strokes have been measured with rising times from hundreds of nano-seconds to more than 10 μs.
- **Regarding the decay time:** Both pulses decay slower than they rise, being the negative first stroke the faster to fall; around 100 μs. While, the positive first stroke might have a decay time of around 2 ms.

Regardless of the general behavior between strokes, the characteristics of lightning strikes varies from one impact to another, from geographic region to another, and between different seasons. Due to this diversity, arises the necessity to establish a common base behavior to characterize a lightning strike.

Therefore, the most important normalization committees along the world have adopted results from different sets of measurement campaigns carried along decades, to compile a data base sufficiently as robust as to establish a confident statistical behavior for the lightning impulse current.

1.2.1 Parameters of a lightning strike useful to conceive protection measures

As previously stated, a statistical approach is often used to characterize the behavior of the return strokes in general. This approach is based on several measurements performed during tens of years, usually the observations of Berger et al. [4] are the reference adopted by the most relevant scientific committees: CIGRE [5], IEC [6] and IEEE [7].

It is important to note that, even with the technology limitations at the moment of Berger's observations (1975), its data continues to be valid. Although, modern efforts to complement it with new observations have been made [8].

In order to evaluate the effects of a lightning strike, four main parameters have been extracted from the observations:

- **The peak current:** accounts for the conduction effects, particularly of the potential rise of the grounded structures, and grounding system.
- **The average rate of change:** also known as the current time derivative, or front steepness. Accounts for the induction effects of the transient propagating through the structure, particularly of the magnetic fields coupling through closed loops.
- **The transfered charge:** accounts for the melting effects at the attachment points.
- **The specific energy:** accounts for the heating and mechanical forces of conductors through which the current propagates.

Each one of these parameters has its own statistical behavior according to the kind of strike and its polarity: first strike or subsequent strike, positive or negative. As an example, figure 1.4 indicates the cumulative probability for the peak of the currents according to Berger's data [4].

Figure 1.4 is a representation of a standardized and globally extended statistical behavior of the peak current of the return stroke. Depending on the engineering application, this behavior is adopted from a different perspective. For example, for installations with the highest importance to human activity and personnel security, the standard of lightning protections IEC 62305-1 [6]; fixes current parameters that helps to conceive a Lightning Protections System (LPS) able to withstand 99 % of the feasible lightning strikes.

Rigorously, when performing lightning transient studies, all the waveforms of the strikes shall be considered, since each one of them accounts for different consequences of a lightning discharge. Nevertheless, in order to represent all the effects, it is common practice recommended in several lightning protection standards to deal only with two of these strikes:

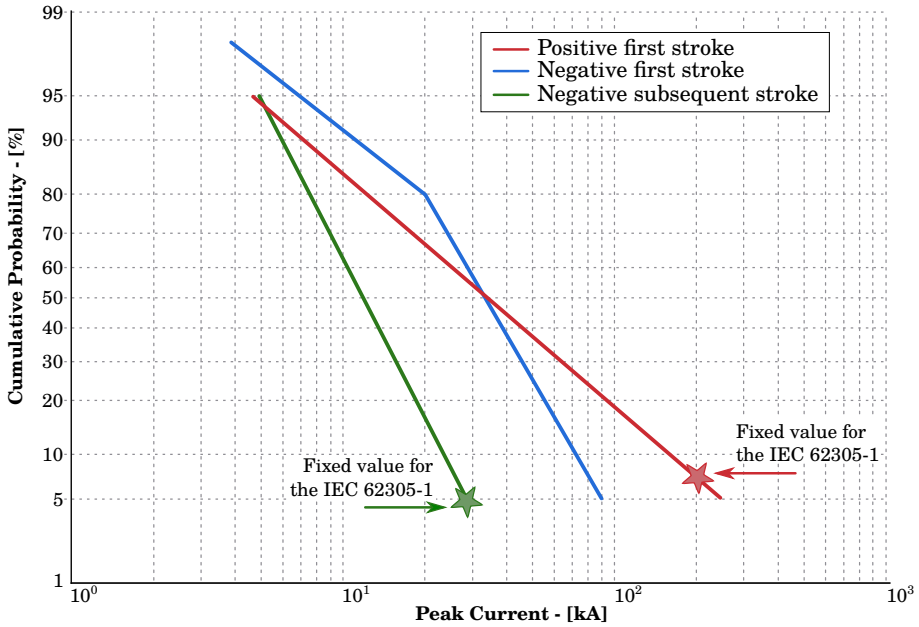

Figure 1.4: Cumulative frequency of the current peak. Adapted from the standard IEC-62305-1 [6]

- **The positive first stroke:** has the maximum transfered charge, current peak, and specific energy. According to the measurements of Berger, these parameters have a strong correlation [9]. Therefore this kind of impulse is useful for assessing the energy withstand of protection elements, as well as potential rise of grounded components.

- **The negative subsequent stroke:** has the highest rate of change, which makes it useful to study inductive effects of a lightning impact.

In order to describe both type of pulses, perform lightning transient studies, and account for all the consequences of a lightning impact, a standard impulse waveform is required. It is common practice, and widely recommended to use the Heidler function [10] to describe a lightning pulse, such as the one depicted in figure 1.5. In a manner that , selecting the peak, the rise and decay time of the function, the pulse emulates the effects of a first or subsequent stroke.

The table 1.1, shows the parameters of the Heidler function [10] that best describe the behavior of the worst case scenarios for the 99 % of feasible lightning strikes to ground. This is, for a first stroke; the maximum amount of transfered charge, and energy. And for a subsequent stroke the highest rate of change, and peak current.

Up until now, the parameters of interest to assess the effects of a lightning discharge have been mentioned: the transfered charge, the specific energy, the peak current and its rate of change. These parameters are conceived to model the effects of a lightning impact over a structure.

In the next section, more detail of the consequences of an impact are going to be

presented, alongside with a brief description the problem of interest of this work: a lightning strike to a PGC.

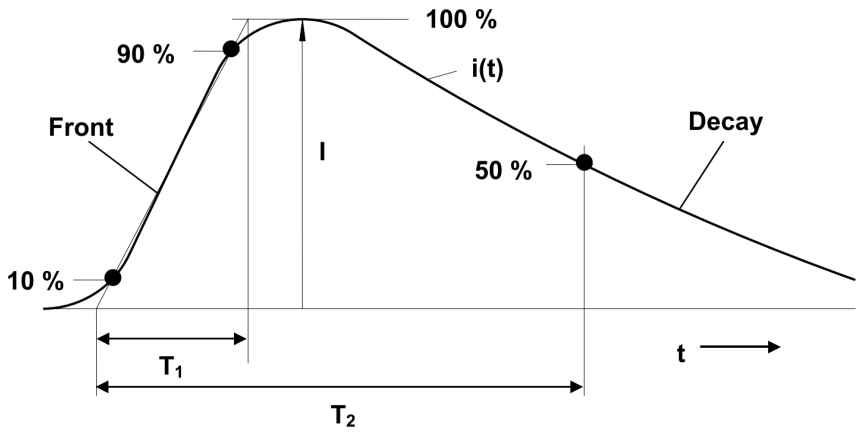

Figure 1.5: Transient behavior of a Heidler pulse. T_1 and T_2 stand for the rise and decay time. (Adapted from [6])

Parameter	Units	Positive First Stroke	Negative Subsequent Stroke
Peak	kA	200	50
Rise time	μs	10	0.25
Decay time	μs	350	100
Transfered charge	C	100	–
Specific energy	MJ/Ω	10	–
Average front steepness	kA/μs	–	200

Table 1.1: Maximum values of the current parameters. Adapted from [9]

1.3 Consequences of a lightning impact on a building

The consequences of lightning impact on a building can be classified following the striking position, this is: a strike near the building or directly into its structure [6].

If the lightning strike in the building it might cause:

- **Damage to humans and living stock** due to dangerous potentials of conductive elements, mainly of the reference conductors: the grounding system, or the carcass of the equipment. This is also known as touch and step potentials.
- **Physical damages tied to fire, and explosions** due to possible sparks close to flammable material. Also mechanical degradation might occur due to electromechanical efforts between close parallel conductors

- **Failure of sensitive equipment** due to the ElectroMagnetic Interference (EMI), mainly radiation from the lightning current propagating through the structure, which induce currents and charges in the conductive elements of the facility.

If the lightning strikes near the building, the principal effect of lightning is the EMI on the equipment inside.

Figure 1.6 synthesizes the effects of a lightning strike to a building. Here, the interest is to observe the effects over sensitive electronic equipment, particularly; the equipment connected to IM cables leaving an impacted building.

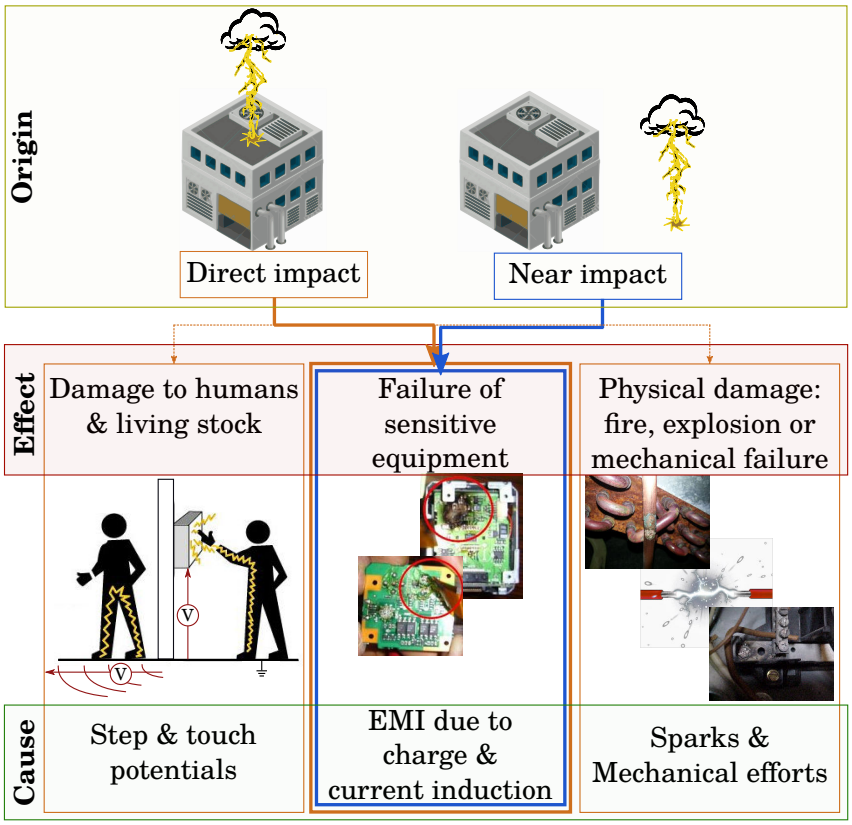

Figure 1.6: Damages caused by a lightning strike to a building in an industrial site

Figure 1.7 presents a synthesis of the problem of interest: A lightning strikes a building, its currents flow from the impact point through the building structure, to the cable leaving the building and the grounding system at the foundations.

To inquire on the EMI at the extremities of a IM cable, it is necessary to consider the current circulating through the cable shield, the potential rise at its connection point, and the induction coming from the coupling of the cable to the building and the grounding system.

The interactions of these phenomena depend on the type of building: its geometry, materials, configurations, type of conductors, its canalizations etc. As that, different approaches can be adopted to assess the lightning interference. At this point, is mandatory to specify the type of facility to examine in this work.

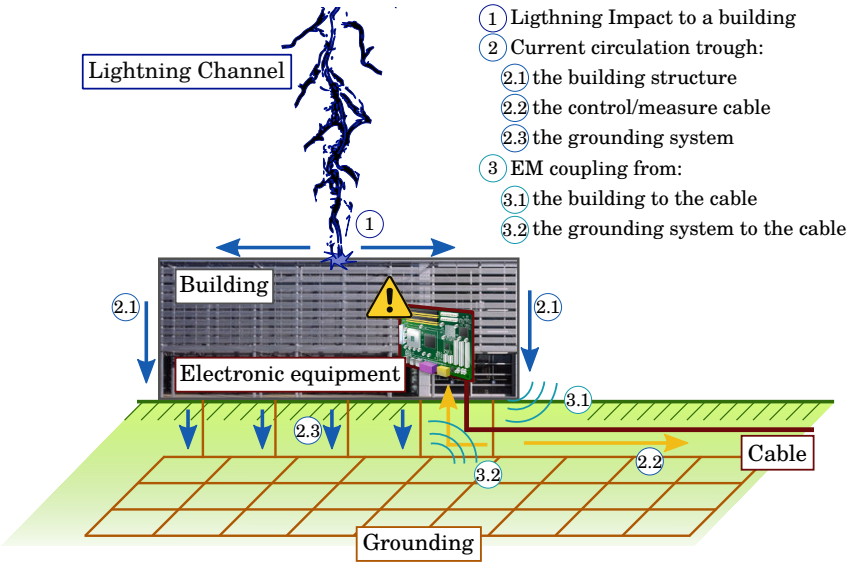

Figure 1.7: Problem of interest: Induced voltages at the termination of a buried IM cable leaving a building stroke by lightning.

Up until this moment, the considerations of the lightning effects have been made over a case of a generic site. Nevertheless, it has been previously stated that the frame of this study are the PGC.

In the next section, the current guidance to assess the lightning induced voltages in IM cables in this type of sites is going to be discussed.

1.4 Lightning induced voltages in IM cables in NPPs

From the point of view of a LPS designer, an standardized procedure is usually followed, to estimate the level of threat to electronic equipment inside a Nuclear Power Plant (NPP). This procedure counts with the approval of national and international experts, academics and manufacturers. The methodology proposed in this procedure is not complex, since it comes from previously observations, tests, measurements, and exhaustive analysis.

In France, one of the procedures followed to assess the LPSs was the guidelines established in the safety standard of the Kerntechnischer Ausschuss (KTA) 2206 (Nuclear Safety Standards Commission) [11], which originally is a German standard focused in the particularities of its own national NPPs. This procedure includes:

- The general requirements an NPP must follow in order to be protected from lightning damages.
- The design recommendations for the LPSs outside and inside the buildings.
- A calculation procedure for Lightning Induced Voltage (LIV) at the terminations of IM cables leaving the building.

- The test procedures to follow for the compliance of the safety of the site.

In this section, the procedure suggested by the standard KTA-2206 to obtain the induced voltages of a IM cable is going to be detailed. Afterwards, the legal framework that challenges this traditional method is going to be presented. And finally, the foundations of the new proposal to obtain the lightning response of IM cables will be laid out.

1.4.1 Procedure recommended in the standard KTA-2206 to compute the Lightning Induced Voltages

The KTA-2206 [11], is a safety standard that specifies the requirements a NPP should fulfill to be protected against lightning. Among its recommendations, there is a general procedure to estimate the level of threat given by a lightning, to the equipment connected to the IM cables leaving an impacted building.

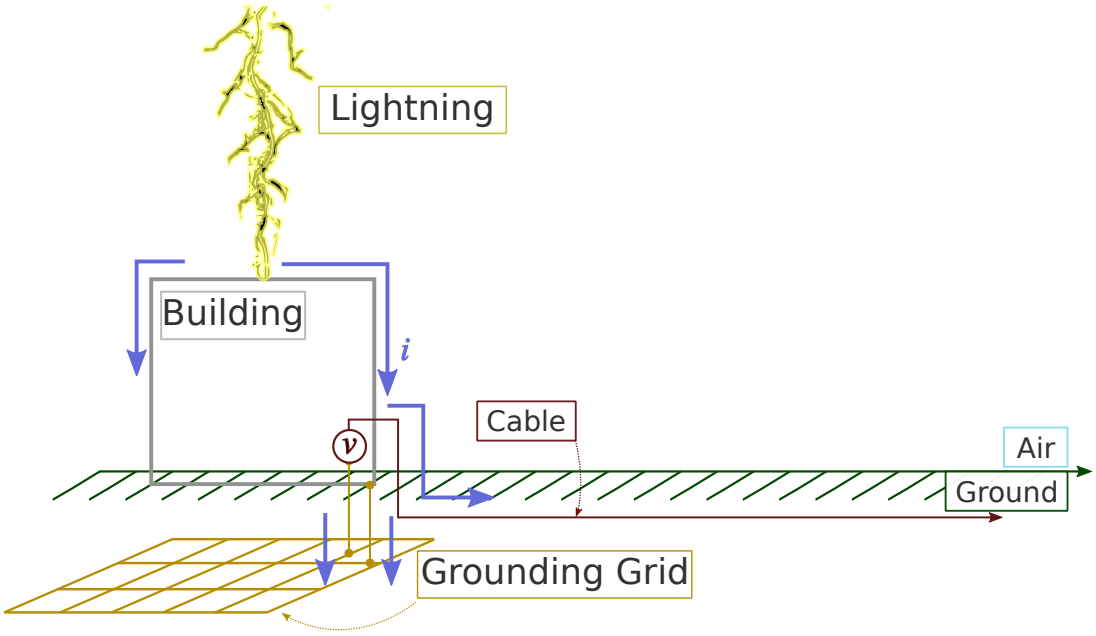

Figure 1.8: General scope of the problem treated in the standard KTA 2206

The general scope of the problem as treated in the KTA standard is depicted in figure 1.8: a lightning impacts a building, its current propagates to the ground and to the conductors leaving the building, and a transient voltage appears at the termination of these conductors. This voltage is referred to as the ”axial voltage´´, but is also commonly known as the *common mode* voltage [12, 13].

The standard allows the computation of the peak value of the transient voltage for IM cables located in two types of routes: Inside a concrete cable duct, or directly in contact with the ground. In this work, the focus is made on cables placed inside

a concrete duct, which might be divided into several segments, joined by metallic bridges at the expansion joints, as depicted in figure 1.9.

The calculation for the transient of cables inside a concrete cable duct depends on three main components: The portion of the lightning current that flows through the duct, the duct length, and an equivalent coupling impedance from the duct to the cable under study. in a manner that, the whole system: lightning-building-grounding-cable is reduced to a simple lumped impedance relationship.

In the following section, the overall procedure to obtain the LIV according to the KTA standard is described. Afterwards, the implications and assumptions behind the methodology are discussed.

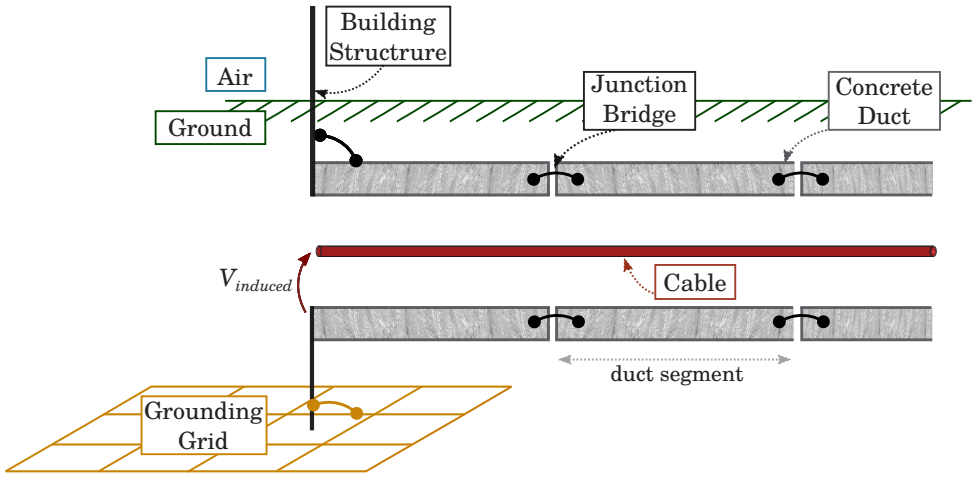

Figure 1.9: Geometry to calculate the induced voltage in a cable duct.

Computation of peak lightning induced voltages in a cable inside a concrete cable duct according to the KTA-2206

To compute the peak voltage a lightning induces in a cable inside a concrete duct, first; a type of current at the base of the lightning channel must be selected. And, in agreement to the statement in section 1.2.1, representative impulses that account for the worst case scenarios of the feasible lightning discharges are suggested.

Table 1.2 shows the variables that describe the transient characteristics of the three impulses suggested by the KTA standard: the peak magnitudes, rise-times (t_{front}), and decay-times (t_{tail})

These impulses are depicted in figure 1.10, they are characterized with the Heidler function [10] depicted in (1.1). The value of the parameters to describe either type of current are detailed in table 1.3.

$$i_B = \frac{I_B}{\eta} \frac{(t/\tau_1)^{10}}{1 + (t/\tau_1)^{10}} \exp(t/\tau_2) \tag{1.1}$$

Type of current at the base	Nomenclature	Magnitude	t_{front}	t_{tail}
Positive first stroke	+FS	200 kA	10 μs	350 μs
Negative first stroke	-FS	100 kA	1 μs	200 μs
Negative subsequent stroke	-SS	50 kA	0.25 μs	100 μs

Table 1.2: Transient characteristics of the return stroke current as suggested by the KTA-2206.

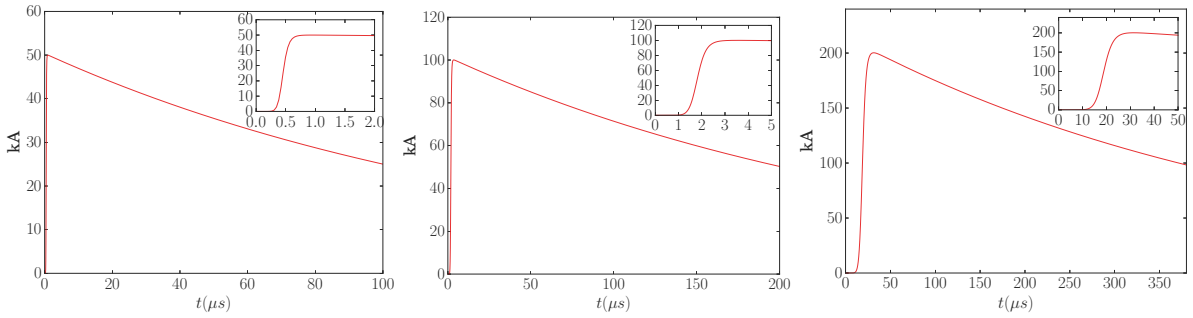

(a) Negative Subsequent Stroke **(b) Negative First Stroke** **(c) Positive First Stroke**

Figure 1.10: Channel base currents as considered in the KTA-2206

Where: $i_B \rightarrow$ Transient current at the base of the lightning channel - [A]
$I_B \rightarrow$ Peak value of the lightning current
$\eta \rightarrow$ Correction factor of the peak.
$\tau_1 \rightarrow$ Rise time constant - [μs]
$\tau_2 \rightarrow$ Decay time constant - [μs]

Parameter	Type of lightning current +FS	-FS	SS
I_B - [kA]	200	100	50
η	0.93	0.986	0.993
τ_1 - [μs]	19	1.82	0.454
τ_2 - [μs]	485	285	143

Table 1.3: Parameters that characterize the current at the base of the lightning channel I_B. according to expression (1.1)

Then, the next three steps must be followed, with no regards to the order:

1. Calculation of the fraction of the lightning current that propagates to the cable duct of interest, according to the amount of conductors leaving the building, and their nature: Grounding conductors, pipelines, cable ducts, etc.

   The portion of current flowing through the cable duct of interest is obtained by the weighting expression (1.2), with relatives weights depicted in table 1.4.

$$I_k = \frac{2}{3} I_B \frac{p_{kk}}{\sum_{v=1}^{n} p_{kv}} \tag{1.2}$$

Where:

$I_k \rightarrow$ Peak value of the fraction of the lightning current through the cable duct
$I_B \rightarrow$ Peak value of the lightning current according to table 1.3
$p_{kk} \rightarrow$ Relative weight of the cable duct
$\sum_{v=1}^{n} p_{kv} \rightarrow$ Sum of relative weights
$n \rightarrow$ Number of conductors in contact with the soil.
$v \rightarrow$ index of considered conductor

Type of cable duct or soil contacting table	Weighting factor p_k
Cable duct (approx. 2×2 m)	3
Threefold or fourfold cable duct (each approx. 2×2 m)	6
Soil contacting cable Ø< 0.1 m (e.g., ground cable)	1
Soil contacting cable 0.1 m ≤ Ø≤ 1 m (e.g., pipe line)	2
Soil contacting cable Ø> 1 m (e.g., pipe line)	3

Table 1.4: Weighting factors p_k to use in (1.2)

2. Calculation of the fictive distance of the cable duct l_f using expression (1.3). This variable is defined as the distance along the cable duct in which the peak of the lightning current does not decreases, after traveling l_f, the peak of the current starts to diminish.

$$l_f = K\sqrt{\rho_e} \tag{1.3}$$

Where: $l_f \rightarrow$ Fictive distance of the cable duct (m)
$K \rightarrow$ Lightning type factor given in table 1.5 $((\Omega\text{m})^{1/2})$
$\rho_e \rightarrow$ Resistivity of the soil (Ωm)

Type of lightning	Lightning type factor K
Positive First Stroke (+FS)	3
Negative First Stroke (-FS)	1
Negative Subsequent Stroke (SS)	0.5

Table 1.5: Lightning type factor K to use in (1.3)

Since l_f is an artifice, it is subjected to the real design conditions of the cable duct of interest: its actual length l_k, and the amount of bridges in each expansion joint:

- The distance to be used is the smaller value between the fictive distance l_f and the actual cable duct length l_k.
- The influence of the expansion joints is considered only in case the value of the fictive distance l_f covers one or several joints. To do so, an additional distance is appended following the expression (1.4). These additions depends on the type of lightning currents considered at the beginning, and on the amount of bridges used in each joint. As depicted in table 1.6.

$$l = l_f + \sum_{v=1}^{N} l_{DFv} \tag{1.4}$$

Where: $l \rightarrow$ Equivalent cable duct length (m)
$l_{DFv} \rightarrow$ Fictive extension for the expansion joint v (m), according to table 1.6
$N \rightarrow$ Amount of cable ducts within l_f

	Amount of bridges per joint			
Type of lightning	**16**	**8**	**4**	**2**
Positive First Stroke (+FS)	15	30	50	70
Negative First Stroke (-FS)	10	20	35	55
Negative Subsequent Stroke (SS)	5	10	20	30

Table 1.6: Fictive extension of the expansion joints l_{DFv} (m)

3. Selection of the value of the coupling impedance per unit of length between the duct and the cable shield. This value depends only on the type of lightning current selected at the beginning, as indicated in table 1.7.

Type of lightning	$\boldsymbol{Z'_M}$ (V/kAm)
Positive First Stroke (+FS)	0.5
Negative First Stroke (-FS)	0.3
Negative Subsequent Stroke (SS)	0.08

Table 1.7: Coupling impedance to use in (1.5)**.**

Finally, the peak induced voltage U_L can be computed following the expression (1.5).

$$U_L = Z'_M \cdot I_k \cdot l \tag{1.5}$$

Where: $U_L \rightarrow$ Peak induced voltage (V)
$Z\prime_M \rightarrow$ Coupling impedance (V/kAm), according to table 1.7

The diagram 1.11 summarizes the procedure to compute the peak induced voltage in a cable inside a concrete duct, according to the standard KTA-2206.

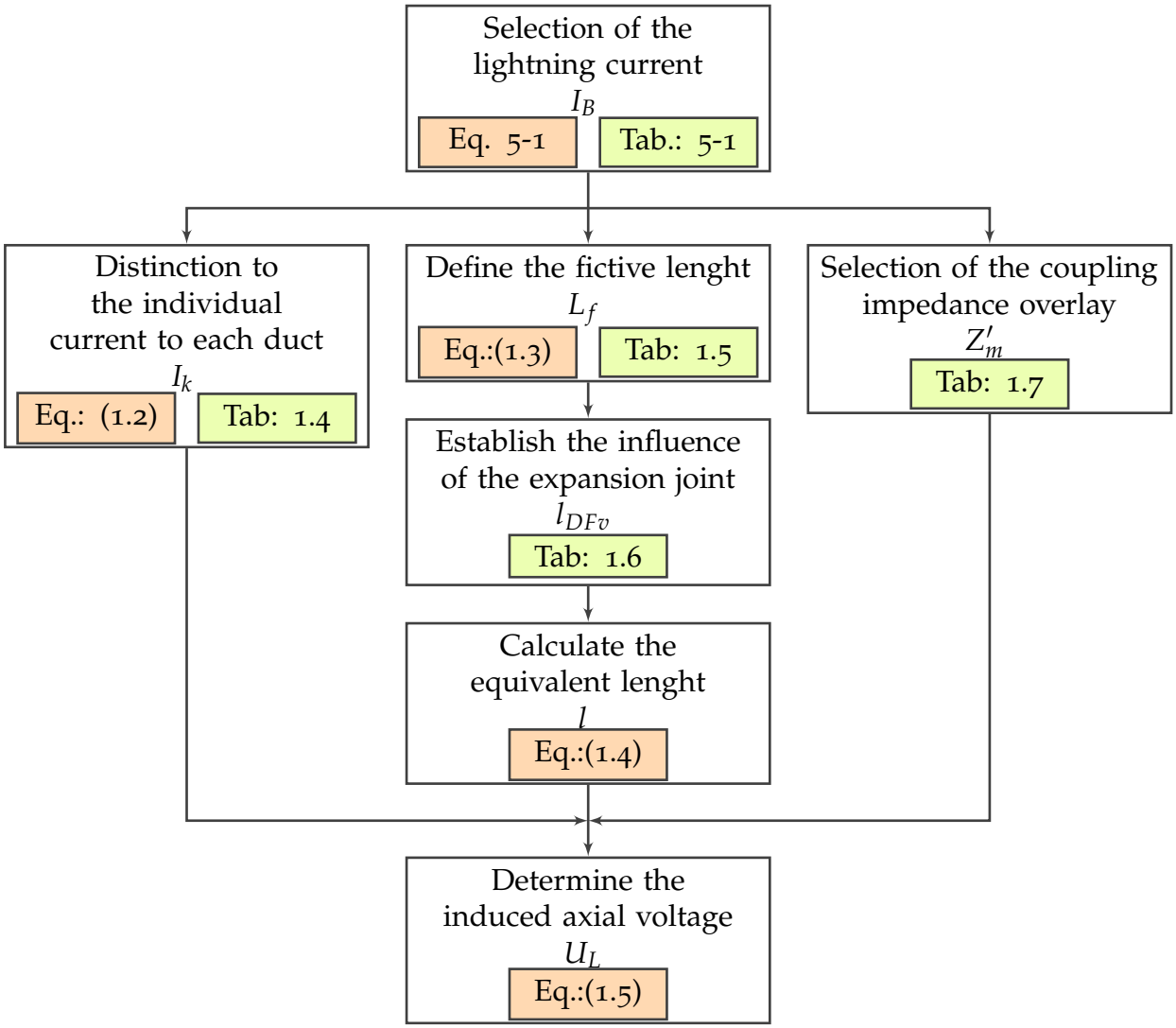

Figure 1.11: Work-flow to compute the peak voltage at the terminations of a cable inside a cable duct according to the standard KTA-2206

Assumptions and hypotheses considered in the standard KTA-2206

The philosophy behind the calculation proposed in the standard is simple: a lightning strikes a building, a fraction of its current flows through the cable duct of interest, and as results a voltage is induced in a cable inside the concrete duct. Nevertheless, this procedure includes several aspects to be presented and discussed.

Main cause of the induced voltages The main assumption behind the methodology states that the coupling between the concrete duct and the inner cable is of inductive nature, which implies that is dependent on the time derivative of the current impulse flowing through the cable duct (di_{duct}/dt).

Moreover, since the rise time of the current decays along its position through the duct, most of the induction is caused by the section of the duct connected to the building. [14].

The reasons to ignore the conduction effect in the voltages at the inner conductor of the cable, lays in the considerations of the connection of the cable to the reference potential at its termination [14]:

- When the cable shield is connected (figure 1.12a): the induction is measured only in the inner conductor.
- When the cable shield is not connected (figure 1.12b): the induction measured in the shield and in the inner conductors is approximately the same.

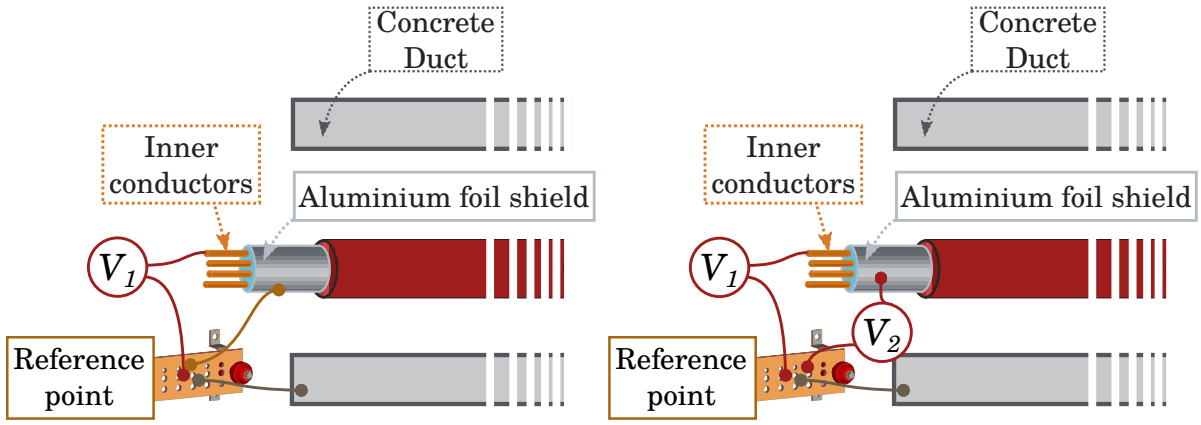

V_1: Voltage induced in one inner conductor

(a) Shield connected to the reference

V_1: Voltage induced in one inner conductor
V_2: Voltage induced in the shield

(b) Shield not connected to the reference

Figure 1.12: Connections of terminations of cable used in [14].

On the definition of the fictive distance l_f The above points are the foundations to the concept of the fictive length l_f. Instead of determining the total induction observing the contribution at each distance from the building, until the value of the contribution is negligible, it is assumed that the induced voltage is proportional to a constant current along a fictive distance. Beyond this distance, the induction is not important to determine the peak voltage.

According to the authors, the calculation of the fictive distance corresponds exactly with the penetration depth of a wave in the soil [14, 15], given in expression (1.6). This is, in the KTA-2206, the distance along the cable duct in which the current keeps its value constant, is treated in a similar manner to the distance to which a low frequency wave penetrates in the soil.

$$\delta = \sqrt{\frac{1}{\pi \mu_0 f}} \sqrt{\rho_e} \tag{1.6}$$

Type of lightning	Equivalent frequency - [kHz]
Positive First Stroke (+FS)	25
Negative First Stroke (-FS)	250
Negative Subsequent Stroke (SS)	1000

Table 1.8: Equivalent frequency of the impulses considered in the KTA-2206 [14]

To illustrate the previous point, observe the expression of the penetration depth given in (1.6), it behaves exactly as expression (1.3). When the values of the frequency f correspond with the equivalent frequency of the lightning impulse. [1] of each of the lightning impulses, given in table 1.8 [13, 14], we obtain the values of K suggested in table 1.5.

The proposed values of the coupling impedance Z'_M The values of Z'_M in table 1.7, were obtained with measurements performed in a section of a real $2\,\mathrm{m} \times 2\,\mathrm{m}$ concrete cable duct. In here, the ratio between the peak voltage and the peak current is taken as the coupling impedance, disregarding the time delay between both measured transients.

This implies, that the peak voltage computed occurs at the same instant that the peak current. This approximation to the behavior of the transients is in disagreement with the previous assumptions regarding the nature of the phenomenon, merely inductive: A transient voltage proportional to the time derivative of the inducing current does not reach its peak at the same time.

[1] The equivalent frequency as defined here, is the frequency of a sinusoidal wave of a quarter of a period equal to the rise time of the lightning impulse $T/4 = t_{front}$

On the influence of the expansion joints Regarding the expansion joints, it has been observed that while less bridges are used, the higher the induced voltages were [16]. Therefore, taking advantage of the definition of the impedance per unit of length Z'_M; the effect of the expansion joints is translated into a contribution to the concept of the fictive distance l_f, which indirectly is, a recognition of an impedance variation.

The premise of the fictive distance is that the induction occurs only during a fraction of the length of the duct, which; applied to the effect of the expansion joints means that only the expansion joints within the range of l_f are considered to affect the induced voltage. This, although logical; rest as a simplification of the problem, since implicates that the presence of the expansion joints does not modifies the ratio of decay of the current rise time, as a first instance.

Implications and limits of the procedure stated in the KTA-2206

All the previous assumptions have implications regarding the application, validity and precision of the standard. Identifying these, is a crucial part on determining whether or not the standard would be suitable for the requirements and particularities of the French NPPs.

First, it was stated that the induced voltage obtained with the procedure of the KTA-2206, corresponds with the potential rise of a cable with respect to the cable duct, as suggested in figure 1.9. This means, that for a single *coaxial* cable inside the duct, this voltage corresponds with the elevation of the potential of its core. Which implies a rise of potential of all the electronic equipment connected to that core.

Moreover, the main assumption of the problem is that the potential rise is caused only by induction from the current flowing through the cable duct, this neglects directly the contribution from the potential rise from the grounding system to which the screen might also connected. This implies that, the contribution to the shield voltage, that comes from the galvanic connection of the shield to the grounding system is not considered. Simultaneously, is worth noting that this shield-grounding connection , is usually close to the wielding points of the cable duct to the building structure.

In the KTA standard, no particularities concerning the type of cables are denoted, mainly: its configuration, geometry, materials, and number of inner conductors. Instead, the recommended values for the induction are obtained from the highest value among a variety of cable types and configurations [16]. This is a measure to simplify the procedure of computation without losing assurance, but ceding detail on the cable of interest.

In the other hand, when treating the current flowing through the cable duct, it is assumed that its waveform is invariant from the original lightning current at the base of the channel, this is; of course, an approximation, only valid for small buildings. When treating larger structures, the total inductance of the building and the nature

of its grounding systems might cause a delay in the current entering the cable duct. This, according to [14] is in agreement with the particularities of the German NPP.

Although the methodology is conceived to estimate the peak induced voltage, along all its procedure exist premises that consider the waveform of the input current: the factor K, the coupling impedance Z'_M, the influence of the expansion joints l_{DFv}. All this components consider that the current flowing through the duct has the original waveform of the channel at the base of the lightning channel.

On the same subject, although the structure of the building has relative low losses, and therefore the current along the cable duct comes mainly from the connection to the building, it is worth noting that some induction from the magnetic field coming from the current flowing through the building is been neglected.

Finally, even if the conductive component is considered to estimate the current flowing through the ducts, the procedure to estimate the fraction of the current that will reach the duct, is based in the assumption that the cable duct is an equivalent Transmission Line (TL) [13], with no resistive part, and no relative coupling to the rest of the conductors leaving the building, like the cable pipes and the bare grounding conductors. Both simplifications are sustained on:

- The type of impulse current depicted in figure 1.10, involves frequencies high enough to consider that the inductive response of the cable ducts and buried conductors is always higher than the resistive response.
- The standard is only interested in the peak induced voltage, mainly caused by the rise time of the injected current, this part of the transient is more depending on the inductive response of the cable duct than on its resistive response. This component will affect mostly the decay part of the current.

Summarizing, the main implications and limits of the procedure established in the standard KTA-2206 are:

- The KTA-2206 gives an estimation of the potential difference between the shield of a coaxial cable and its concrete cable duct.
- The voltage is not subject of contribution of a conductive component, given mostly by the connection of the shield to the grounding system.
- The delay of the current at the base of the lightning channel is not considered.
- Only the conductive component of the current flowing through the cable duct is considered, the inductive component coming from the building radiated magnetic field is neglected.
- The model to estimate the current division among all the buried conductors is based on the approximation of inductive and uncoupled TLs.

The above considerations imply that although coherent, and with a range of validity, is needed to test the weight of the standard hypotheses on the final LIV calculations.

Additionally, it was estated the missing considerations of more complex phenomena. Therefore, in order to estimate with more precision the LIV of electronic equipment connected to a IM cable, a more comprehensive tool to assess the response is needed.

In this section, the philosophy behind the methodology proposed in the KTA standard has been revised, along with some of its main assumptions and technical limitations. In the next section, another consideration that stimulates the development of a more comprehensive tool of computation is going to be addressed.

1.4.2 Introduction of a new regulation for the lightning protection of Power Generation Centers in France

Given the nature of the Power Generation in France, in which 77 % is produced in NPP [3], it is a matter of national interest to guarantee the continued and secure operation of the facilities. Considering this, a current legislation; the mandate INB of February 2012 [17], makes an effort to outline the guidelines that these facilities must follow, mainly three aspects are indicated:

- The lightning is advised to be always considered as an external aggression to the site. Therefore all the protection means available to the present must be considered to avoid damages caused by an impact.
- When evaluating the performance against an external aggression to the site, such as the lightning; the state-of-the-art methods and tools are encouraged to be used, in order to give the best protection with the available technology.
- The methods and tools must be validated, and its limits and margins of error well estimated, in order to know its accuracy and pertinence.

Up until now, to evaluate the performance of IM cables against a lightning strike, the guidelines of the standard KTA 2206 (2009-11) [11] have been used. As estated in the previous section, this is a standard developed for German NPPs, therefore not conceived for the particularities of the French NPPs. As a consequence, is needed to test the validity of its hypothesis and assumptions.

A robust conception of the French NPP has led them to operate safely and continuously. Nevertheless, with regards to the new requirements by law, the methodology to evaluate the lightning performance of IM cables needs to be revised, the uncertainties to be assessed, and with a better understanding of the phenomena, contribute to an optimal canalization of the investments in protection means.

Therefore, the NPPs administrators are concerned in developing a new tool that allows for the study of the lightning performance of IM cables, in a manner more adapted to the reality of the present and future NPPs. This tool should:

- Include state-of-the-art methods.
- Have known hypothesis, assumptions, and margin of errors.
- Lead to more efficient investments in the conception of the protection systems.

In the previous section we have commented all the approximations and limits of the actual methodology used to compute the induced voltages in cables, and; as estated in this section, a more comprehensive approach must be considered. In the following, some strategies to assess this problem are going to be discussed, as well as the final proposition of this work.

1.4.3 Numerical strategies to assess the lightning induced voltages in cables

It has been discussed that the voltage developed at the terminations of IM cable depends on the interaction of several phenomena: the current conduction and induction coming from the building, the induction from the concrete cable duct, the potential rise of the grounding system, among others. The interaction of all these effects is hardly reachable by analytics methods, therefore needs the implementation of numerical methods.

Among the numerical methods available to the present to solve for this problem, three main types can be distinguished:

- Methods based on the equivalent TL theory, or the solution of the so-called telegraphist equations [18]
- Methods based on the solution of the Maxwell equations, also called full wave approach. [19]
- Hybrid methods, that try to combine the precision of the solution of the Maxwell equations, with the practicality of the TL approximation.

In the following sections, these methods are going to be briefly discussed, along with its implications and limits.

Transmission Line Theory Methods

The TL theory methods allow for the computation of the induced voltages and currents in *electrically large* components, i.e., components in the system that have sizes large enough to as to be compared with the wavelength of its excitation [12]. This components might be grounding conductors, aerial lines, buried cables, pipe lines, among other.

A component modeled as a TL is described as a distribution of circuit parameters, usually in a *π-distribution*, as suggested by figure 1.13. The value of these RLCG parameters depends on the materials of the component of study, its geometry, and its excitation [12].

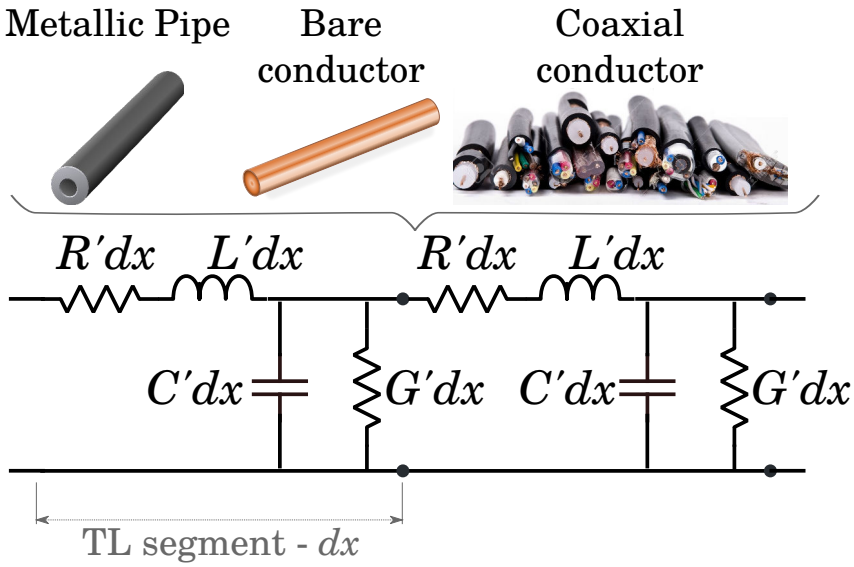

Figure 1.13: Circuit distribution of electrical parameters in the TL model.

In order to model a component with the TL theory, it must fulfill two characteristics:

- Its cross sectional area must be electrically small, this is, smaller than one tenth of the minimum significant wavelength of its excitation.
- The separation distance from the reference conductor must be smaller than its total length.

With the previous conditions, the main simplifications of the model are:

- The propagation mode of currents and charges occurs only in the axial direction, therefore, producing fields that are transversal to the conductor, as indicated in figure 1.14. This is also known as Transverse ElectroMagnetic (TEM).
- The "common-mode" currents are neglected [12], and only the "differential-mode" currents are considered. As suggested by figure 1.15

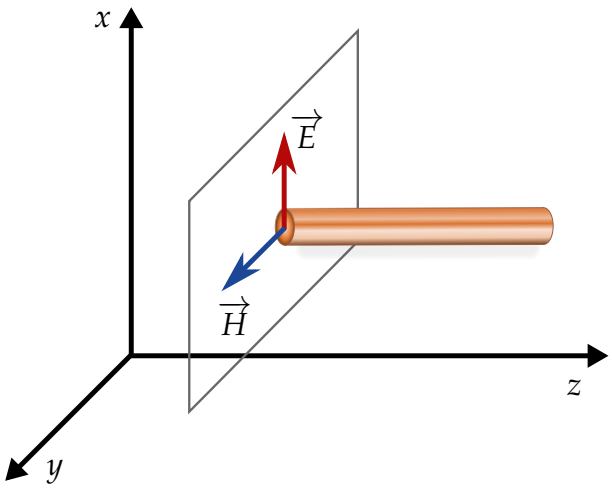

Figure 1.14: Structure of ElectroMagnetic (EM) fields in the TEM mode.

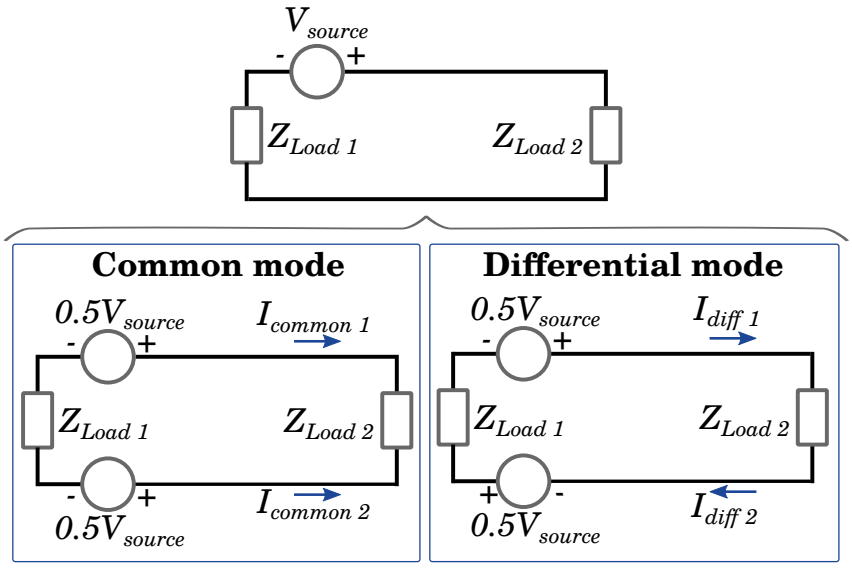

Figure 1.15: Excitation in common mode and differential mode. Adapted from [12]

These simplifications have their limitations:

- The TEM response of the line is only valid up to a specific frequency, above this frequency, higher order Transverse Electric (TE) and Transverse Magnetic (TM) propagation modes appear [18].
- Even for lines with electrically small cross sectional areas, the "differential-mode" has an influence in determining the currents along the line. Nevertheless, at the extremities of the line, the influence is severely reduced [12, 20], which makes the TL models suitable to study the response of the loads at the terminations.

It has also been stated that for lines of finite length, even if the line has a small section, in the presence of lossy ground, the TL model fails to predict all the resonance frequencies of the component, particularly for excitations of high frequencies [21].

The TL model has been extensible used to solve for lightning transients in a wide variety of applications, because of its simplicity and the fast computational times of its solution. Nevertheless, it is not a suitable model to our problem, since the presence of the building and the grounding system around the connection of the cable duct have an influence on the current induced along the cable duct, and to the shield potential rise. As suggested in figure 1.16.

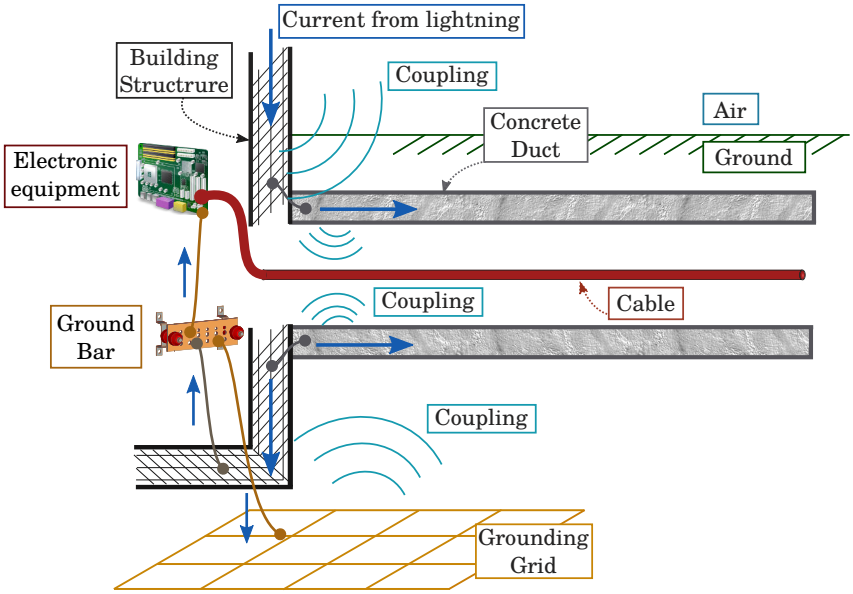

Figure 1.16: Detail of the phenomena interacting at the cable duct connection to the building.

In order to consider these effects, an approach able to evaluate the whole EM environment in the vicinity of the connection of the cable duct to the building is needed. This is going to be covered in the following section.

Full Wave Methods

The full wave EM numerical methods allows one to solve for the complete electromagnetic environment of a given structure in a three dimensional space. There is a variety of these methods, in here, the most used in lightning transient studies are going to be mentioned:

- **The Finite Difference (FD) methods** are based on the discretization of the Maxwell Equations in its differential form. In here, the EM fields and potentials are the unknowns in an meshed and structured volume. It can be solved in the time domain (FDTD), or in the frequency Domain (FDFD). One of the main problems with this approach, is the nature of the object to be solved, since the meshing has a Cartesian structure, forcing the use of staircase approximations of the boundaries that are not aligned with the space discretization. Although recently, progress has been made to approximate these complex boundaries with non-uniform meshes, taking advantages on parallel computing.

- **The Integral Equation (IE) Methods** are based on the solution of the Maxwell equations in its integral form, being the Method of Moments (MoM) one of its most extended applications. In here, the unknowns are the currents and charges in the surface of the conductive and dielectric elements. It is often used when the structure of interest is composed mainly of wire elements such as transmission lines, building meshes, or grounding conductors.

- **The Variational Methods** such as the Finite Element Method (FEM) or the Garlekin Method (GM) try to approximate the solution of a set of the Maxwell equations in its Partial Differential form in an arrangement of small sub-domains, in a manner that, a global set of partial differential equations with known answers can describe the whole problem starting from its initial conditions. Although they allow one to easily represent complex configurations of boundaries, they also require a high amount of computational resources and time to find a solution.

These methods are well suited for complex problems, from the electronics domain, to the aeronautics, and the power industry. Since they allow the considerations of the complete EM environment of the structure, with all its physical properties, and the interaction of all its field components. Depending on the type of structure to study, one method presents different advantages against the others.

Independently of this, they all have in common that for problems electrically large, they demand an elevated amount of computational resources. Which, sometimes makes them impractical to use, specially in the industry environment.

To circumvent this flaw, several efforts have been made to reduce the amount of memory and time needed to solve a big structure. One of this strategies is to

hybridize the full wave methods with the TL methods. There is a wide variety of hybrid methods, and to account for all of them is outside the scope of this work. Instead, the direct proposal to solve for our problem is going to be presented in the next section.

1.5 Proposal of a computational tool to assess lightning transients in Power Generation Centers.

As previously estated, the interest is to study the transient voltages at the terminations of IM cables leaving a building stroke by lightning in a NPP. The most interesting case presents when the cables are located inside a concrete duct, since at its termination, the duct structure is welded to the building walls, and relative close to the grounding grid. These connections and proximities between conductors, favors couplings that require the use of a full wave method in order to be considered.

Nevertheless, as seen in the previous section, a full wave method demands a high amount of computational resources: time and memory for each specific configuration to solve. Therefore, additional models to extend the application of the the original full wave approach are needed. In this work, the Finite Differences Time Domain (FDTD) method is going to be used, since it offers a direct solution in the time domain, up until the time of interest, which can severely reduce the computational time.

In addition, in order to improve the capabilities of the FDTD original approach, a model to include conductive elements of small transversal areas is going to be considered: a modification of the thin wire formalism of Holland [22–25]. This will allow one to model all the meshed structures of the NPP: The building structure and foundation, the grounding grid, the steel cable duct, and the IM cable, without the use of a relative small discretization of the space of computation.

To increase the potentiality of the FDTD with the thin wire formalism of Holland, a Message Passing Interface (MPI) [26] protocol is used to solve the system within multiple cores of computation.

With this set of tools, a single lightning strike to an NPP of a couple of hundreds of meters can be studied. To our knowledge, this is the first time the problem is assessed in the industry with this level of complexity, and with an adequate investment of computational resources. This becomes more relevant, considering the relevance of NPP in France.

Nevertheless, as we have seen, the problem is a combination of several parameters, and the pertinence, and influence of each one of them have not been elucidated. Therefore, it becomes necessary to understand their interaction, and to translate it in a versatile study tool.

It is a complex problem, a lot of parameters intervene, and a simple analysis tool is needed: it is not practical to perform an FDTD simulation to study each particular

energy production center. Therefore, the proposal is to obtain the lightning induced voltage in the terminations of a cable, with a surrogate model, or meta-model. This will allow one to vary the most influential parameters, and perform additional studies without investing time and computational resources.

The meta-model is based on carefully selected combinations of input parameters, to do that the technique of Design of Experiments (DoE) [27] is used. As a consequence the number of simulations to perform are reduced, and the parameter influence is accounted in an efficient way.

At the end, a simple tool to estimate with a known degree of precision the load voltages in a IM cable is proposed. The tool is supported on simulations based at the same time on validated EM models of the components of an NPP.

In light of this proposal, the objectives of this work are:

1.5.1 General Objective

The aim of this work is to develop a computational tool to compute the lightning transient voltages in instrumentation and measurement cables in a Power Generation Center.

1.5.2 Specific Objectives

To reach the main objective, several specific objectives are proposed:

- To validate the developed tool against another computational method, and results previously published.
- To identify the most influential parameters that affects the behavior of the transient voltages.
- To evaluate statistically the pertinence of these influential parameters.
- To establish the error margins and limitations of the developed tool.
- To compare the results of the developed tool against the results given by the approach of the standard KTA.

References

[1] Martin A. Uman. *The Lightning Discharge*. Vol. 39. International Geophysics. Elsevier, 1987. ISBN: 9780127083506.

[2] Vernon Cooray. *The Lightning Flash*. Ed. by Vernon Cooray. The Institution of Engineering and Technology, Michael Faraday House, Six Hills Way, Stevenage SG1 2AY, UK: IET, Jan. 2003. ISBN: 9780852967805. DOI: 10.1049/PBP0034E. URL: http://digital-library.theiet.org/content/books/po/pbpo034e.

[3] RTE. *Bilan électrique 2014*. Tech. rep. 2014, p. 56.

[4] K. Berger, R.B. Anderson, and H. Kroeninger. "Parameters of lightning flashes". In: *Electra* 41 (1975), pp. 23–37.

[5] WG C4.407. *Lightning Parameters for Engineering Applications*. Tech. rep. CIGRE, 2013.

[6] International Electrotechnical Commission (IEC). *IEC 62305-1. Protection against lightning. Part 1: General principles*. 2010.

[7] IEEE Power Society, Energy, and Substation Committee. *IEEE Guide for Direct Lightning Stroke Shielding of Substations*. Vol. 2012. April. 2013, pp. 1–227. ISBN: 9780738180373. DOI: 10.1109/IEEESTD.1996.81546.

[8] V. A. Rakov et al. "CIGRE technical brochure on lightning parameters for engineering applications". In: *2013 Int. Symp. Light. Prot. SIPDA 2013* (2013), pp. 373–377. DOI: 10.1109/SIPDA.2013.6729246.

[9] Fridolin H. Heidler et al. "Parameters of Lightning Current given in IEC 62305. Background, Experience and Outlook". In: *29th Int. Conf. Light. Prot.* June (2008), pp. 1–22.

[10] F. Heidler. "Analytische Blitzstromfunktion zur LEMP Berechnung". In: *18th Int. Conf. Light. Prot. (ICLP 1985), Munich* (1985), pp. 63–66.

[11] Nuclear Safety Standards Commission (KTA). *Design of Nuclear Power Plants Against Damaging Effects from Lightning*. 2009.

[12] Frederick M. Tesche and Torbjörn Karlsson. *EMC Analysis Methods and Computational Models*. 1997, p. 623. ISBN: 047115573X.

[13] Fridolin Heidler et al. "Induced Overvoltages in Cable Ducts Taking into Account the Current Flow into Earth". In: *Light. Prot. (ICLP), 1998 Int. Conf.* 1. Birmingham, UK, 1998, pp. 270–275.

[14] W. J. Zischank et al. "Assesment of the lightning transient coupling to control cables interconnecting structures in large industrial facilities and power plants". In: *25th Int. Conf. Light. Prot.* September. Rhodes, Grec, 2000, pp. 691–696.

[15] Edward F. Vance. *Coupling to Shielded Cables*. 1st. Wiley, 1978, p. 183. ISBN: 0471041076.

[16] W. J. Zischank et al. "Shielding effectiveness of reinforced concrete Cable Ducts Carrying Partial Lightning Currents". In: *Int. Conf. Light. Prot.* Birmingham, 1998, pp. 735–740.

[17] JORF. *Régles générales relatives aux installations nucleaires de base*. 2012.

[18] Paul Clayton. *Analysis of Multiconductor Transmission Lines*. Ed. by Wiley Interscience. 2nd. New Jersey: Wiley-Interscience, 2008, p. 780. ISBN: 978-0-470-13154-1.

[19] O. C. Zienkiewicz. *The Finite Element Method*. Ed. by McGraw-Hill Companies. 3rd. 1986. ISBN: 13: 9780070840720.

[20] Farhad Rachidi. "A review of fieldtotransmission line coupling models with particular reference to lightninginduced voltages". In: *10th Int. Symp. Light. Prot. ...* 1 (2009), pp. 67–88.

[21] Dragan Poljak and Vicko Doric. "Electromagnetic field coupling to overhead wires: comparison of wire antenna and transmission line model in the frequency and time domain". In: *Int. Conf. Appl. Electromagn. Commun.* 1. Dubrovnik, 2007, pp. 1–4. DOI: 10.1109/ICECOM.2007.4544432.

[22] Richard Holland and Larry Simpson. "Finite-Difference Analysis of EMP Coupling to Thin Struts and Wires". In: *IEEE Trans. Electromagn. Compat.* EMC-23.2 (1981), pp. 88–97. ISSN: 0018-9375. DOI: 10.1109/TEMC.1981.303899.

[23] Christophe Guiffaut and Alain Reineix. "Cartesian shift thin wire formalism in the FDTD method with multiwire junctions". In: *Antennas Propagation, IEEE ...* 58.8 (2010), pp. 2658–2665.

[24] Christophe Guiffaut, Alain Reineix, and Bernard Pecqueux. "New Oblique Thin Wire Formalism in the FDTD Method With Multiwire Junctions". In: *IEEE Trans. Antennas Propag.* 60.3 (2012), pp. 1458–1466. ISSN: 0018-926X. DOI: 10.1109/TAP.2011.2180304.

[25] Christophe Guiffaut and Alain Reineix. "Des fils obliques pour une modélisation conforme et sans maillage des câbles dans la méthode FDTD. Bilan et extensions". In: *17ème Colloq. Int. Expo. sur la Compat. Electromagnétique - CEM 2014*. Clermont-Ferrand, France, 2014.

[26] M Snir. *MPI–the Complete Reference: The MPI core*. Mass, 1998. ISBN: 9780262692151.

[27] F Pukelsheim. *Optimal Design of Experiments*. Classics in Applied Mathematics. Society for Industrial and Applied Mathematics (SIAM, 3600 Market Street, Floor 6, Philadelphia, PA 19104), 1993. ISBN: 9780898719109.

Chapter 2

FDTD Modeling of a Large Industrial Site

2.1 Introduction

In general, the problem of a lightning strike to a Nuclear Power Plant (NPP) can be described with five main components of an industrial site: buildings, the electronic equipment inside, the soil, the grounding system, the cables and conductors inside and between buildings. To completely evaluate the effects of a lightning strike in facilities with this level of complexity, a numerical simulation that considers the complete ElectroMagnetic (EM) environment, is required.

However, the size and the complexity of the geometry of such a facility requires large computational resources. Thus, it is important to assess the numerical methodologies to achieve an acceptable computational time and memory use.

The FDTD method [1] is often used to perform lightning transient studies, since it gives a direct solution in the time domain, and allows for further implementation of non-linear components. However, the original FDTD algorithm as proposed by Yee [2] does not allow one to efficiently perform lightning studies on large industrial sites, especially when considering the cables leaving building.

The relative large industrial site proposed in this work can be described with several configurations of mesh structures, therefore, as a complex arrangement of wire elements. In FDTD, it is not computationally efficient to deal with objects of relative small transversal area, therefore; the implementation of a kind of sub-cellular models is needed.

A conductive element with a transversal area small with respect to the cell size, is also known as a thin wire. There are several ways to include a thin wire inside the FDTD method [3–5]. The model used in this work is based on the formalism proposed by Holland and Simpson [6], and has been modified to overcome the original limitations, and to extend its domain of application.

This thin wire formalism is versatile enough to model all the components of the

large industrial site mentioned previously. To show this, an implementation for each separate component is going to be validated, in a manner that, a reliable final complete FDTD model of the whole problem can be studied.

The chapter is organized as follows: in section 2.2 the thin wire model based on Holland's formalism is going to be introduced. Afterwards, in sections 2.3 to 2.6, its implementations to model separately the different components of an industrial site are going to be validated, starting by the lightning return stroke channel, continuing by the building, the Instrumentation & Measurement (IM) cable and the grounding system. Finally, in section 2.7 a complete case that integrates all the components is going to be presented.

2.2 The thin wire formalism of Holland

The thin wire formalism of Holland [6] considers a bare conductor along an edge of a classic Finite Differences Time Domain (FDTD) cell [2] with an equivalent transmission line illuminated by the cell electric field, as depicted in figure 2.1. As that, the current and the charge in the conductor introduce a set of two additional equations to be solved at the same time as the six field equations of the traditional FDTD scheme [2]. These auxiliary equations are given in (2.1) and (2.2).

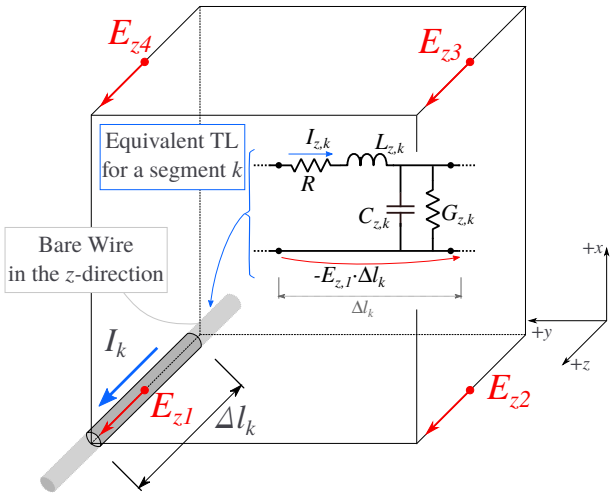

Figure 2.1: Bare wire in a FDTD cell according to Holland's formalism [6]

$$L_l\left(\partial_t I + v^2 \partial_r Q\right) + R_l I = E_r\left(r\right) \tag{2.1}$$

$$\partial_t Q + \frac{\sigma}{\varepsilon} Q + \partial_r I = 0 \tag{2.2}$$

Where the unknowns are I and Q, respectively the current and the charge per unit of length along a conductor segment; σ, ε and v are the conductivity, permittivity and velocity of propagation in the medium surrounding the wire; $E_r\left(r\right)$ is the tangential

electric field at a distance r from the segment, and R_l and L_l are the linear resistance and inductance per unit of length.

As it was originally proposed, the model of Holland has some limitations regarding its uses:

- The path of the wire must be located parallel to the Cartesian axis, moreover, particularly on the cell edge. This prohibits oblique trajectories and forces smaller cell sizes to perform equivalent staircase trajectories.
- It only considered bare wires.

To overcome these limitations three extensions to the formalism have been included in the TEMSI-FD code:

- The consideration of wires with oblique trajectories [7].
- The presence of the insulation [8].
- The model of shielded coaxial conductors [9].

In the following, these extensions are explained.

2.2.1 A thin wire shifted in the FDTD cell

The limitation of trajectory inherent to the formalism of Holland is a consequence of the way of computing the in-cell inductance L_l. In [7] a new method to compute the inductance is proposed, in a manner that the inductance of an oblique wire inside a cell is a mean value within that volume. To do this, the inductance is computed 12 times: each time with respect to a cell volume centered on each of the electric field components surrounding the wire, as indicated in figure 2.2. The numerical computation of the inductance follows the expression (2.3).

$$\left\langle L_{u,j,m} \right\rangle = \frac{\mu_0}{2\pi} \frac{\iiint_{r>a, V_{u,j,m}} \ln\left(\frac{r(x,y,z)}{a}\right) dxdydz}{\Delta x \Delta y \Delta z} \tag{2.3}$$

Where $\left\langle L_{u,j,m} \right\rangle$ is the in-cell inductance, u corresponds with one of the three directions x, y or z, subscript j indicates one of the four field components in the direction u, m denotes the number of the cell crossed by the conductor, $r(x,y,z)$ is the radial length between any point $M(x,y,z)$ inside the integration volume $V_{u,j,m}$, and Δu is the cell size in the direction u.

As well as with the inductance, the electric field in equation (2.1) is a mean weighted magnitude along the direction of the cable. This weighting is performed with respect to the relative proximity of the wire to each of the twelve E-field components surrounding it. According to figure 2.3, the weight coefficients in any

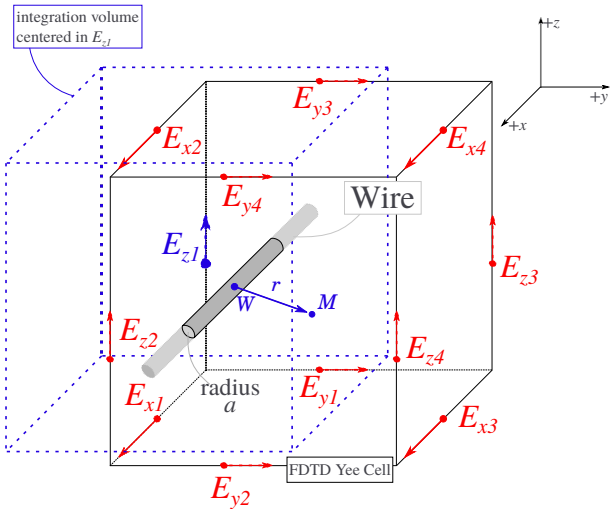

Figure 2.2: Integration volume centered on the component $E_{z,1,m}$, to compute the inductance $L_{z,1,m}$. Taken from [7]

r-direction can be obtained using expressions (2.4a) to (2.4d). The details of this computation are explained in [7].

$$p_{u,1,k,m} = \left(1 - \frac{\delta v}{\Delta v}\right)\left(1 - \frac{\delta w}{\Delta w}\right) \tag{2.4a}$$

$$p_{u,2,k,m} = \frac{\delta v}{\Delta v}\left(1 - \frac{\delta w}{\Delta w}\right) \tag{2.4b}$$

$$p_{u,3,k,m} = \frac{\delta w}{\Delta w}\left(1 - \frac{\delta v}{\Delta v}\right) \tag{2.4c}$$

$$p_{u,4,k,m} = \frac{\delta v}{\Delta v}\frac{\delta w}{\Delta w} \tag{2.4d}$$

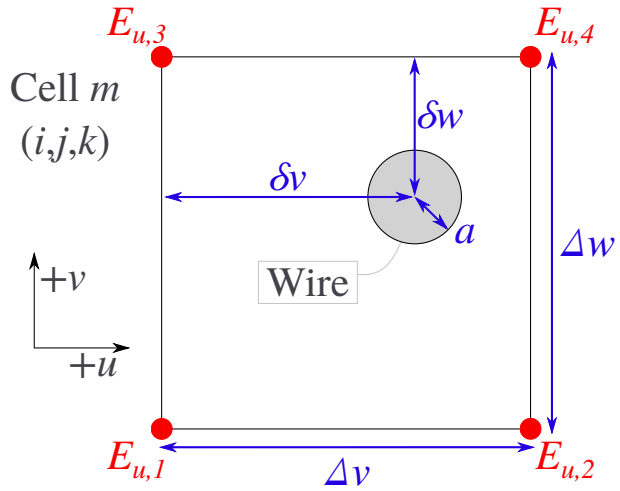

Figure 2.3: Thin wire of radius a crossing a Yee cell, $(u,\ v,\ w)$ take any Cartesian direction $x,\ y$ or z in circular permutation. Taken from [7]

Using these weight coefficients, the coupling of a wire segment, to all the field components of the cell can be found by solving expression (2.5). The wire is assumed following the oblique direction r, given by the unitary vector $\overrightarrow{r} = r_x\widehat{x} + r_y\widehat{y} + r_z\widehat{z}$.

$$L_k\left(\partial_t I_k + v^2\partial_r Q\right) + RI_k = \langle E_k\rangle \tag{2.5}$$

$$L_k = \sum_{u=x,y,z}\left\{\sum_{m,m\bigcap k}\left[\frac{\delta l_{k,m}}{\Delta l}\sum_{j=1}^{4}\left(\langle L_{u,j,m}\rangle p_{u,j,k,m}\right)\right]\right\} r_u^2 \tag{2.6a}$$

$$\langle E_k\rangle = \sum_{u=x,y,x}\left\{\sum_{m,m\bigcap k}\left[\frac{\delta l_{k,m}}{\Delta l}\sum_{j=1}^{4}\left(\langle E_{u,j,m}\rangle p_{u,j,k,m}\right)\right]\right\} r_u^2 \tag{2.6b}$$

$$\sum_{u=x,y,x} r_u^2 = 1 \tag{2.6c}$$

Where $\langle E_k\rangle$ is the mean electric field of the twelve components around the conductor segment k. $\langle L_k\rangle$ is the segment inductance, $\delta l_{k,m}$ is the segment length inside the cell m, Δl is the conductor length, and the notation $(m, m\bigcap k)$ indicates the cells intersecting with the segment k.

To better handle the junctions nodes in the cable, the concept of in-cell capacitance is introduced, in a manner that the charge in expression (2.2) is replaced by a voltage V_k and a capacitance per unit length Cl_k in each side of the segment node k. This capacitance is a function of the in-cell inductance as indicated in expression (2.7). As a result, the modified formalism of Holland introduces a set of Transmission Line (TL) equations in the FDTD scheme.

$$C_k = \frac{\Delta l}{2}\left(Cl_{k-} + Cl_{k+}\right) = \frac{\Delta l}{2}\left(\frac{1}{v^2 L_{k-}} + \frac{1}{v^2 L_{k+}}\right) \tag{2.7}$$

Using the well-known relations between charge and voltage $Q_k = Cl_k V_k$, equations (2.1) and (2.2) can be rewritten as a set of auxiliary equations of a TL model. Figure 2.4 illustrates this model for a cable segment k of longitude Δl_k, oriented in the z direction, and illuminated by a mean electric field $\langle E_{z,k}\rangle$

$$L_{lk}\partial_t I_k + R_l I_k + \partial_r V_k = \langle E_k\rangle \tag{2.8a}$$

$$C_k\left(\partial_t V_k + \frac{\sigma}{\varepsilon}V_k\right) + I_{k-} - I_{k+} = 0 \tag{2.8b}$$

It is important to note, that the updating of the electric field components is made using the current density of the wire segments crossing the cell m, following the expression of Ampere-Maxwell given in (2.9a).

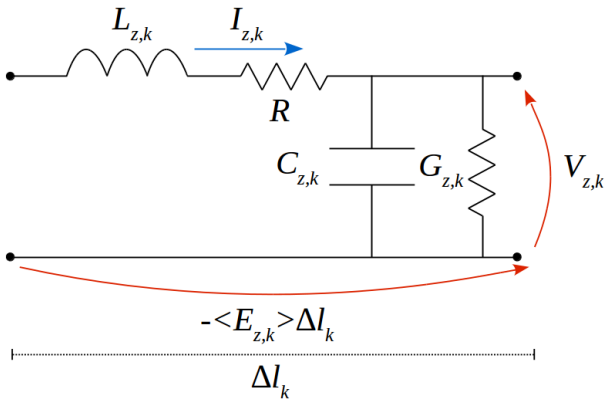

Figure 2.4: TL equivalent circuit for a thin wire

$$E_{u,j,m}^{n+1} = E_{u,j,m}^{n} + \frac{\Delta t}{\varepsilon_0 \varepsilon_r}\left[\left(\nabla \times \overrightarrow{H}\right) \cdot \overrightarrow{u} - J_{u,j,m}\right]^{n+1/2} \tag{2.9a}$$

$$J_{u,j,m} = r_u \sum_{k,k\cap m} p_{u,j,m} \frac{\delta l_{k,m}}{\Delta l} J_k \tag{2.9b}$$

$$J_k = \frac{I_k \Delta l}{\Delta x \Delta y \Delta z} \tag{2.9c}$$

Where:
- $m \rightarrow$ FDTD index of space
- $n \rightarrow$ FDTD index of time
- $u \rightarrow$ Direction of the component of interest: x, y, z
- $j \rightarrow$ Index of the adjacent field component: 1,2,3,4
- $k \rightarrow$ Index of the wire segment inside the cell
- $J_{u,j,m} \rightarrow$ Total current density associated to the field component $E_{u,j,m}$
- $J_k \rightarrow$ Current density of a single wire segment k

It is worth noting a special consideration for obliques thin wires, in order to avoid small parasite oscillations. A last condition must be fulfilled: the current trace continuity must be respected in all the cells containing a wire segment.

According to figure 2.5, the node m of a cell containing a cable segment has six edge current weighting coefficients Pc_u, given by the six cell edges joining at the node. As defined in expression (2.10), this edge weight coefficients depend on the coupling weight coefficients $p_{u,j,k,m}$ of the cell with the wire segments, depicted in equations (2.4).

When two wires are in junction in the vicinity of the node, the current weighting coefficient results from the contributions of both wires. To do that, the currents in the segments must be similarly oriented, as suggested by figure 2.5. If a multi-wire junction is present, the current continuity trace must be verified for each combination of two wires [7].

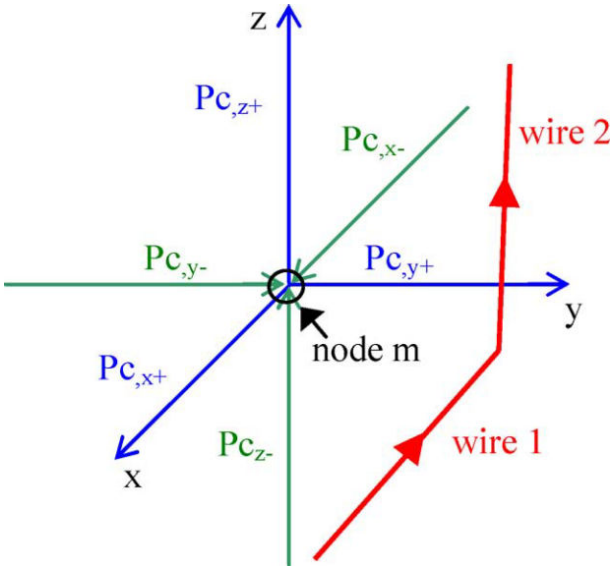

Figure 2.5: Current weighting coefficient Pc_u of the cell node m resulting from the contribution of all wires in the vicinity. Adapted from [7]

$$Pc_{u,j,m} = \frac{r_u}{\Delta_u} \sum_{k,k\cap m} p_{u,j,k,m} \delta l_{k,m} \tag{2.10}$$

$$\sum_{u=x,y,z} Pc_{u+,m} - Pc_{u-,m} = 0 \tag{2.11}$$

Finally, the numerical stability of the formalism is kept by maintaining the conductor radius a inferior to $\Delta/10$, where Δ is the spatial step of an uniform FDTD cell [7].

2.2.2 An insulated thin wire

To consider an insulated conductor, the system in (2.8a) and (2.8b) is modified to include the additional capacitance introduced by the insulation. The total capacitance considered in the previous section is separated into two components: one for the insulation ($C_{g,k}$), and one for the medium surrounding the cable ($C_{e,k}$). Each of them forces the use of new auxiliary voltage; $V_{g,k}$ and $V_{e,k}$ respectively.

The values of $C_{g,k}$ and $C_{e,k}$ are obtained with respect to their own inductances $L_{g,k}$ and $L_{e,k}$ respectively. In a similar way as in section 2.2.1, for the sides of a segment node k, the capacitances can be calculated following expressions (2.12) and (2.13).

$$C_{g,k} = \frac{\mu_0 \varepsilon_g \Delta l_{k-}}{2L_{g,k-}} + \frac{\mu_0 \varepsilon_g \Delta l_{k+}}{2L_{g,k+}} \tag{2.12}$$

$$C_{e,k} = \frac{\mu_0 \varepsilon_e \Delta l_{k-}}{2L_{e,k-}} + \frac{\mu_0 \varepsilon_e \Delta l_{k+}}{2L_{e,k+}} \tag{2.13}$$

Where $L_{g,k}$ and $L_{e,k}$ are the weighted mean values of the 12 in-cell inductances computed using expressions (2.14) and (2.15) respectively.

$$\langle L_{g,u,j,m} \rangle = \frac{\mu_0}{2\pi} \ln\left(\frac{r_g}{a}\right) \frac{\iiint_{r>a, V_{u,j,m}} dxdydz}{\Delta x \Delta y \Delta z} \tag{2.14}$$

$$\langle L_{e,u,j,m} \rangle = \langle L_{u,j,m} \rangle - \langle L_{g,u,j,m} \rangle \tag{2.15}$$

Finally, the new auxiliary expressions rewritten as TL equations are (2.16a), (2.16b) and (2.16c). They characterize the cable model given in 2.6.

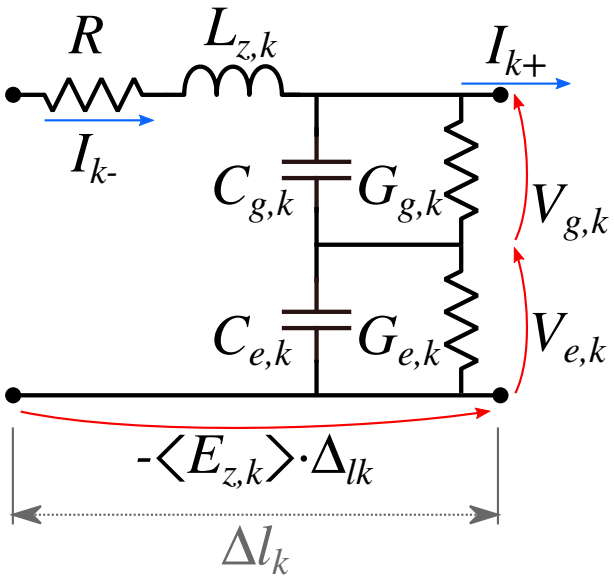

Figure 2.6: TL equivalent circuit for an insulated single core thin wire. Adapted from [9].

$$L_k \partial_t I_k + \partial_r V_{g,k} + \partial_r V_{e,k} + R_l I_k = E_k \tag{2.16a}$$

$$C_{g,k}\left(\partial_t V_{g,k} + \frac{\sigma_g}{\varepsilon_g} V_{g,k}\right) = -\left(I_{k+} - I_{k-}\right) \tag{2.16b}$$

$$C_{e,k}\left(\partial_t V_{e,k} + \frac{\sigma_e}{\varepsilon_e} V_{e,k}\right) = -\left(I_{k+} - I_{k-}\right) \tag{2.16c}$$

2.2.3 A coaxial thin wire

A single core shielded cable can be treated as two coupled circuits, in a manner that each circuit is solved with different strategies:

1. An external circuit, formed by the metallic shield with its insulation: is solved with the modified formalism of Holland explained in 2.2.2, in which the conductor radius is the external radius of the shield and the insulation external radius is the cable external radius.

2. An internal circuit: composed by the core and the inner insulation: is solved with a TL model considering the transfer impedance of the cable, and a dependent voltage source to account for the induction from the external circuits [10, 11].

Although these circuits are coupled, an assumption is made: the coupling is unidirectional from the external circuit to the internal circuit. Thus, the currents and voltages in the core do not influence back those in the shield. The TL system depicted in figure 2.7 and ruled by expressions (2.17a) and (2.17b), is used to solve the currents and voltages along the core.

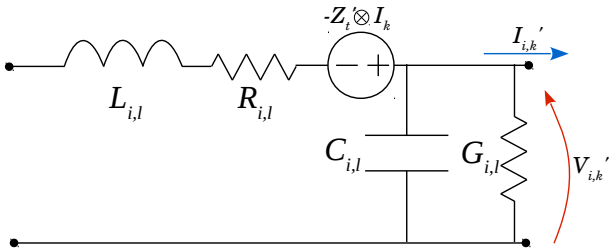

Figure 2.7: TL equivalent for the inner circuit of a shielded cable

$$\partial_r V_{i,k} + L_{i,l}\partial_t I_i + R_{i,l} I_i = Z'_{T,l} \otimes I_k \tag{2.17a}$$

$$C_{i,l}\partial_t V_{i,k} + G_{i,l} V_{i,k} = -\partial_r I_{i,k} \tag{2.17b}$$

Where the inputs are I_k and V_k, the current and voltages in segment k of the shield, the unknowns are $I_{i,k}$ and $V_{i,k}$, the current and voltages in segment k of the inner conductor, $R_{i,l}$, $L_{i,l}$, $C_{i,l}$ and $G_{i,l}$ are the linear resistance, inductance, capacitance and conductance of a coaxial cable, given by its geometry and material properties [10]. $Z_t{}'$ is the transfer impedance per unit of length of the shield. In this model the transfer admittance is not considered. The right-hand term in equation (2.17a) is the result of a convolution product ($\otimes$) between the inverse Fourier transform of the transfer impedance, and the transient current in the shield I_k.

The transfer impedance $Z_{T,l}{}'$ is described with a generic first order model in the frequency domain, as established in (2.18). In a manner that, if measures are available, they can be translated to an analytical model through a Vector Fitting technique [12].

$$Z_{T,l} = R_{T,l} + j\omega L_{T,l} + \sum_{i=1}^{N_p} \frac{a_i}{c_i + j\omega} \tag{2.18}$$

In general, as indicated in figure 2.8, the electric and magnetic fields in the cell are computed using the conventional FDTD algorithm, if the cable has a coaxial configuration; the currents and voltages in the shield are computed using the extended thin wire formalism in [9, 13], and the currents and voltages in the core

are computed using the TL method. While if the cable has single core configuration, only the extended thin wire formalism is used.

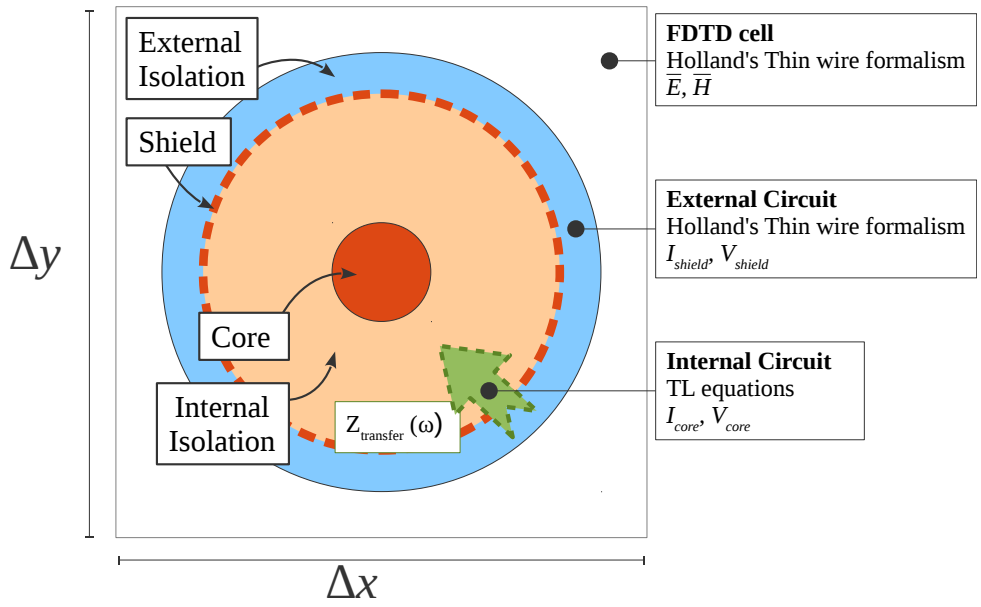

Figure 2.8: Solution methods for each component in a cable

As mentioned earlier, the thin wire described in this section is the base for the electromagnetic models to study a lightning impact to a large industrial site in FDTD. All the main components: the lightning strike, the building, the grounding grid and the IM cable are going to be constructed meshing different thin wire structures. In the next sections, the validation of the individual components is going to be shown.

2.3 The return stroke

When studying the effects of lightning, four different kinds of models exist [14]: the thermo-electrical models, the transmission line models, the electromagnetic models and the so called engineering models. All of them with more or less complexity and accuracy try to emulate the energy content of a lightning strike, either direct or indirect.

In this work, the electromagnetic models (EM) are going to be considered, since the problem that concern us (a lightning strike to a building) is mainly a direct interaction (conduction), but also has indirect effects in the surroundings (radiation). Therefore, the interest is to model an adequate current to the building, and a fair electromagnetic environment to some tens of meters from the channel, in a manner that, the connection of the cable to the building is affected by both phenomena.

The EM models are geometrical constructions that emulates the electromagnetic environment of a lightning strike. They are not based on physical parameters, but

they try to emulate two physical variables usually measured: the current propagation along the channel, and the radiated fields.

In general, the return stroke electromagnetic models can be described as a vertical straight conductor, surrounded by a material. Both conductor and material have unrealistic properties and geometries. They can be lossless, uniformly lossy, or variably lossy, with a set of inductances and capacitances distributed along the conductors, or embedded in a material with any values of electrical permittivity or magnetic permeability. This configuration is usually excited at its bottom with a voltage or current source, as indicated in figure 2.9.

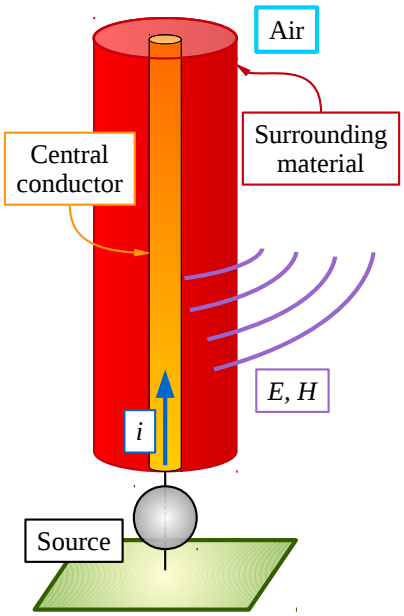

Figure 2.9: Generic EM model of a lightning channel

It is important that the chosen configuration fulfills a set of conditions previously established as physical parameters of the lightning return stroke. These conditions were identified for the first time by Nucci et al. [15] based on the measurements of Lin et al. [16].

The conditions are the followings:

1. The speed of the propagation of the current front shall be less than the speed of light c, it must be between $c/3$ and $2c/3$
2. The vertical component of the electric field flattens at tens to hundreds of meters within around 15 ms from the beginning of the return stroke (See figure 2.10a).
3. A sharp initial peak in both electric and magnetic field waveforms at a few kilometers and beyond (See figures 2.10b, 2.10c, and 2.10d).
4. A slow ramp following the initial peak in electric field waveforms measured within few tens of kilometers (See figure 2.10b).

5. A hump following the initial peak in magnetic field waveforms measured within several tens of kilometers(See figure 2.10c).

6. A zero-crossing within tens of microseconds in both electric and magnetic field waveforms measured at 50 km and beyond (See figure 2.10d).

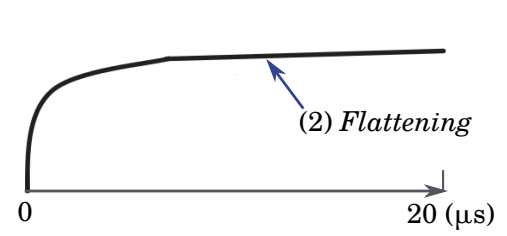

(a) Vertical electric field at 50 m from lightning channel base

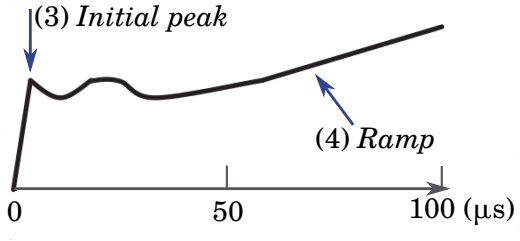

(b) Vertical electric field at at 5 Km from lightning channel base

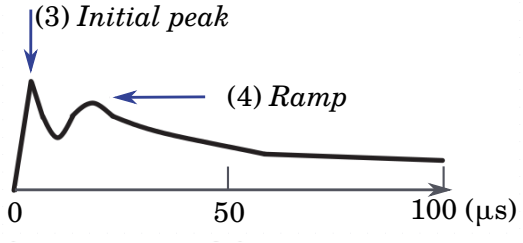

(c) Azimuthal magnetic field at 5 Km from lightning channel base

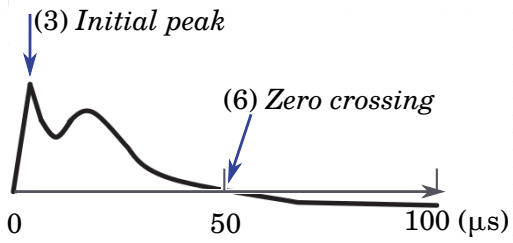

(d) Azimuthal magnetic at 50 Km from lightning channel base

Figure 2.10: Characteristics of the electromagnetic environment of a return stroke. Adapted from [17]

Although these conditions exist, and help with the construction of an electromagnetic model of a return stroke, conditions 4, 5 and 6, will not be taken into account, since they concern regions further than our case of interest. In this work, the interest is in the electromagnetic environment of some hundreds of meters at most.

The condition regarding the velocity of propagation of the current front wave, to our knowledge; is the most important requirement that an EM model must fulfill. Since the velocity of propagation is going to affect directly the conduction of currents in the building and conductors, as well as the risetime of the electromagnetic fields.

In the next section, examples of four different electromagnetic models with geometries that fulfill the previously mentioned conditions, are going to be detailed and implemented in FDTD. The models are:

- A lossless wire with a radius of 0.675 m surrounded by air
- A lossless wire with a radius of 0.675 m surrounded by a dielectric material of $\varepsilon = 9\varepsilon_0$

- A lossy wire with a radius of 0.675 m and 0.25 Ω/m, surrounded by a material of $\mu = 5\mu_0$ and $\varepsilon = 5\varepsilon_0$
- A lossy wire with a radius of 0.675 m surrounded by a material of $\mu = 5\mu_0$ and $\varepsilon = \varepsilon_0$. With different values of the distributed resistance: $R = 1\Omega/m \ \forall \ z \in (0\ ,\ 0.5)$km, $R = 0.3\Omega/m \ \forall \ z \in (0.5\ ,\ 4)$km,$R = 0.5\Omega/m \ \forall \ z \in (4\ ,\ 7.5)$km and $R = 5\Omega/m \ \forall \ z > 7.5$km.

The EM models implemented in this work, are compared with those proposed in [18, 19], and shown in figures 2.11. It is also worth noting that, they are flexible enough as to be implemented with any full wave numerical method either: FDTD, FEM or MoM.

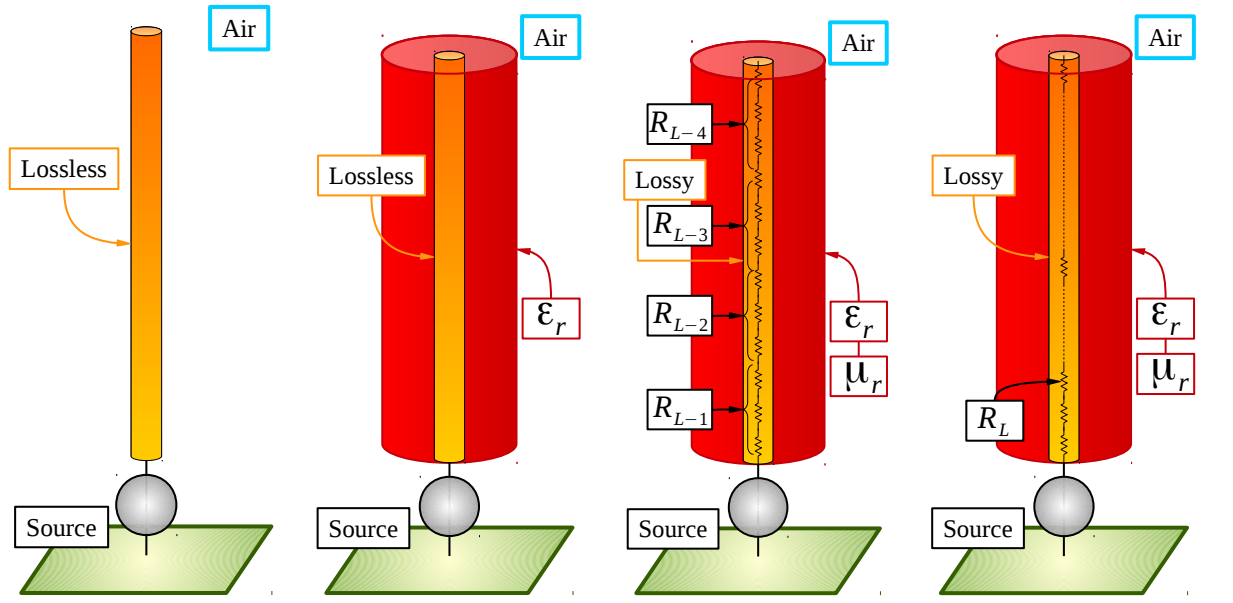

(a) Lossless wire in Air **(b) Lossless wire in dielectric** **(c) Lossy wire inside dielectric/magnetic** **(d) Non-uniform lossy wire inside dielectric/magnetic**

Figure 2.11: EM models for the lightning channel

For all of these models, the propagated current along the channel is calculated using FDTD and compared with the results showed in [18, 19].

A satisfactory behavior of the current is not good enough to determine whether an EM model is suitable or not. Some observations of the radiated fields must be also considered.

To validate the radiated fields, the EM model described in figure 2.11d is considered. This model is compared to the fields radiated by several vertical electric dipoles (VED) over a perfectly conducting ground. The fields of the VED are solved using Bannister equations [21].

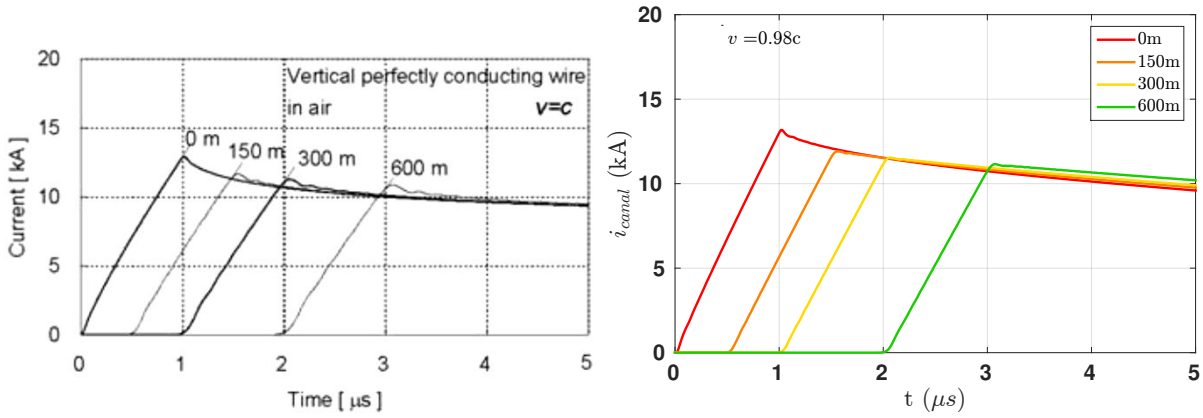

(a) Reported by Baba and Rakov [18] **(b) Implemented in FDTD**

Figure 2.12: Current distribution for a perfectly conducting wire in air

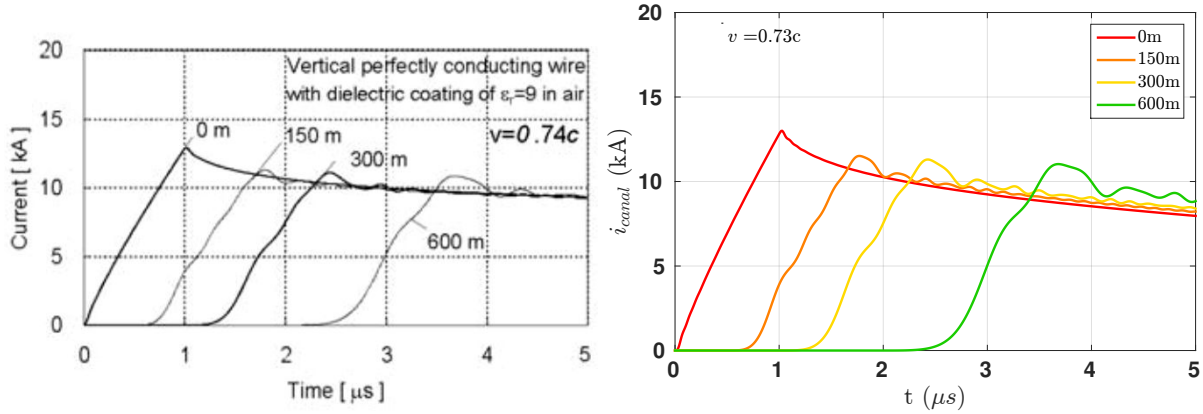

(a) Reported by Baba and Rakov [18] **(b) Implemented in FDTD**

Figure 2.13: Current distribution for a perfectly conducting wire embedded in a 4 m×4 m dielectric of $\varepsilon_r = 9$

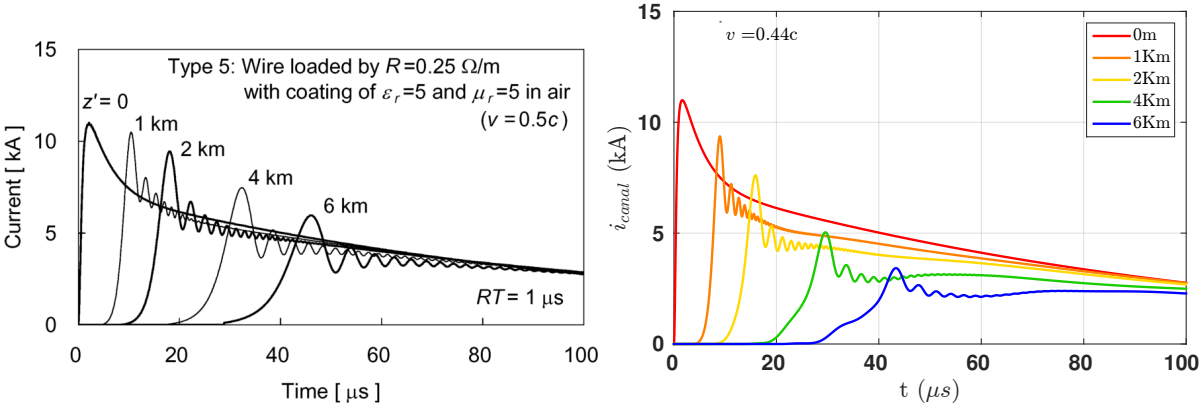

(a) Reported by Baba and Rakov [19] **(b) Implemented in FDTD**

Figure 2.14: Current distribution for a lossy wire with uniform distributed resistances, embedded in a material of $\varepsilon_r = 5$ and $\mu_r = 5$ with 20 m×20 m of transversal area

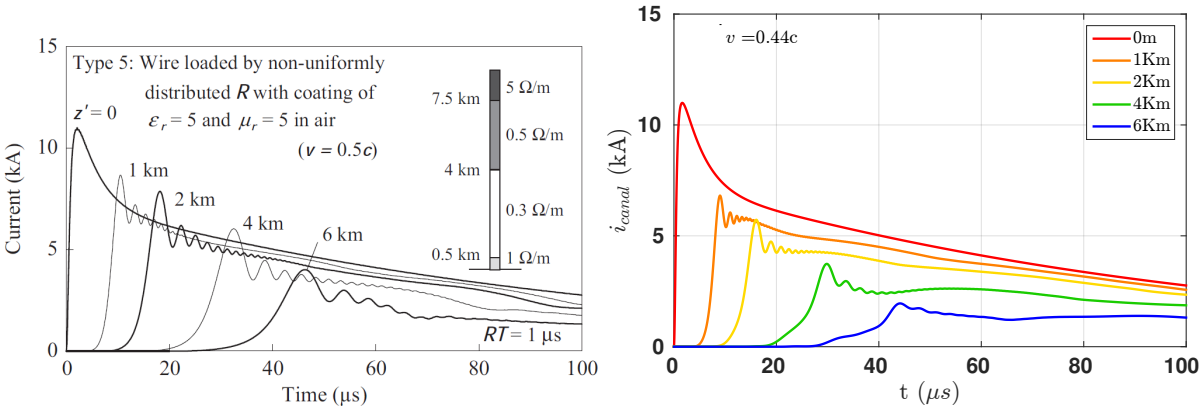

(a) Reported by Baba and Rakov [19] **(b) Implemented in FDTD**

Figure 2.15: Current distribution for a lossy wire with non uniform distributed resistance, embedded in a material of $\varepsilon_r = 5$ and $\mu_r = 5$.

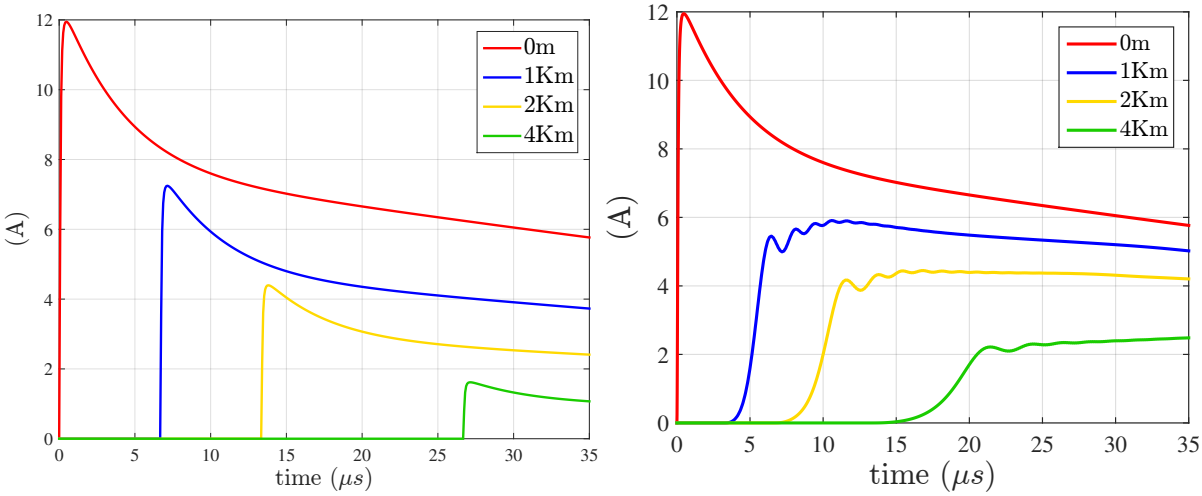

(a) Given by the MTLE propagation model [20] **(b) Given by the electromagnetic model of figure 2.15.**

Figure 2.16: Current propagation for two different return strike models

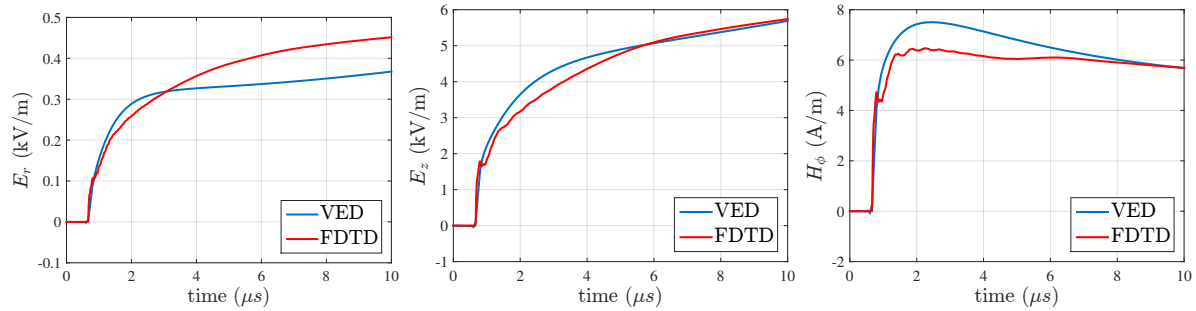

(a) Radial electric field at the surface of the soil **(b) Vertical electric field at the surface of the soil** **(c) Azimuthal magnetic field at the surface**

Figure 2.17: Fields radiated at 200 m for two different lightning channel numerical models

The Bannister equations depend on the current distribution along the channel. There are several models to represent this distribution [22], in this work; the Model of Transmission Line Modified Exponentially (MTLE) [14] is used.

Figure 2.16 shows a comparison of the current distribution for the two return stroke models. As it can be seen, they show similar propagation velocities and current behaviors. The small discrepancies are expected, since the nature of the models is different.

Finally, the fields generated by both the VED arrangement, and the EM model in FDTD are compared in 2.17. In here, the fields over a perfectly conductive soil are computed at ground level, and 200 m from the channel base. The observed discrepancies due are mainly to the different nature of the models of the return stroke, nevertheless; the fields agree reasonably well.

The EM model indicated in figure 2.15 is the one of the fairest models to emulate the electromagnetic environment of a lightning strike.

An special consideration concerning the type of excitation at the channel based must be assessed, for engineering studies; the return stroke current at the base of the channel is a standardized value. Therefore, the use of an ideal source that forces the behavior of the current at the striking point, is advisable. Nevertheless, this kind of source suggests a separation of current propagation paths, i.e., the reflections of currents from the base of the building and grounding grid, are not going to travel to the lightning channel.

In this section it has been revised several EM models for the return stroke to be implemented in FDTD, and it has been observed that the model depicted in figure 2.15 is fairly representative of the electromagnetic environment of a lightning strike, and of the current propagation velocity. Nevertheless, it is also a relative complex model, and, for a case already demanding in computational resources, it is advised to use a simpler and less consuming model, like the one depicted in figure 2.12.

2.4 The building

There are several ways to model a building in FDTD, in this section, three models are going to be briefly discussed: a composition of perfectly metallic cubes or plates, as lossy conductive plates, or as conductive beams forming a mesh structure.

2.4.1 Perfectly metallic structure

In the classical Yee scheme for the FDTD, an ideal metallic structure is constructed with a Perfect Electric Conductor (PEC) material. This kind of material is implemented forcing boundary conditions in their interface, i.e., establishing the tangential electric fields, and the normal magnetic field to a null value, as depicted in figure 2.18. The rest of the fields are updated following the classical FDTD algorithm.

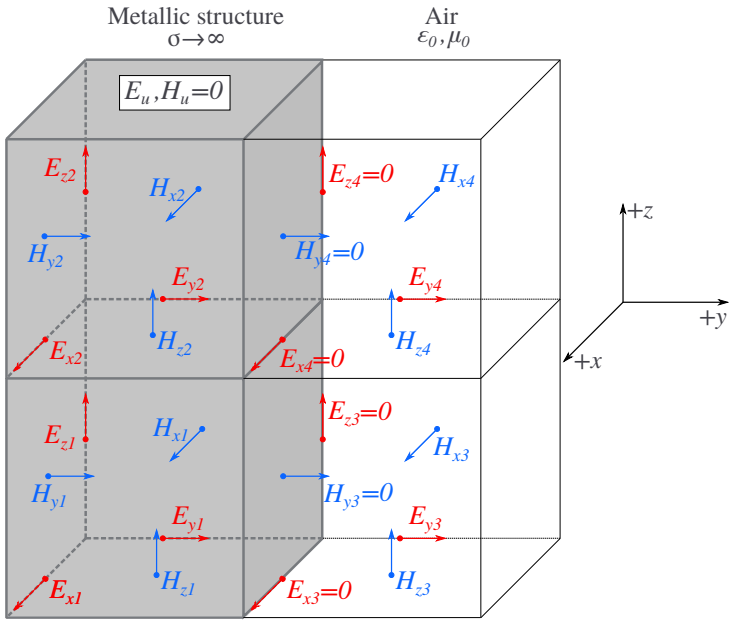

Figure 2.18: Boundary between a metallic volumetric structures and air cells in FDTD.

This is the simplest approach to model a building structure, nevertheless, it rest as an approximation to the real construction of buildings in a Power Generation Center (PGC). Not all the buildings are completely metallic structures, in fact; usually they are constructed with steel beams inside concrete walls.

This kind of structure, inherently carries a conductivity different from infinity, and affects the current propagation at lower frequencies. In order to consider this phenomena, more complex models are needed.

2.4.2 Lossy conductive plates

A building wall can be considered with a thin lossy plate, with its thickness smaller than the cell size, a surface impedance in both sides of the plate, and a transfer impedance to communicate the field information of both sides of the plate. As depicted in figure 2.19. This model is also known as a Bilateral Impedance Boundary Condition (BIBC).

To model the losses in the surface, the expression depicted in (2.19) is used. While the transition between the two medias is treated with the use of a transfer impedance, as shown in expression (2.21).

$$Z_s = \frac{jk_m}{\sigma_s} \coth(jk_m d) \tag{2.19}$$

$$k_m = (1 \pm j)\sqrt{\frac{2\pi f \mu \sigma}{2}} \tag{2.20}$$

$$Z_t = \frac{k_m}{\sigma \sin k_m d} \tag{2.21}$$

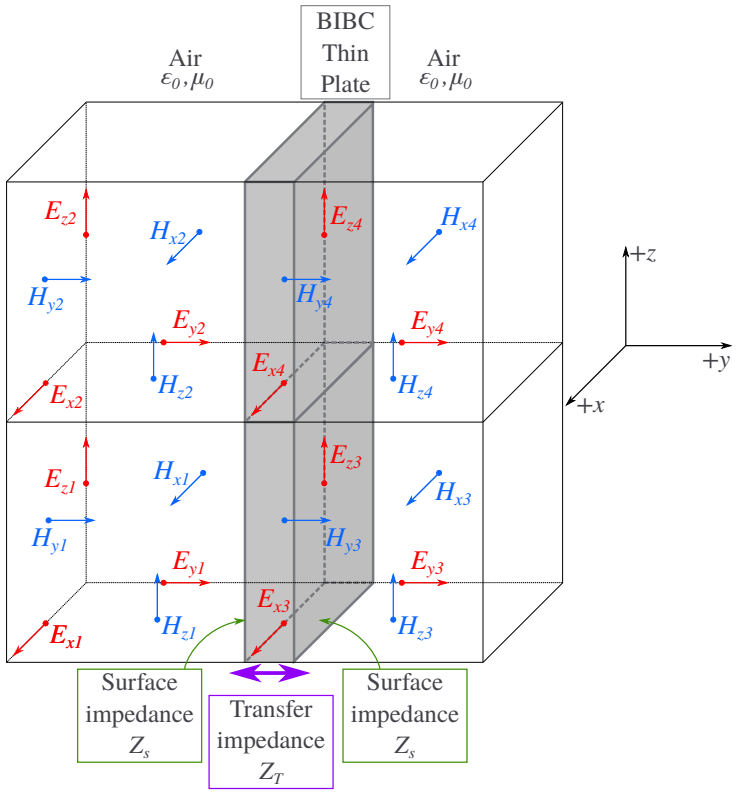

Figure 2.19: Thin lossy plate with BIBC in FDTD.

Where: $Z_s \rightarrow$ Thin plate surface impedance
$\sigma_s \rightarrow$ Low frequency surface conductivity
$d \rightarrow$ Thin plate thickness
$k_m \rightarrow$ Wave number of the surface.

This kind of model allows one to consider the electromagnetic environment inside a building, contrary to the perfect metallic walls, in here the fields can penetrate and have an influence in electronic equipment not shield or grounded, for example.

2.4.3 A junction of lossy thin wires

Finally, another approach that can be used to model the building walls is to consider them as a meshed structure of several lossy thin wires. In order to do so, a wire junction for the extended formalism of Holland is going to be considered as depicted in figure 2.20. The interest is to establish the boundary condition at the junction, therefore, three conditions must be met:

- The voltage in the node V_0 is a continuous variable (See expression (2.22)).
- The current $I_{k,0}$ follows Kirchoff law (See expression (2.23)).
- The charge $Q_{k,0}$ in each segment adjacent to the node conserves (See expression (2.24)).

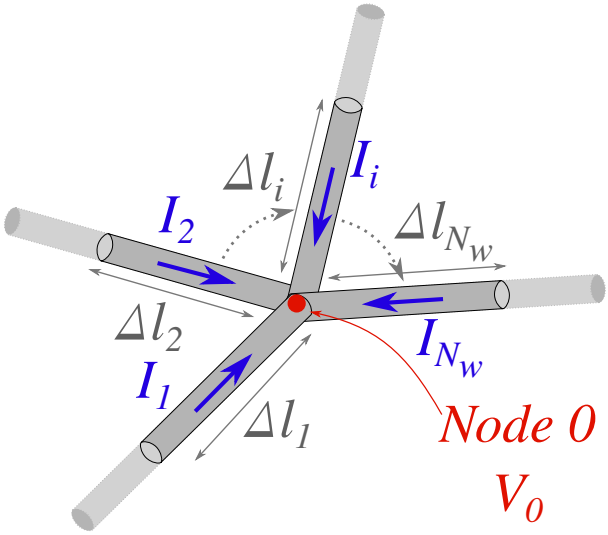

Figure 2.20: Junction of multiple wires.

$$\frac{Q_{k,0}}{C_k} = V_0; \quad k = 1, \ldots, N_w \tag{2.22}$$

$$\sum_{k=1}^{N_w} I_{k,0} = 0 \tag{2.23}$$

$$\frac{\Delta l_k}{2} \partial_t Q_{k,0} = -\left(I_{k,0} - I_k\right) \tag{2.24}$$

All three conditions added, give the boundary condition of the node (2.25), in which the equivalent capacitance $C_{eq,0}$ is noted in expression (2.26).

$$C_{eq,0}\left(\partial_t V_0 + \frac{\sigma}{\varepsilon} V_0\right) = \Delta t \sum_{k=1}^{N_w} I_k \tag{2.25}$$

$$C_{eq,0} = \sum_{k=1}^{N_w} C l_k \frac{\Delta l_k}{2} \tag{2.26}$$

In the following section, a case of lightning impact to a building is going to be considered, in order to validate the computational tool.

2.4.4 Validation of transients in a building

The electromagnetic model of a building to validate will be a mixture between volumetric metallic structures (PEC cells), and the thin wire of Holland [6, 7, 23]. Figure 2.21 illustrates the considered case study for this validation, as proposed in [24]. A lightning strikes at the top of a building, and the induced voltages inside an electrical wiring is studied.

The building structure is located over perfect metallic surface and modeled using

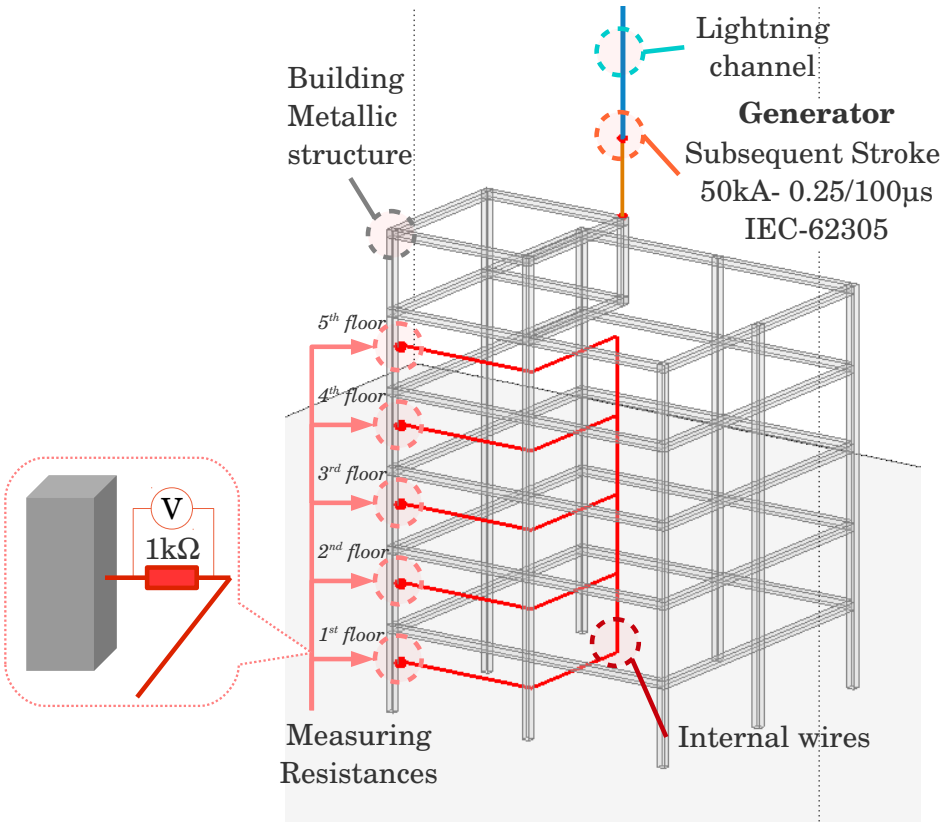

Figure 2.21: Schematic of a building as proposed in [24]

volumetric metallic structures of 0.5 m×0.5 m of transversal surface, while the internal electrical wires are modeled using the thin wire proposed in [7], with a radius of 0.5 cm. As a first approach, no losses were considered in both components.

The lightning channel is modeled using a bare thin wire [7] of radius 0.05 cm, with a distributed resistance of $1\,\Omega/m$. The excitation is a current source with an internal resistance of 600 Ω. The waveform of the current source is given by the Heidler function [25], as depicted in expression (1.1), with typical parameters of a lightning subsequent stroke: 50 kA - $0.25/100\,\mu s$ as given in [26].

The figure 2.22 shows the induced voltages at the junction between the internal wire and the building structure. At this point a high resistance ($1\,k\Omega$) is used to model electrical isolation of the wire with respect to the building. So the induced voltages are actually the potential differences along the resistances.

The figure 2.23 shows the currents flowing through the junction between the internal wiring and the building structure. In this case, the junction resistance is 0 Ω.

As it can be seen from figures 2.22 and 2.23, the induced voltages and currents obtained with the FDTD model are in good agreement with the results obtained in [24]. The slight discrepancies are due to the difference between the models used in each case. In [24], the thin wire of Noda and Yokoyama [27] is used, which leads to assume that the building structures and the wires have circular transversal area. In

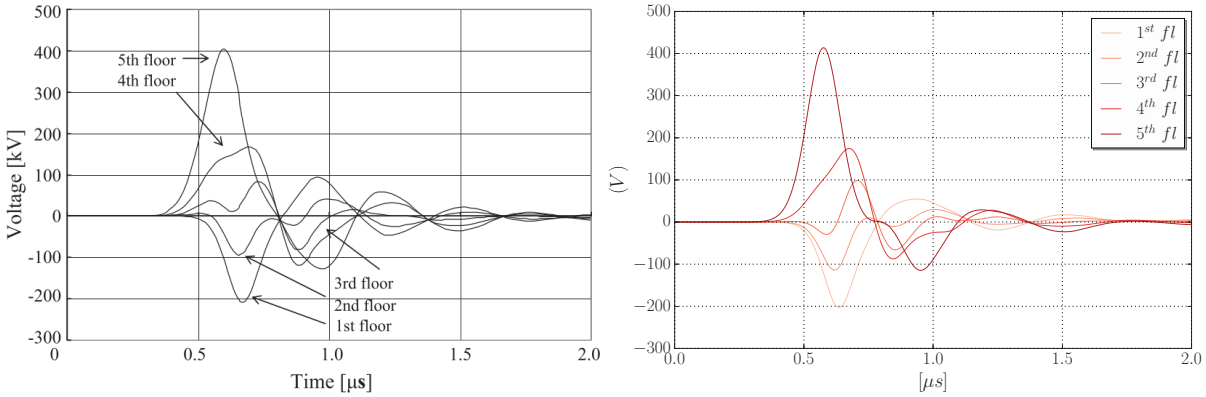

(a) As reported in [24] **(b) As computed with FDTD**

Figure 2.22: Induced voltage in the junction of the electrical wiring and the building structure

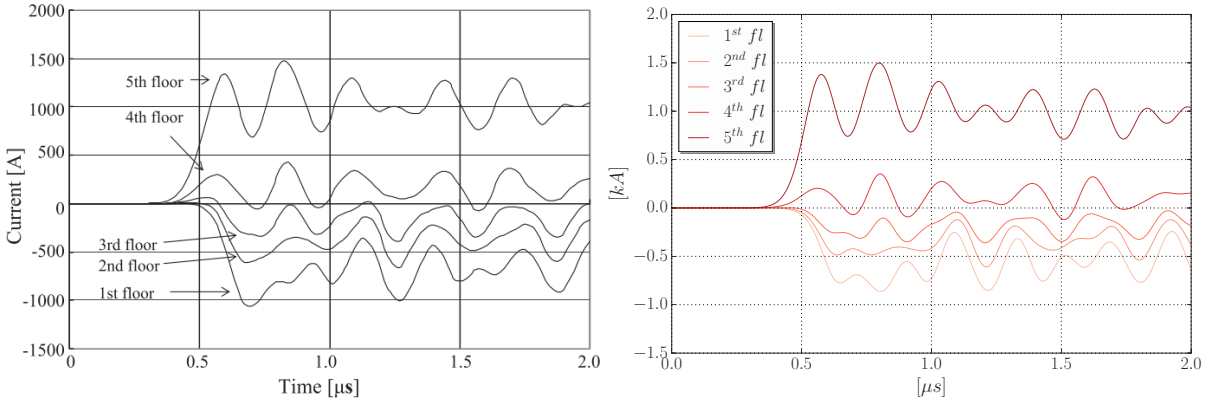

(a) As reported in [24] **(b) As computed with FDTD**

Figure 2.23: Current in the junction of the electrical wiring and the building structure

our models, the building structure has square transversal area (a conventional metallic volume in FDTD) and the electrical wires are modeled with the modified Holland thin wire model of [7].

These results allows one to validate the model of a lightning impact on a building, based on the thin wire formalism of Holland and ideal metallic structures properties. Further implementation of different walls like; a steel mesh, or a lossy thin plate, are going to be considered in the following sections.

2.5 The instrumentation and measurement cable

As mentioned previously, to model the cables, the modified version of the formalism of Holland is going to be used. The basis of the formalism were treated at the beginning of the chapter, in section 2.2. Therefore, in this section, only a validation case is going to be presented.

Consider the case proposed in [28], a simple buried coated conductor of 1 km, is excited at one of its extremities by a double exponential current source with two different rise times: 0.1 μs and 10 μs. Two different types of isolation permittivity are considered: $\varepsilon = 2\varepsilon_0$ and $\varepsilon = 5\varepsilon_0$. The interest is to observe the current at 150 m and 300 m from the source. Figure 2.24 describes the case.

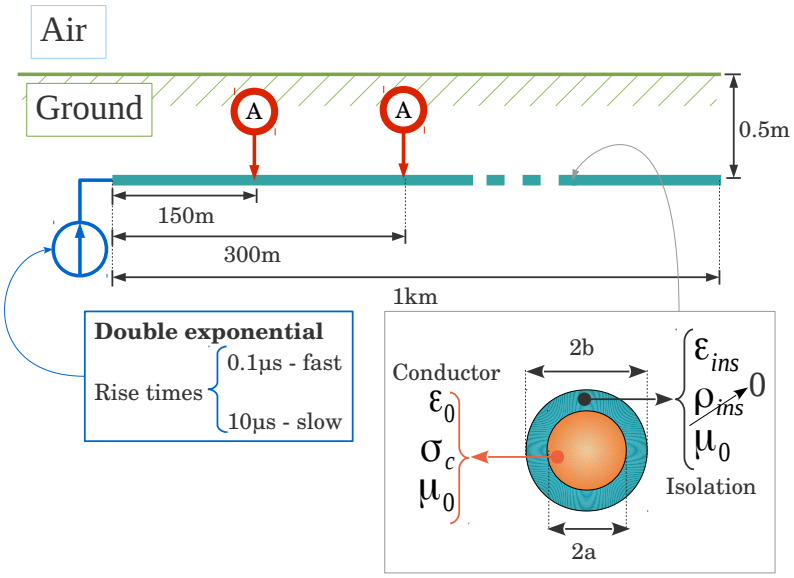

Figure 2.24: Geometry of the case to validate the thin wire formalism to model an horizontal conductor.

The results presented in [28] were obtained using a TL approach. They are going to be used as reference in the next section, to compare with two numerical solutions: a FDTD solution using the thin wire formalism of Holland, and a TL solution in the frequency domain as proposed by [10].

2.5.1 A Transmission Line solution for the current propagation in a buried conductor

The expression (2.27), proposed in [10], is used to find the current in the frequency domain at any distance x from the current injection point, and then the inverse Fourier Transform is used to find the transient response.

In order to solve the current, it is necessary to know the series impedance per unit length Z', and the shunt admittance Y'. This values depends mainly of two aspects: the cable configuration, and the ground properties. The series impedance, as denoted in expression (2.28a), depends on the internal impedance of the conductor Z'_w, the inductive reactance $j\omega L'$, and the ground impedance Z'_g, depicted in expressions (2.28b),(2.28c), and (2.28d) respectively. The internal impedance is approximated by its high frequency behavior [11], while the ground impedance is a model recently proposed in [28].

Regarding the shunt admittance shown in expression (2.29a), it can be seen that it depends on the capacitive susceptance $j\omega C'$ (expression (2.29b)), and the ground admittance Y'_g approximated with expression (2.29c) [10, 11]. The losses of the insulation are neglected.

$$I(x) = \frac{\exp(-\gamma x) - \rho_2 \exp(-\gamma(x-2L))}{2(1-\rho_1\rho_2\exp(-2\gamma L))}[1+\rho_1] Z_c I_0 \tag{2.27}$$

Where:
- $I(x) \rightarrow$ Current at position x from the source
- $\gamma \rightarrow$ Propagation constant equal to $\sqrt{Z'Y'}$
- $Z_c \rightarrow$ Characteristic impedance of the cable $\sqrt{Z'/Y'}$
- $\rho_i \rightarrow$ Reflection coefficient at terminal i, given by: $\frac{Z_i - Z_c}{Z_i + Z_c}$
- $I_0 \rightarrow$ Input current source.

$$Z' = Z'_w + j\omega L' + Z'_g \tag{2.28a}$$

$$Z'_w \simeq \frac{1+j}{2\pi a}\sqrt{\frac{\omega\mu_0}{2\sigma_w}} \tag{2.28b}$$

$$L' = \frac{\mu_0}{2\pi}\log\left(\frac{b}{a}\right) \tag{2.28c}$$

$$Z'_g = \frac{j\omega\mu_0}{2\pi}\left[\log\left(\frac{1+\gamma_g b}{\gamma_g b}\right) + \frac{2\exp(-2d|\gamma_g|)}{4+\gamma_g^2 b^2}\right] \tag{2.28d}$$

$$\gamma_g = \sqrt{j\omega\mu_0(\sigma_g + j\omega\varepsilon_g\varepsilon_0)} \tag{2.28e}$$

$$Y' = Y'_g + j\omega C' \tag{2.29a}$$

$$C' = \frac{2\pi\varepsilon_{ins}\varepsilon_0}{\log\left(\frac{b}{a}\right)} \tag{2.29b}$$

$$Y'_g \simeq \frac{\gamma_g^2}{Z'_g} \tag{2.29c}$$

$$\tag{2.29d}$$

Where:
- $\gamma_g \rightarrow$ Propagation constant in the ground
- $\sigma_g \rightarrow$ Ground conductivity
- $\varepsilon_g \rightarrow$ Ground relative permittivity
- $\sigma_w \rightarrow$ Conductor conductivity
- $\varepsilon_{ins} \rightarrow$ Insulation relative permittivity
- $d \rightarrow$ Burial depth
- $b \rightarrow$ Isolation external radius
- $a \rightarrow$ Isolation internal radius

2.5.2 Comparison of methods to compute the transients in a buried cable

As stated in section 2.5, the interest is to compare the transient currents obtained with the formalism of Holland, to the TL approaches described in section 2.5.1, and used in [28].

For the FDTD volume of computation depicted in figure 2.25, the cubic cells are 1 m length, the current injection is ideal, and its return path goes into the Perfectly Matched Layers (PML) boundary in order to avoid a numerical singularity in that point.

The comparison is depicted in figures 2.26, as it can be seen, the agreement between both transmission line responses is good, as well as the solution obtained with the extended model of Holland. These results validate our approach for representing an underground isolated conductor.

In the next section, this model is extended to a more complicated scenario: the grounding system.

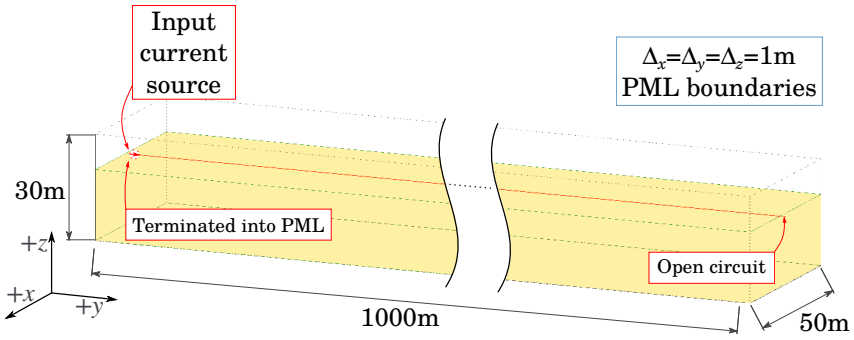

Figure 2.25: FDTD implementation of the case study depicted in figure 2.24

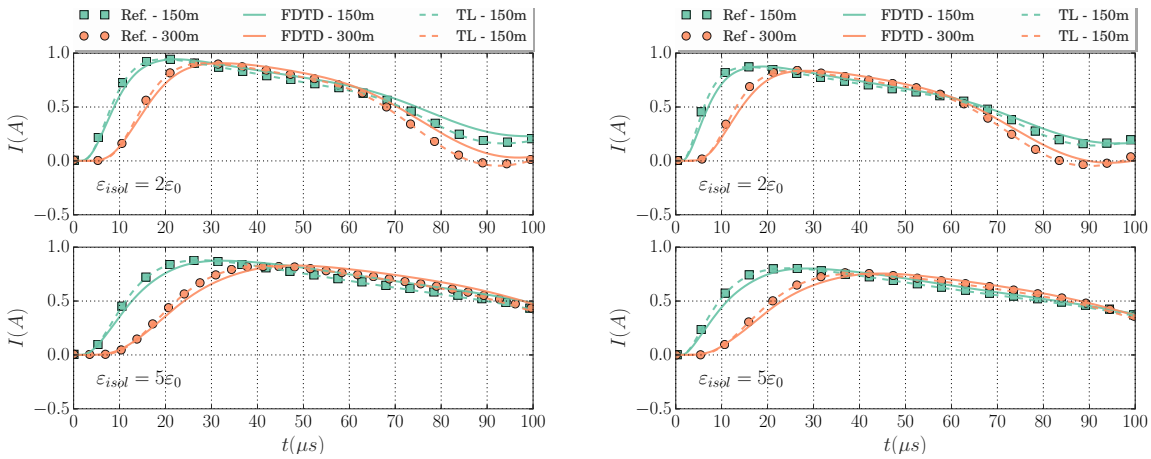

(a) Slow excitation **(b) Fast excitation**

Figure 2.26: Currents in the buried horizontal cable depicted in figure 2.24. "*Ref.*" are the results extracted from [28]. "*FDTD*" are the results obtained using the thin wire formalism of Holland, and "*TL*" are the results computed solving expression (2.27)

2.6 The grounding system

To model the grounding system in FDTD the thin wire formalism of Holland as described in section 2.2 is going to be used. Nevertheless, in order to validate the model against measurements and simulations of different case study, it is necessary to distinguish a problem not treated until now: The potential rise of a conductor when modeled with the formalism of Holland.

The extended model of the thin wire formalism of Holland, establishes an accurate coupling between the current circulating along the wire, and the tangential electric field surrounding it. In this formalism, the radial electric field (useful for the determination of the potential) close to the wire does not have to be evaluated, but can be reconstructed by the FDTD solver. When making such a calculation, particularly in the cell containing the wire, its precise value would be inaccurate and even wrong depending on the location of the wire:

- For a wire shifted inside a FDTD cell, as suggested in 2.27a, the radial electric field $E_{r,-}$ from one side is opposite to the one from the other side $E_{r,+}$, whereas only one radial component can be calculated by the FDTD, i.e. solving directly for both sides of the wire is not possible.
- If the wire is along a cell edge (see figure 2.27b), the radial electric field of the wire will ideally coincide with the FDTD computation, however, the FDTD nature of fields unknowns is averaging the field over an area of the cell. This presents a problem in the cell in which the wire is located, since the wire introduces a strong singularity that counteracts the averaging of the FDTD algorithm. The convergence between both quantities, usually is obtained from the second cell, i.e. from a distance more than one spacial step.

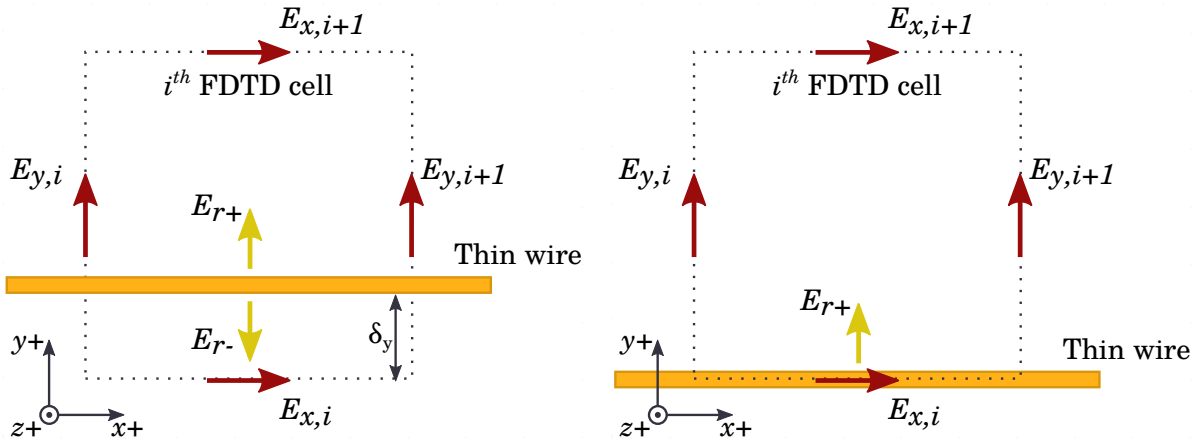

(a) Thin wire shifted a distance δ_y inside a FDTD cell

(b) Thin wire along a cell edge

Figure 2.27: Electric field in a FDTD cell around a thin wire

These inaccuracies to determine the electric field close to the conductor, hinder the computation of the potential rise, since the line integral highly depends on the behavior of the field immediately close to the surface of the conductor. Therefore, in the following section, a formulation to assess the potential rise of the conductor close to its surface is proposed. This formulation is based on the previous works of Noda and Yokoyama[27], and has been extended to suit the formalism of Holland when the conductor is located inside the cell and has any inclination.

2.6.1 Potential rise of a Hollands Thin Wire

Lets consider the situation in which a thin wire of radius a is located along the z-axis, as suggested in figure 2.28 the wire is shifted δ_x from the edge of the cell. The origin of the system is the center of the wire. The potential in a single cell i is defined by (2.30)

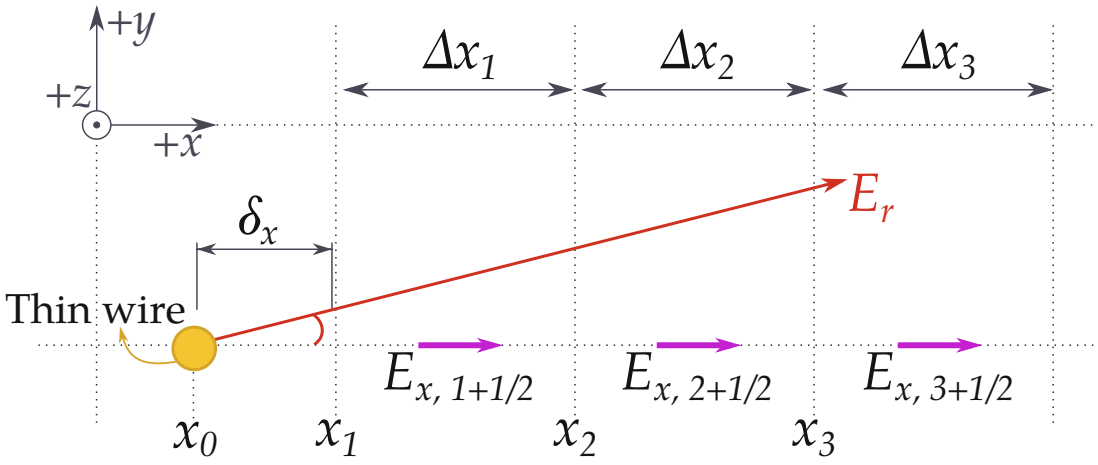

Figure 2.28: Thin wire oriented along z-axis. Close radial components along x-axis.

$$V_i = -\int_{x_i}^{x_{i+1}} e_{x,i}\,(x)\,dx \tag{2.30}$$

In a uniform FDTD grid, $x_i = \delta_x + (i-1)\,\Delta x$.

The value of the electric field in the FDTD is computed at the location $i + 1/2$, where $E_{x,i+1/2}$ is the value of the field at the i-th cell. The formulation to obtain the potential close to the conductor assumes that the radial electric field is inversely proportional to the distance from the center of the conductor ($E_r \propto 1/r$), as indicated in (2.31). In here, the radial direction corresponds with the x-direction, as suggested by figure 2.28.

$$e_{x,i} = E_{x,i+1/2}\frac{x_i + \Delta x_i/2}{x} \tag{2.31}$$

Using expression (2.31), the average field along the x-direction $\langle E_{x,i}\rangle_x$ can be computed for the closest cells to the conductor: i =0,1,2,3, as suggested by the generic expression (2.33).

$$\langle E_{x,i}\rangle_x = \frac{x_i + {}^{\Delta x_i}/_2}{\Delta x_i} E_{x,i+1/2} \int_{x_i}^{x_{i+1}} \frac{1}{x} dx \tag{2.32}$$

$$= \frac{x_i + {}^{\Delta x_i}/_2}{\Delta x_i} \log\left(\frac{x_{i+1}}{x_i}\right) E_{x,i+1/2} \tag{2.33}$$

For simplification, let us consider the case proposed in [3] in which the conductor is in the cell edge, and the grids are uniform. ($\delta_x = 0$ and $\Delta x = \Delta y = \Delta z$). Using (2.33), the average in the first three cells is given by (2.34), (2.35) and (2.36) respectively.

$$\langle E_{x,1}\rangle_x = \frac{1}{2} \log\left(\frac{\Delta x}{a}\right) E_{x,1+1/2} \tag{2.34}$$

$$\langle E_{x,2}\rangle_x = \frac{3}{2} \log\left(\frac{2\Delta x}{\Delta x}\right) E_{x,2+1/2} \approx 1.0397 E_{x,2+1/2} \tag{2.35}$$

$$\langle E_{x,3}\rangle_x = \frac{5}{2} \log\left(\frac{3\Delta x}{2\Delta x}\right) E_{x,3+1/2} \approx 1.0137 E_{x,3+1/2} \tag{2.36}$$

From (2.34), (2.35) and (2.36) it can be seen that the computed field at $i = 2 + 1/2$ is a good approximation to the average field along the cell edge $i = 2$. This is not true for the cell $i = 1$, where the average value depends on the ratio between the spatial step and the radius of the wire. Thenceforth, the proposition of this work is to extrapolate the value of $i = 2$ to assess the field closer to the conductor surface, this is $\langle E_{x,1}\rangle_x$, and $\langle E_{x,0}\rangle_x$, as indicated in (2.37) and (2.38).

$$\langle E_{x,1}\rangle_x = \frac{1}{\Delta x_1} \log\left(\frac{\delta x + \Delta x_1}{max\,(\delta x, a)}\right) \left(x_2 + \frac{\Delta x_2}{2}\right) E_{x,2+1/2} \tag{2.37}$$

$$\langle E_{x,0}\rangle_x = \frac{1}{\delta x} \log\left(\frac{\delta x}{a}\right) \left(x_2 + \frac{\Delta x_2}{2}\right) E_{x,2+1/2} \tag{2.38}$$

Expression (2.38) is obtained for $\delta x \neq 0$.

Finally the potential close to the conductor (i=0,1,2) is given by the expression (2.41).

$$V_{x,\ 0,1,2} = \delta x \langle E_{x,0}\rangle_x + \Delta x_1 \langle E_{x,1}\rangle_x + \Delta x_2 \langle E_{x,2}\rangle_x \tag{2.39}$$

$$\begin{aligned} V_{x,\ 0,1,2} = {} & \log\left(\frac{\delta x}{a}\right) \left(x_2 + \frac{\Delta x_2}{2}\right) E_{x,2+1/2} \\ & + \log\left(\frac{x_2}{max\,(\delta x, a)}\right) \left(x_2 + \frac{\Delta x_2}{2}\right) E_{x,2+1/2} \\ & + (x_2 + {}^{\Delta x_2}/_2) \log\left(\frac{x_3}{x_2}\right) E_{x,2+1/2} \end{aligned} \tag{2.40}$$

$$V_{x,\ 0,1,2} = \log\left(\frac{x_3}{a}\right)\left(x_2 + \frac{\Delta x_2}{2}\right) E_{x,2+1/2} \tag{2.41}$$

Since the interest is to compute the Transient Ground Potential Rise (TGPR), a path integral is required from the surface of the conductor to a point sufficiently far away from it, where the field would be negligible. This path is going to be split into two terms: the first concerns the potential rise close to the conductor, and the second the rest of the path. Therefore, the expression (2.41) can be used alongside with a traditional numerical integration. As that, the TGPR can be obtained using expression (2.43).

$$TGPR = V_{x,\ 0,1,2} + \sum_{i=3}^{n} \Delta x_i \left\langle E_{x,i} \right\rangle_x \tag{2.42}$$

$$= \log\left(\frac{x_3}{a}\right)\left(x_2 + \frac{\Delta x_2}{2}\right) E_{x,2+1/2} + \sum_{i=3}^{n} \Delta x_i \left\langle E_{x,i} \right\rangle_x \tag{2.43}$$

Observe that expression (2.43) depends on the relation between the distances x_3 and a, according to figure 2.28. Therefore, it is in coherence with a thin wire of Holland shifted along the FDTD, as developed in [23].

2.6.2 Validation of the formulation for the potential rise

To test the proposed formulation, three configurations of grounding conductors are considered:

- A single vertical rod. Reported in [29].
- A single horizontal counterpoise. Reported in [30].
- A grounding grid. Reported in [31].

The formulation for the TGPR proposed in the previous section is compared to these results, and to other numerical methods and models. In the following sections, the details of all the case of study are presented.

Single vertical rod

The case presented in [3, 29, 32], consists of a single vertical conductor of 6 m length, 8 mm radius, buried in a soil with 20 $^{mS}/_{m}$ of conductivity and 15 ε_0 permittivity.

The general case is depicted in 2.29a. The rod is excited with an impulsive current source of 0.52 μs rise-time and 33.2 A of amplitude, as depicted in figure 2.30. Also, the source has an auxiliary vertical conductor of 1 m used for the current return path, this conductor is 21 m away from the testing rod, and is connected to the source through an overhead wire at 0.9 m from the ground surface.

The TGPR is evaluated along a perpendicular axis of 60 m along the surface of the ground, as depicted in figure 2.29b. The computation is performed for two relative locations of the rod with regard to the FDTD cell: along the edge and in the center of the cell, as depicted in 2.31.

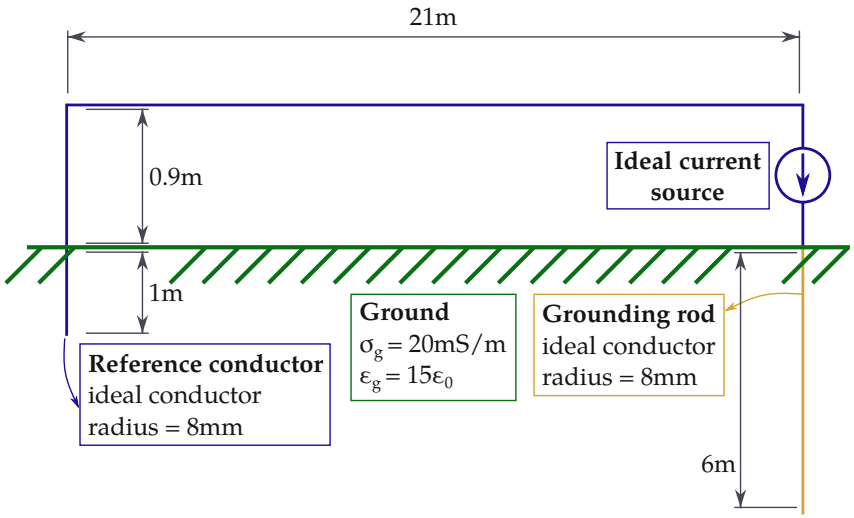

(a) General description

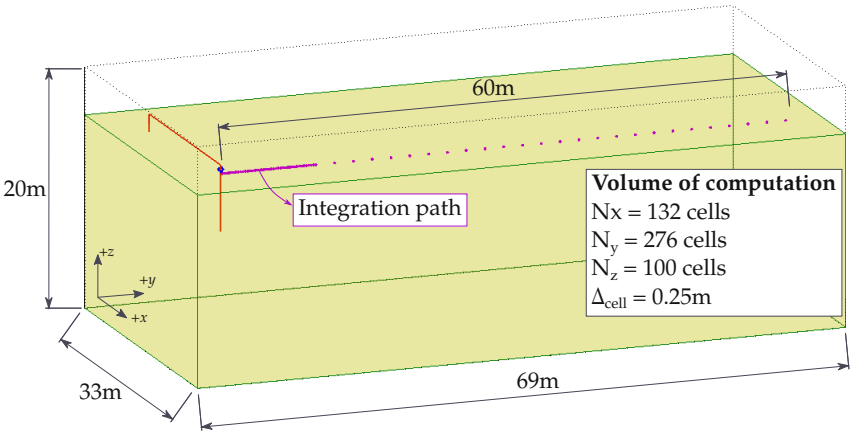

(b) Integration path

Figure 2.29: Case study of a single vertical rod.

The TGPR for a vertical rod is shown in 2.32a, for both relative locations along the cells. As it can be seen, expression (2.43) is in good agreement with the results reported in [3], for both relative positions of the cable along the FDTD cell.

In figure 2.32b, the contribution of each member of expressions (2.43) to the TGPR can be observed. Following the contribution of the potential close to the conductor given by (2.41), it can be observed that there is no significant difference when the rod is located along the cell edge and in the middle of the cell.

Nevertheless, the rest of the contribution to the TGPR, which is the integration of the field along the rest of the path, is different for each relative location of the conductor. This is because the integration paths for both cases, have all the field components in common, except for the first component; the one closer to the

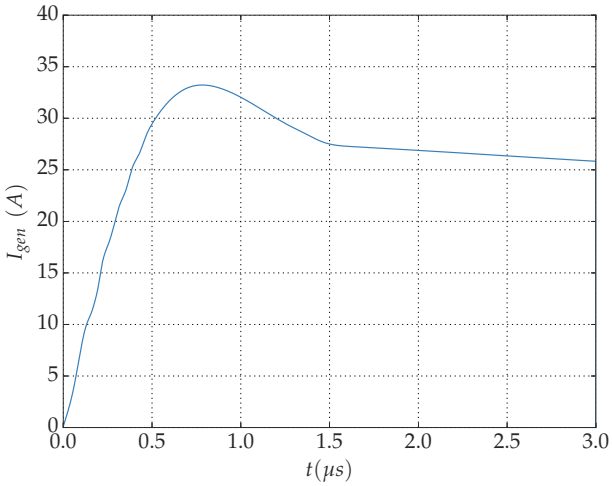

Figure 2.30: Current injected to the vertical rod.(Adapted from [29])

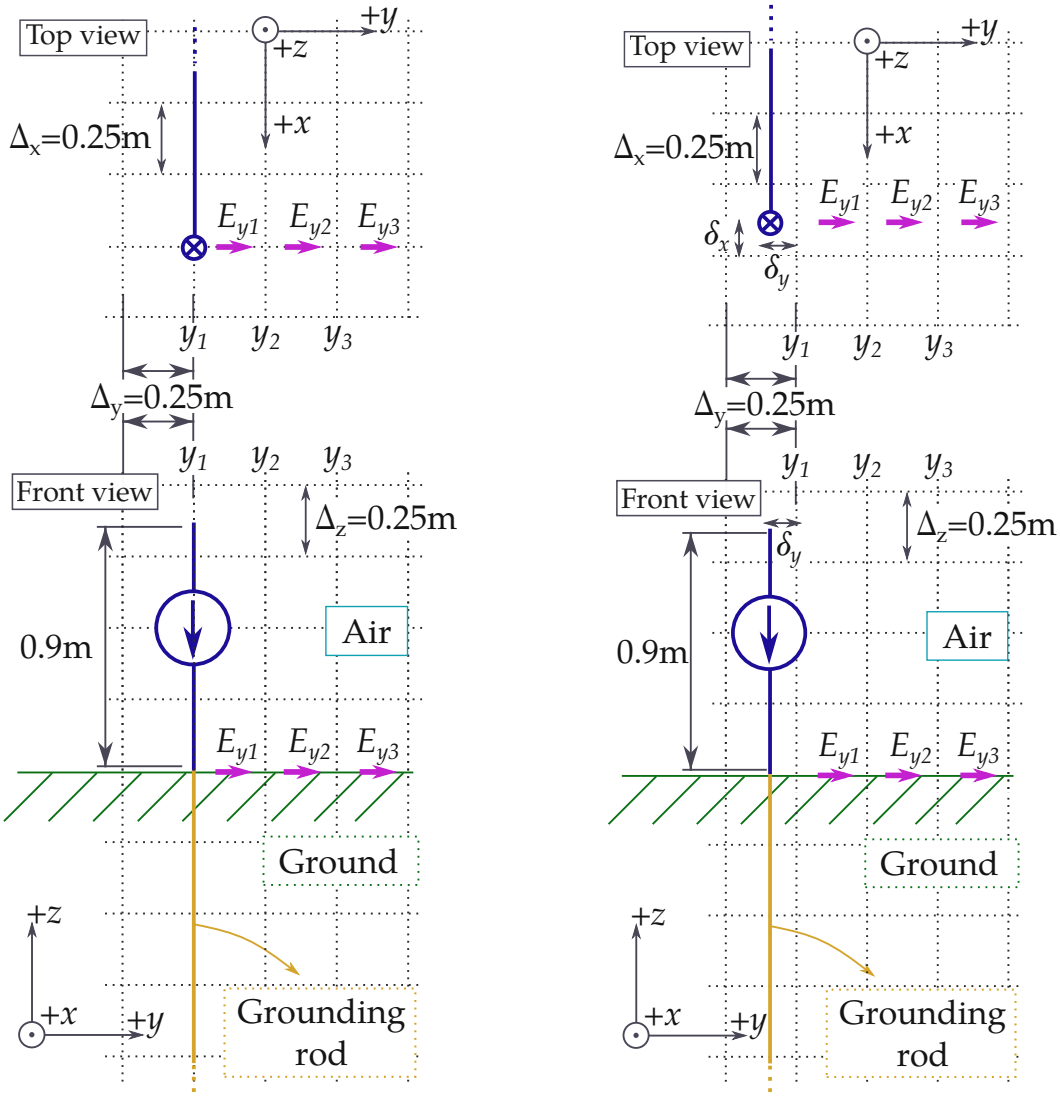

(a) In the cell edge **(b) In the cell center.**

Figure 2.31: Detailed view of the buried vertical rod in the FDTD scheme.

conductor. When the conductor is a the center of the cell, this component is weaker, and therefore the numerical integration becomes smaller than when the conductor is at the cell edge.

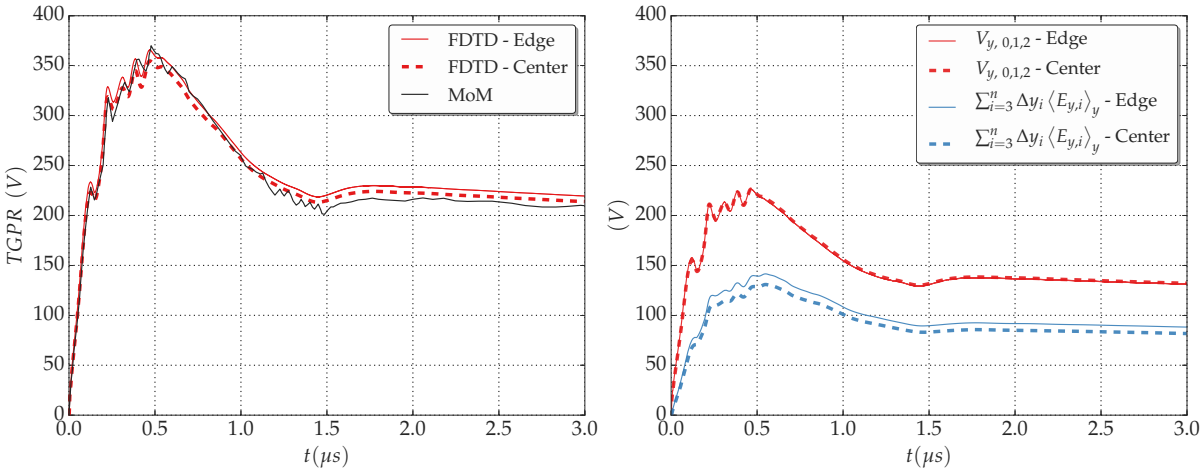

(a) Total TGPR.

(b) Contribution of the different components of (2.43) to the TGPR.

Figure 2.32: Transient potential rise of a vertical conductor.

Single horizontal counterpoise

This case has been proposed in [30] to validate the measurements performed in [33]. It consist of a 8.1 m long horizontal copper conductor, with radius of 4.4 mm, and buried 1 m depth. This configuration is also known as a counterpoise, and is depicted in 2.33a.

The counterpoise is excited with an impulsive source of 2.4 μs of time rise and 22.2 kA of peak, shown in figure 2.35. The source uses an overhead conductor at 1 m of height, to connect to a current return conductor located 20 m from the injection point. The TGPR is measured along a perpendicular path of 150 m as suggested by 2.33b, and as in the previous case, the computation is performed when the conductor is located along the cell edge, and in the center of the cell, as suggested by figures 2.34a and 2.34b.

The computation of the TGPR is compared with the results in [3], as well as with computations performed with another numerical tool based on the Method of Moments (MoM). The main results can be observed in figure 2.36a.

The contribution of each member of expression (2.43) to the TGPR can be observed in figure 2.36b. As in the previous case, the approximation given in (2.41) gives similar results despite the location of the conductor along the cell. Nevertheless, this displacement causes a logical reduction on the results of computation of the rest of the integration path.

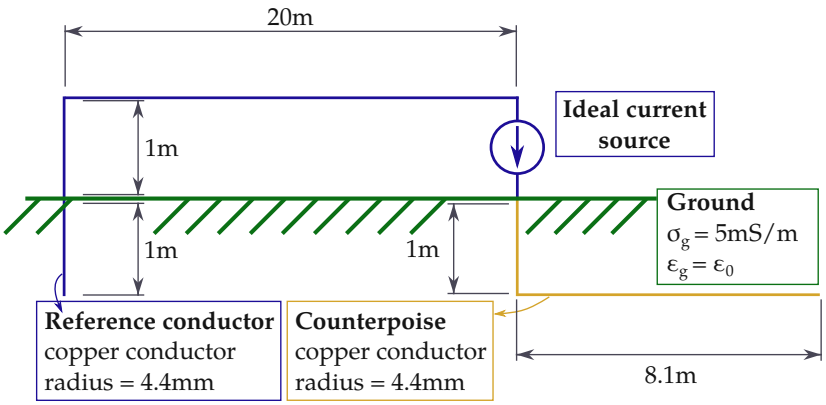

(a) General description

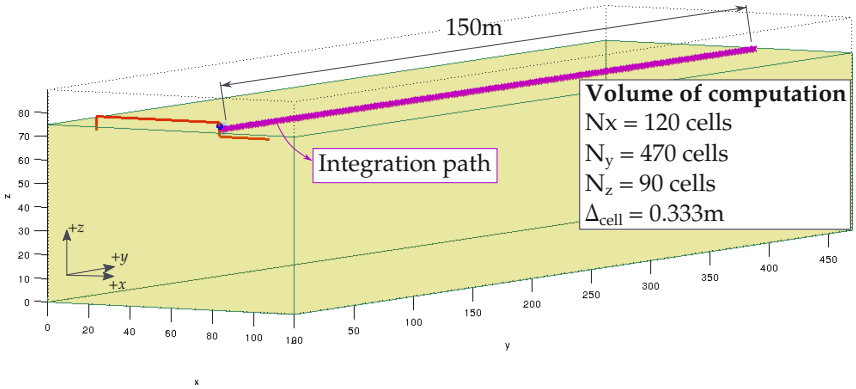

(b) Integration path

Figure 2.33: Case study of a counterpoise.

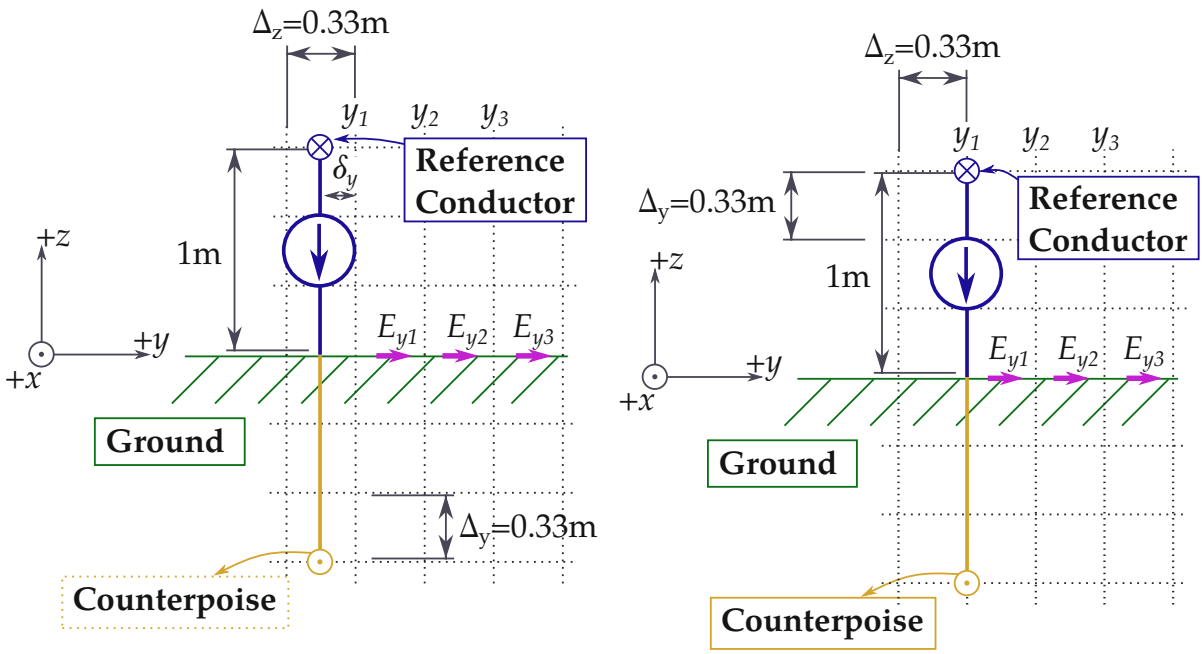

(a) In the center of the FDTD cell **(b) In the edge of the FDTD cell**

Figure 2.34: Detailed view of the buried counterpoise in the FDTD scheme.

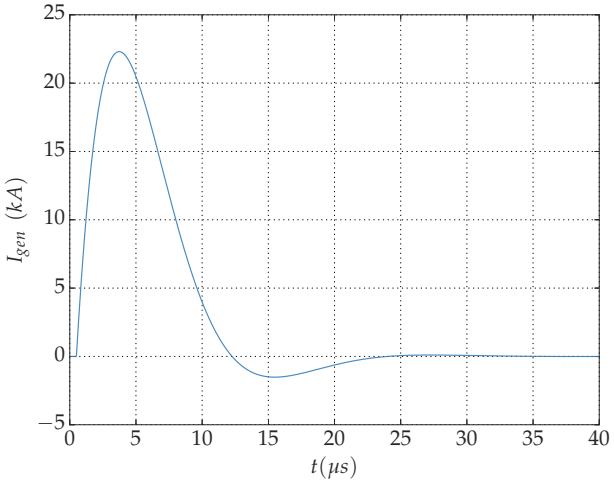

Figure 2.35: Current excitation of the buried counterpoise

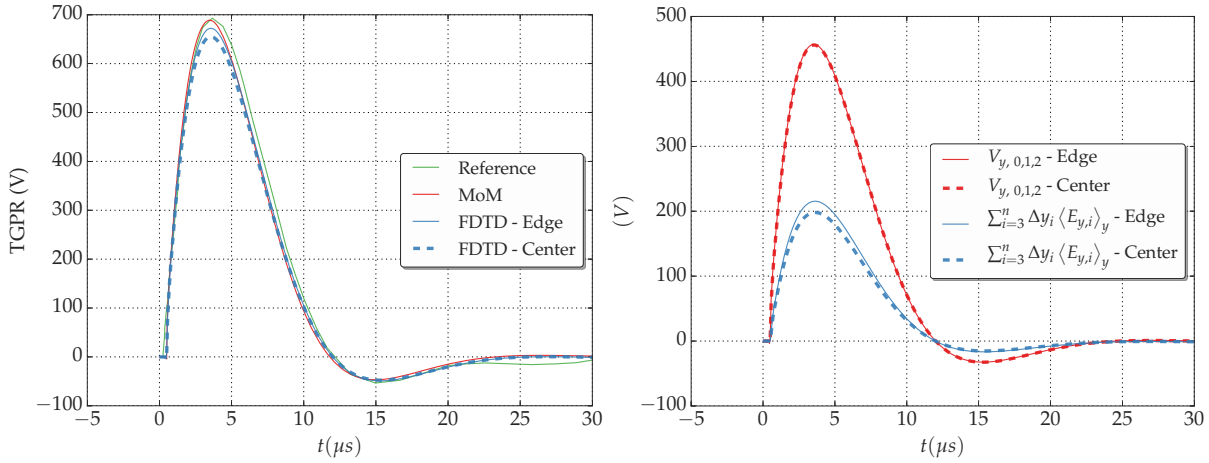

(a) Total TGPR.

(b) Contribution of the different components of (2.43) to the TGPR.

Figure 2.36: Transient potential rise of a buried counterpoise.

Grounding grid

Finally, the grounding grid studied in [31, 34] is considered. The grid is buried 50 cm, has a size of $60 \times 30\,\mathrm{m}^2$, with inner squares of 10 m sides. It is built with copper conductors of 4.37 mm radius, and excited with a voltage ramp source of 20 μs rise-time. The source is connected to an overhead current reference wire, with 1.59 mm of radius, 100 m of length and at 0.5 m from the surface of the ground. The potential rise is measured with another overhead copper wire of 0.8 mm of radius, located 1.5 m from the ground surface, 45.5 m from the grid and connected to a buried reference electrode at 120 m of distance, as suggested in figures 2.37a and 2.37b.

The voltage source is adjusted to deliver 1 A in stationary state, as shown in 2.38. The potential is observed at 15 m from the injection point at the grid level, as indicated in 2.37b. To do so, a vertical integration path from the grid to the voltage reference wire is followed. In this path, the approximation for the potential close to the conductor must be used for both the conductor of the grid, and the voltage reference wire.

The results concerning the grounding grid include the simulations and measurements performed by the authors in [31]. Here, the simulations reported were performed following the model thin wire based on [3]. For this case, the formulation for the potential rise proposed in this work, has been implemented only when the conductor is in the edge of the FDTD cell.

In figure 2.39 can be observed the results of the total TGPR, they show good agreement between the measurements and both models of thin wire in a FDTD scheme.

Up until this moment, the main components interacting in the problem at task have been considered separately, in the next section, a case of a relative big volume,

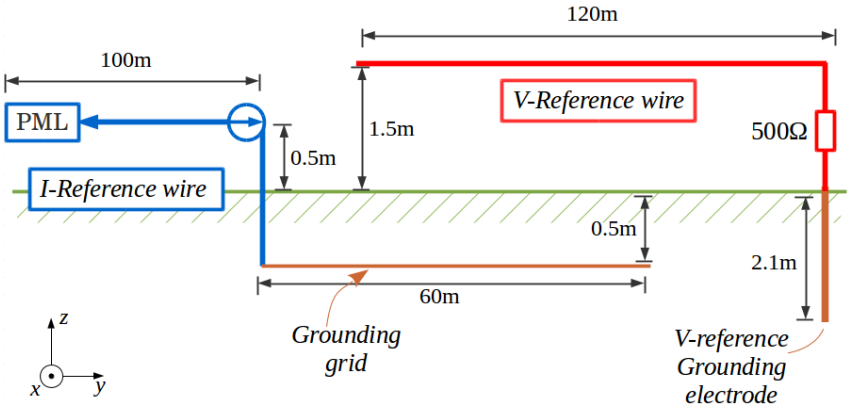

(a) Lateral view

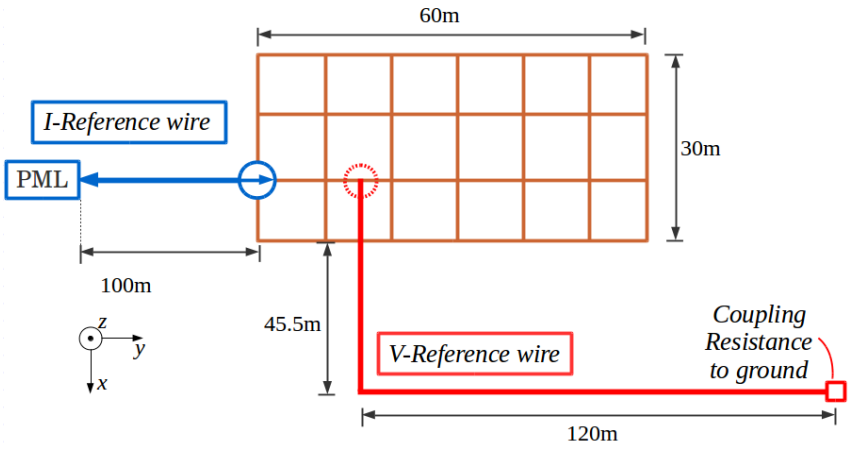

(b) Top view

Figure 2.37: Case study of a grounding grid

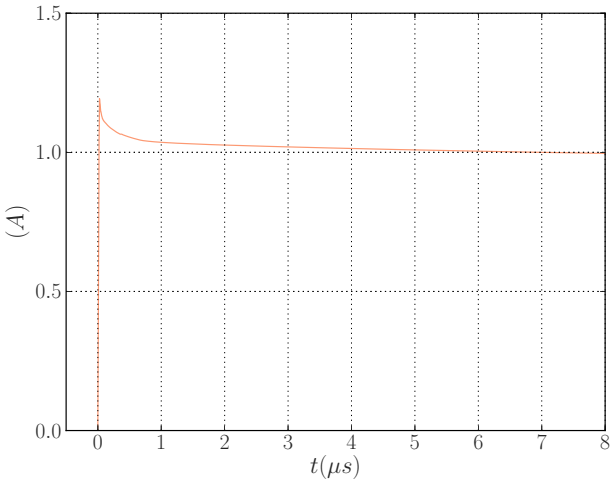

Figure 2.38: Current injected in the grid.

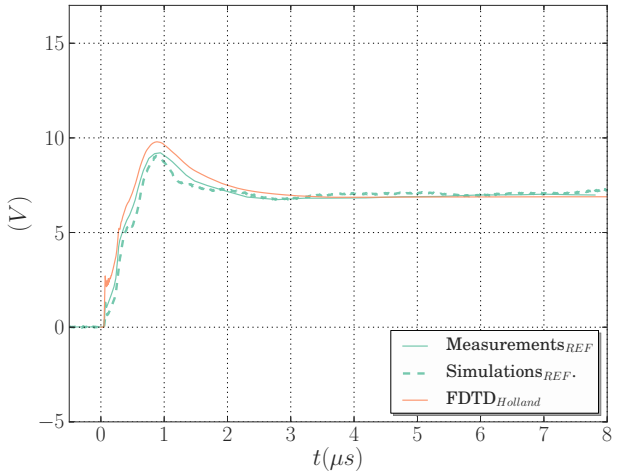

Figure 2.39: Potential rise of the point in the grounding grid depicted in 2.37b.

including all the components; is going to be presented.

2.7 A first approach to a complete case

The validation cases shown in previous sections allowed one to get to this point: a FDTD simulation of a lightning impact on a relative big industrial facility, composed of elements of relative different sizes, conductor configurations, and surrounding media.

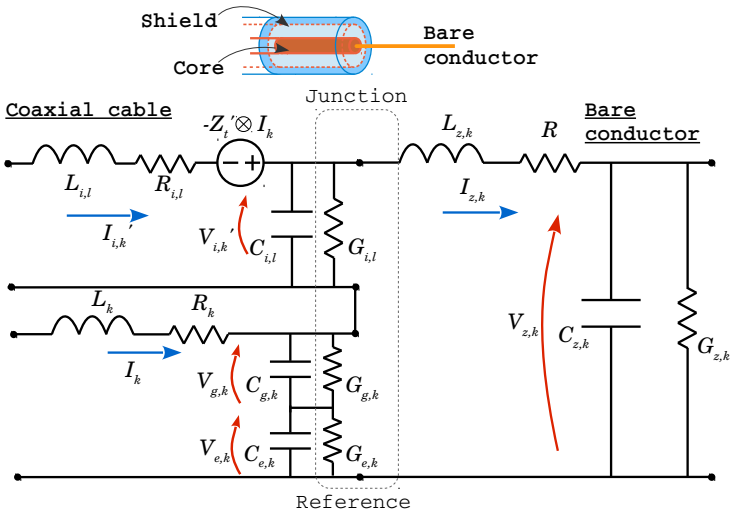

Figure 2.40: Equivalent circuit for the junction of a coaxial cable and a bare conductor.

Concerning the numerical results, first; the interest is to validate the whole FDTD implementation, in particular the discussed thin wire model; with a more consolidated method. The Integral Equation (IE) technique is used, by means of FEKO software which operates in the frequency domain, and demands a relative high amount of computational resources.

After the validation, the correspondence between the currents of a coaxial cable and an equivalent single core insulated conductor is observed. And finally, the transient behavior of the voltage at the terminations is inspected, considering the effect of the transfer impedance and the cable termination auxiliary wires.

Before assessing the realistic problem, a special consideration concerning the junctions of different type of conductors must be made, particularly of the coaxial cable. The case depicted in figure 2.40 represents the equivalent circuits of a junction between a shielded cable and a bare conductor. To solve for the junction, an Ordinary Differential Equations (ODEs) system is built at each junction point, with regard to the current continuity between conductors.

2.7.1 Case Study: A large industrial site

The case study selected is indicated in figure 2.41, and as mentioned previously is composed of a building, the grounding grid, a buried cable, and the lightning channel.

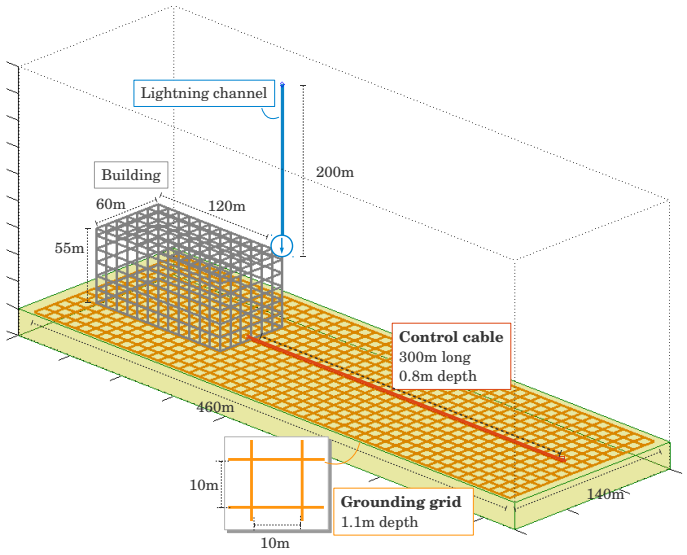

Figure 2.41: Study case of a buried cable connected to a building stroke by lightning

The IM cable is 300 m long, buried 0.8 m deep, with geometry depicted in figure 2.42a. In this case, a coaxial cable is considered. The shield and the core are both copper conductors with 11.3 mΩ and 5.488 $m\Omega$ of linear resistance respectively. It has a transfer impedance of $Z_{T,l} = 10m\Omega + j\omega 1\mu H$ and null transfer admittance. As a first instance, the terminations are going to be considered connected to two auxiliary ideal bare wires: one for the shield and one for the core, as depicted in figures 2.43a and 2.43b, one cable connects the shield to the grounding grid directly, while the other connects the core to a 50 Ω series resistance, which represents the impedance of the electronic equipment, this element is also connected to the grounding grid. The cable is the structure of main interest, therefore results will be given considering the currents along the path and the voltages at the 50 Ω terminations.

The building is a $60\times120\times55\,m^3$ meshed structure, with $5\times5\,m^2$ grids, modeled with bare ideal thin wires of 60 mm diameter. No grid is considered in the lower XY plane, the conductors of the building connect directly to the grounding grid. The grounding system is a perfectly metallic grid of 460x140 m^2, with buried conductors of 15.35 mm diameter, at 1.1 m in a soil of 800 Ωm of resistivity, and $10\varepsilon_0$ permittivity. Each mesh has a size of $10\times10\,m^2$.

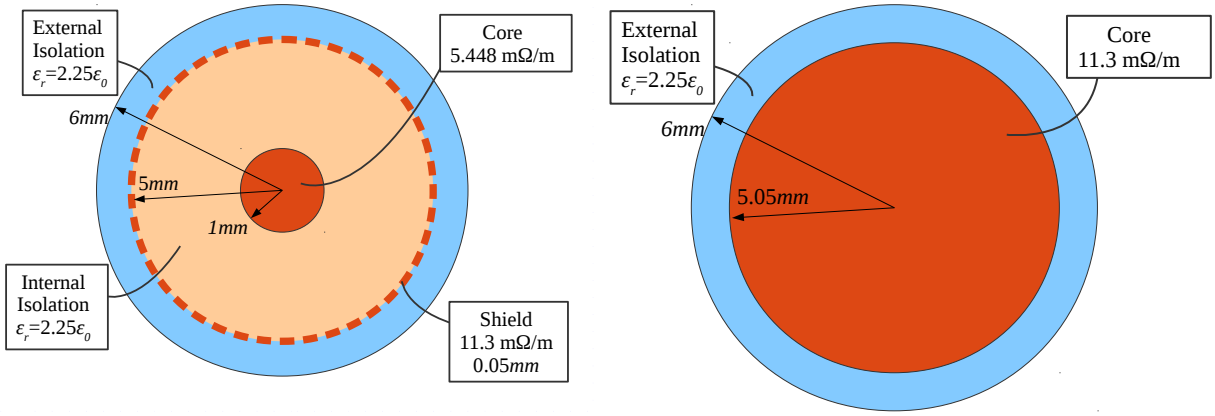

(a) Coaxial cable **(b) Equivalent single core cable**

Figure 2.42: Geometry and material properties of the cable under study

Finally, the lightning channel is a 200 m long, bare conductor with 20 cm of diameter and $1\Omega/m$ of linear losses, with a Heidler current source at the bottom. The source corresponds to a normalized subsequent stroke with a 50 kA magnitude. The channel is terminated in the PML frontier [35].

2.7.2 Validation of the FDTD Thin Wire Model

The comparison against the MoM tool is depicted in figure 2.44, which shows the currents in a single core cable at different distances, measured from the point in which the cable is connected to the building. We observe the behavior of the currents along a wide spectrum of the excitation. The currents are normalized with respect to the source in the frequency domain.

As shown in figure 2.44, there is a good agreement between both methods. We observe a resonance point at around 50 kHz which may be due to the longest conductor element: the grounding grid. This element is embedded in a soil with relative permittivity of 10 and conductivity of 800 Ωm, and the length of its diagonal is 480.8 m, which approximately corresponds to one quarter of the wavelength at 50 kHz. Also, slight differences appear between both responses which can be explained by:

- The different lightning channel model used: an "infinite" channel for the FDTD tool, and a 1 km long channel for the MoM tool. The latter, in order to eliminate

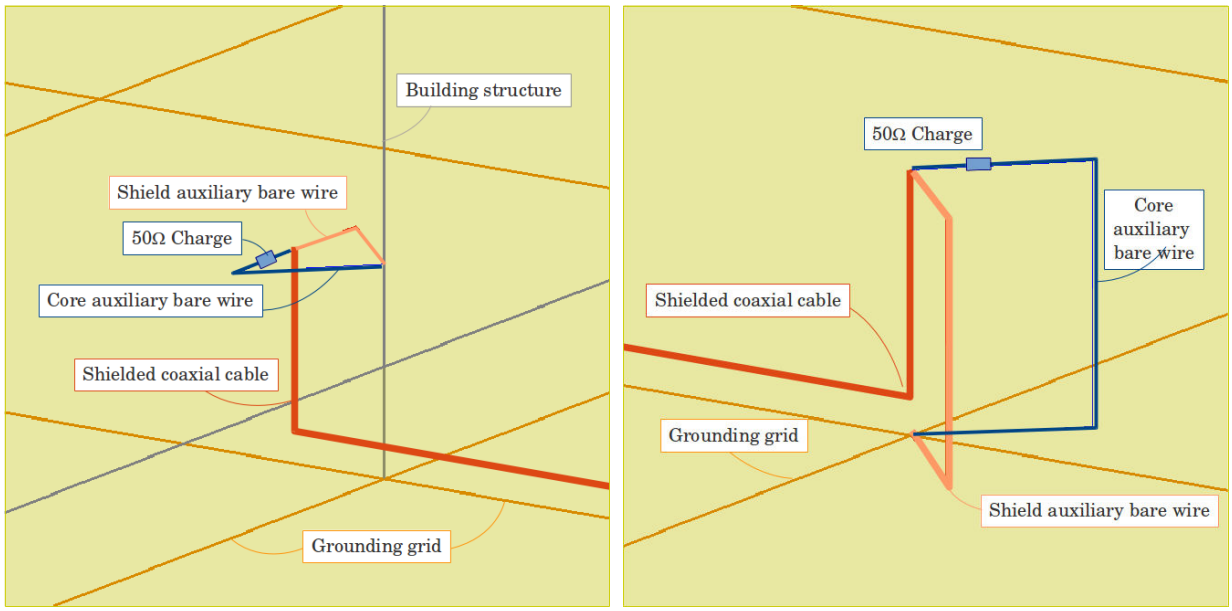

(a) At the building **(b) At 300 m from the building**

Figure 2.43: Details of the terminations in the FDTD case

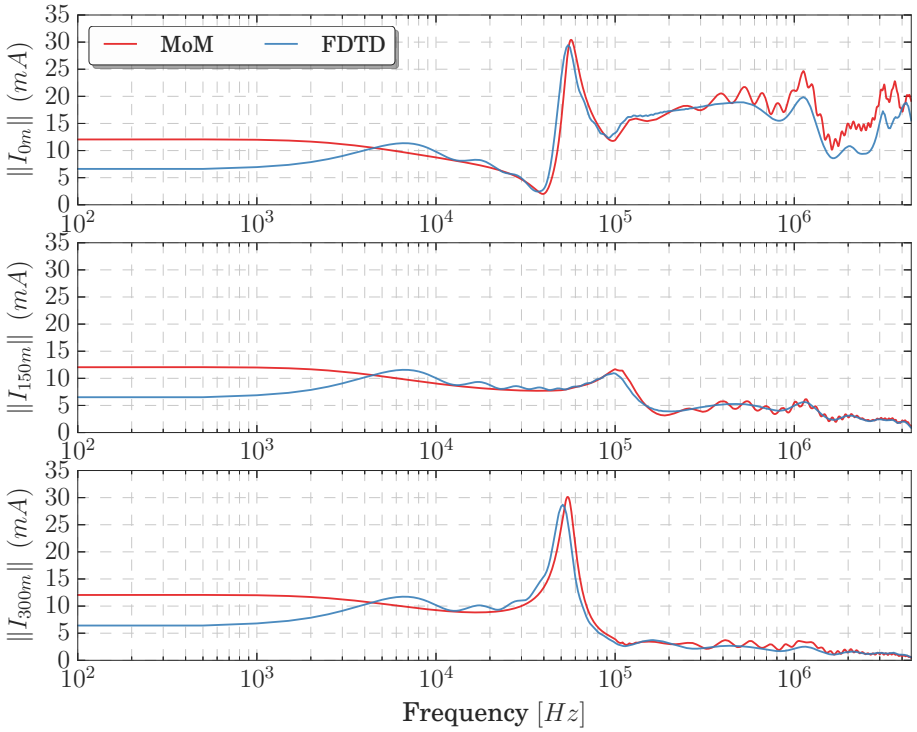

Figure 2.44: Normalized current in the single core cable for two computational tools, at three positions along the cable.

small oscillations at high frequencies. As an example, observe figure 2.45, for an equivalent FDTD case with an open 1 km channel instead of the channel terminated inside the PML frontier, the high frequency response is similarly oscillatory than the MoM response.

- The weak convergence at low frequencies for the FDTD, which depends on the maximum duration of the transient response (1 ms), and the attenuation of the signal at that time. Which produces a smooth breakdown of the FDTD response between 1 kHz and 10 kHz.

However the differences observed in the high frequency band and at the very beginning of the low frequency band, have a slight impact on the transient response of a typical 50 kA subsequent stroke [36], as shown in 2.46. This is due to the fact that not all the frequencies have the same energy content in the spectrum. The transient response is obtained by multiplying the normalized current with the excitation source in the frequency domain and by transforming it to the time domain using an inverse Fast Fourier Transform (FFT) algorithm.

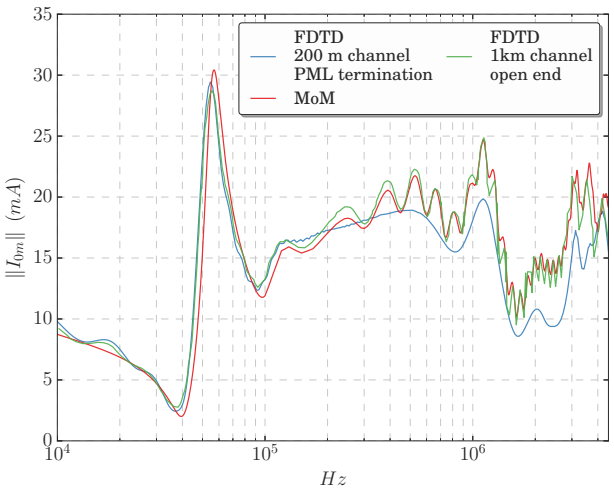

Figure 2.45: Normalized current in the single core cable at the building side. For two different computational tools. Comparison of lightning channel implementations.

It is also worth noting that a simulation of a case study with these dimensions takes several days to solve with the MoM tool in a 2.4 GHz 8 core processor, considering a frequency range from 100 Hz to 5 MHz. In contrast, the FDTD method takes a couple of hours for an observation time of 1 ms. This suggest that the thin wire model makes the FDTD more efficient in terms of computational resources.

2.7.3 Currents in the coaxial cable

Once the thin wire technique has been validated, it is used to consider the coaxial cable model described in 2.2.3. First, the currents in the shield of the coaxial cable

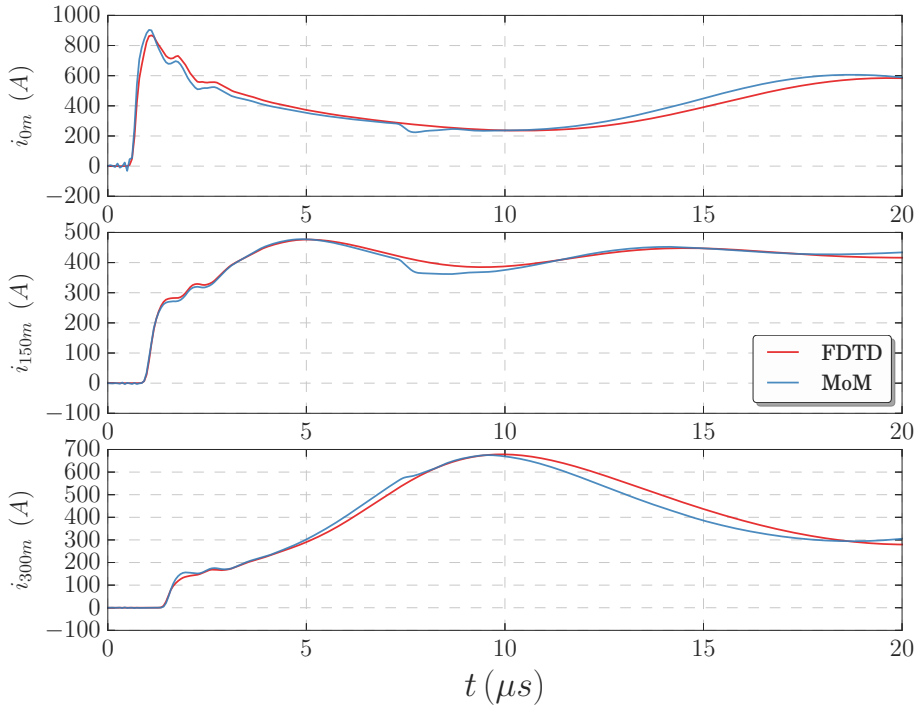

Figure 2.46: Transient current in the single core cable for two computational tools, at three positions along the cable.

and in the core of an equivalent insulated cable (see figure 2.42b) are compared at three different points along the cable path. Results are shown in 2.47. As expected, there is no difference between both observed currents.

The current obtained in the core of the coaxial cable is given in 2.48. As it can be observed: the peak magnitude of the current in the core is about four times smaller than in the shield, as well as the damping of the oscillations in the core is 20 times faster. This shows the influence on the shield in diminishing the external inductions along the cable path.

2.7.4 Voltages at the extremities of a coaxial cable

Finally, as mentioned in section 2.7.1, it is of interest to know the transient voltage at the equipment location. For this study the effect of shielding will be examined. To do this, three different cases will be considered:

- The reference case study of a cable connected to two auxiliary wires with a non-perfect shield (Figure 2.49a).
- The cable with perfect shielding (No transfer impedance) terminated in two separated auxiliary wires (Figure 2.49b).
- The cable terminated directly in the 50 Ω loads (inner the shield), which implies no outgoing wires for the core, only one conductor from the shield to the ground

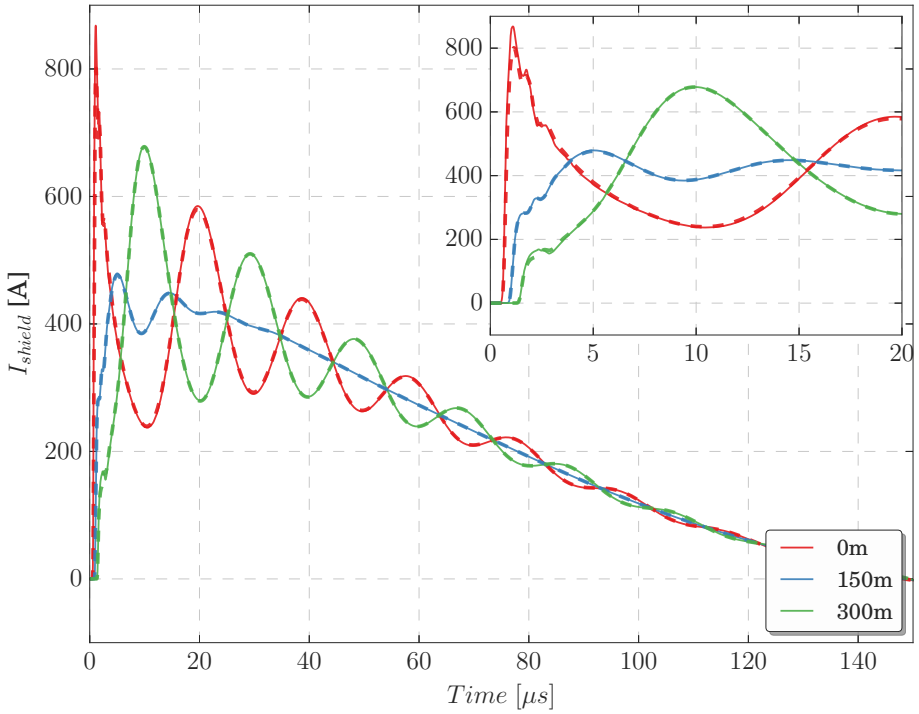

Figure 2.47: Transient current in the conductor of a single core cable (solid line) and in the shield of an equivalent coaxial cable (dotted line).

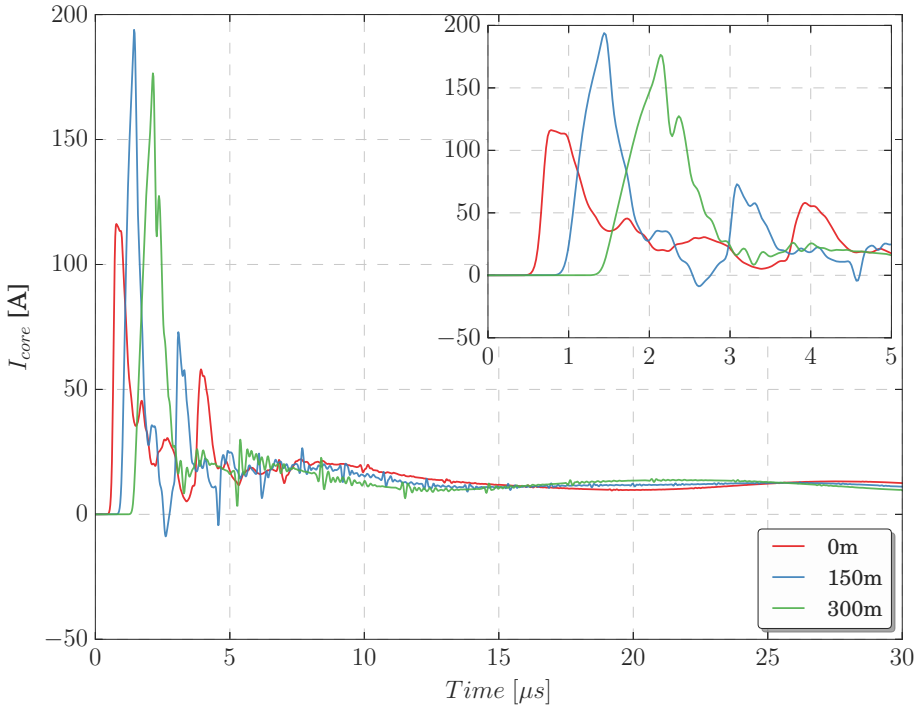

Figure 2.48: Transient current in the core conductor of the coaxial cable.

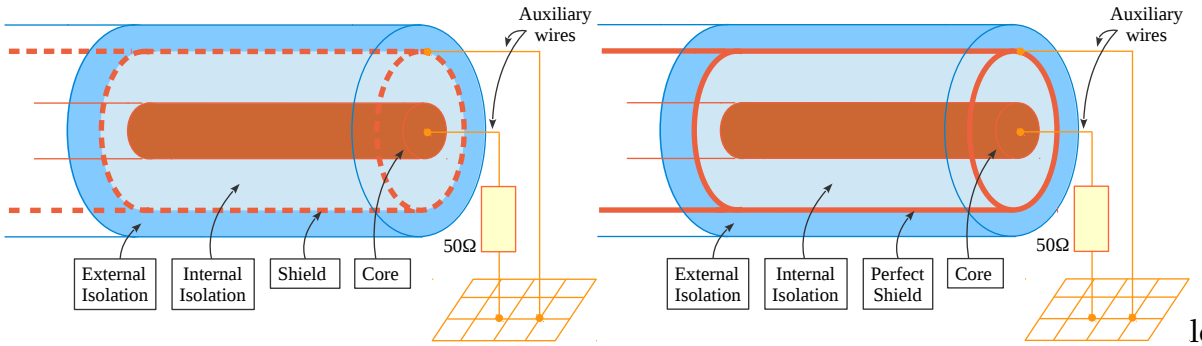

(a) Non-perfect shield with auxiliary wires. **(b) Perfect shield with auxiliary wires.**

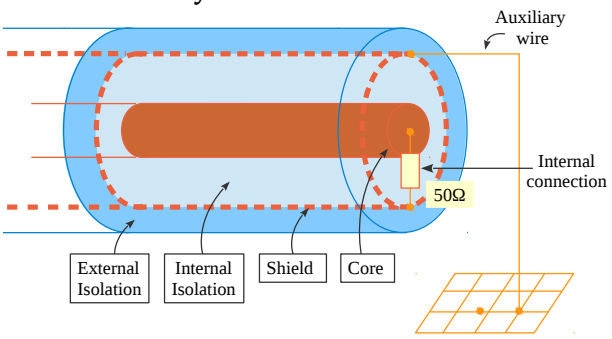

(c) Non-perfect shield without core auxiliary wire.

Figure 2.49: Variations on the connection of the termination impedance

location (Figure 2.49c).

The results of the voltage computation are shown in figure 2.50, they depict a higher rise-time in the cases in which the auxiliary wire is physically connecting the core to the grounding grid (2.49a and 2.49b), this implies that the aforementioned connection permits the circulation of high frequencies perturbations. Therefore, when considering coaxial cables, it is suggested to not include the auxiliary wire for the core, as indicated in 2.49c.

Finally, in the cases related to 2.49a and 2.49c, it can be observed a slow decay time, which indicates that the presence of a non-perfect shield allows for the penetration of low frequency perturbations.

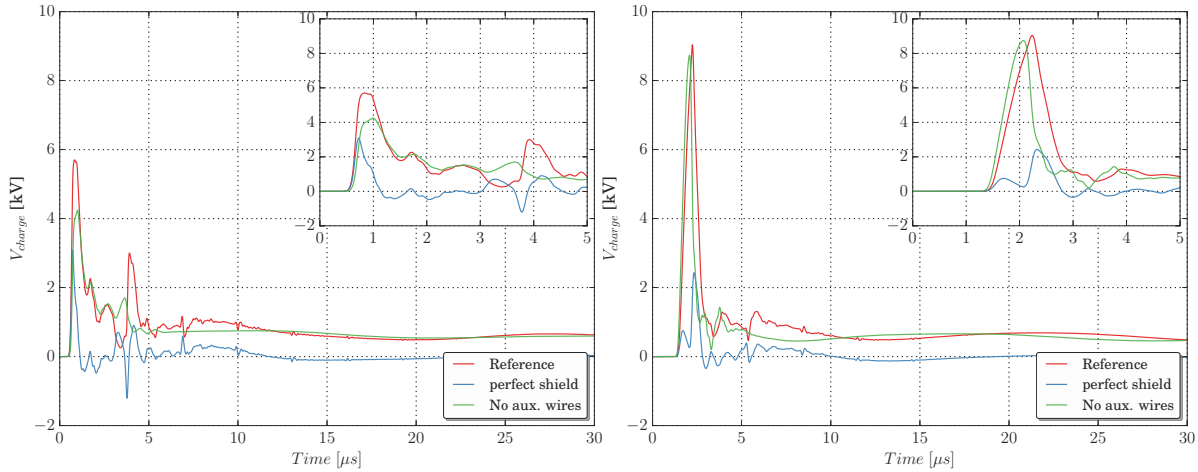

(a) At the building side **(b) At 300 m from the building**

Figure 2.50: Transient voltage at the 50 Ω load in the terminations.

2.8 Conclusions

In this chapter, the electromagnetic conception of a lightning impact to a Power Production Center was decomposed into four main structures: The building, the grounding grid, the lightning strike and the IM cable. Each structure was modeled using different implementations of the thin wire formalism of Holland, to finally validate it as a feasible, reliable, and computationally efficient tool to assess the problem at task.

In the next section, the problem is going to be analyzed in detail, considering the influences of different parameters in the behavior of the transient voltages at the extremities of the coaxial cable.

References

[1] Allen Taflove and Susan C Hagness. *Computational Electrodynamics: The Finite-Difference Time-Domain Method*. 3 edition. Boston: Artech House, May 2005. ISBN: 9781580538329.

[2] K S Yee. "Numerical solution of initial boundary value problems involving Maxwells equations in isotropic media". In: *IEEE Trans. Antennas Propag.* 14.3 (1966), pp. 302–307.

[3] Yoshihiro Baba, N. Nagaoka, and A. Ametani. "Modeling of Thin Wires in a Lossy Medium for FDTD Simulations". In: *IEEE Transactions on Electromagnetic Compatibility* 47.1 (Feb. 2005), pp. 54–60. ISSN: 0018-9375. DOI: 10.1109/TEMC.2004.842115.

[4] C J Railton, D L Paul, and S Dumanli. "The Treatment of Thin Wire and Coaxial Structures in Lossless and Lossy Media in FDTD by the Modification of Assigned Material Parameters". In: *IEEE Transactions on Electromagnetic Compatibility* 48.4 (Nov. 2006), pp. 654–660. ISSN: 0018-9375. DOI: 10.1109/TEMC.2006.884452.

[5] Y Taniguchi et al. "Modification on a Thin-Wire Representation for FDTD Calculations in Nonsquare Grids". In: *IEEE Transactions on Electromagnetic Compatibility* 50.2 (May 2008), pp. 427–431. ISSN: 0018-9375. DOI: 10.1109/TEMC.2008.921034.

[6] Richard Holland and Larry Simpson. "Finite-Difference Analysis of EMP Coupling to Thin Struts and Wires". In: *IEEE Trans. Electromagn. Compat.* EMC-23.2 (1981), pp. 88–97. ISSN: 0018-9375. DOI: 10.1109/TEMC.1981.303899.

[7] Christophe Guiffaut, Alain Reineix, and Bernard Pecqueux. "New Oblique Thin Wire Formalism in the FDTD Method With Multiwire Junctions". In: *IEEE Trans. Antennas Propag.* 60.3 (2012), pp. 1458–1466. ISSN: 0018-926X. DOI: 10.1109/TAP.2011.2180304.

[8] C Guiffaut et al. "New thin coated wire formalism for {FDTD} method". In: *2011 Int. Conf. Electromagn. Adv. Appl.* 2011, pp. 386–389. DOI: 10.1109/ICEAA.2011.6046371.

[9] Christophe Guiffaut and Alain Reineix. "Des fils obliques pour une modélisation conforme et sans maillage des câbles dans la méthode FDTD. Bilan et extensions". In: *17ème Colloq. Int. Expo. sur la Compat. Electromagnétique - CEM 2014*. Clermont-Ferrand, France, 2014.

[10] Frederick M. Tesche and Torbjörn Karlsson. *EMC Analysis Methods and Computational Models*. 1997, p. 623. ISBN: 047115573X.

[11] Edward F. Vance. *Coupling to Shielded Cables*. 1st. Wiley, 1978, p. 183. ISBN: 0471041076.

[12] B. Gustavsen and A. Semlyen. "Rational approximation of frequency domain responses by vector fitting". In: *IEEE Trans. Power Deliv.* 14.13 (1999), pp. 1052–1061.

[13] Christophe Guiffaut, Alain Reineix, and Bernard Pecqueux. "Extension du formalisme des fils obliques minces aux câbles blindés dans la méthode FDTD". In: *17ème Colloq. Int. Expo. sur la Compat. Electromagnétique - CEM 2014*. Rouen, France, 2012, Session 4C.

[14] Vladimir A Rakov and Farhad Rachidi. "Overview of recent progress in lightning research and lightning protection". In: *Electromagn. Compat. IEEE ...* 51.3 (2009), pp. 428–442.

[15] Carlo Alberto Nucci et al. “Lightning return stroke current models with specified channel-base current: A review and comparison”. In: *J. Geophys. Res.* 95.D12 (1990), p. 20395. ISSN: 0148-0227. DOI: 10.1029/JD095iD12p20395.

[16] Y. T. Lin et al. “Characterization of lightning return stroke electric and magnetic fields from simultaneous two-station measurements”. In: *J. Geophys. Res.* 84.C10 (1979), p. 6307. ISSN: 0148-0227. DOI: 10.1029/JC084iC10p06307.

[17] Vladimir A. Rakov and Martin A. Uman. “Lightning Return Stroke Models Including Some Aspects of Their Application”. In: *IEEE Trans. Power Deliv.* 40.4 (1998), pp. 403–426.

[18] Yoshihiro Baba and Vladimir a. Rakov. “Electromagnetic models of the lightning return stroke”. In: *J. Geophys. Res.* 112.D4 (Feb. 2007), p. D04102. ISSN: 0148-0227. DOI: 10.1029/2006JD007222.

[19] Yoshihiro Baba and Vladimir a. Rakov. “Electric and Magnetic Fields Predicted by Different Electromagnetic Models of the Lightning Return Stroke Versus Measured Fields”. In: *IEEE Trans. Electromagn. Compat.* 51.3 (Aug. 2009), pp. 479–487. ISSN: 0018-9375. DOI: 10.1109/TEMC.2009.2019122.

[20] Vladimir A. Rakov and Martin A. Uman. *Lightning: Physics and Effects*. Vol. 2007. 2007, p. 687. ISBN: 0521035414.

[21] Peter Bannister. *Simplified expressions for the electromagnetic fields of elevated, surface, or buried dipole antennas*. Newport R.I.: Naval Underwater Systems Center Newport Laboratory, 1987.

[22] Vernon Cooray. *Lightning Electromagnetics*. 1st. Institution of Engineering & Technology, 2012, p. 950. ISBN: 978-1-84919-215-6.

[23] Christophe Guiffaut and Alain Reineix. “Cartesian shift thin wire formalism in the FDTD method with multiwire junctions”. In: *Antennas Propagation, IEEE ...* 58.8 (2010), pp. 2658–2665.

[24] Masaru Ishii, Keiji Miyabe, and Akiyoshi Tatematsu. “Induced voltages and currents on electrical wirings in building directly hit by lightning”. In: *Electr. Power Syst. Res.* 85 (Apr. 2012), pp. 2–6. ISSN: 03787796. DOI: 10.1016/j.epsr.2011.07.001.

[25] F. Heidler. “Analytische Blitzstromfunktion zur LEMP Berechnung”. In: *18th Int. Conf. Light. Prot. (ICLP 1985), Munich* (1985), pp. 63–66.

[26] International Electrotechnical Commission (IEC). *IEC 62305-1. Protection against lightning. Part 1: General principles*. 2010.

[27] Taku Noda and Shigeru Yokoyama. “Thin Wire Representation in Finite Difference”. In: *IEEE Trans. Power Deliv.* 17.3 (2002), pp. 840–847.

[28] Nelson Theethayi et al. “External impedance and admittance of buried horizontal wires for transient studies using transmission line analysis”. In: *IEEE Trans. Dielectr. Electr. Insul.* 14.3 (June 2007), pp. 751–761. ISSN: 1070-9878. DOI: 10.1109/TDEI.2007.369540.

[29] Leonid D. Grcev. “Computer analysis of transient voltages in large grounding systems”. In: *IEEE Trans. Power Deliv.* 11.2 (1996), pp. 815–823. ISSN: 08858977. DOI: 10.1109/61.489339.

[30] Ken Otani et al. “FDTD surge analysis of grounding electrodes considering soil ionization”. In: *Electr. Power Syst. Res.* 113 (2014), pp. 171–179. ISSN: 03787796. DOI: 10.1016/j.epsr.2014.02.032.

[31] Akiyoshi Tatematsu and Taku Noda. “Three-dimensional FDTD calculation of lightning-induced voltages on a multiphase distribution line with the lightning arresters and an overhead shielding wire”. In: *IEEE Trans. Electromagn. Compat.* 56.1 (2014), pp. 159–167. ISSN: 00189375. DOI: 10.1109/TEMC.2013.2272652.

[32] R Fieux, P Kouteynikoff, and F Villefranque. “Measurements of Impulse Response of Grounding to Lightning Currents”. In: *Int. Conf. Light. Prot.* Uppsala, Sweden, 1979.

[33] S. Sekioka et al. “Measurements of grounding resistances for high impulse currents”. In: *IEE Proc. - Gener. Transm. Distrib.* 145 (1998), p. 693. ISSN: 13502360. DOI: 10.1049/ip-gtd:19982009.

[34] Luis Diaz et al. “FDTD transient analysis of grounding grids. A comparison of two different thin wire models”. In: *IEEE International Symposium on Electromagnetic Compatibility and EMC Europe*. Dresden, Germany, 2015.

[35] Jean-Pierre Berenger. “A perfectly matched layer for the absorption of electromagnetic waves”. In: *Journal of Computational Physics* 114.2 (Oct. 1994), pp. 185–200. ISSN: 0021-9991. DOI: 10.1006/jcph.1994.1159.

[36] Fridolin H. Heidler et al. “Parameters of Lightning Current given in IEC 62305. Background, Experience and Outlook”. In: *29th Int. Conf. Light. Prot.* June (2008), pp. 1–22.

Chapter 3

Parametric Study of a Lightning Impact to a Large Industrial Site

3.1 Introduction

As it has been stated, the interest of this work is to assess the behavior of the voltages that develop at the extremities of a Instrumentation & Measurement (IM) cable when a lightning strikes its building. In the previous chapter, was introduced the conception of all the components interacting in a FDTD solution of this problem. In this chapter, the details concerning the configurations, materials, dimensions and properties of particular components are going to be inspected.

The interest is to detail the influence of each element interacting in the phenomenon, to infer its importance as a design parameter to consider in numerical simulations or system construction.

This kind of study aims to serve as a ground and guidance to the establishment of the parameters to consider in the future meta-model of the problem, if they ought to be included, and how are they going to be considered; their nature and boundaries.

The selection of parameters is a compilation between a-priori ubiquitous variables, and variables of interest to conceptualize the lightning protection system of the Power Generation Center (PGC):

- The lightning current at the channel base.
- The soil resistivity.
- The type of canalization of the IM cable.
- The building size.
- The grounding connections of the external concrete cable duct.
- The connections to ground of the shield of the coaxial cable

- The external grounding system configuration.
- The length of the IM cable.
- The point of strike of the lightning in the building.
- The EM model for the building wall.
- The inclusion of cable trays inside the concrete cable duct.
- The inclusion of the expansion joints between concrete cable ducts.

In order to perform the parametric study, it is necessary to establish a reference case, to compare all the variations and cases mentioned. Therefore, the first section of this chapter is going to discuss this reference case. Afterwards, the subsequent sections will describe the influence of each of the previously mentioned parameters.

3.2 The reference case

The main case study is depicted in figure 3.1. At the center of the volume of computation is a building with a cubic structure of 50 m×50 m×50 m, composed of grids of 5 m×5 m of steel beams of 3 cm of radius and 0.269 $m\Omega/m$ of linear losses. The foundations of the building are buried at 5 m in the ground.

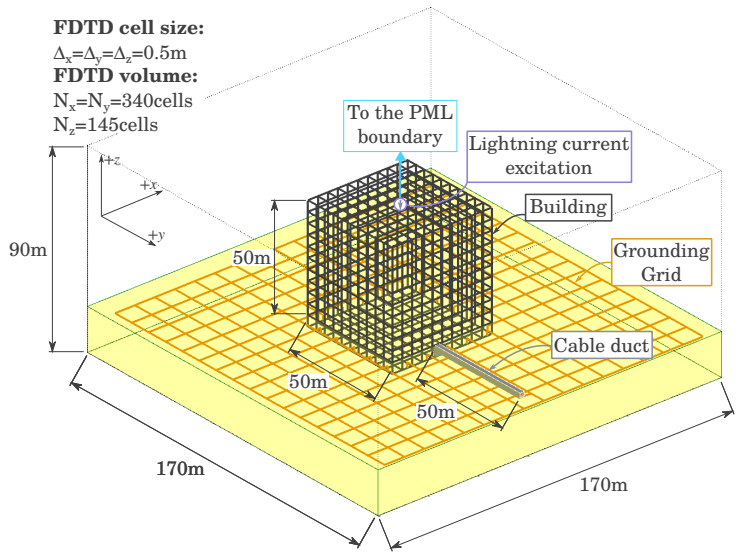

Figure 3.1: Main case of study, a 50 m cubic building hit by lightning, with one 50 m IM cable inside a buried cable duct.

The foundations of the building are connected to an external grounding grid with meshes of 10 m×10 m, constructed with bare copper conductors of 185 mm of section and 93.84 $\mu\Omega/m$ of linear losses.

At one side of the building a buried concrete duct leaves, within a IM cable inside, this duct is a 50 m long structure, with a transversal surface of 2 m×2 m constructed with bare steel beams of 1 cm of radius, separated 50 cm. As indicated in the figure 3.2.

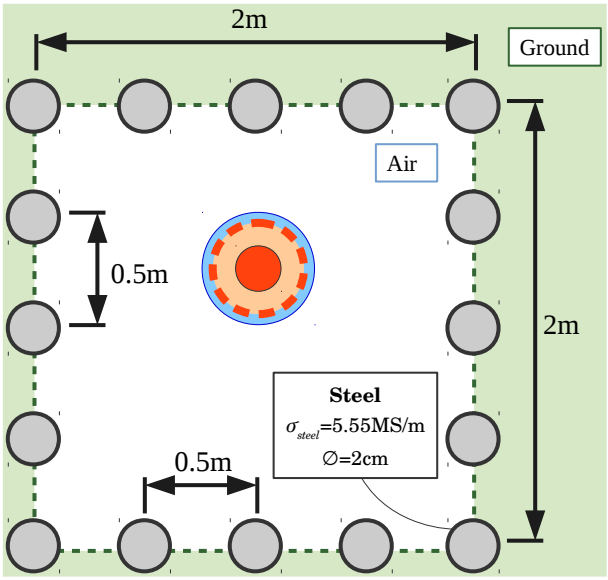

Figure 3.2: Transversal view of the cable duct under study.

For the reference case, one extremity of the cable duct is connected to the building, and the other extremity to the grounding system, as suggested by figure 3.3. The concrete around the beams is not considered, therefore they are directly in contact with the soil.

The IM cable is modeled as a mono-polar coaxial conductor, with configuration depicted in 2.42a. It has a non-perfect shield, therefore; a coupling from the shield to the core occurs. This coupling is represented by a transfer impedance with a simple inductive model of $Z_{T,l} = 1m\Omega + j\omega 10^{-8}H$.

The shield and the core are made of copper with $1.72{\cdot}10^{-8}\,\Omega$m. The material for both insulations jackets is an homogeneous lossless dielectric of $\varepsilon = 2.25\varepsilon_0$.

At the end of the coaxial cable, the electronic equipment of interest is going to be modeled with a 50 Ω load, which is connected between the shield and the core, following the configuration depicted in figure 2.49c from section 2.7.4. In this manner, only an auxiliary copper conductor is used to connect the shield to the cable duct, as depicted in figure 3.3a.

This model of termination implies that the voltages observed at the electronic equipment are a direct consequence only from the induction of the current flowing through the shield, by the means of the transfer impedance. Therefore, no external conductive component is considered.

The soil is an homogeneous lossy medium of 100 Ωm with permittivity ε_0 and permeability μ_0.

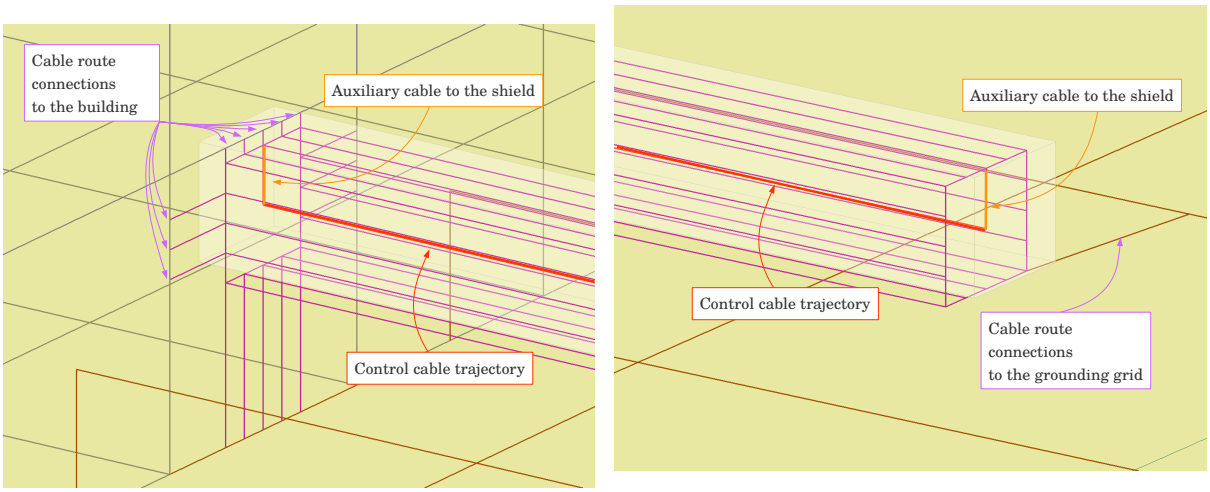

(a) At the building side

(b) At the remote termination from the building

Figure 3.3: Details of the terminations of the cable duct

The lightning strikes the top center of the building, a single bare conductor of 10 cm of radius and 1 Ω/m of losses is used as return stroke channel. An ideal current source is at the channel base. This model for the lightning channel is selected since requires less computational resources, and it has also been observed that from the perspective of the transient voltages at the termination loads, this model does not represent a significant difference with regard to more complex EM models of the lightning channel.

In the following sections, the parametric study is described in detail.

3.3 Effect of the current at the channel base

To evaluate the effects of lightning to protect equipment, different type of excitation currents are usually recommended, this work considers the three current types suggested in the KTA-2206 standard, and described in section 1.4.1. These are: a positive first stroke, a negative first stroke, and a negative subsequent stroke.

To fully illustrate the induction of voltages in the extremities of the IM cable, it is interesting to observe the currents flowing through the cable duct and in the shield of the cable. The first, is shown in figure 3.4c, indicating the current at the building side flowing to the cable duct, this current is the addition of all the currents flowing from each of the sixteen steel beams composing the cable duct.

Regarding the current flowing through the cable duct at the building side, it can be appreciated that division ratio of the currents from the lightning channel to the cable duct is independent of the type of excitation used. Observing the peak of the currents in table 3.1, it can be seen that for all the lightning current types, the ratio with respect to the excitation is similar. Which is in agreement with the basis of the

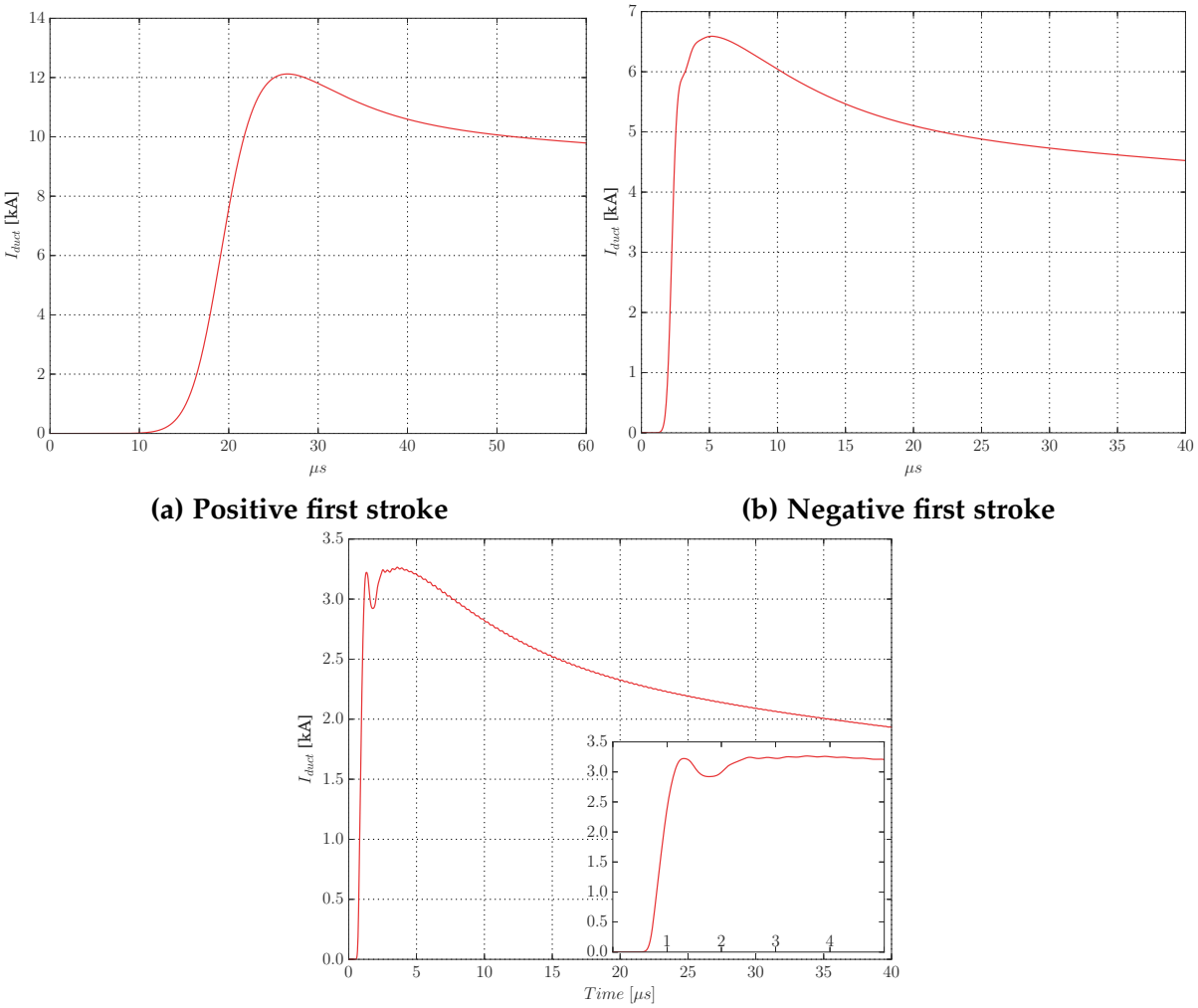

(a) Positive first stroke

(b) Negative first stroke

(c) Negative subsequent stroke

Figure 3.4: Current flowing through the cable duct at the building side. For the case depicted in figure 3.1

standard KTA-2206 [1].

The above reinforced with the comparison of rise-times indicated in table 3.2, which suggests that; although there is a reasonable delay between the times, the order of magnitude is not highly affected.

Excitation	$\max(I_B)$	$\max(I_{duct})$	$\max(I_B)/\max(I_{duct})$
Positive first stroke	200 kA	12.12 kA	16.5
Negative first stroke	100 kA	6.32 kA	15.82
Negative subsequent stroke	50 kA	3.27 kA	15.3

Table 3.1: Ratio of current division from the channel base to the cable duct.

Excitation	$t_f\,(I_B)\,[\mu s]$	$t_f\,(I_{duct})\,[\mu s]$
Positive first stroke	9.98	8.9
Negative first stroke	0.994	1.44
Negative subsequent stroke	0.256	0.50

Table 3.2: Rise time of the current at the channel base and at the entrance of the cable duct.

The above suggest that, in order to study the induced voltages of a cable inside a cable duct, it is not a bad approximation to consider that the transient behavior of the current entering to the cable duct is proportional to the current at the channel base, as it is inferred from the procedure recommended in the KTA standard.

The current circulating through the cable duct induces a current in the shield of IM cable, at the same time; this current is also subject to a conductive component coming from the bare auxiliary wire connected at its termination.

In figure 3.5 the current in the shield can be appreciated. Here, the positive and negative first stroke are only presented at the building side, since the transients at both sides does not show a distinction between. Nevertheless, for the negative subsequent stroke, these differences are slightly observable, as indicated in figures 3.5c and 3.5d.

Observing the current in the shield, when the building is hit by a negative subsequent stroke a resonance frequency appears. This resonance has a value of 2.83 MHz, which corresponds with a wavelength $\lambda_{resonance}$ =106 m. This is expected since, the cable has a length of 50 m, which roughly gives $L_{cable} \simeq \lambda_{resonance}/2$.

The resonance does not appear for the slower excitations of the positive and negative first stroke, this is due to the low energy of these excitations at the resonance point of a 50 m conductor. In other terms, it can be seen that the transient is sufficiently slow as to superpose its reflections of both extremities.

Finally, it is worth noting that the above resonance frequency corresponds with a velocity of propagation $v_\phi = c$, which is only possible in a medium with permittivity $\varepsilon = \varepsilon_0$. As consequence, the resonance observed at the loads cannot

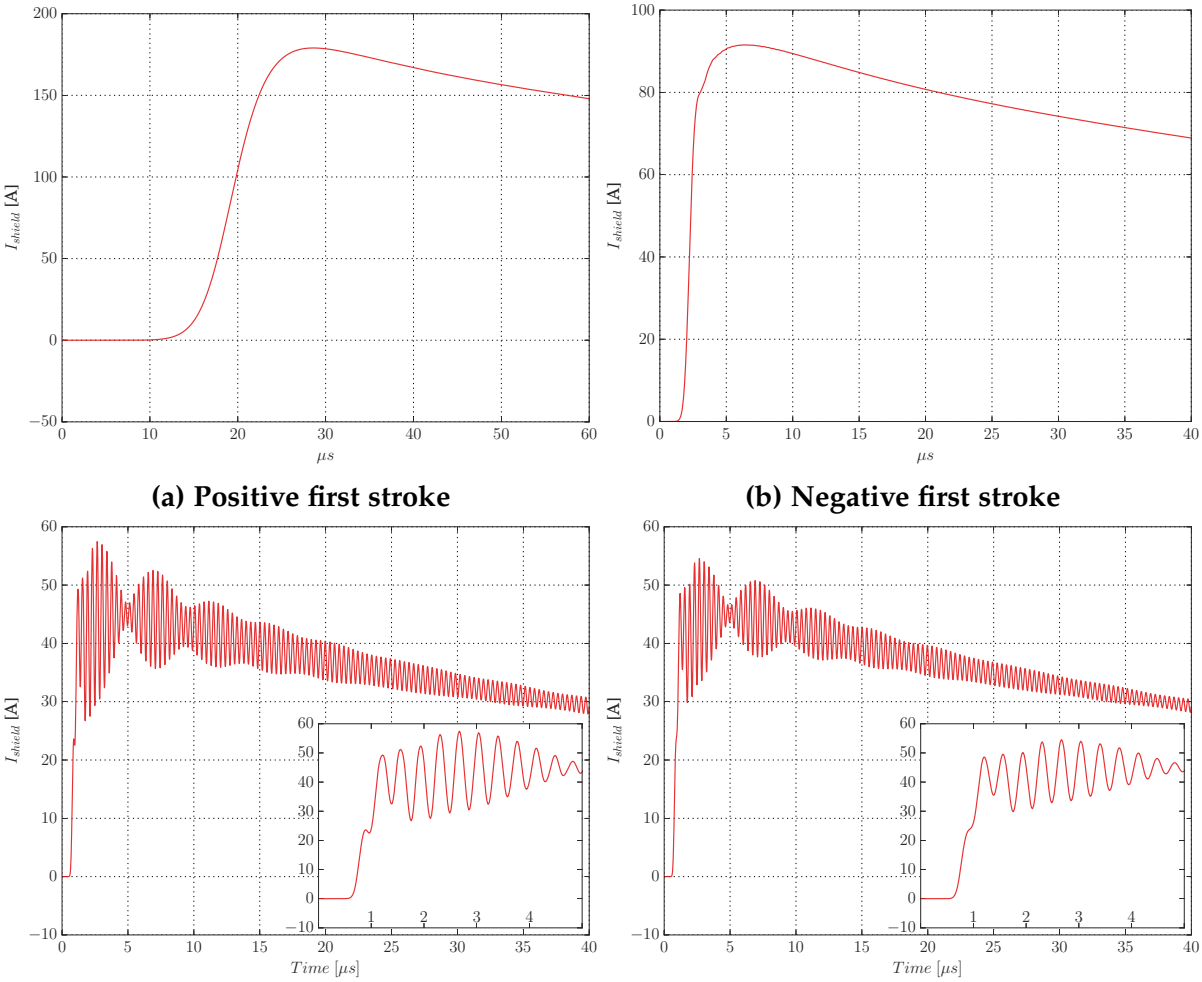

(a) Positive first stroke

(b) Negative first stroke

(c) Negative subsequent stroke - At the building side

(d) Negative subsequent stroke - At 50 m from the building

Figure 3.5: Current flowing through the cable shield. For the case depicted in figure 3.1

be originated inside the coaxial cable, since the shield and the core are isolated with an homogeneous lossless dielectric material with $\varepsilon_{ins} = 2.25\varepsilon_0$. This suggests that the resonance might come from the "coaxial configuration" between the cable duct and the shield of the coaxial cable.

The above suggestion can be explained if we observe the current in the shield and the current in the cable duct, in figures 3.5c and 3.4c respectively. In figure 3.5c, the oscillations are of the same nature than in figures 3.6c and 3.6d. Therefore, suggesting perhaps that the perturbations are also outside the coaxial cable.

We know that the model used to include the coaxial cable inside an FDTD scheme is an uni-directional model. This is, the currents in the core are affected by the currents in the shield, and this relation is not reciprocal. Therefore, taking into account that the resonance is also observed in the shield, we cannot conclude that comes from within the coaxial cable, but outside. Ultimately penetrating to the core through the shield transfer impedance.

This is perhaps the more interesting phenomenon observed, since this resonance has enough energy to travel through the transfer impedance, and induced higher voltages than the ones caused by the positive an negative first strokes, as it can be appreciated in figure 3.6.

From the model of transfer impedance used in this case, it can be expected to observe a voltage in the load with less content of low frequency. To the point that, the excitation with higher frequency content, causes higher transient voltages. At the same time, this is the source that introduces a perturbation caused by a resonant behavior, in this case originated in the equivalent coaxial arrangement of the duct and the shield of the cable.

Finally, it must be noted that, although the positive and negative first strokes have higher peaks, they do not induce the highest voltage at the location of the electronic equipment. In general, because of two main reasons:

- they are slower excitations, with relative low risetimes.
- the coupling of the inner conductor to the external excitation is mainly inductive. To the shield through a transfer impedance with an $R + j\omega L$ model, and the shield to the cable duct through a lossless medium like air.

In general, it can be seen that in terms of understanding the phenomenon, the positive and the negative first strokes give roughly the outcome. Therefore, for simplification, in the rest of the sections of the chapter, only the extreme excitations are going to be considered: the slowest; the positive first stroke, and the fastest; the negative subsequent stroke.

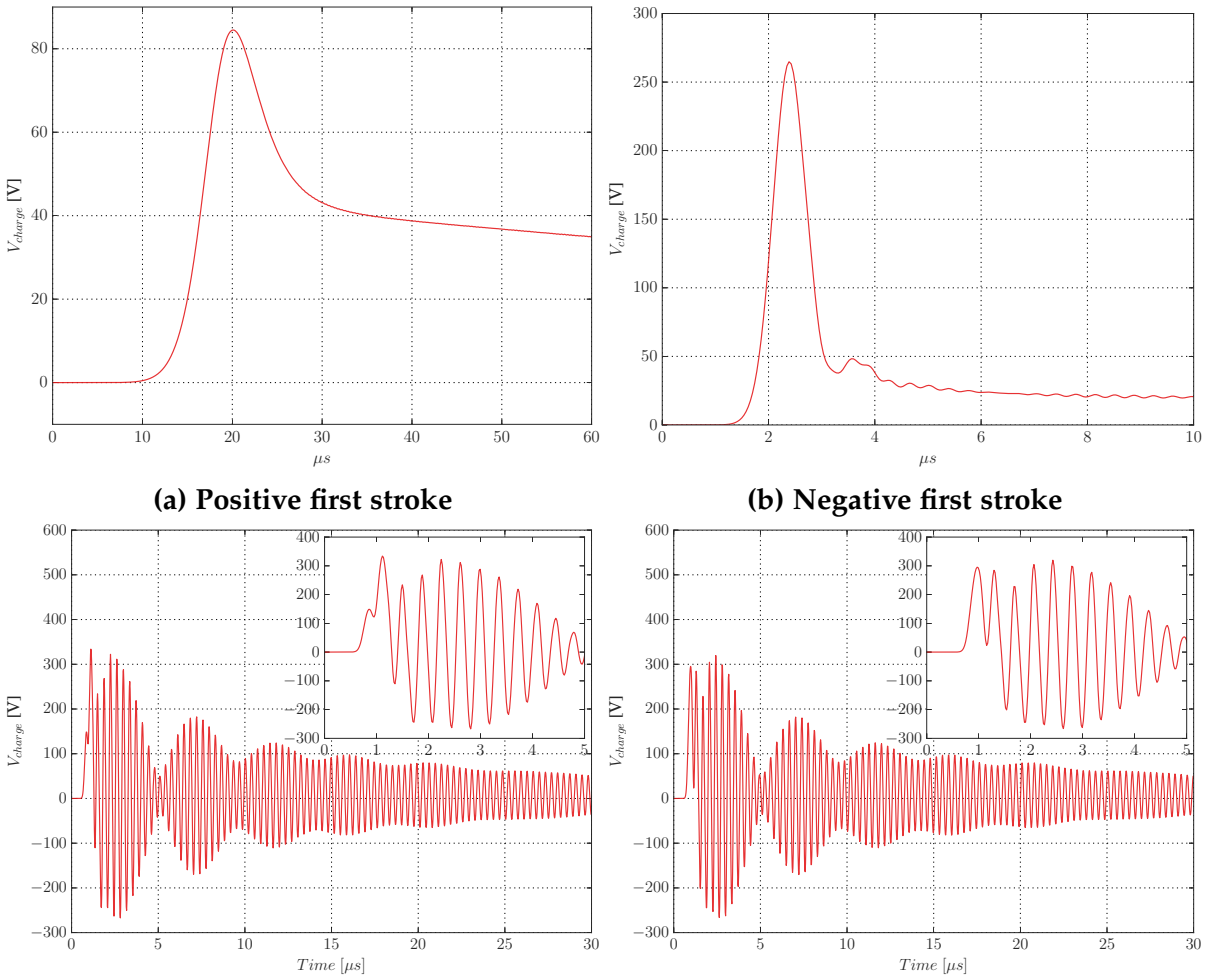

(a) Positive first stroke

(b) Negative first stroke

(c) Negative subsequent stroke - At the building side

(d) Negative subsequent stroke - At 50 m from the building

Figure 3.6: Voltage at the 50 Ω load. For the case depicted in figure 3.1

Synthesis of the effect of the current at the channel base

- The excitations with higher amplitude are the positive and negative first strokes, at the same time they are the slowest excitations, contrary to the negative subsequent stroke.
- The portion of the current that propagates from the channel base, to the cable duct is independent of the type of excitation considered.
- The negative subsequent stroke excites the resonant circuit formed by the coaxial configuration of the cable duct and the shield of IM cable, which suggests a differential mode propagation.
- The resonance has enough energy to penetrate the cable shield, and through the transfer impedance; induces greater voltages at the $50\,\Omega$ load than excitations with much bigger peaks.

3.4 Effect of the ground resistivity

One of the main parameter to include when performing lightning studies, is the resistivity of the soil, especially when the conductors are buried. In the problem treated in this work, the grounding system is an element that cannot be neglected, as that; the soil resistivity plays an important part in its behavior [2, 3].

Therefore, to observe the extent of its influence in the transient voltages in a IM cable; a variation of three values for this parameter are considered, within the range of expected values in French soils: $100\,\Omega$m, $500\,\Omega$m and $1000\,\Omega$m.

Although it is well known that the soil can be characterized with frequency dependent resistivity and permittivity [2], in this work it is considered as an homogeneous medium. Therefore, only a fixed value of the resistivity changes, maintaining the permittivity equal to ε_0 (It has been observed that variations of the permittivity does not significant affect the voltages at the loads). The case study is depicted in figure 3.1.

3.4.1 Transients in a IM cable for different soil resistivities

The voltage at the terminal load at the IM cable is observed in figure 3.7, for the three types of current at the channel base mentioned in the previous section.

As it can be seen, a variation in the soil resistivity has more influence on the peak of the voltages originated by a negative subsequent stroke, and a negative first stroke, than those originated by a positive first stroke.

To illustrate this behavior, it is convenient to observe the currents entering to the cable duct, and the currents in the shield, showed in figures 3.8 and 3.9 respectively.

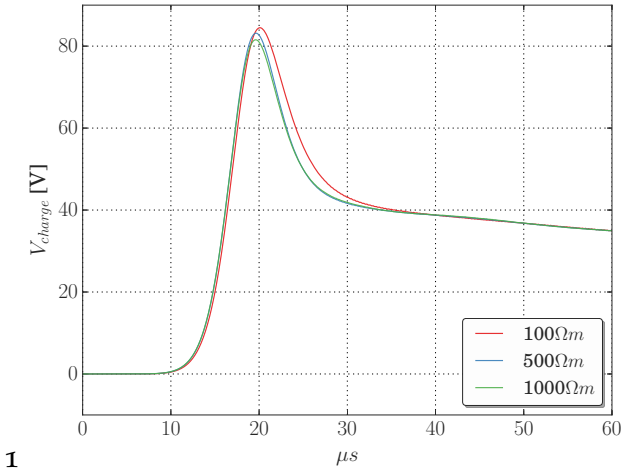

1

(a) Positive first stroke

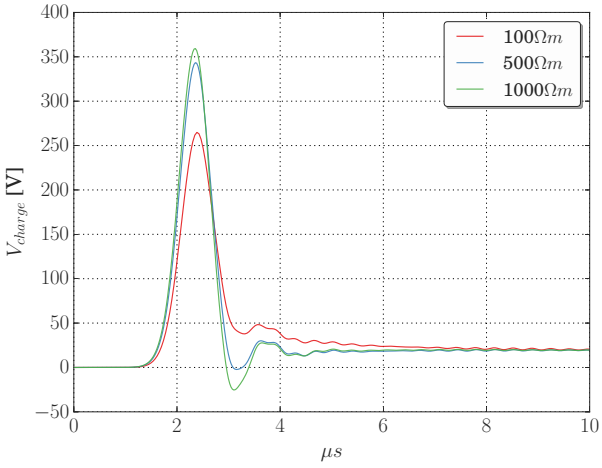

(b) Negative first stroke

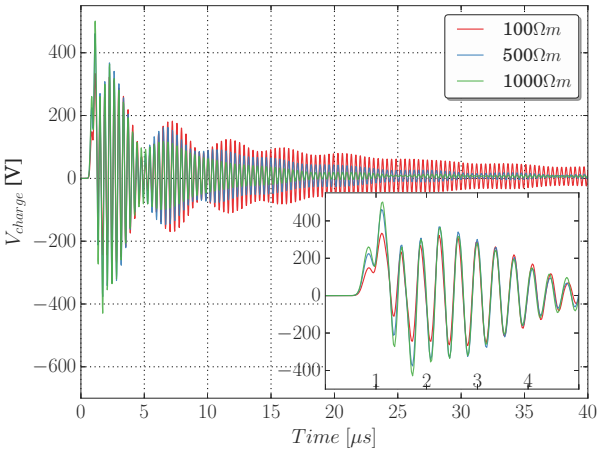

(c) Negative subsequent stroke - At the building side.

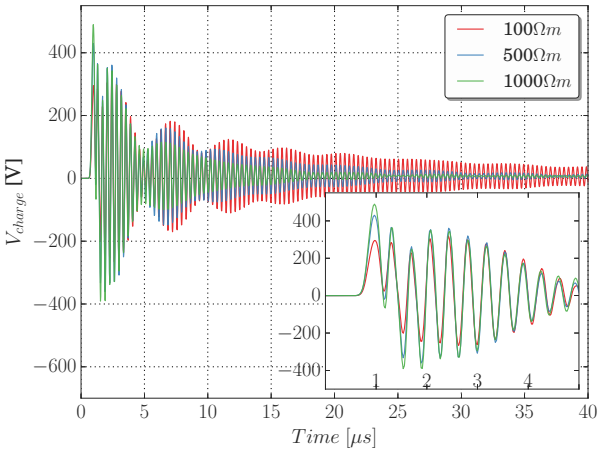

(d) Negative subsequent stroke - At 50 m from the building.

Figure 3.7: Influence of the soil resistivity in the voltage at the 50 Ω load. For the case depicted in figure 3.1

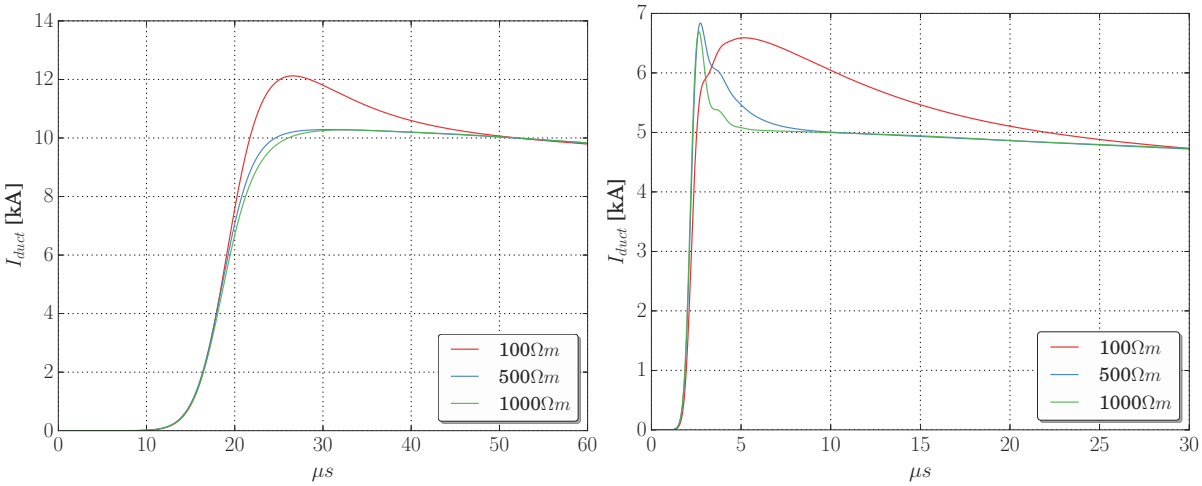

(a) Positive first stroke **(b) Negative first stroke**

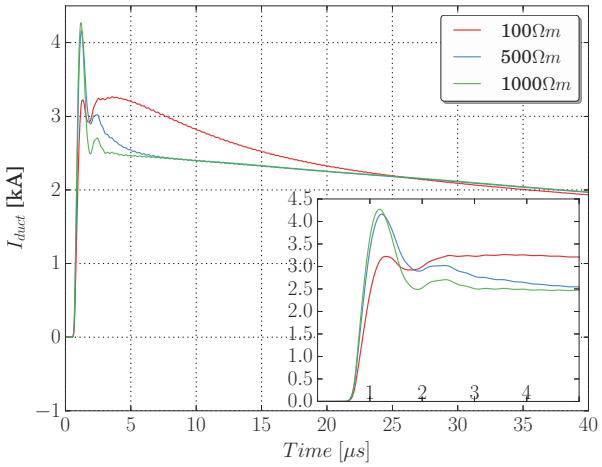

(c) Negative subsequent stroke - At the building side.

Figure 3.8: Influence of the soil resistivity in the current entering to the cable duct from the building. For the case depicted in figure 3.1

The cable duct is composed of bare conductors in direct contact with the soil, therefore, the soil resistivity directly affects its current propagation. The response for soils of 500 Ωm and 1000 Ωm is similar for all the type of currents at the channel base. This suggests that, in general, the range of variation for the soil resistivity to be significant is relatively small, depending on the soil characteristics of the country, and its seasonal variation [4].

In addition, it can be seen that for the slowest excitation, the positive first stroke, the soil of 100 Ωm causes the higher amplitude, which suggest that, the buried duct represents a higher conduction path as the soil resistivity decreases, like the low frequency response of a grounding electrode.

The opposite occurs for fastest excitations, when the soil resistivity is low, less current actually enters the cable duct, since the current propagation to ground from the rest of the buried conductors around the duct, rises. And, at higher values of resistivity, the soil no longer acts as an interesting propagation media, and the inductive and capacitive couplings determine the current propagation through each of the buried metallic structures.

This phenomena has also interesting influence on the rise-time of the currents, it can be seen that, for fastest excitations, the lower the soil resistivity is, the longer the rise-time becomes. Once again, for lower resistivities, more current flows into the ground, and less flows into the cable duct.

The effect on the rise-time is fundamental, since it determines the magnitude of the induction in the cable shield, and as consequence, in the cable core. Figure 3.9 indicates the current flowing in the cable shield.

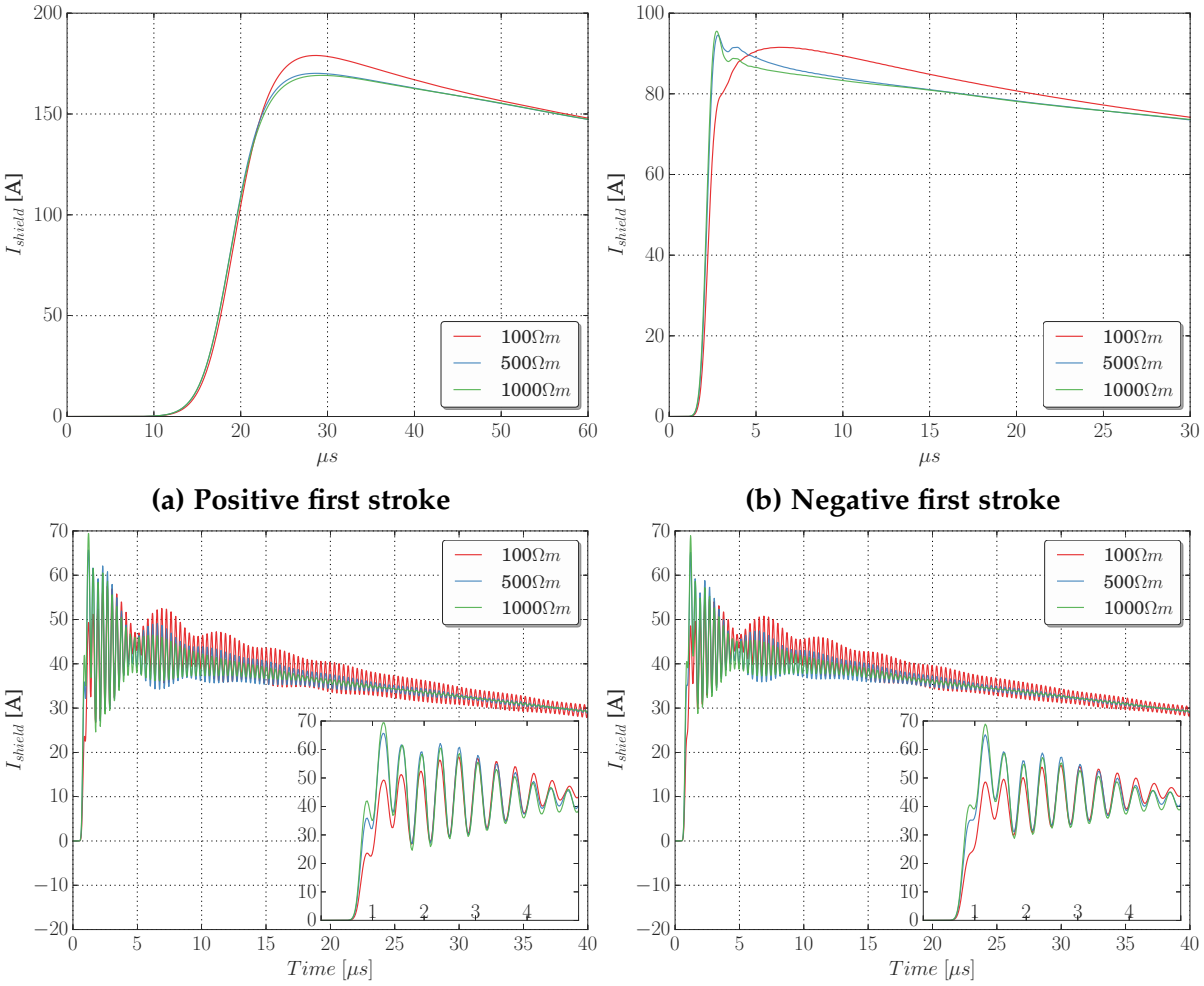

(a) Positive first stroke

(b) Negative first stroke

(c) Negative subsequent stroke - At the building side.

(d) Negative subsequent stroke - At 50 m from the building.

Figure 3.9: Influence of the soil resistivity in the current flowing through the cable shield. For the case depicted in figure 3.1

3.4.2 Synthesis of the effect of the soil resistivity

- The range of variation of the soil resistivity to be influent is relatively small, lower than 500 Ωm.
- The soil resistivity is a parameter that affects the rise-time of the current flowing through the cable duct, in an inverse proportional manner; the higher the resistivity, the lower the rise-time of the current flowing through the cable duct.
- The rise-time of the current entering through the cable duct, is the important parameter to observe; when determining the effect of the soil resistivity in the transient voltages at the ends of the IM cable.
- For a slow excitation like the positive first stroke, the soil resistivity has little influence on the rise-time of the current in the duct, therefore; the induced voltages in the IM cable are not affected in a significant manner. The opposite occurs for the fastest excitations of the negative first and subsequent strokes.

The behaviors observed in this section repeat for the following considerations and case of study of the chapter. Therefore, this parameter is not going to be varied further, and the value to be considered in the rest of the chapter is 100 Ωm, unless indicated the contrary.

3.5 The building size.

One of the first effect of special interest to observe, is the size of the building hit by the lightning. In this section, four scenarios are presented; cubic buildings of 15 m, 35 m, 50 m, and 75 m of side, as depicted in figures 3.1 and 3.10.

The mesh density of the building, length of the cable duct, the geometry of the grounding grid, the soil properties and the configuration of the IM cable are maintained exactly as in the reference case.

The transient voltages are observed for the slowest and fastest excitation: the positive first stroke, and the negative subsequent stroke.

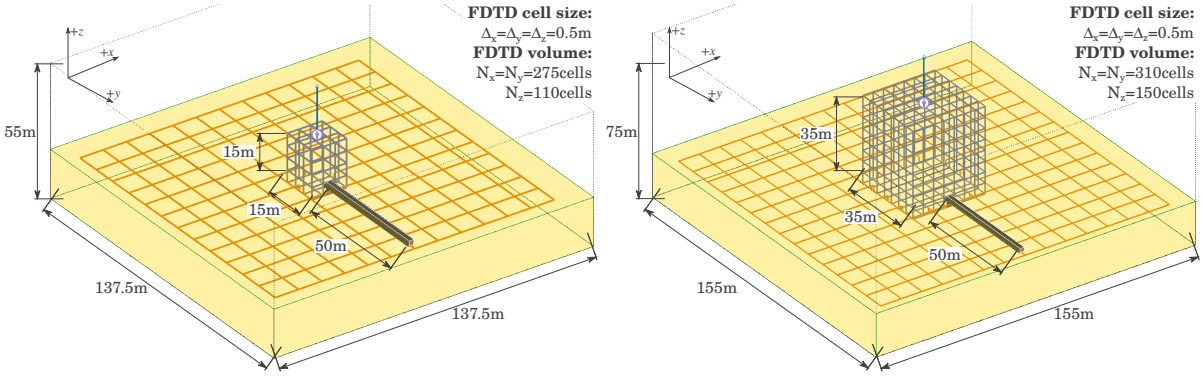

(a) $15\times15\times15$ m^3 building **(b) $35\times35\times35$ m^3 building**

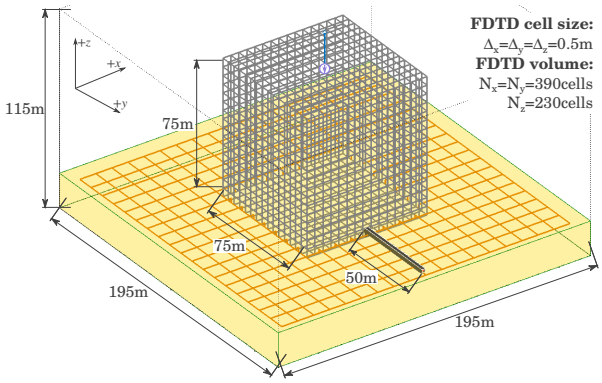

(c) $75\times75\times75$ m^3 building

Figure 3.10: Geometry of the cases for evaluate the effect of the building size.

3.5.1 Transients in a IM cable connected to building of different sizes

The voltages at the 50 Ω load at the terminations of the cable, are presented in figure 3.11. As it can be seen, the building size is an influent and relevant parameter in the complete transient behavior: the smaller the building, the higher the amplitude of the voltage.

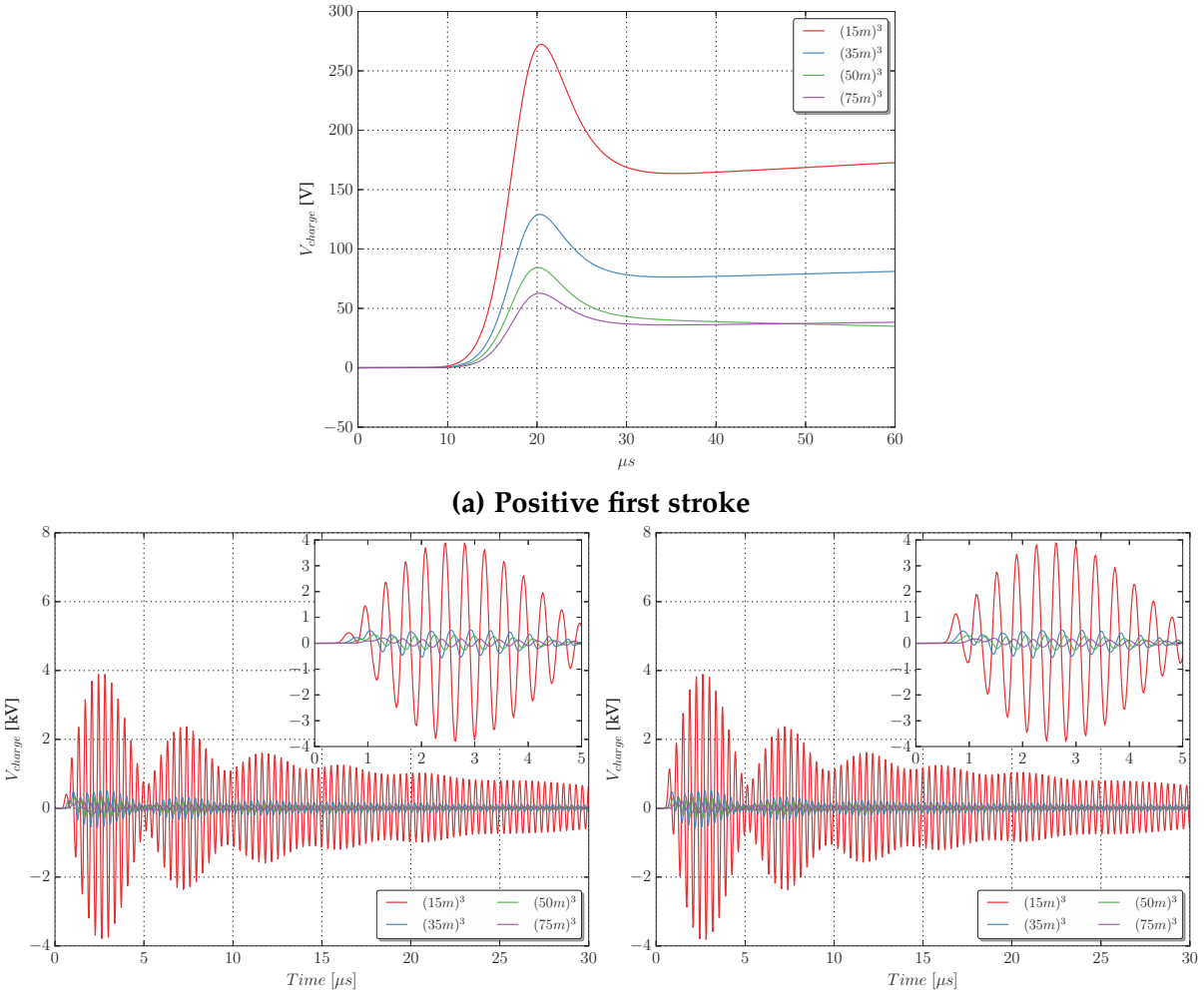

(a) Positive first stroke

(b) Negative subsequent stroke - At the building side

(c) Negative subsequent stroke - At 50 m from the building

Figure 3.11: Influence of the size of the building in the voltages at the terminations of the cable.

In the case of the positive first stroke, no oscillations are observed, as in the previous sections. But for a negative subsequent stroke, the figures 3.11b and 3.11c suggest that the smaller the size of the building, the higher the amplitude of the oscillations.

This is a direct consequence of the amount of current circulating through the cable duct indicated in figure 3.12 The smaller the building, less buried building conductors

to drain lightning current to the ground, therefore, more current circulating through the cable duct, which is proportional to the induced current in the shield, observed in figure 3.13.

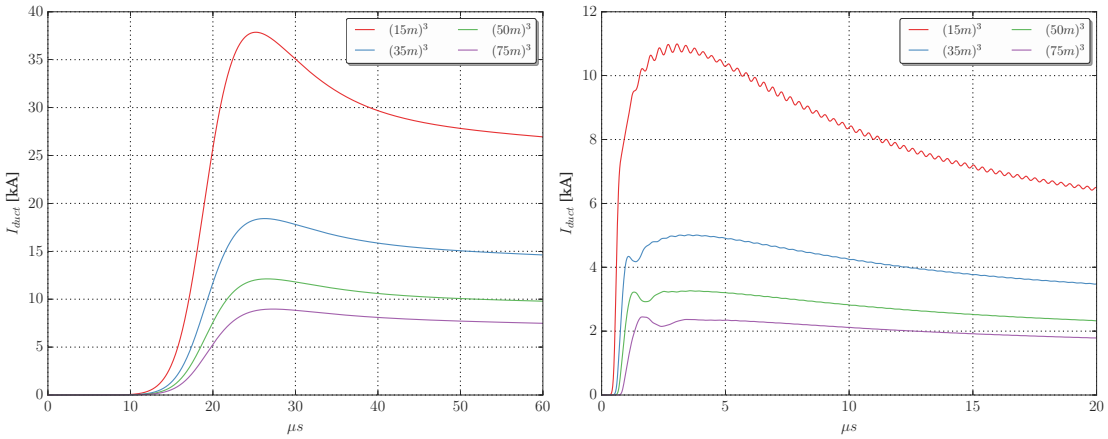

(a) Positive first stroke **(b) Negative subsequent stroke**

Figure 3.12: Influence of the size of the building in the current entering to the cable duct.

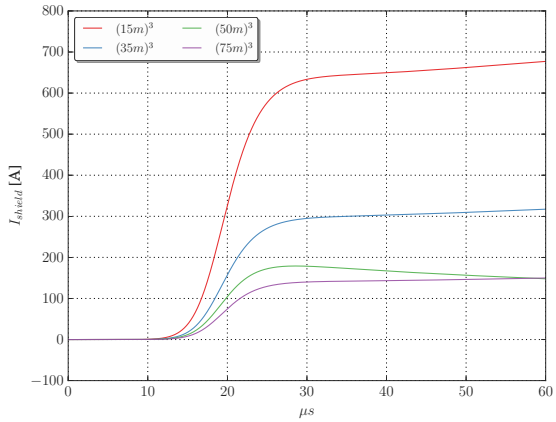

(a) Positive first stroke

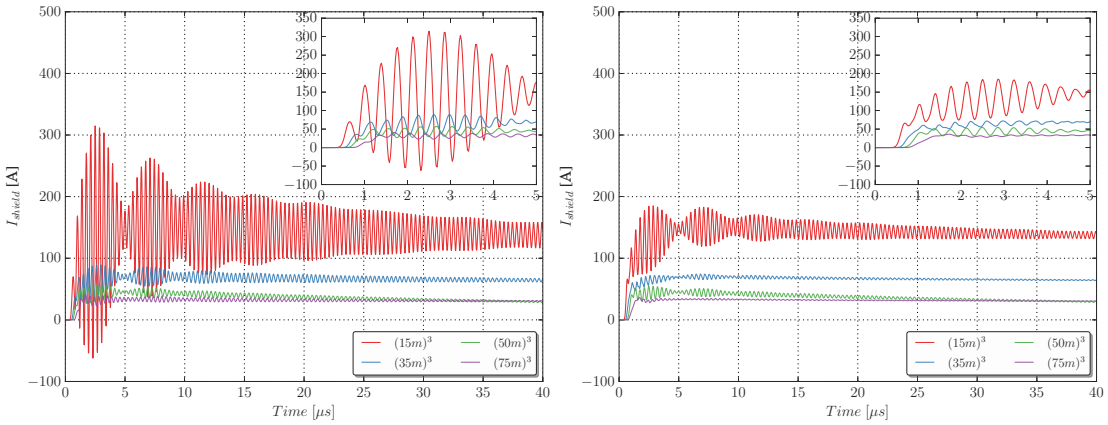

(b) Neg. Sub. Stroke - At building side **(c) Neg. Sub. Stroke-50 m from building.**

Figure 3.13: Influence of the building's size in the current of the cable shield.

3.6 The grounding connections of the concrete cable duct.

Regarding the grounding of the cable duct, it is known that at the building side is always somehow connected to ground, but along the rest of its trajectory different grounding points can also exist. To perform this kind of installations, imply an elevation of construction costs that, at least from the point of view of the transient voltages at the extremities of a IM cable, have not been justified.

In this section, the effect of the grounding connections of the cable duct are going to be observed. To do that, the reference case of a 50 m×50 m×50 m depicted in figure 3.1 is going to be used. Considering the following three configurations:

- The cable duct is left open at the remote extremity.
- The cable duct is connected to the grounding grid only at the remote end. As indicated in 3.14a.
- The cable duct is connected to the grounding grid each 10 m. As indicated in 3.14b.

The grounding of the cable duct is performed with a bare copper conductor of 185 mm² of transversal area. And, as it can be seen in figure 3.14, is performed between one conductor of the cable duct and the lower grounding grid.

It is important to note that for all the scenarios considered in this section, the shield of the IM cable is always connected at both extremities of the cable duct. The effect of the grounding of the shield is going to be observed in the next section.

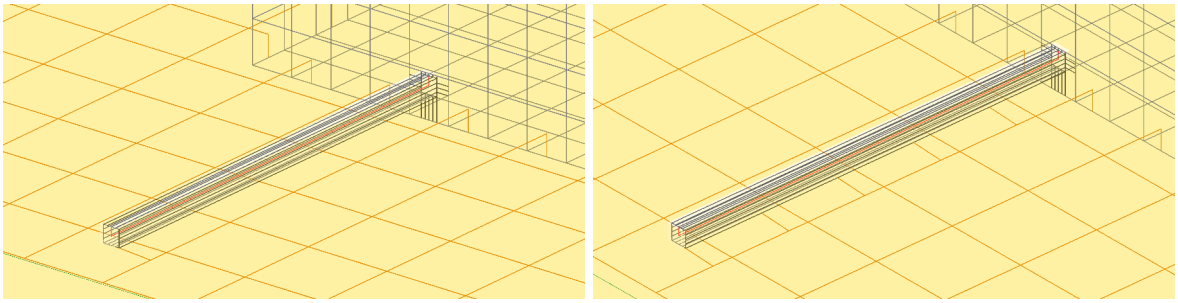

(a) Grounding at the remote end only. **(b) Grounding distributed each 10 m**

Figure 3.14: Detail of the grounding connections considered for the cable duct.

3.6.1 Transients in the IM cable for different grounding connections of the cable duct

The voltages at the cable terminations for the negative subsequent stroke and the positive first stroke are shown in figures 3.15 and 3.16 respectively.

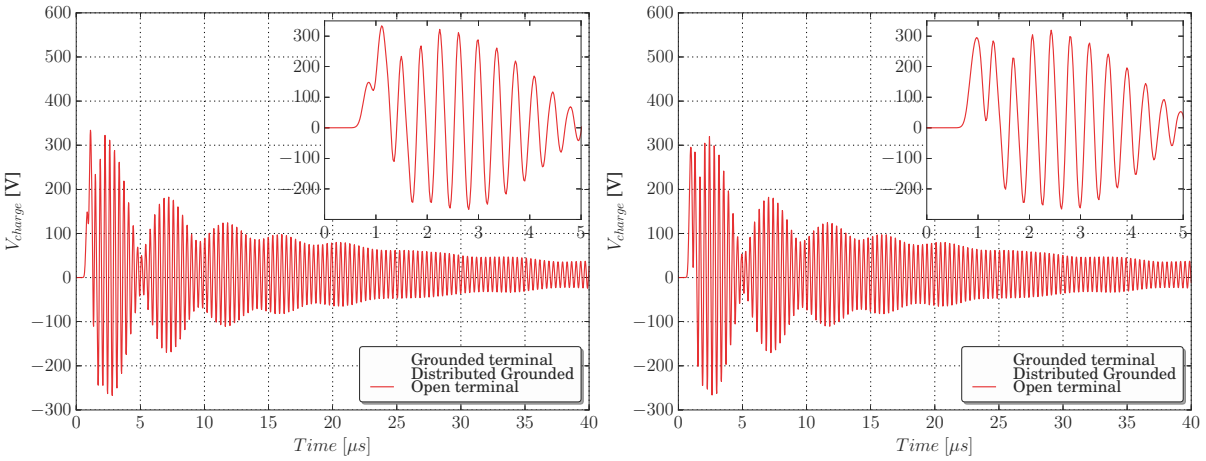

(a) At the building side **(b) At the remote termination.**

Figure 3.15: Effect of the grounding on the cable duct in the voltage at the 50 Ω load. For a negative subsequent stroke

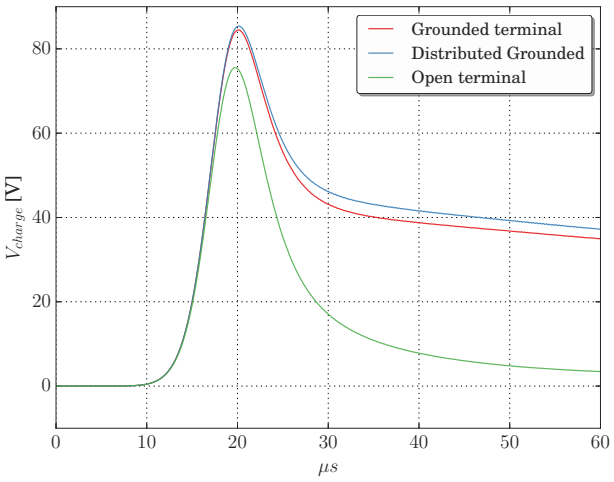

Figure 3.16: Effect of the grounding on the cable duct in the voltage at the 50 Ω load. For a positive first stroke

At first sight, it can be observed that for a fast excitation as the negative subsequent stroke, the type of grounding of the cable duct does not affect the voltages in observed at the terminations. This suggest that the grounding of the cable duct has an effect at lower frequency content, as for the positive first stroke, here the difference in the magnitude of the impulse are more notorious: if the cable duct is left open at the remote termination, the peak voltages are lower than if the cable duct is grounded.

The low frequency effect of the grounding of the cable duct, can be confirmed by observing the response of the current shield in figures 3.17 and 3.18, and the current entering to the cable duct in figures 3.19a and 3.19b. For all those currents, the decay time reduces when the cable duct is left open.

The above phenomenon is interesting, since an open cable duct imposes a boundary condition at the remote termination that forces the current to be null. Therefore, the duct becomes a "less attractive" path for current circulation. On the contrary, when is grounded, the current coming from the building can continue its propagations to the remote extremity and to the grounding grid.

Finally, it is also worthy to mention that, from the point of view of the transient behavior of the IM cable, there is no difference between the use of a distributed grounding, and a grounding at the termination. Which suggests that, with good continuity along the cable duct construction, there is no need to perform extra connections to the external grounding system. This practice, does not effectively modifies the nature of the transient voltages observed in the IM cables.

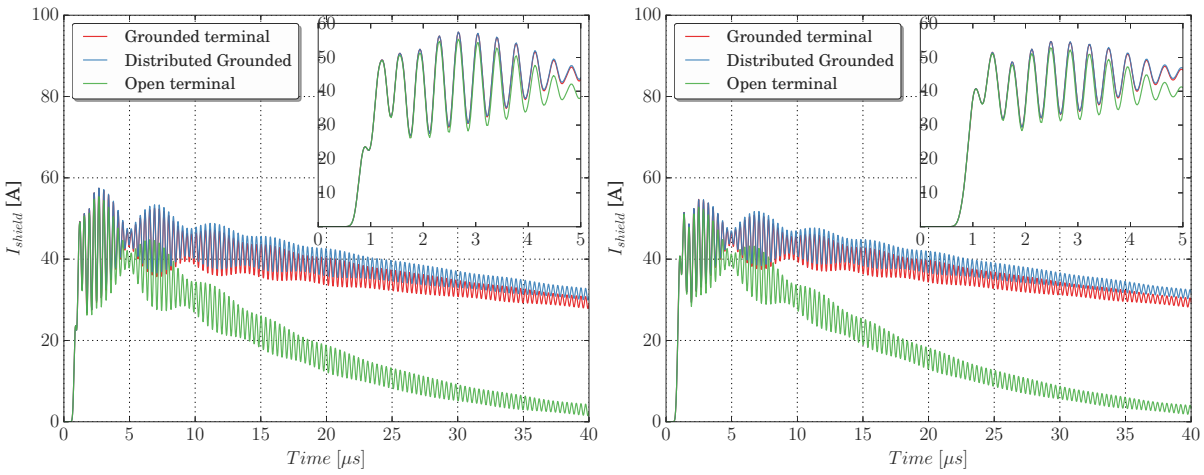

(a) At the building side **(b) At the remote termination**

Figure 3.17: Effect of the grounding on the cable duct in the shield current. For a negative subsequent stroke

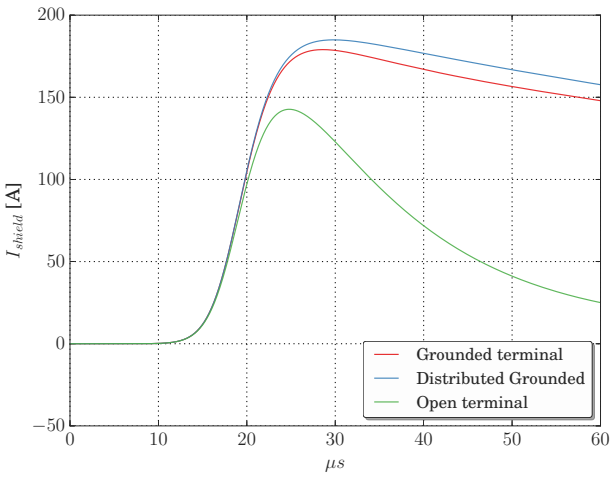

Figure 3.18: Effect of the grounding on the cable duct in the shield current. For a positive first stroke

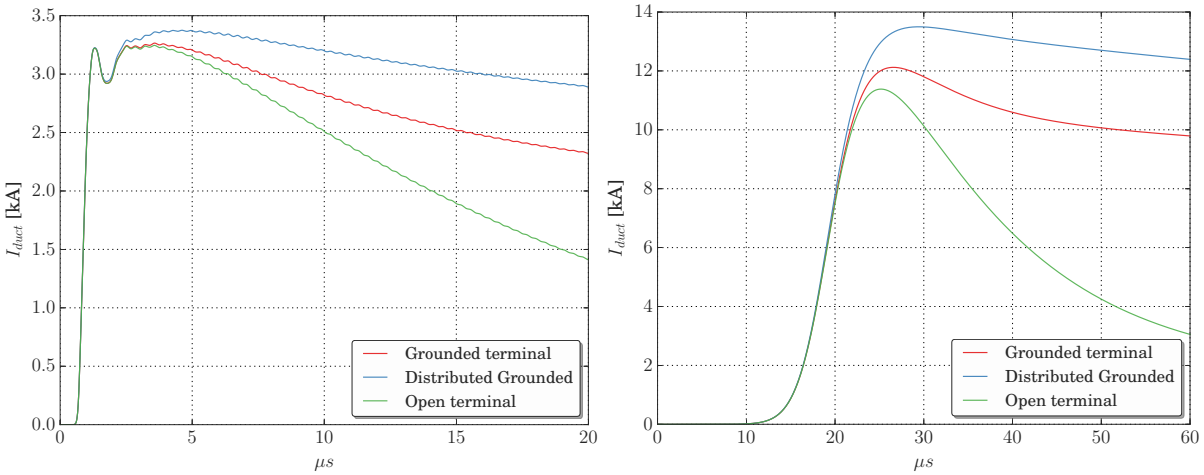

(a) For a negative subsequent stroke. **(b) For a positive first stroke.**

Figure 3.19: Effect of the grounding on the cable duct in the current entering from the building.

3.6.2 Synthesis on the effect of the grounding of the cable duct in the transient voltages

- For fast excitations, the type of grounding considered in the cable duct does not affect the transients voltages at the termination of the IM cable.
- For slower excitations when the cable duct is connected to ground at its remote location, the voltage at the extremities in the coaxial cable are higher than when the cable duct is left open.
- Regardless of the type of grounding: distributed or at the terminal, the voltages in the IM cable are unaltered.

3.7 The connections to ground of the shield of the coaxial cable

In this section it is going to be presented how the grounding connection of the shield affects the transient voltages at the extremities of the IM cable. To do that, the auxiliary wire connecting the shield to the cable duct is going to be retired from the FDTD case. Three scenarios were considered:

- Both terminations of the cable shield connected.
- Only the termination at the building side is connected.
- Only the remote termination is connected.

As in previous sections, the scenarios are going to be evaluated for both excitations: positive first stroke, and negative subsequent stroke.

It is worth recalling that, this kind of connection does not affect the emplacement of the $50\,\Omega$ load representing the electronic equipment, since in the thin wire model of a coaxial cable, this load is internally connected between the core and the shield. As explained in section 2.7.4.

3.7.1 Transients in a IM cable for different connections of the shield

In figures 3.20 and 3.21 it can be seen the voltage at the $50\,\Omega$ load. At first, it can be observed that for a subsequent stroke excitation, the magnitude of the transient voltages does not differ in an important manner from one scenario to another.

Nevertheless, the energy contained for each of the cases is severely different, given the intensity of the resonances caused by each shield connection. Under this perspective, the case in which the shield is connected only at the building side, is the situation with higher resonances.

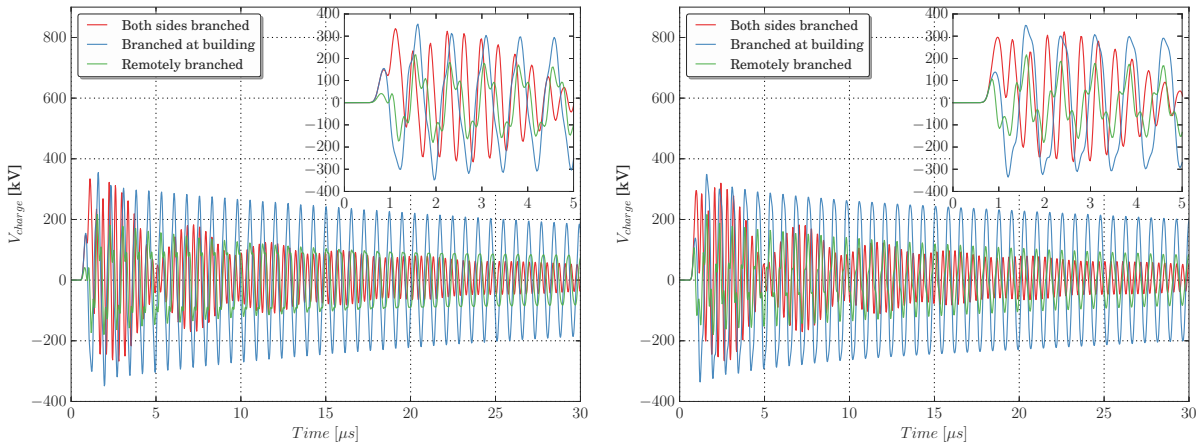

(a) At the building side. **(b) At 50 m from the building.**

Figure 3.20: Voltage at the 50 Ω load for a subsequent stroke.

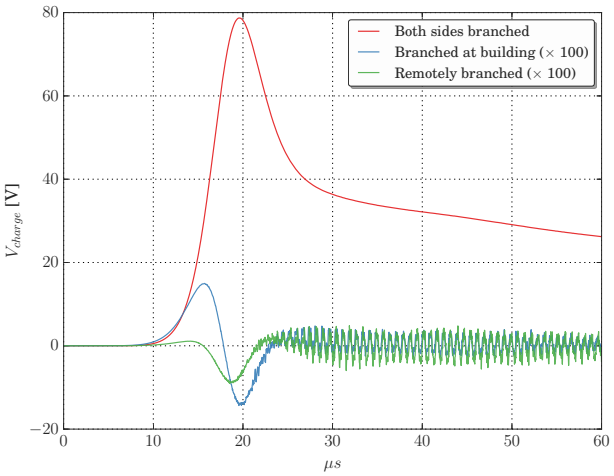

Figure 3.21: Voltage at the 50 Ω load for a first stroke. At the building side. *Note:* observe that the blue and green curves are amplified by 100

This is not the case for an impact with a positive first stroke, shown in 3.21. Here, the cases in which the shield is open in either extremity causes a negligible voltage, with regards to the case in which the shield is branched at both extremities.

This behavior can be explained if the current in the shield is observed; take figures 3.22 and 3.23. It can be seen that the current circulating through the shield is significantly lower when the building is hit by a slower excitation, with a wavelength significantly higher than the length of the conductor, this is, a positive first stroke.

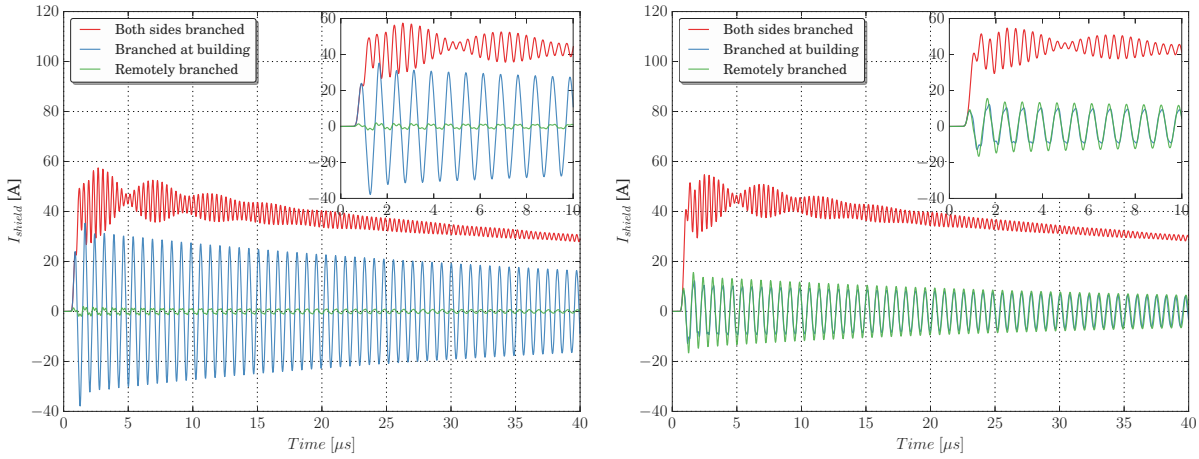

(a) At the building side. **(b) At 50 m from the building.**

Figure 3.22: Current in the shield for a subsequent stroke.

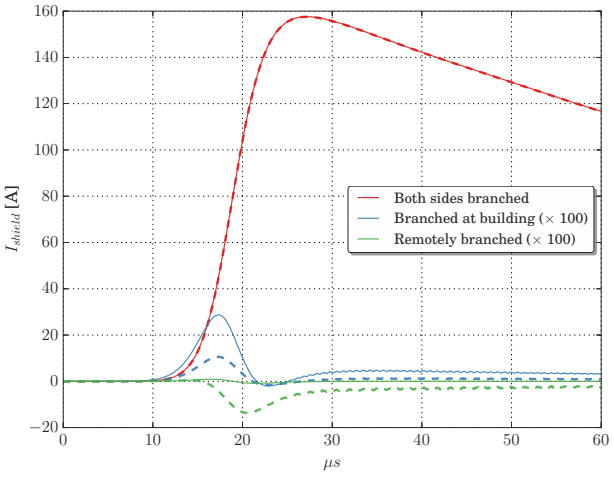

Figure 3.23: Current in the shield for a first stroke. Solid line: At the building side. Dotted line: At 50 m from the building. *Note:* observe that the blue and green curves are amplified by 100

In terms of a transient behavior, it can be understood that, a positive first stroke is sufficiently slow as to "see" the coaxial cable as a lumped circuit and not as propagation medium. Therefore, an open circuit at one extremity, is practically a general open circuit, forcing the current to propagate through a nearby conductive channel, which in this case is the cable duct.

Figure 3.24 depicts the current at the cable duct, here; for the first stroke excitation, when the shield is left open, the current entering through the cable duct is higher than the case the shield is connected in both extremities. The latter scenario adds a circulating path to the current, therefore reducing the fraction of the current entering the duct.

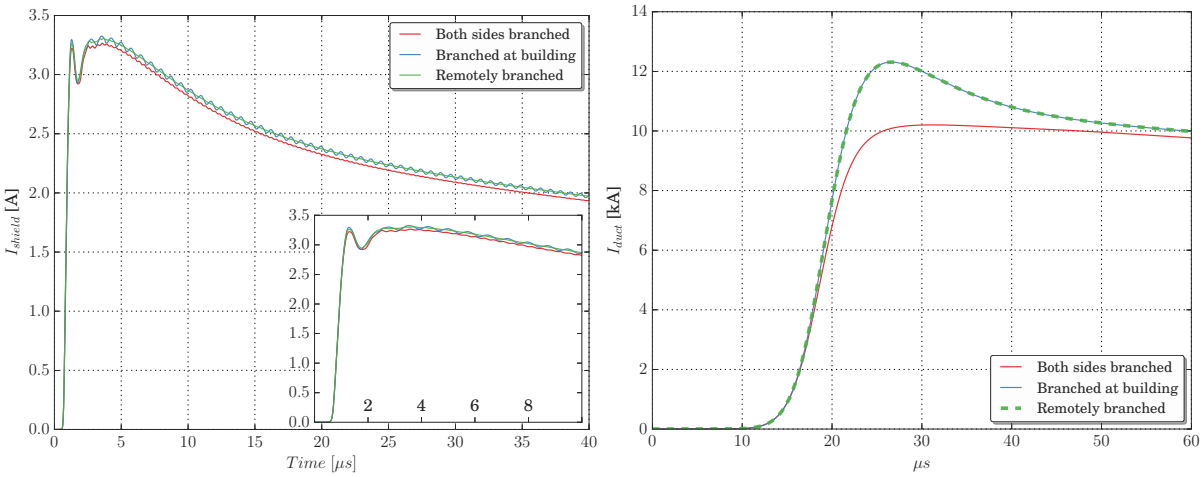

(a) For a subsequent stroke **(b) For a first stroke**

Figure 3.24: Current entering from the building to the cable duct.

On the other hand, it is possible to justify the results at this point to the model used for the coaxial cable. Particularly, considering that is a model that neglects the transfer admittance of the conductor. Therefore, in the next section a model that includes the effect of the transfer admittance is considered.

3.7.2 Effect of the inclusion of the transfer admittance.

In section 2.2.3, it was stated that the coupling of the shield to the coaxial cable can be studied considering a transfer impedance between both conductors. In reality, this coupling also includes a transfer admittance. While the impedance accounts for the induced current into the core, the admittance accounts for the electric charge.

Usually this last variable is neglected, given the good shielding characteristics of modern IM cables used in most of the Nuclear Power Plants (NPPs). Nevertheless, in light of the results of the last section, it seemed interesting to evaluate the effect of a classical model of transfer admittance, in the transient voltages at the extremities of a coaxial cable.

To study the effect of the transfer admittance, the equivalent Transmission Line (TL) model of the coaxial cable of figure 3.25 will be used. The shunt current source depends on the convolution product of the transfer admittance and the distributed shield potential. In the following sections, the strategy followed to compute both parameters is explained.

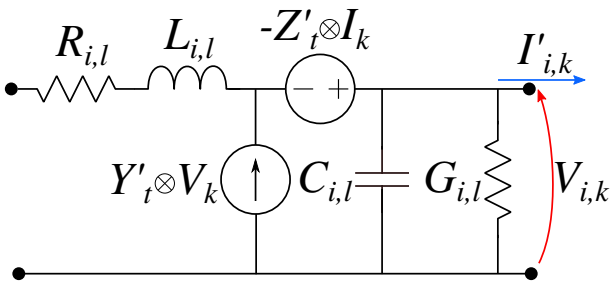

Figure 3.25: Equivalent TL model for a coaxial cable considering the transfer impedance.

The potential rise of the shield

To obtain the distributed voltage along the cable shield, a reference point is necessary. In this case, the point is a steel conductor of the cable duct structure, since at both extremities the shield is connected to the cable duct.

Finally, the expression (2.41) of section 2.6.1 is going to be used to determine the distributed potential of the shield. Since the potentials close to the shield and to the cable duct are needed, the expression (2.41) is used twice. When performing this computation, the two integral paths overlap, therefore, the cell section of this superposition of paths is subtracted. Figure 3.26 illustrates the integration paths, and expression (3.1) indicates the computation of the distributed potential of the shield with respect to the cable duct.

$$V'_k = V_z|_{z_{shield}}^{z_{shield}+1.5\Delta_z} + V_z|_{z_{duct}-1.5\Delta_z}^{z_{duct}} - \Delta_z \cdot E\left(z_{shield} + 2.5\Delta_z\right) \tag{3.1}$$

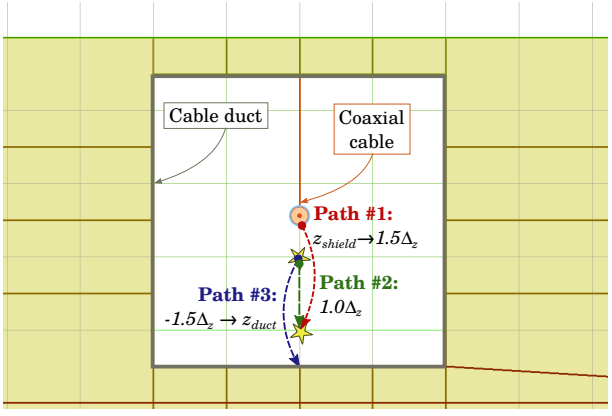

Figure 3.26: Transversal view of the cable duct and the points used to measure the electric field to compute the distributed source V_{si}

The expression for the transfer admittance

To compute the transfer admittance, the analytical expression (3.2a) is used. The parameters of the IM cable are depicted in table 3.3, they are taken from a typical IM cable configuration.

$$Y'_T = \frac{j\omega\pi\varepsilon_{eq}C'_{core}C'_{shield}}{6N_c\varepsilon_{core}\varepsilon_{shield}}\sqrt[3]{(1-K)^2}\frac{1}{E(e)} \tag{3.2a}$$

$$\varepsilon_{eq} = \frac{2\pi\varepsilon_{shield}\varepsilon_{core}}{\varepsilon_{core}+\varepsilon_{shield}} \tag{3.2b}$$

$$C_{shield} = \frac{2\pi\varepsilon_{shield}}{\log\left(\frac{r_{shield}}{r_{core}+T}\right)} \tag{3.2c}$$

$$C_{core} = \frac{2\pi\varepsilon_{core}}{\log\left(\frac{r_{core}}{r_{cond}}\right)} \tag{3.2d}$$

Where: $Y'_T \rightarrow$ Transfer admittance per unit of length. $[S/m]$
$C'_{core} \rightarrow$ Capacitance per unit of length of the coaxial region $[F/m]$
$C'_{shield} \rightarrow$ Shield capacitance per unit of length $[F/m]$
$\varepsilon_{eq} \rightarrow$ Equivalent permittivity of the materials inner and external to the shield [
$E(\cdot) \rightarrow$ Complete elliptic integral of the first kind.

Parameter	**Symbol**	**Value**
Optical coverage of the shield	K	0.8
Number of carriers in the shield	N_C	16
Electric permittivity of the material external to the shield	ε_{shield}	$2.25\,F/m$
Electric permittivity of the material inner to the shield	ε_{core}	$2.25\,F/m$

Table 3.3: Coaxial cable parameters used to compute the transfer admittance (3.2a)

Transient voltages in a IM cable considering the transfer admittance.

Figures 3.27a and 3.27b show the transient voltage at the $50\,\Omega$ load when the building is hit by a negative subsequent stroke. As it can be seen, when the transfer admittance is considered, there is a modest increase in the magnitude of the voltage, and a small delay in the oscillations.

This new element of the coaxial cable is not going to be further considered, since it does not contributes significantly to the peak transient voltage and unnecessarily adds computational effort.

3.7.3 Synthesis of the effect of the connection of the shield

For a subsequent stroke, the emplacement of the shield connections does not alter the magnitude of the induced voltage at the ends of the coaxial cable. Nevertheless, the amount of energy for each case is severely affected. This is an important issue not to neglect when selecting Surge Protection Devices (SPDs)

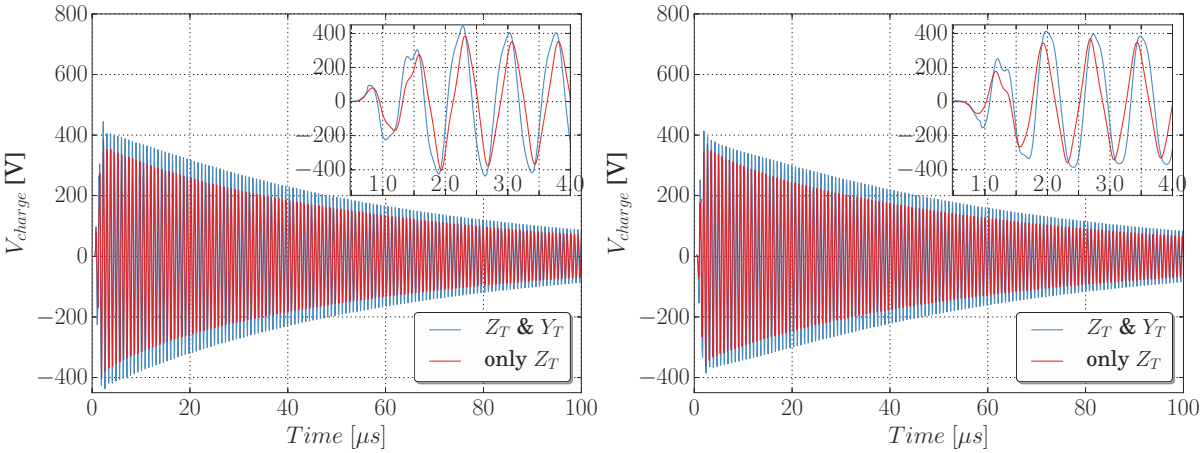

(a) At the building side. **(b) At 50 m from the building.**

.

Figure 3.27: Voltage at the load

For a First Stroke, the only configuration that generates induced voltages is when both extremities of the shield are connected. Since, the excitation has a larger wavelength as to "see" the 50 m coaxial cable as a lumped circuit, therefore; an open circuit at one extremity is a general open circuit.

3.8 The external grounding system configuration.

One of the most important elements conceptualized for the lightning protection system is the grounding. In this section, the effect of the most common configurations of grounding systems in Power Production Centers is going to be examined. To do that, four configurations were considered:

- A simple ring 1 m from the building structure, buried at 2.5 m of depth. The ring has two variations:
  - With one connection to the building (In a corner).
  - With connections around the building each 10 m. (See figure 3.28a)
- A grounding grid with segments of 10 m $\times$ 10 m (See figure 3.28b)
- No external grounding system, only the foundations of the building.

Seemingly as the previous sections, two lightning strikes were considered: the positive first stroke of 200 kA, and the subsequent stroke of 50 kA.

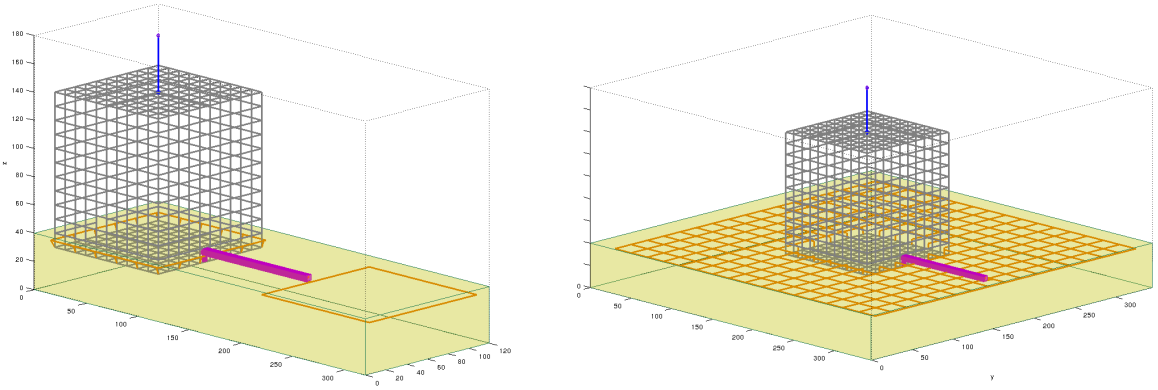

(a) With a ring

(b) With grounding grid.

Figure 3.28: General view of the case studies that concerns the study of the grounding system

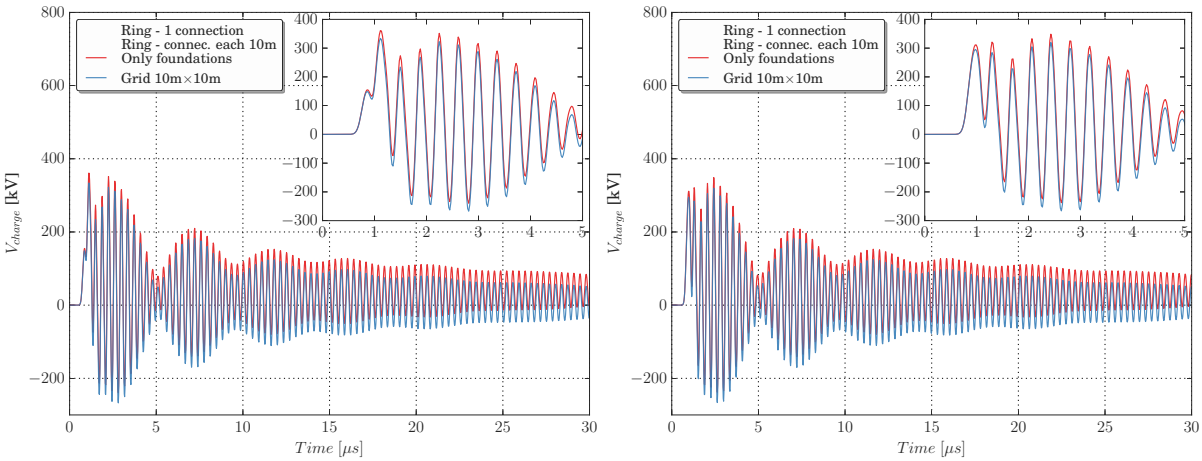

(a) At the building side.

(b) At 50 m from the building.

Figure 3.29: Voltage at the 50 Ω load for a negative subsequent stroke

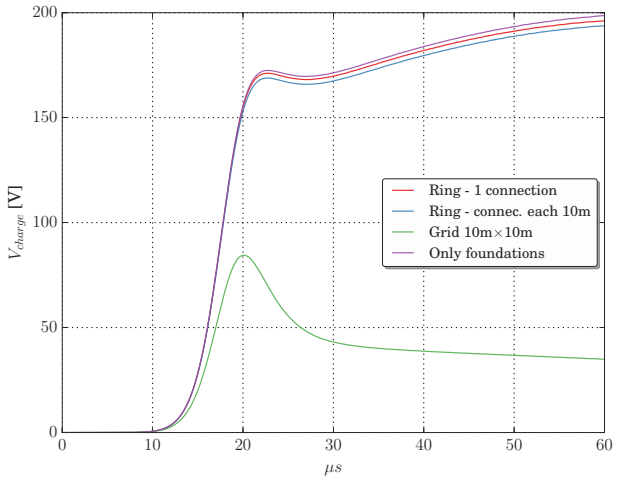

Figure 3.30: Voltage at the 50 Ω load for a positive first stroke.

3.8.1 Transients in a IM cable for different configurations of grounding

The voltages at the loads of 50 Ω are shown in figures 3.29 and 3.30. For the scenarios when the excitation is a subsequent stroke, the three cases different from the grid are grouped in one response, since all of them behave in the same manner.

In a similar manner, for a positive first stroke, there is no significant difference in the responses for a grounding system different than a grounding grid. Which suggests that, the different configurations of the grounding system have a more important influence under low frequency excitations.

In section 3.3, it has been indicated that the nature of the resonant behavior observed for the subsequent stroke excitation, are the reflections along the shield of the cable. From figure, 3.29, alongside its frequency response in 3.31, it can be observed that the resonant peak is invariable for the different grounding configurations. Which implies that at least for a cable as big as 50 m, the grounding system is not influential to interfere in a resonant condition.

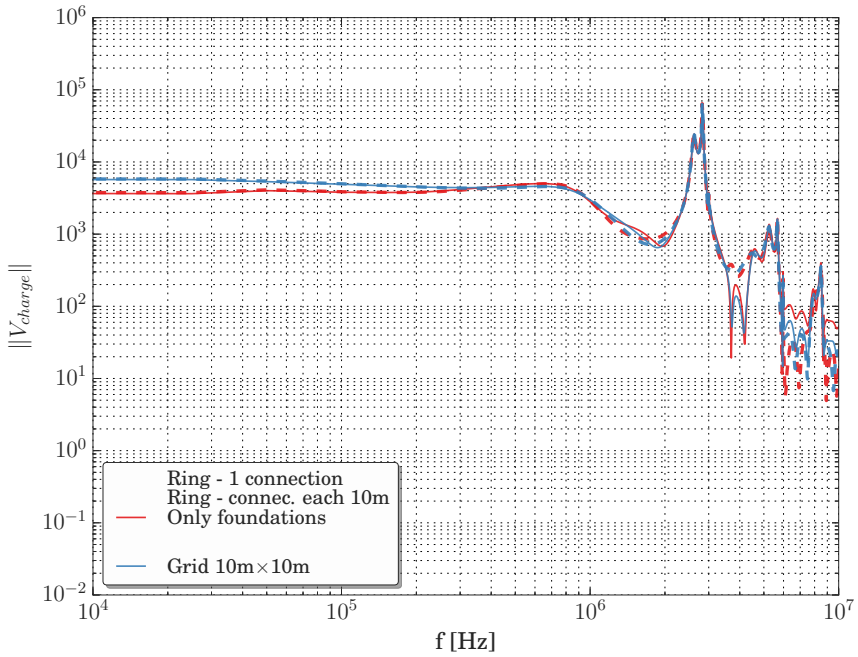

Figure 3.31: Frequency response of the voltage at the at the 50 Ω load for a subsequent stroke. Solid line: At the building side. Dotted line: at 50 m from the building

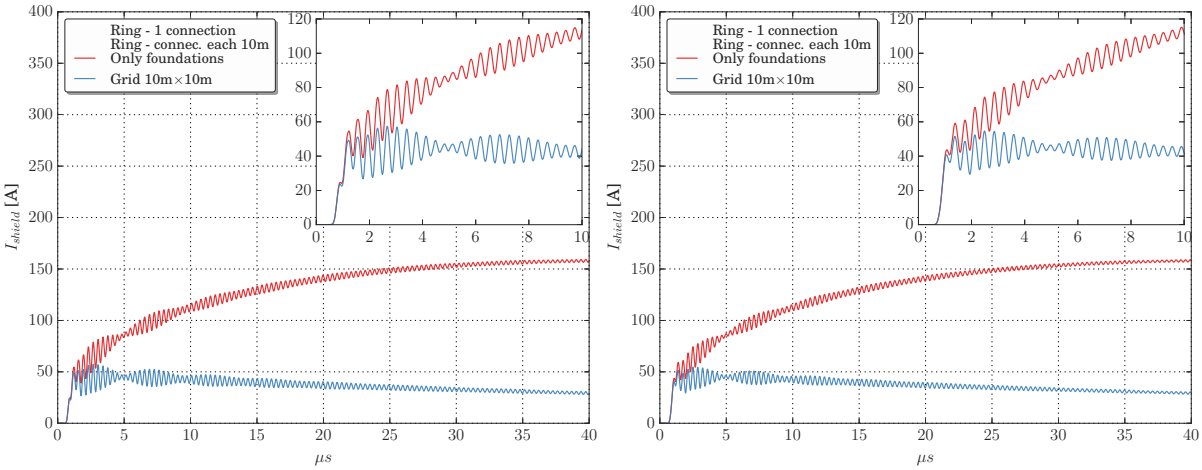

(a) At the building side. (b) At 50 m from the building.

Figure 3.32: Shield current for a negative subsequent stroke

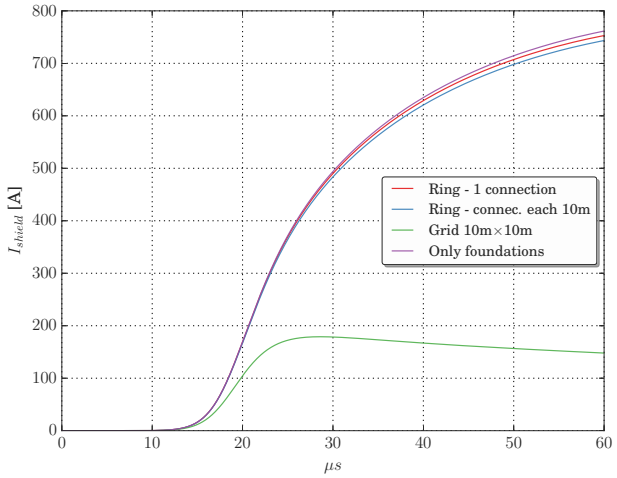

Figure 3.33: Shield current at the building side for a positive first stroke.

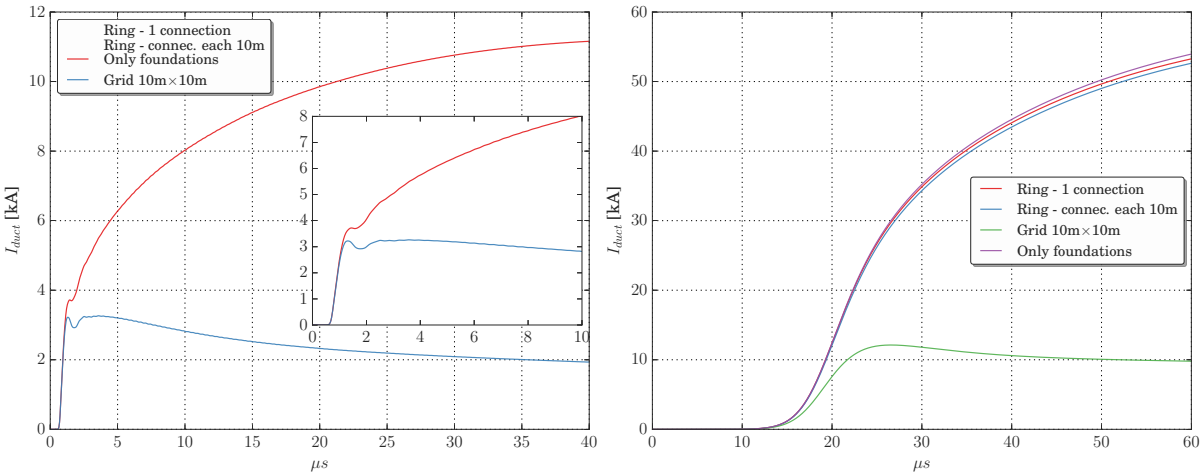

(a) For a subsequent stroke (b) For a first stroke

Figure 3.34: Current entering from the building to the cable duct.

Special consideration: A connection between neighbor grounding systems

It is common practice in Power Production Centers to link two adjacent grounding systems with a buried, bare conductor, in order to reduce the relative potential rise from one grounding system to another. In this section, the effect of this connection is studied for the case of a grounding ring connected at one point to the building, as suggested by figure 3.35.

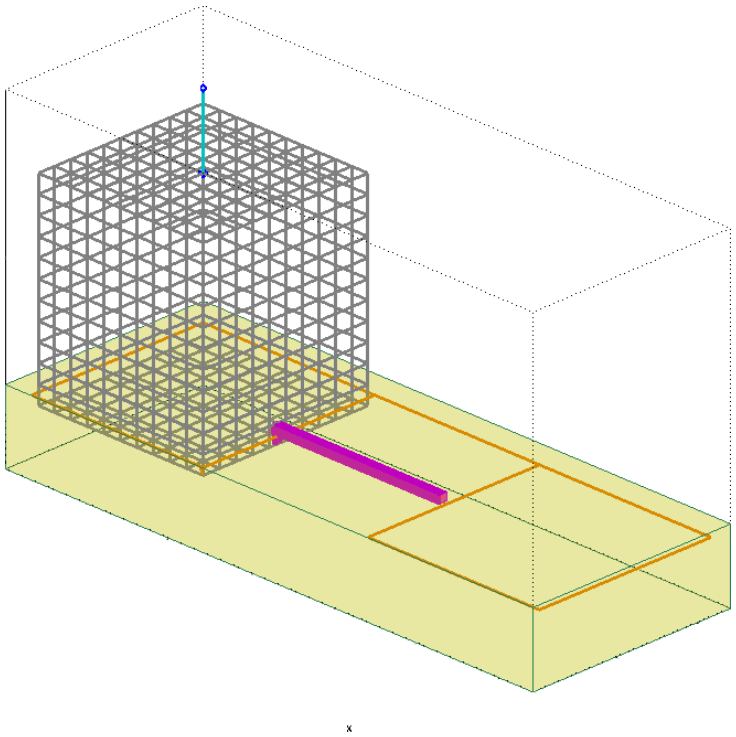

Figure 3.35: Case study of two grounding rings connected.

The currents circulating through the cable shield are shown in figures 3.36 and 3.37, while the voltages at the 50 Ω loads are in figures 3.38 and 3.39. As expected from the results in the previous section, connecting both grounding systems does not have an important influence in the behavior of the transient voltages at the extremities of the conductor.

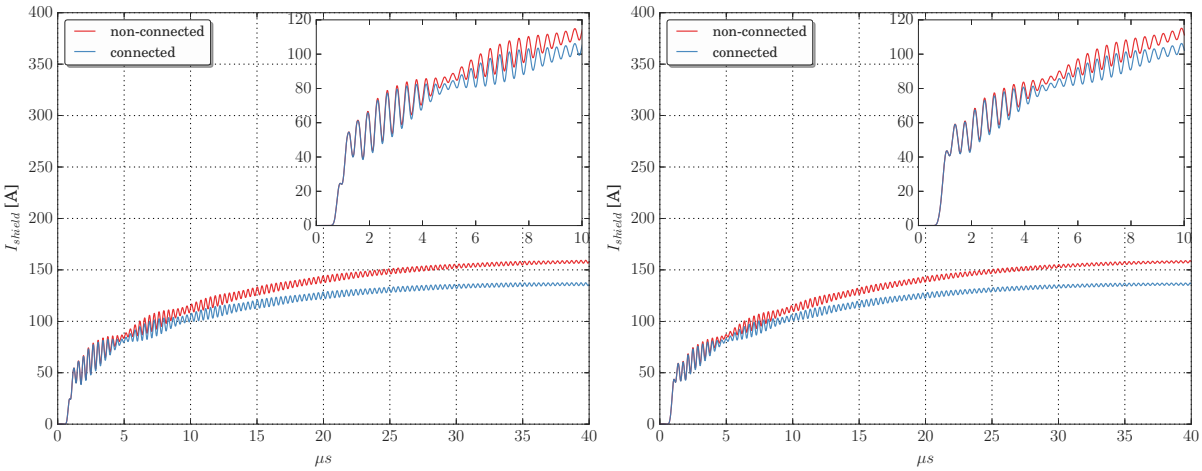

(a) At the building side. (b) At 50 m from the building.

Figure 3.36: Effect of connecting two grounding systems in the shield current for a negative subsequent stroke.

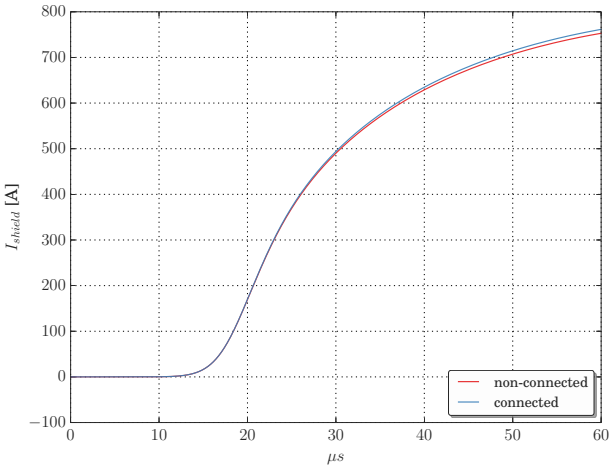

Figure 3.37: Effect of connecting two grounding systems in the shield current for a positive first stroke.

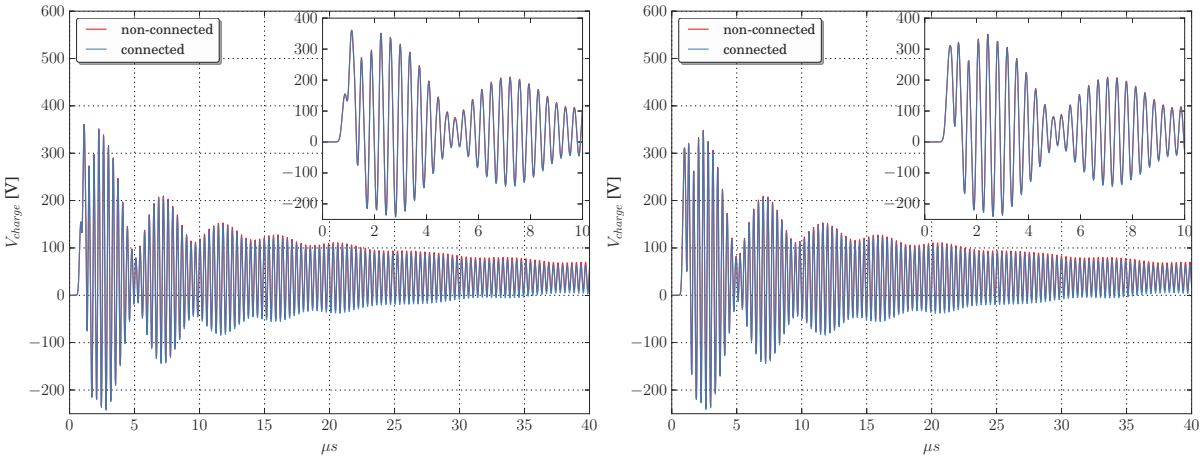

(a) At the building side. **(b) At 50 m from the building.**

Figure 3.38: Effect of connecting two grounding systems in the voltage at the 50 Ω load for a negative subsequent stroke

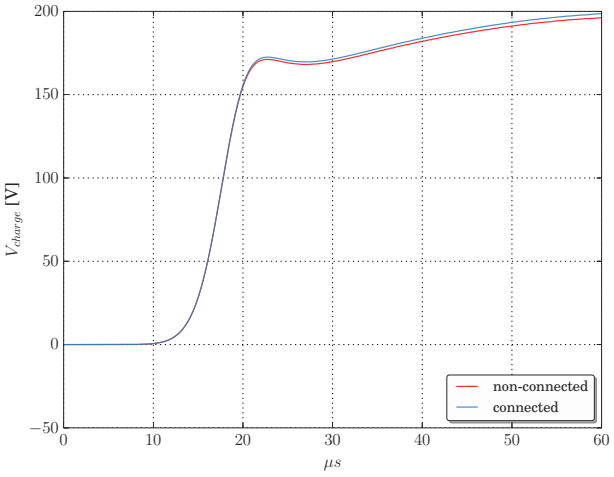

Figure 3.39: Effect of connecting two grounding systems in the voltage at the 50 Ω load for a negative subsequent stroke

3.8.2 Synthesis of the effect of the external grounding system configuration.

- Regarding the transient voltage at the extremities of the coaxial cable, there is no significant difference in the use of the following grounding schemes: A ring with one connection to the building, a ring with multiple connections to the building, and the use of the building foundations as grounding system.
- General variations of the configurations on the grounding systems have more significant influence for low frequency excitations. In other words, for an excitation with high frequency content as a subsequent stroke, the connection of the grounding system is not determinant on the voltage observed in the 50 Ω load.
- The cable duct and the shield of the coaxial cable form a kind of coaxial configuration that resonates at a frequency corresponding to half of the wavelength of the structure.
- The phenomena of resonance appears only with high frequency excitations, this is, for a subsequent stroke. And, although the subsequent stroke has a peak amplitude four times lower than a first stroke, its transient voltages are of almost the double of those obtained with a first stroke.

3.9 The length of the IM cable.

It has been suggested in section 3.3 that the length of the cable is an important parameter to consider, since it determines the nature of the resonance observed at the extremities of the cable, particularly when a negative subsequent stroke is used as an excitation.

In this section, the effect of the length of the cable is going to be inspected, considering three scenarios: 100 m, 50 m and 25 m. As before, the reference case is a 50 m-side building, as used in figure 3.1 of section 3.2.

3.9.1 Transients in a IM cables of different lengths

The voltages at the 50 Ω load is depicted in figures 3.40 and 3.41. Here, two aspects arise: independently of the excitation, there is a proportionality between the length of the cable duct and the voltage peak, and for a subsequent stroke, the presence of resonances.

The proportionality between length and voltage magnitude is expected, since for longer cables, the amount of equivalent distributed induction sources along its path is higher, which results in greater voltages at the terminations.

Concerning the resonance for a subsequent stroke, it can be observed that the resonant frequency is inversely proportional to the length of the cable. Implying that, for longer cables, the resonant frequencies are going to be smaller, and at the same time; with more energy content from the excitation, resulting in more intense oscillations.

To illustrate this point, the frequency response of the voltages is showed in figure 3.42, here; it can be seen that the resonances for the different scenarios are approximately: $f_{res}^{100m} \approx 1.432\,\text{MHz}$, $f_{res}^{50m} \approx 2.831\,\text{MHz}$, $f_{res}^{25m} \approx 5.549\,\text{MHz}$. Which are frequencies that corresponds with associated wavelengths of roughly the double of the cable length: $\lambda_{100m} = 209.5\,\text{m}$, $\lambda_{50m} = 105.9\,\text{m}$ and $\lambda_{25m} = 54\,\text{m}$.

This is an interesting phenomenon, since supports the statements of the previous section 3.3: The coupling of the duct to the shield of the cable generates a resonant coaxial configuration. And, the resonances observed in the shield, penetrates to the core, reaching the load at the extremities.

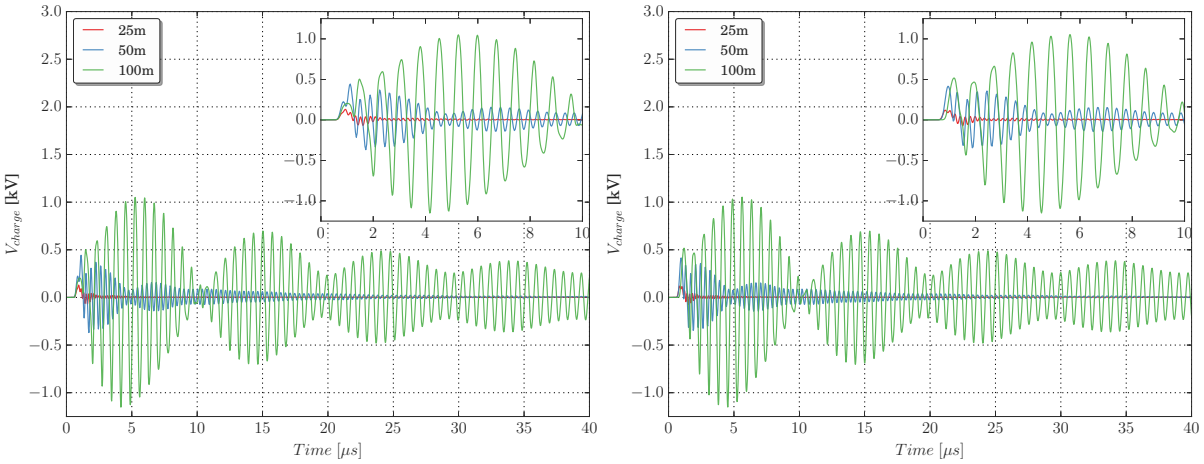

(a) At the building side. **(b) At 50 m from the building.**

Figure 3.40: Effect of the length of the cable in the voltage at the 50 Ω load for a negative subsequent stroke

3.9.2 Synthesis of the effect of the cable length in the transient voltages.

- The larger the cable duct, the higher the peak of induced voltages at the extremities of the control cable.
- The subsequent stroke current excites resonant frequencies of realistic cable lengths.
- The larger the cable, the resonances decrease their frequency, and increase their magnitude.

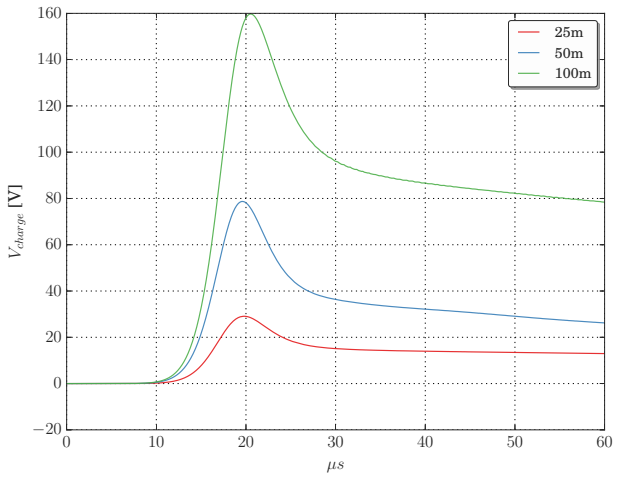

Figure 3.41: Effect of the length of the cable in the voltage at the 50 Ω load for a positive first stroke

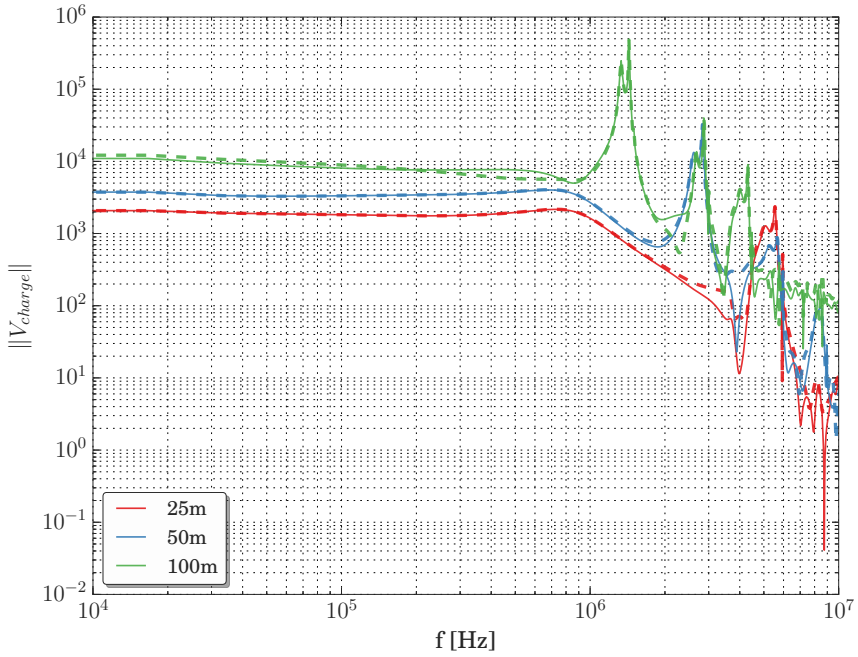

Figure 3.42: Frequency response of the voltage at the at the 50 Ω load for a subsequent stroke. Solid line: At the building side. Dotted line: at 50 m from the building

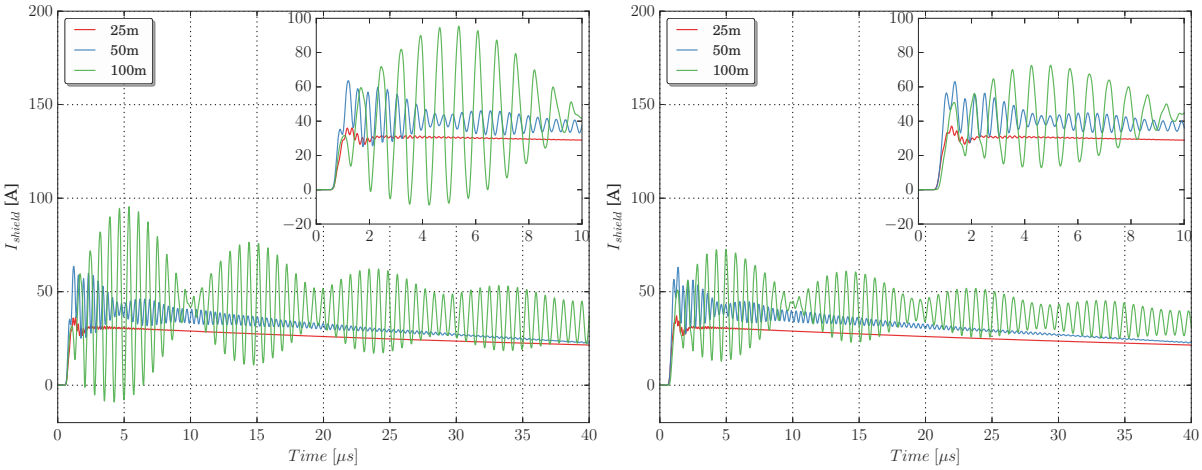

(a) At the building side.

(b) At 50 m from the building.

Figure 3.43: Effect of the length of the cable in the current at the shield for a negative subsequent stroke

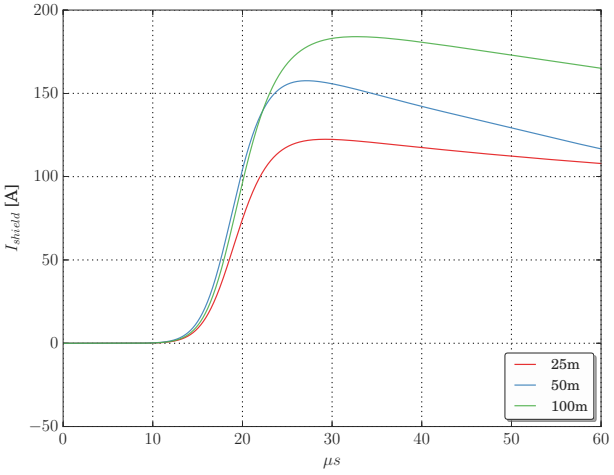

Figure 3.44: Effect of the length of the cable in the current at the shield for a positive first stroke

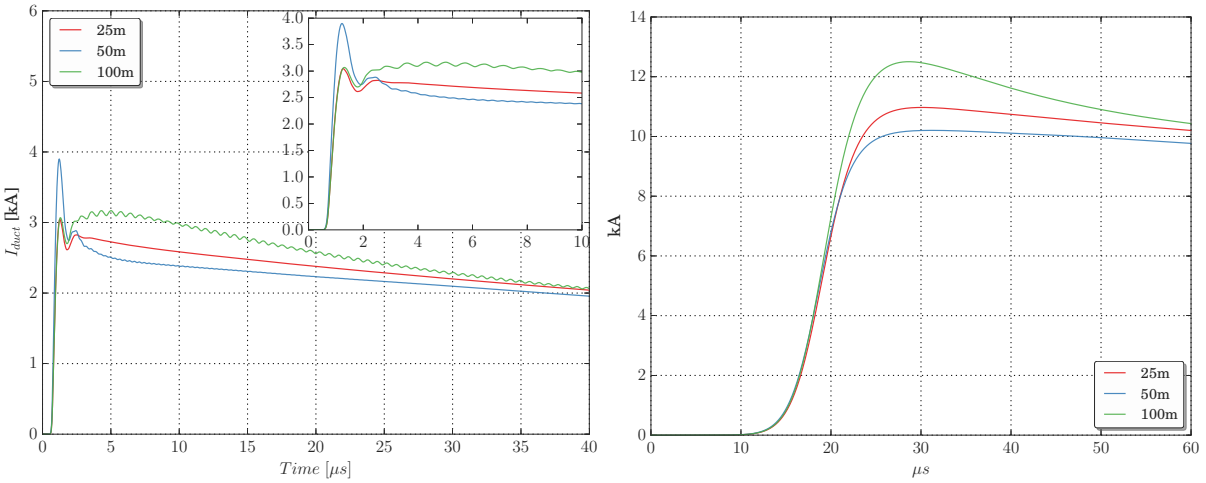

(a) For a subsequent stroke **(b) For a first stroke**

Figure 3.45: Effect of the length of the cable in the current entering at the cable duct from the building

3.10 The connection point of the lightning channel to the building.

Up until this section, the lightning strike has been considered hitting in the center of the rooftop of the building, nevertheless, it is also feasible that hits the corner of the building. Therefore the interest to observe, to which extend, this location is relevant to the computations of transients in the external IM cable.

To observe the influences, three striking points in a building are chosen, as indicated in 3.46.

- At the center of the building.
- At one corner close to the cable duct.
- At one corner far to the cable duct.

3.10.1 Transients in a IM cable for different lightning striking position

The voltages at the 50 Ω loads are shown in figures 3.47 and 3.48. As it can be seen, for both type of excitations there is an important influence of the striking point location: the farther the lightning strike is, the lower the voltages are.

Although the above behavior is expected, it is also interesting to observe the relative difference between the three locations, for a first stroke current; the voltages for a strike in the far corner are 15 % lower than the voltages for a strike at the center.

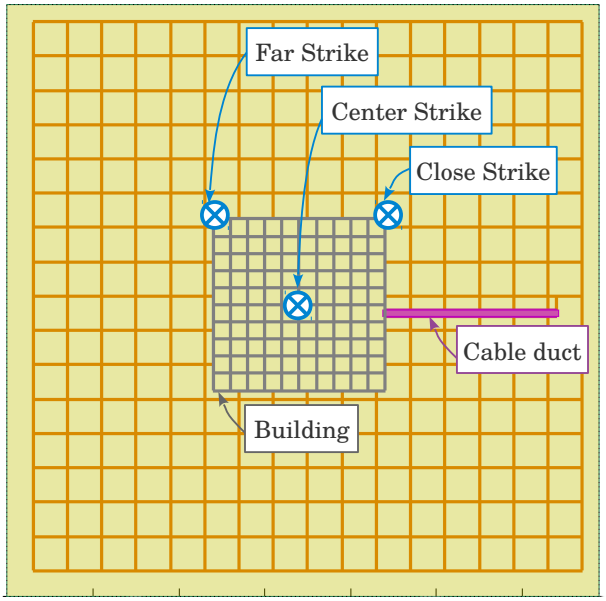

Figure 3.46: Top view from the case study. Different lightning strike locations

In a similar manner, the voltages for a strike in the close corner are 13.5 % higher than those obtained when the lightning strikes the center of the building.

These differences are more unbalanced when the excitation is a subsequent stroke: the voltages are 40 %-45 % higher for the close impact, and 2 %-5 % lower for the far impact.

To the moment, and for previous studies, it has been considered cases in which the lightning strikes the center of the building, which can give an underestimation of the voltages up until 45 %. This is not an acceptable tolerance for the cases in which there is only one cable duct, nevertheless, usually a building has multiple cable ducts around, alongside with pipeline cables, and directly buried conductors.

For these cases, and to guarantee an equally intense perturbation, the striking position that should be considered, is the top center of the rooftop. Otherwise, for a single conductor, it is advice to consider a lightning impact in a closer corner of the building.

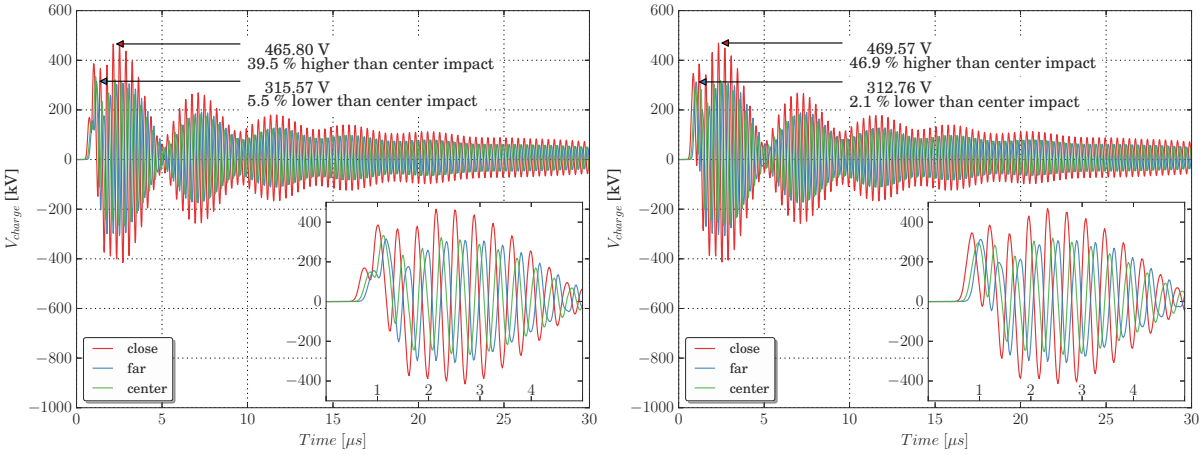

(a) At the building side. **(b) At 50 m from the building.**

Figure 3.47: Effect of the striking position in the voltage at the 50 Ω load for a negative subsequent stroke

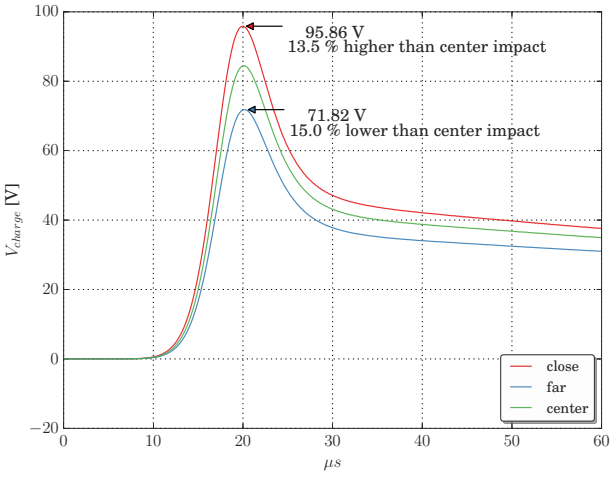

Figure 3.48: Effect of the striking position in the voltage at the 50 Ω load for a positive first stroke

3.10.2 Synthesis of the effect of the lightning striking position

- There is an important influence of the lightning strike location on the voltage observed at the extremities of a coaxial cable. The strike closer to the location of the cable, generates stronger transient voltages.
- Although it is advisable to always consider the lightning strike in the closest position to the cable duct, when multiple cable ducts are connected around the strike is recommended to strike at the center of the building.

3.11 The EM model for the building wall.

In the previous chapter it was mentioned that a building could be modeled with different strategies inside a FDTD volume. Here, two of those strategies are going to be implemented, in order to observe their influence on the transient induced voltages of the IM cable: a building modeled with a mesh of lossy beams, and modeled with a lossy thin plate, as described in 2.4.2.

The two models are used to test three scenarios of building walls:

- A lossy steel grid of $5\,\mathrm{m}\times 5\,\mathrm{m}$ of density
- A lossy steel grid of $10\,\mathrm{m}\times 10\,\mathrm{m}$ of density
- A thin wall of $10\,\mathrm{cm}$ of a material of $\sigma_{wall} = 2000\,\mathrm{S/m}$ and $5\,\mathrm{m\Omega}$ of surface impedance.

The last scenario was tested and recommended in [5], to perform electromagnetic penetration studies inside a typical building of a French PGC.

3.11.1 Transients in a IM cable for different EM models of building walls.

The response of the voltages of the cable connected to a building modeled with different walls is shown in figures 3.49 and 3.50. As it can be seen, for both types of excitations, the highest voltages come from the building modeled with a $10\times 10\,\mathrm{m^2}$ mesh grid, followed for the voltages obtained for a grid of $5\times 5\,\mathrm{m^2}$, and the voltages obtained for the lossy thin plate.

The results suggest that for denser building walls, less current gets to the cable duct, and therefore, less voltage is induced finally to the IM cable core. This is coherent, since the denser the walls are, more equivalent current propagation paths to the ground exists, and as consequence, less current propagates to the cable duct, as indicated by figures 3.51a and 3.51b.

The above is mainly a conductive effect that has low frequency implications. Take for example the current at the shield in figures 3.52 and 3.53, the decay times of the for both types of excitations is higher when the building wall is less meshed. This is, less denser walls facilitate lower frequency perturbations, or seemingly, since less paths are available, more time takes the current to propagate to the soil.

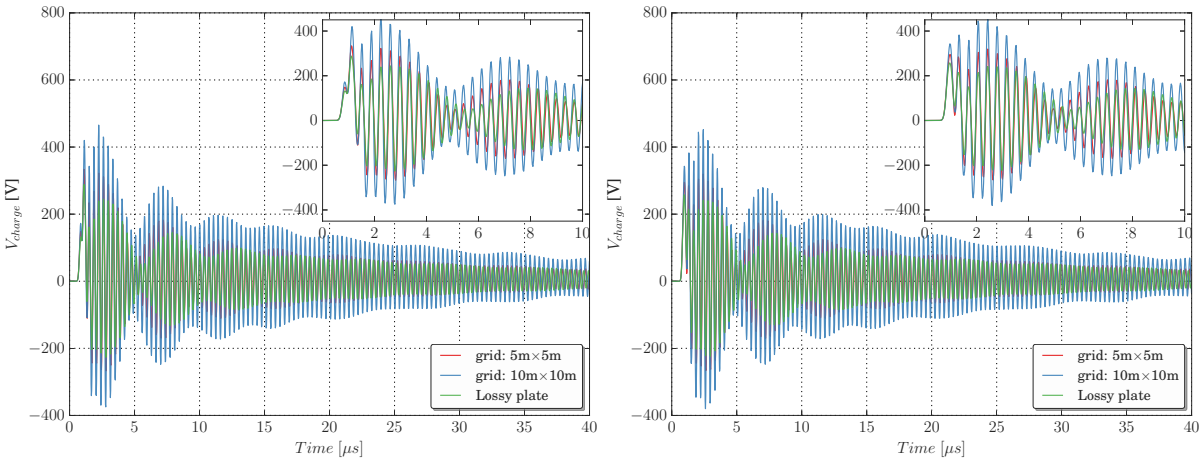

(a) At the building side. **(b) At 50 m from the building.**

Figure 3.49: Effect of the EM model of the building in the voltage at the 50 Ω load for a negative subsequent stroke

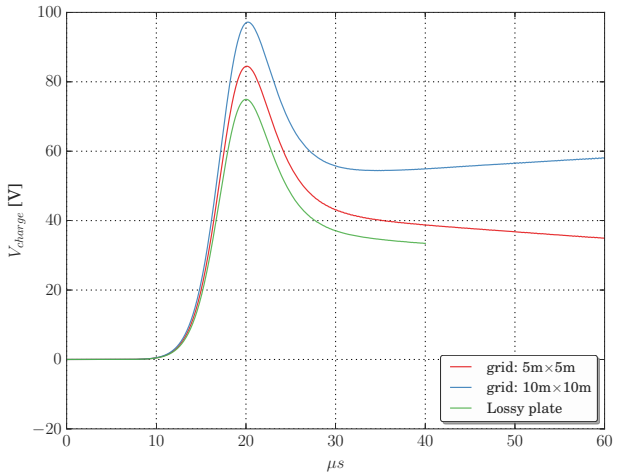

Figure 3.50: Effect of the EM model of the building in the voltage at the 50 Ω load for a positive first stroke

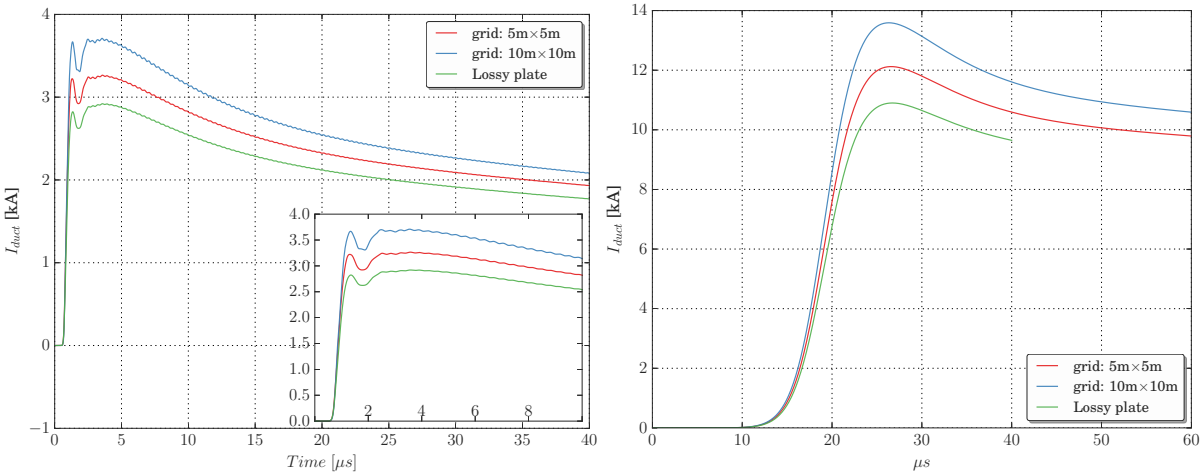

(a) For a subsequent stroke (b) For a first stroke

Figure 3.51: Effect of the EM model of the building in the current entering to the cable duct from the building.

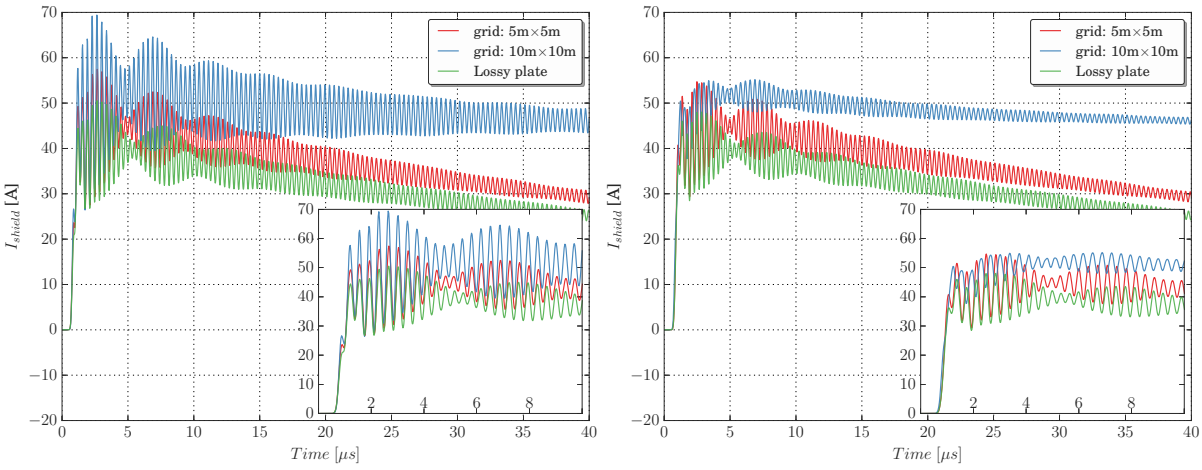

(a) At the building side. (b) At 50 m from the building.

Figure 3.52: Effect of the EM model of the building in the shield current for a negative subsequent stroke

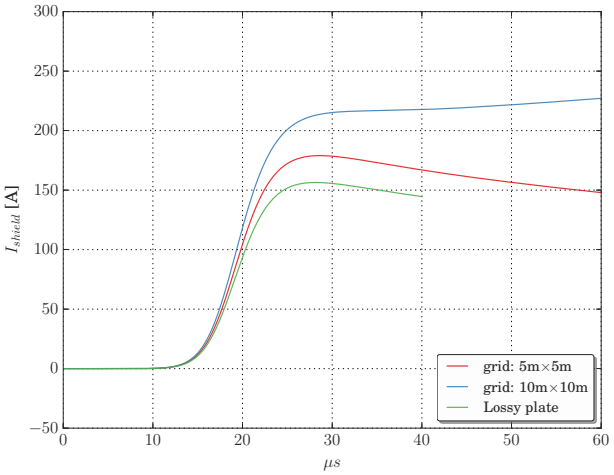

Figure 3.53: Effect of the EM model of the building in the shield current for a positive first stroke

3.11.2 Synthesis of the effect of the model of the building wall

- For a denser grid, exist more paths for the lightning current to propagate to the ground, therefore, less current reaches the cable duct.
- As a consequence, independently of the type of excitation, the voltages in the cable are lower while the walls are modeled with a denser wall.
- The resonance frequency for the negative subsequent strokes is unchanged, which reinforces the idea exploited in section 3.3, that the resonance is mainly depending on the geometry of the cable duct.

3.12 The inclusion of cable trays inside the concrete cable duct.

In reality, the IM cables are not "floating" in the middle of the air inside the cable duct, as it has been proposed in the reference case 3.1. They are resting over a conductive structure called: cable tray. These trays can be constructed in several manners, it can be simple plates, ladder route or enclosed structure, as depicted in figure 3.54

Sometimes the trays are made of non-conductive material, but it is not unusual for these structures to be metallic, and as that, they are bounded to be grounded to the potential reference, in this case, to the metallic cable duct structure.

An extra set of grounded metallic structure around the IM cable, suggest a certain amount of shielding, depending on the nature of the cable trays. Therefore the special interest to observe the effect of this conductive structures, running in parallel to the cable of study.

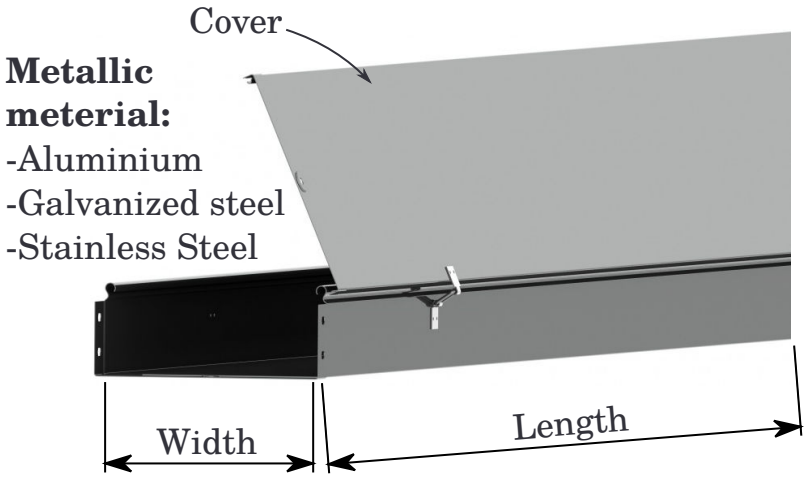

Figure 3.54: Generic metallic closed cable duct.

To include a cable tray inside the FDTD case study, four PEC plates are going to be considered at each side of the cable duct, as suggested in figure 3.55. The IM cable is between two of those plates, and its shield is connected to the cable duct.

To avoid close current paths in the terminations, the plates are grounded at each terminal point to the cable duct through one conductor.

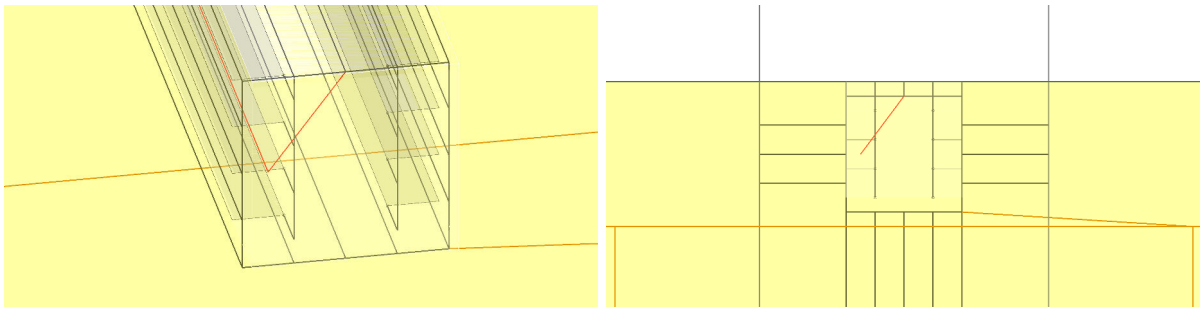

(a) 3D view **(b) YZ plane**

Figure 3.55: Detail of the cable duct with trays at the remote end.

3.12.1 Effect of the cable trays in the transient voltages of an IM cable

From the proposed case studies in figure 3.55, it can be inferred that the cable trays form a parallel circulation path for the current along the cable duct. In fact, when observing the current entering from the building to the cable duct in figure 3.56, it can be seen diminish almost half of its original value without cable trays. For both excitations: Positive first stroke, and negative subsequent stroke.

The effect of the cable trays is observed for the positive first stroke and the negative subsequent stroke, for three grounding scenarios:

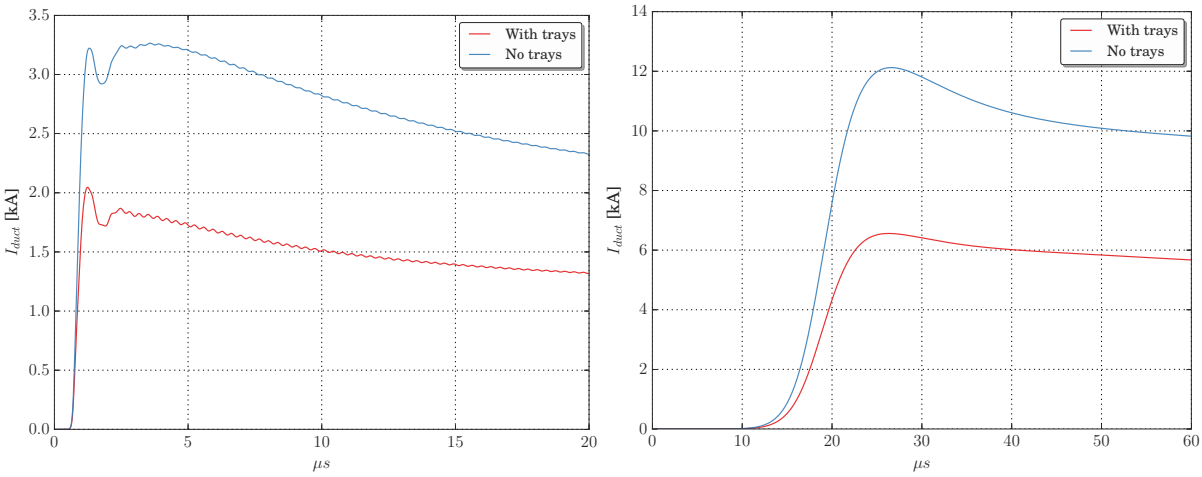

(a) For a subsequent stroke **(b) For a first stroke**

Figure 3.56: Effect of the presence of cable trays in the current entering to the cable duct from the building.

- When the cable duct is not grounded at the remote termination, but the shield of the IM is connected to the cable duct. In figure 3.57.
- When the cable duct is grounded at the remote termination, and the shield of the IM cable is left open in that point. In figure 3.58.
- When the cable duct is grounded at the remote termination, and the shield of the IM cable is also connected to the cable duct in that point. In figure 3.59.

The shield of the cable is connected to the cable duct at the building termination for all three scenarios.

As expected, including the cable trays parallel to the cable duct diminishes the peak of the transient voltages, this reduction is between 80 %-70 % of the peak of the voltages when no cable trays are considered.

Moreover, the presence of the trays attenuates in general the whole behavior of the transients observed in the terminal loads. Nevertheless, this effect does not eliminate the resonant behavior, as confirmed in figure 3.60. The resonant frequency for the cases in which the shield is connected, does not varies a lot, regardless of the presence of the cable trays.

This last behavior is of importance, since these resonances are going to reach the electronic equipment, and depending on its nature, a level of threat is possible.

It is interesting to observe that, again for this case, the parameter that determines the behavior of the transient in general, is the nature of the connection of the shield, and not the connection of the cable duct. When the shield is connected, both responses with open and grounded cable duct are similar. The same comparison can be made when the shield is left opened.

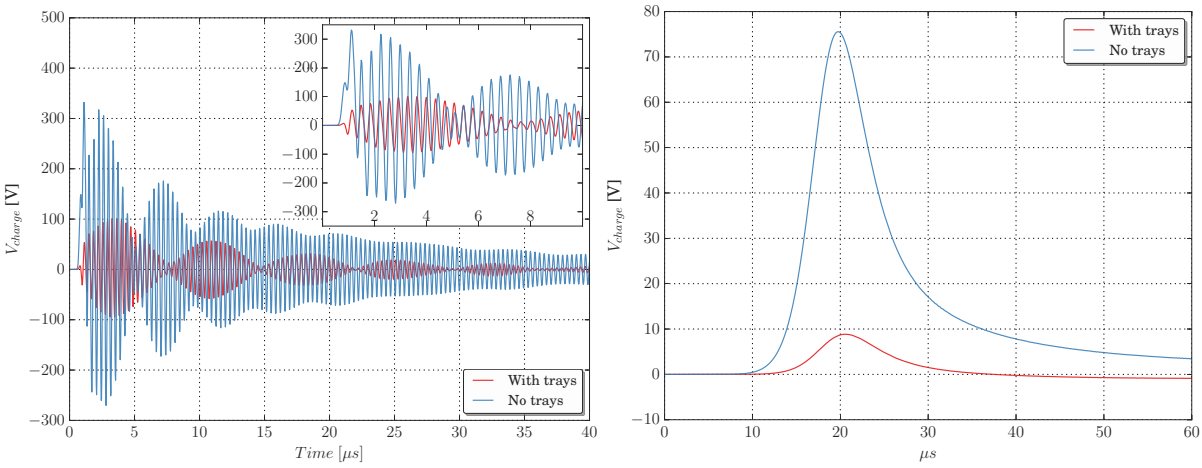

(a) Negative subsequent stroke. **(b) Positive first stroke.**

Figure 3.57: Effect of the presence of cable trays in the voltage at the 50 Ω load, at the building side. For an open cable duct and a connected shield.

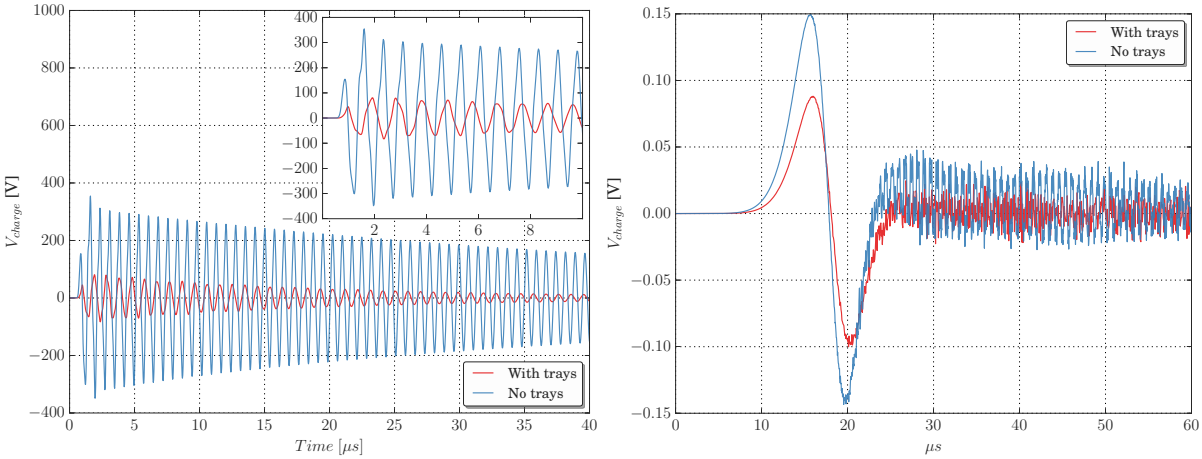

(a) Negative subsequent stroke. **(b) Positive first stroke.**

Figure 3.58: Effect of the presence of cable trays in the voltage at the 50 Ω load, at the building side. For a grounded cable duct and an open shield.

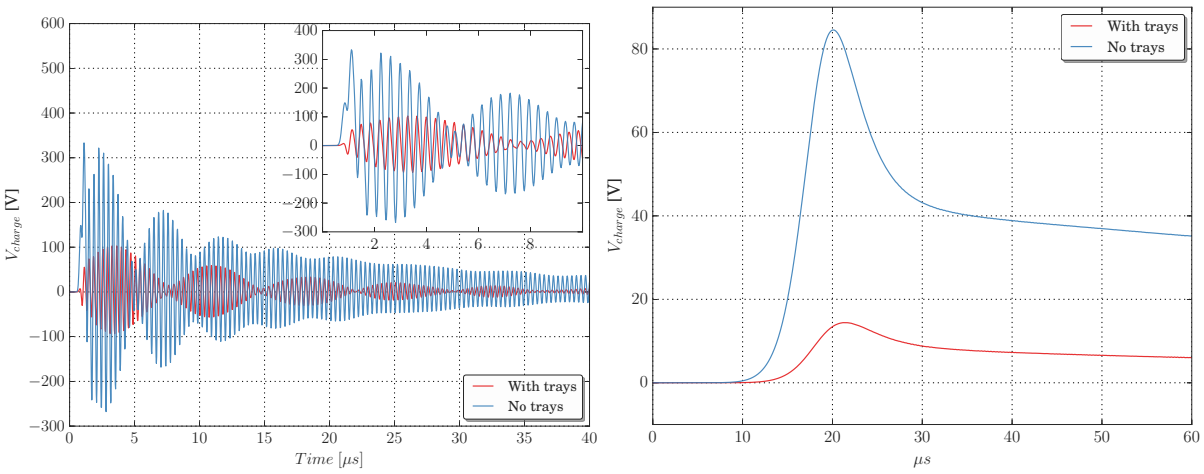

(a) Negative subsequent stroke. **(b) Positive first stroke.**

Figure 3.59: Effect of the presence of cable trays in the voltage at the 50 Ω load, at the building side. For a grounded cable duct and a connected shield.

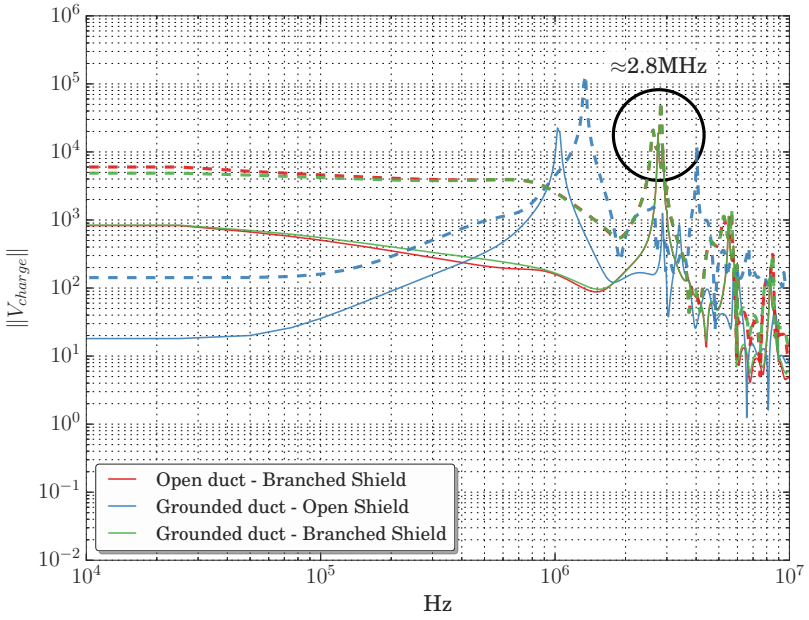

Figure 3.60: Frequency response of the effect of the voltage at the 50 Ω load, at the building side. Evaluation of the presence of the cable trays for a negative subsequent stroke. Solid line: with cable trays. Dotted line: without cable trays.

3.12.2 Synthesis of the effect of the cable trays

- Since the cable trays are connected to the cable duct structure at both terminations, they act as a parallel conductor element, diminishing the actual current circulating through the duct structure.
- The presence of the cable trays severely attenuates the transient response of the voltages at the terminations of the IM cable, acting as a shield along the cable path.
- The resonance frequency of the voltages is almost unchanged with the presence of the cable trays, which poses a level of threat to the electronic equipment connected to the cable.

3.13 The inclusion of the expansion joints between concrete cable ducts.

One important aspect of the construction of the cable ducts is its mechanical stability, therefore a long cable duct is separated in several shorter segments. The space between segments is known as an expansion joint, and, in the standard KTA-2206 [1] it is recommended to be made each 20 m of cable duct.

An electrical continuity is required between each duct segment, in consequence, it is necessary to perform a bridging with highly conductive metal strips around the perimeter of the expansion joint. The amount of bridges is diverse, in this section the presence of expansion joint of different quantity of bridges is presented.

The cable duct of 50 m of the reference case is divided in two segments of 25 m. They are separated with expansion joints of 30 cm, and are connected through copper bridges of 70 mm^2 of transversal area. Four configuration were considered: 2, 4, 8, 16 bridges uniformly distributed around the transversal cut of the cable duct. The figure 3.61 shows the detail of the construction of one expansion joint of a cable duct, with copper bridges.

3.13.1 Transients in a control cable for different amount of expansion bridges

In figures 3.63 and 3.62, are depicted the transient voltages at the 50 Ω. As it can be seen, for a negative subsequent stroke, the presence of expansion joints in the cable ducts does not significantly modify the amplitude of the transient voltages.

Nevertheless, including an expansion joint severely attenuates the intensity of the resonance of the cable. In fact, in the frequency response indicated in figure 3.64, it can be observed the lack of a “resonant peak” for the cases with expansion joints,

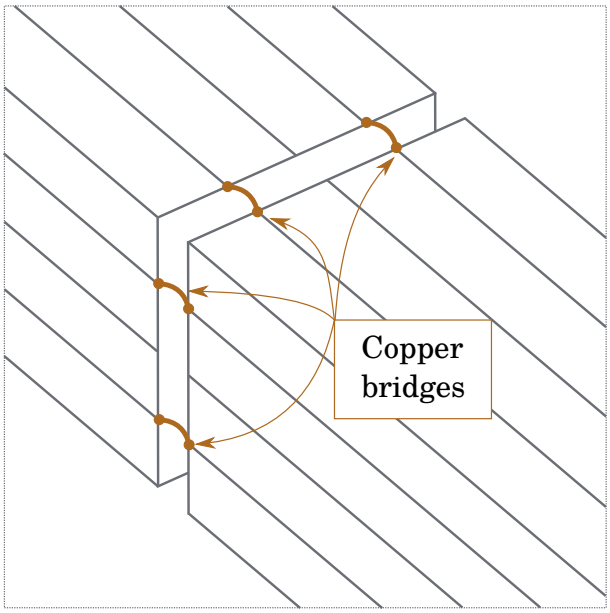

Figure 3.61: Detail of the schematic of one expansion joint, with copper bridges uniformly distributed around the perimeter of the cable duct.

which is directly translated into an attenuated oscillatory behavior of the transient response.

In the other hand, for the positive first strike, the influence on the magnitude of the induced voltage is more notorious: less bridges are used, higher are the voltages at the cable terminations. This suggests that the presence of an expansion joint affects the lower frequency spectrum.

The above can be confirmed observing the currents in the shield in figures 3.65 and 3.66.

At least for this model of the expansion joint, it does not seems to be an interesting variable to consider in the transients analysis of induced voltages, contrary to the recommendations of the standard KTA-2206. But, once again, as it was noted in section 1.4.1, this part of the calculation in the standard has several assumptions that were obtained for a reduced section of the problem. Afterwards, those assumptions were accepted as valid for the complete scenarios of a lightning impact to a building.

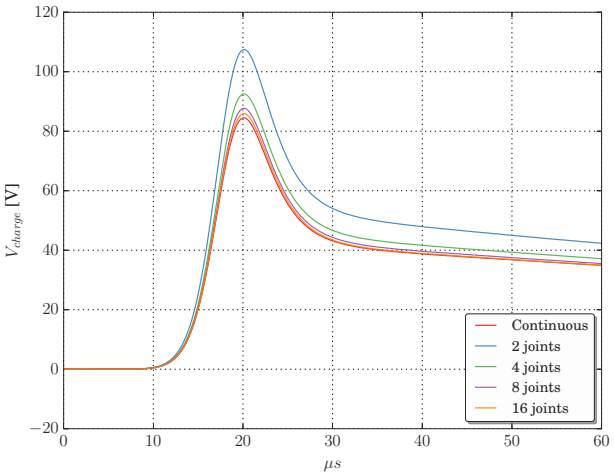

Figure 3.62: Effect of the presence of expansion joints in the voltage at the 50 Ω load, for a positive first stroke.

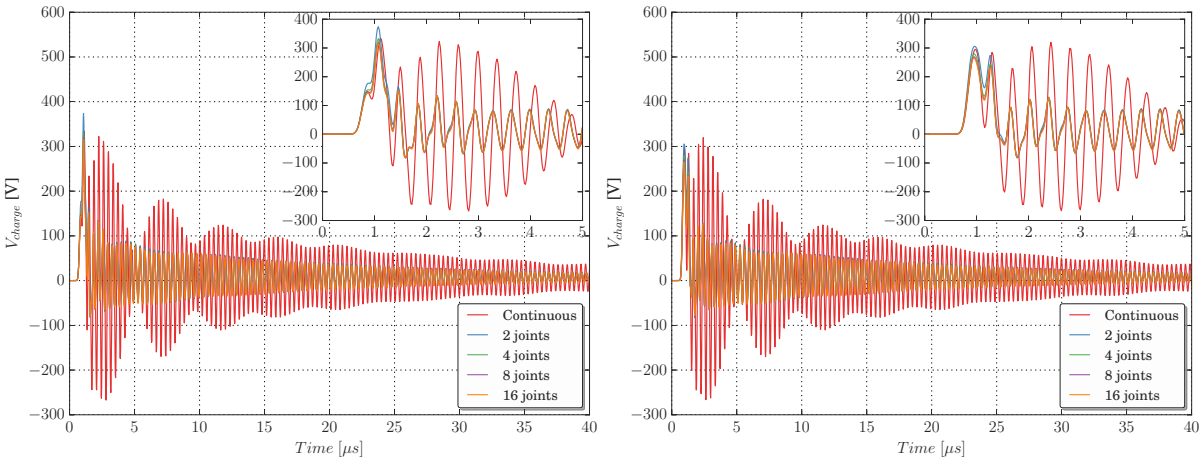

(a) At the building side. **(b) At the remote side.**

Figure 3.63: Effect of the presence of expansion joints in the voltage at the 50 Ω load, for a negative subsequent stroke.

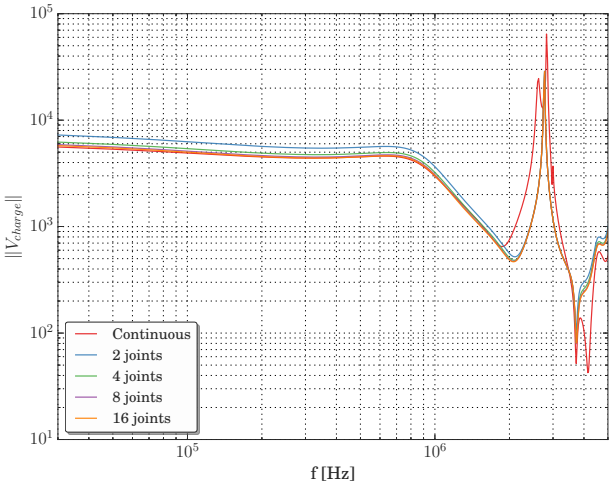

Figure 3.64: Effect of the presence of expansion joints in the frequency response of the voltage at the 50 Ω load. Building side. For a negative subsequent stroke.

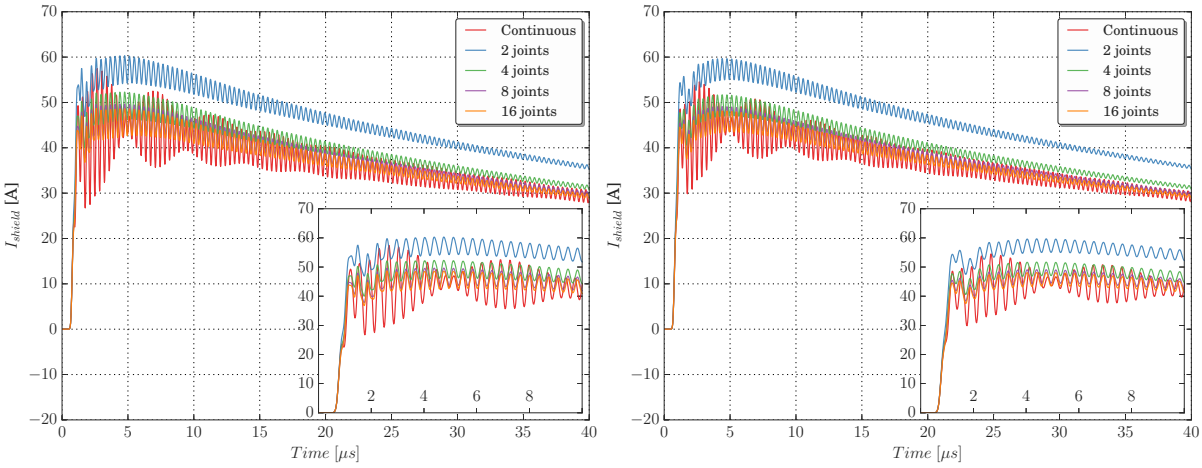

(a) At the building side. **(b) At the remote side.**

Figure 3.65: Effect of the presence of expansion joints in shield current. For a negative subsequent stroke.

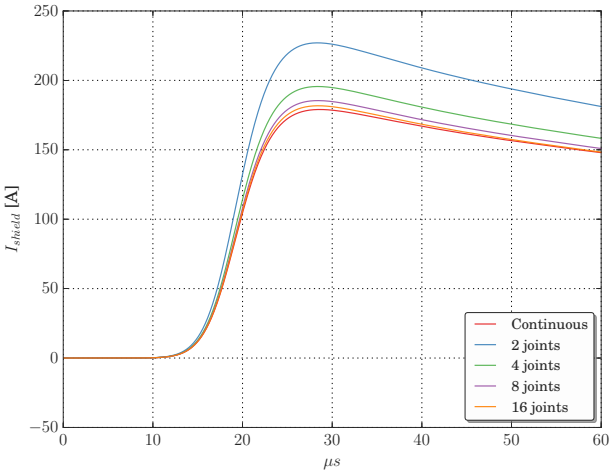

Figure 3.66: Effect of the presence of expansion joints in shield current. For a positive first stroke.

3.14 The type of canalization of the IM cable.

Up until now, the IM cable has been considered inside a cable duct, but in general it can be placed along different types of canalizations or routes, it can be directly buried into the soil, or inside a dielectric pipeline. In this section, different type of routes are going to be presented, in order to observe their influence on the transient voltages at the extremity of the cable.

The four different types of cable routes are:

- An equivalent PVC pipe of $3\,\varepsilon_0$ and $\varnothing$=4 inches
- An square air trench of equal side than the FDTD cell (0.5 m)
- A cable duct as depicted in 3.2
- A directly buried coaxial cable.

The general case study to test the different cable routes is the reference 50 m$\times$50 m$\times$50 m building of figure 3.1. Here to correspond each case, the axis of the control cable is maintained, this is, the conductor in a pipe, directly buried or in an air trench, is located along the same horizontal axis as the conductor inside the cable duct of the reference case.

The EM model for all but one of the canalizations considered have been explained, the case of the cable running inside a pipeline is of special interest, since an equivalent model adapted to the thin wire formalism of Holland must be implemented. In the next section this subject is briefly assessed.

3.14.1 Equivalent model of a pipeline for a Holland thin wire

To model a dielectric pipeline, an special consideration must be made to the modified version of the formalism of Holland [6]: a coaxial cable inside a pipeline, as suggested in figure 3.67, is modeled with a modified insulation jacket, in which the dielectric material has an equivalent permittivity given by (3.3) [7], and an external radius equal to that of the pipeline.

$$\varepsilon_{eq} = \frac{\log(\frac{r_{pipe}+T_{pipe}}{r_{iso\ \ in}+T_{shield}})}{\frac{\log(\frac{(r_{iso\ \ ext})}{r_{iso\ \ in}+T_{shield}})}{\varepsilon_{iso\ \ ext}} + \frac{\log(\frac{r_{pipe}}{r_{iso\ \ ext}})}{\varepsilon_0} + \frac{\log(\frac{r_{pipe}+T_{pipe}}{r_{pipe}})}{\varepsilon_{pipe}}} \tag{3.3}$$

In the next section, the comparison of the transients for different type of canalizations are presented.

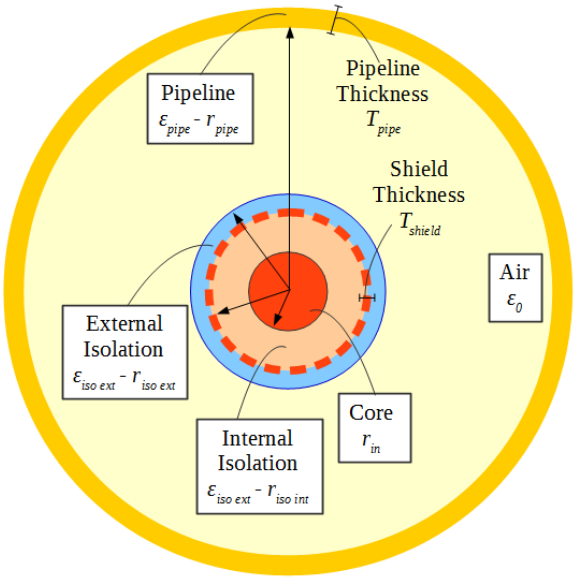

Figure 3.67: A coaxial cable inside a dielectric pipeline

3.14.2 Transients of a IM cable for different canalizations

The voltages at the 50 Ω load for a negative subsequent stroke are shown in figures 3.68a and 3.68b.

At first, it can be observed that the transient voltages when the cable is inside a cable duct are severely attenuated that for the rest of the cable routes. This is expected, since the cable duct acts not only as a shielding element from external fields penetrating into the soil, but as a current conductor element that otherwise, propagates into the cable shield.

Then, it is interesting to note that when the cable is in a pipeline and directly buried, the voltages are slightly higher at the remote extremity than at the building extremity. This might be caused by the induction from nearby components along the cable route: the building, the foundations and the grounding grid. Here, equivalent distributed sources along the cable shield, add to the conductive component entering from the building side. This effect is accentuated for the case of a pipeline, in which the equivalent shunt capacitance of the shield is higher, contributing more to the cumulation of electrical charge along the path, therefore inducing more voltage at the remote end.

The above phenomenon does not replicates for a cable passing through an air trench, since the air-ground interface stops the radiated fields from nearby components to reach the cable shield in the same manner. In reality, the equivalent dielectric pipeline should behave more like this, since the cable is laying inside and air medium, isolated from the ground through the pipeline walls.

Nevertheless, for a negative subsequent stroke; it can be seen that the differences in rise-time and peak voltage between the routes different from the cable duct are

relative small. Which suggest that these case scenarios are mainly governed by a conductive effect: the current entering to the shield through the junction with the building.

Finally, for a positive first stroke; figure 3.69 indicates that if the cable runs outside the cable duct the response is the same independently of the canalization. And, more important, reaching an amplitude potentially dangerous to the electronic equipment.

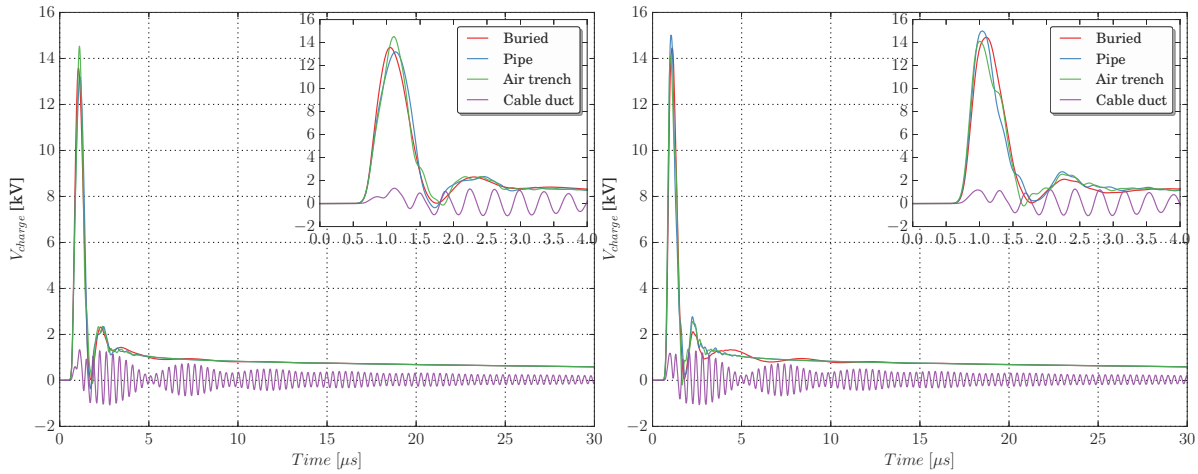

(a) At the building side **(b) At 100 m from the building**

Figure 3.68: Effect of the presence of metallic trays in the voltage at the 50 Ω load, for a negative subsequent stroke.

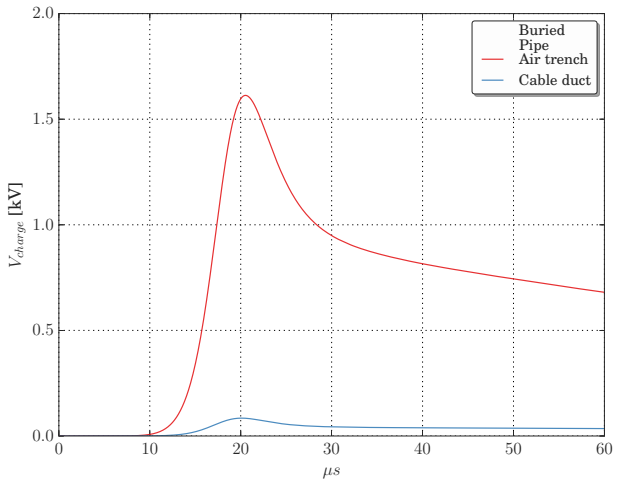

Figure 3.69: Effect of the presence of metallic trays in the voltage at the 50 Ω load, for a positive first stroke.

3.14.3 Synthesis of the effect of the cable route

- The induced voltages of a cable inside a cable duct depends highly of the induced component into the cable shield. Contrary to the voltages of the cable

running in a different route, which highly depends on a conductive component flowing into the shield.

- The cables directly buried and running in a pipeline, are susceptible of induction along the cable path, from the nearby components: building, foundations, and grounding grids, which contributes to higher transient values at the remote end.
- Governing the rise-time and voltage peaks, there are no major difference between the use of canalizations different from the cable duct.

3.15 Synthesis of the parametric study.

Table 3.4 resumes the main conclusions of the effects studied in this chapter.

Table 3.4: Synthesis of the effects considered on the voltages at the cable terminations.

Effect	Variation considered	Negative subsequent stroke		Positive first stroke	
		Voltage magnitude	Transient waveshape	Voltage magnitude	Transient waveshape
Soil resistivity	100 Ωm, 500 Ωm, 1000 Ωm	The peak is proportional to ρ. Most significant variation at lower values of ρ. Influence of high ρ does not differ between scenarios.	The risetime is inversely proportional to ρ.	Same effect as for the negative subsequent stroke	Same effect as for the negative subsequent stroke
Building Size	15 m, 35 m, 50 m, 100 m	Heavily proportional to the building size.	The risetime and the resonant oscillations are proportional to the building size.	Same effect as for the negative subsequent stroke.	Same effect as for the negative subsequent stroke.
Grounding of the cable duct	Open end / Distributed grounding / Grounded end	No influence		Lower magnitude when is open. No influence when a method of grounding is used	Less decay time when is open. No influence when a method of grounding is used.

Continued on next page

Table 3.4: Synthesis of the effects considered on the voltages at the cable terminations.

Effect	Variation considered	Negative subsequent stroke		Positive first stroke	
		Voltage magnitude	Transient behavior	Voltage magnitude	Transient behavior
Grounding of the shield	At both sides / At the building / At remote point.	Lesser value when is remotely grounded.	Less attenuation when is only grounded at the building.	Negligible values when is open at any extremity	
External grounding grid	Foundations - Ring - Grid	No significant difference for each case		Significantly lower values when the grid is used. Non significant difference between the rest of the cases.	Reduced decay time for the grid. Similar decay behavior for the rest of the configurations.
Cable length	25 m, 50 m, 100 m	Proportional to the cable length.	The risetime and the intensity of the resonances are proportional to the length.	Same effect as for the negative subsequent stroke.	The risetime is inversely proportional to the cable length.

Continued on next page

Table 3.4: Synthesis of the effects considered on the voltages at the cable terminations.

Effect	Variation considered	Negative subsequent stroke		Positive first stroke	
		Voltage magnitude	Transient behavior	Voltage magnitude	Transient behavior
Lightning strike position	far corner - center - close corner	Higher values the closer to the cable duct.	Relative small amplification of the resonances the closer the impact is. Unaltered resonant frequencies.	Same effect as for the negative subsequent stroke	Small proportionality between the risetime and the closer the impact is.
EM model building wall	5 m grid - 10 m grid - Lossy wall	Inversely proportional to the density of the wall.	Unaltered resonant frequencies.	Same effect as for the negative subsequent stroke	Decay time inversely proportional for the denser wall. Similar risetimes between all.
Cable trays	With – without	The presence of trays significantly diminish the peak voltage.	The presence of cable trays diminish the resonant frequencies.	Same effect as for the negative subsequent stroke	The presence of trays reduces the risetime

Continued on next page

Table 3.4: Synthesis of the effects considered on the voltages at the cable terminations.

Effect	Variation considered	Negative subsequent stroke		Positive first stroke	
		Voltage magnitude	Transient behavior	Voltage magnitude	Transient behavior
Expansion joints	2 bridges - 4 bridges - 8 bridges - 16 bridges	No significant influence.	Regardless of the amount of bridges, the presence of expansion joints severely diminish the resonant behavior. Relative unchanging its frequency.	Inversely proportional to the amount of bridges.	No significant influence.
Type of canalization	Pipeline - buried cable duct	The cable duct offers a significant reduction of the peak voltages. Otherwise, relatively large and dangerous voltages appear.	The resonant behavior appears only at the cable duct scenario.	Same effect as for the negative subsequent stroke	The risetime augments for the scenario with cable duct.

References

[1] Nuclear Safety Standards Commission (KTA). *Design of Nuclear Power Plants Against Damaging Effects from Lightning*. 2009.

[2] S. Visacro et al. "Lightning Response of Grounding Grids: Simulated and Experimental Results". In: *IEEE Transactions on Electromagnetic Compatibility* 57.1 (Feb. 2015), pp. 121–127. ISSN: 0018-9375. DOI: 10.1109/TEMC.2014.2362091.

[3] S. Visacro. "What Engineers in Industry Should Know About the Response of Grounding Electrodes Subject to Lightning Currents". In: *IEEE Transactions on Industry Applications* 51.6 (Nov. 2015), pp. 4943–4951. ISSN: 0093-9994. DOI: 10.1109/TIA.2015.2445738.

[4] R. J. Gustafson, R. Pursley, and V. D. Albertson. "Seasonal grounding resistance variations on distribution systems". In: *IEEE Transactions on Power Delivery* 5.2 (Apr. 1990), pp. 1013–1018. ISSN: 0885-8977. DOI: 10.1109/61.53115.

[5] E. Bachelier et al. "Protection against lightning of reinforced concrete buildings". In: *Lightning Protection (ICLP), 2014 International Conference o*. Oct. 2014, pp. 735–740. DOI: 10.1109/ICLP.2014.6973220.

[6] Christophe Guiffaut and Alain Reineix. "Des fils obliques pour une modélisation conforme et sans maillage des câbles dans la méthode FDTD. Bilan et extensions". In: *17ème Colloq. Int. Expo. sur la Compat. Electromagnétique - CEM 2014*. Clermont-Ferrand, France, 2014.

[7] Mohammad E M Rizk et al. "Investigation of Lightning Electromagnetic Fields on Underground Cables in Wind Farms". In: *IEEE Trans. Electromagn. Compat.* 58.1 (2016), pp. 143–152. ISSN: 0018-9375. DOI: 10.1109/TEMC.2015.2493206.

Chapter 4

A meta-model for the lightning induced voltages in IM cables

4.1 Introduction

As shown in the previous chapter, the lightning induced voltages in the terminations of an Instrumentation & Measurement (IM) cable is a complex study that involves a wide range of parameters. From the parametric study performed, it is not obvious to determine precisely the manner in which all those parameters interact and influence the transients.

Up until now, the effects of the parameters have been evaluated separately around a reference case, this strategy excludes the possibility of evaluating parameter relations, effects reinforcements or reduction. For example, it has been seen that the peak voltage is proportional to the cable length, and inversely proportional to the building size. This causes that the response of a long conductor connected to a large building cannot be easily extrapolated from the previous studies.

In general, for such a complex case study all the different parameters interact, and whether these interactions cause more or less influence on the final response of the cable is yet to know.

In addition to continue the study of the parameters interactions, at the beginning of this work; it was estated that a computationally efficient tool is necessary to assess the induced voltages at the terminations of a IM cable. Therefore, the proposal of this chapter is to develop a statistical meta-model, based on the parameters of interest studied in the previous chapter.

This meta-model is going to be obtained from a set of scenarios that consider different parameter combinations. Since the nature of these parameters is diverse, and the amount of different scenarios is elevated, a special technique to efficiently vary the parameters is adopted: The Design of Experiments (DoE).

Therefore, in this chapter the generalities of the DoEs techniques are explained, alongside with the criteria to generate the scenarios to study. Then, the details of the

technique implementation to our problem of interest are explained. And finally, at the end of the chapter, the resulting meta-models are presented.

4.2 Overview of the Design of Experiments technique

The Design of Experiments (DoE) technique is an approach to conceive a set of tests, or experience to execute during a study. This technique has evolved from the early years of the 20^{th} century and the agricultural industry [1], to our days in which is used in almost every area of human activities: social sciences, manufacture industry, biology and chemical laboratories, and computer sciences.

Experiments are needed to understand a phenomenon or test a given hypothesis, nevertheless; the amount of experiences that can be performed is as limited as the resources available. The Design of Experiments technique helps to optimize the results and conclusions of a set of tests [2], particularly; in computational simulations with a large set of input parameters, the DoE allows one to select a manageable amount of cases in an efficient manner [3].

In general, the DoE allows one to:

- Understand the influence of the input parameters in the response of a phenomenon. In a manner that:
  - The most relevant parameters are discerned.
  - If some interactions or correlations between parameters exist, they can be detected.
  - The nature of the influence can be established: linear, quadratic, inverse proportional,...
- Develop a meta-model that can predict the response of the phenomenon to parameter combinations that have not been tested.
- Find a parameter combination that helps to optimize the response, i.e., the combination that maximize or minimize the output of the developed model.

In terms of the DoE, the input parameters are known as *factors* (x_i), and the output parameters are known as *responses* (Y_i). In the following section, brief considerations of factors and responses in DoE are presented.

4.2.1 The factors of a DoE

The factors of a DoE can have different natures, but in general, they can be classified as two types:

- **Quantitative factors:** are variables of numeric nature. They can be continuous or discrete. They are usually described with two *levels*: "low" and "high", representing the lower and upper bound respectively [4]. More levels can be possible, specially for the discrete factors. Typical quantitative factors are: distances, temperatures, pressure, volume,...

- **Qualitative factors:** are variables of nominal value. They can be described with more than two levels, with no special proportion or quantifiable relation between them. Examples of qualitative factors are: the state of a switch: on-off, the name of the technician performing the test, the gender of a test subject,...

Numerically, the levels of the factors are treated as -1 and +1, for the "low" and "high" level respectively. The difference in the treatment is that, the quantitative factors can adopt values in-between those lower-upper bounds. While qualitative factors are usually restricted (but not exclusively) to those two levels.

The above is important, since DoE techniques take advantages of the continuing spectrum of quantitative factors to simplify the amount of scenarios to evaluate, while in general for the qualitative factors, the scenarios are forced to always perform both level evaluations. Therefore, for now; it can be estated that a DoE becomes more restricted or less practical while the number of qualitative factors augment in quantity and in levels.

The numerical arrangements of the factors combinations are known as a Design Matrix (DM), this matrix is composed in its columns by the arranged factors, and in its rows by the factor combinations to execute. Each factor combination is also known as a Design Point (DP),or an *experience*.

The DM is not generally square, it can have any shape and composition, depending on the type of factors composing the problem, the objective of the experiment, and the type of response desired. As that; the DM is assembled depending on the DoE technique considered.

In the next section, some comments concerning the response of a DoE are going to be addressed.

4.2.2 The response of a Design of Experiments

Regarding the response, the idea is not necessarily to obtain a physical coherent relation between input parameters and experiment response, but to develop a mathematical expression that relates all the factors and approaches to the main objective of the study: to simulate the "real" response, to maximize or minimize its value, or to carefully screen for factors influences and dependencies.

Usually the expression to generate a model is in the form of a Response Surface Metamodels (RSM) [3, 5], which is a practical expression that can be obtained through

a regression, and allows one to address linear (x_i), quadratic (x_i^2), or cubic (x_i^3) effects, along with its interactions ($x_i x_j \ldots x_i x_j x_k \ldots$).

The expression (4.1) is an example of a quadratic RSM of quantitative continuous values, with an independent random error ε of null mean value. The qualitative factors can also be included if the Analysis of Variance (ANOVA) regression is used [3].

$$Y = \beta_0 + \sum_{i=1}^{n} \beta_i \left(x_i - \overline{x_i}\right) + \sum_{i=1}^{k} \sum_{\substack{j=1 \\ j \geq i}}^{k} \beta_{ij} \left(x_i - \overline{x_i}\right) \left(x_j - \overline{x_j}\right) + \varepsilon \tag{4.1}$$

The RSMs are not the only type of expressions to characterize the response of a DoE, but in general problems of the industry, it has been shown that 2^{nd} order RSMs optimize with an acceptable incertitude the response of an experience [6].

The selection of the meta-model might be important to determine the DM, that depends on the type of DoEs technique considered. In the next section, some aspects concerning the types of techniques to design an experiment are going to be assessed.

4.2.3 Types of Design of Experiments

The choice of the type of DoE depends in several aspects:

- The amount of factors to vary.
- The nature of those factors: quantitative and continuous, quantitative and discrete, or qualitative.
- The amount of levels for the discrete and qualitative factors.
- The restrictions in the possible factor combinations.
- The type of response model: with only main effects, interaction effects, or higher order effects.
- The interest of the analysis: the screen for effect influence, to optimize, or to maximize the response

Two kind of experimental designs are going to be treated in this section: the factorial design, and the I-optimal designs.

The factorial design helps to illustrate the process of generating the DM, as well as the inconvenience to represent designs with a big amounts of factors.

Factorial designs

Factorial designs examine all the possible combinations for the levels of all the factors interacting in an experiment. The notation suggests that, for a set of k factors of m levels, a design to be called m^k-factorial.

They are particularly useful for design with quantitative continuous factors, since they only have two levels: -1 and 1.

To compute a 2^k-factorial design first, the amount of design points $N = 2^k$ is needed, this will indicate the amount of rows of the DM. Then it starts the constructions of the columns of the single factors $x_1 \dots x_k$: the first column is written interchanging "low " and "high" levels, the second column this is done in groups of 2, the third in groups of 4, and so on following the powers of 2.

To illustrate this procedure, take the classical 2^3-factorial design with the design points at the corners of a cube given in figure 4.1, with all the design points related to its DM in table 4.1. For more factors, the design becomes an "hypercube", and which is not possible to represent graphically in three dimensions.

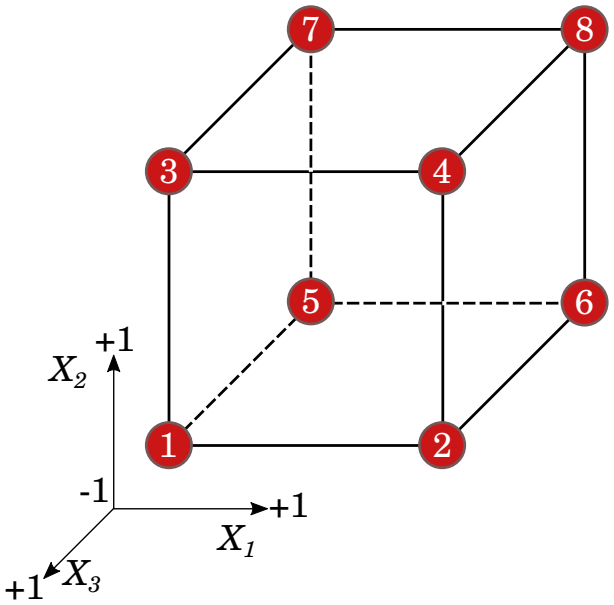

Figure 4.1: Design cube for 2^3-factorial plan

Usually, a factorial design of N experiences can contribute to determine principal effects and first order interactions. For higher order models, additional inner design points of the hypercube, or replications of the experiments are needed. The idea is to maintain enough Degrees of Freedom (DF) to adjust a reliable meta-model, this is; to have more DP than model unknowns.

A factorial design becomes cumbersome for experiments with an elevated amount of factors, or with factors with more than 2 levels. Take for example a small design with 6 factors: 2 with three levels, and four with 2 levels. That will make a design with $N = 3^2 \cdot 2^4 = 144$ experiences. Whether this number is acceptable or not, is at the

Design point	X_1	X_2	X_3
1	1	1	1
2	-1	1	1
3	1	-1	1
4	-1	-1	1
5	1	1	-1
6	-1	1	-1
7	1	-1	-1
8	-1	-1	-1

Table 4.1: Design Matrix for 2^3-factorial plan.

criteria of the designer, who estimates the resources available and the reproducibility of each experience.

To the problem of the size of the experiment N, it must be added the amount of experiences needed in order to construct a response model in agreement with the objectives of the study: if only direct factor influence is needed, a first order linear model can be used, to which a factorial design usually is well suited. But, for higher order models that aims to optimize the response, additional design points that consider the inner space of the hypercube are needed.

Finally, experimental designs of factorial type are not recommended for discrete or qualitative factors, specially when they take more than 2 levels. Also, factor combinations with restrictions are not possible. This types of design demand for a different or more complex techniques: Latin Hypercubes, optimal designs. In the next section, the optimal designs are going to be briefly assessed.

4.2.4 Optimal Design of Experiments

Optimal DoE are conceived for large amount of factors, with special inclusion of discrete and qualitative ones. They heavily depend on the type of response model desired for the set of input factors, and try to optimize the generation DM following a specific criteria related to the objectives of the experience.

Mainly, two kinds of optimal design are commonly used: D-optimal and I-optimal. The first tries to minimize the amount of experiences in order to better scan the effects and their influence on the response. The second tries to optimize the prediction of the response, demanding perhaps more DP than an D-optimal design.

Since the criterion of I-optimality is conceived to obtain a better prediction of the experiment response, it finds any factor setting that produces the desired response. This is specially useful to this work, since the case of interest is to obtain the transient voltages efficiently: fast, precisely, and within an acceptable flexibility concerning the variation of the input parameters.

In our case, using an I-optimal design will allow us:

- To know which factor combination gives a voltage closest to the FDTD simulations.
- To determine the regions of the design space where the voltage is below an acceptable value.

Since the aim of an I-optimal DoE is to generate a meta-model that predicts the response within an acceptable amount of uncertainty, the used optimality criterion is to minimize the average prediction variance in expression (4.2)[**Siafitry2015**, 1, 6]. To solve the minimization, different optimization algorithms can be used, in any case; each execution will stop for a local minimum, and therefore; for the same set of factors, different DMs can be obtained.

$$\min\{Avg.Variance\} = \min\left\{TRACE\left[\left(\boldsymbol{X}^T\boldsymbol{X}\right)^{-1}\boldsymbol{M}\right]\right\} \tag{4.2}$$

$\boldsymbol{X}$ $\rightarrow$ is the Design Matrix
$\boldsymbol{M}$ $\rightarrow$ is the Moments Matrix $\boldsymbol{M} = \int_R f(x) f'(x)\, dx$
$f'(x)$ $\rightarrow$ A single row of the Design Matrix.
R $\rightarrow$ The entire domain of the factors.

This type of DoE carries intrinsically two limitations:

- They are highly dependent on the chosen meta-model to described the phenomenon. And although in general a quadratic model suits most of the cases, in reality no model can be entirely adapted to a problem [7]. Therefore, there is always the possibility of choosing a design based on a model not suited to the particular problem.
- The optimization process stops at a local minimum, therefore; there is no entitled warranty that the DM is the absolute optimal planning for the problem of interest [6, 8].

Nevertheless, observing the approach in this work to the problem of Lightning Induced Voltage (LIV) in IM cables, it can be justified the use of an I-optimal DoE:

- Different types of parameters of interest (factors) are involved: continuous (distances), discrete (number of expansion joints bridges), and qualitative (grounding connections of the shield).
- There are constraints between the feasibility of factor combinations.
- Although the FDTD simulations are relatively fast with respect to other numerical methods, they still require a couple of minutes-to-hours to solve. Once the meta-model is established, its solution is almost instantaneous.

- The focus of the meta-model is to predict the response of an equivalent FDTD simulation within an acceptable margin of error.

In the next section, the implementation of a DoE I-optimal design adapted to the problem of interest is going to be shown.

4.3 The Design of Experiments adapted to the lightning induced voltages in IM cables

At this point, it is worth noting that, all the algorithms related to the DoE, model fit and statistical analysis are carried out with the toolbox available in the JMP software [9].

To obtain a meta-model using DoEs, first the amount and type of factors must be established, and then the base meta-model must be constructed. With those two steps, an I-optimal algorithm can generate a DM.

4.3.1 The factors for the problem of LIV in IM cables

As estated previously, the first step is to generate a DM, the amount of factors, as well as their nature and domain of validity.

In general, in order to have a final meta-model that accurately predicts the response of an experiment, two DMs are generated. The first one is smaller, and is used to perform a screening DoE that helps in the selection of the most influential parameters. Then, a second DoE is performed with those "influential" parameters, this time with more refinement on their selection, their range of variation, and specially focusing in the construction of a more precise meta-model.

The effect screening part was covered in detail in the chapter 3, in which a set of parameters was carefully varied to observe its influence in the transient voltages. These first extensive studies, resulted in special information concerning the way in which each parameters shall be considered inside a DoE: the nature of the factors, and its range of variation.

According to the observations of the previous chapter, the feasibility of the implementation in the computational FDTD code, and the prospective size of the DM, the most influential parameters selected are:

- **The cable length:** It is treated as continuous factor between 10 m and 100 m. By extension, the structure of its canalization, the cable duct or the dielectric pipeline, have the same distance.

- **The building size:** Since it is a cubic structure, it is considered through its side dimension, as continuous factor between 15 m and 55 m.

- **The Soil resistivity:** It is a continuous factor between $100\,\Omega$m and $1000\,\Omega$m
- **The amount of bridges in the expansion joints:** It is a numerical discrete factor with the range $\{2, 4, 8, 16\}$ bridges per joints, with a maximum section of cable duct of $20\,$m.
- **The connection of the shield:** It is considered as a qualitative factor with two level: Connected to the reference potential at the remote termination, code: "CC". Or open at the remote termination, code: "CO". The termination at the building side is always connected.
- **The amount of conductors around the building:** It is considered as a discrete numerical factor, within the range of $\{1, 4, 7\}$ conductors uniformly distributed around the building. This range is imposed specially from the minimal building size, it is unpractical and unrealistic to surround a building with side walls of $15\,$m with more than 8 cable ducts.
- **The Type of conductor canalization:** It is a qualitative factor with two levels: running inside a cable duct, or running inside a dielectric pipe.
- **The model for the building wall:** It is considered as a qualitative factor with two levels: A metallic grid of steel conductors, code: "Grid". Or a lossy thin plate, code: "Plate"
- **The configuration of the external grounding grid:** It is also a qualitative factor with two level: A copper grounding grid, code: "Grid". Or an external ring running through the edge of the volume of computation, code: "Ring". In any case, the grounding of the building are its foundations.

A special comment shall be made regarding the implementation of the type of conductor canalization and the amount of conductors around the building. It is not advisable to mix together these two factors as they are, otherwise; all the conductors surrounding the building will be the same type of canalization. In order to make a discretization, these two factors are substituted by other two: the amount of cable ducts around a building, and the amount of cable running inside dielectric pipes.

This new conception of the factors forces the use of a restriction: the total amount of conductors around the building cannot exceed 8. Therefore, the DoE must be made with two extra numerical discrete factors, that fulfill the restriction.

In general, for all the case scenarios some parameters will be considered exactly as in the previous chapter:

- The geometries of the cable duct, and the pipeline.
- The model of the coaxial cable: its configuration, and transfer impedance.

- The lightning strikes at the same corner of the building.
- No cable trays are considered inside the cable ducts.
- Whenever the cable is inside a cable duct, the remote extremity of the duct is connected to the closest point in the external grounding system. This, in general is the actual situation for all the Power Generation Center (PGC).

The choice of some of these considerations was made to favor a conservative approach in the study of the induced voltages. This is: the type of transfer impedance, the lightning striking position, and the absence of cable trays, are all parameters that can easily be varied to diminish the induced voltages. Instead, they were fixed to a value known to propitiate higher LIV in IM cables.

Also, a more practical approach must be assessed; to reduce the amount of input factors, is to reduce the size of the DM, and therefore the amount of simulations to perform.

Finally, the input factors to consider for the I-optimal DoE are summarized in table 4.2.

Factor	DoE Variable	Type of variable	Range
Cable length	X_1	Continuous	10 m- 100 m
Building size	X_2	Continuous	15 m- 55 m
Soil resistivity	X_3	Continuous	100 Ωm- 1000 Ωm
Number of bridges	X_4	Discrete	$\{2, 4, 8, 16\}$
Shield grounding	X_5	Qualitative	"CC" or "CO"
Amount of pipes	X_6	Discrete	$\{1, 4, 7\}$
Amount of ducts	X_7	Discrete	$\{1, 4, 7\}$
Wall type	X_8	Qualitative	"Grid" or "Plate"
External grounding	X_9	Qualitative	"Grid" or "Ring"
Restriction		$X_6 + X_7 \leq 8$	

Table 4.2: Summary of the factors considered for the meta-model of LIV in IM cables.

In section 4.2.4 it was noted that an I-optimal design requires the definition not only of the factors, but of the responses and the meta-model to describe those responses. In the next section, this aspect is going to be treated.

4.3.2 The meta-model for the response of the LIV in IM cables

The lightning induced voltages at the terminations of IM cables are described with a transient behavior. This behavior is not trivial to describe with a single output variable. Therefore, a practical approach to the problem is suggested; to consider only the peak induced voltage for each excitation, and each cable canalization. This is:

- It is known that three normalized current sources are recommended to be considered for lightning studies: positive and negative first strokes, and negative subsequent strokes. And, in the previous chapter it was observed that the factors interact differently for each excitation, therefore, here they are going to be assumed as uncorrelated [10].

- The cables run in two types of canalizations: cable duct and dielectric lines. It is also going to be assumed that both responses are not correlated, this is; a variation in one, does not affects the other.

In a manner that, for a single DP, three FDTD simulations are executed, and two output variables obtained: the maximum induced voltages among all the cable ducts, and the maximum induced voltages among all the cables running inside dielectric pipelines.

Each one of the six unrelated output variables, is going to be modeled with the same base meta-model: a 2nd order surface model, such as the one depicted in expression (4.3).

$$Y = \sum_{i=1}^{9} \beta_i \left(\frac{x_i - \overline{x_i}}{D_i^{max}} \right) + \sum_{i=1}^{9} \sum_{\substack{j=1 \\ j \geq i}}^{9} \beta_{ij} \left(\frac{x_i - \overline{x_i}}{D_i^{max}} \right) \left(\frac{x_j - \overline{x_j}}{D_j^{max}} \right) \tag{4.3}$$

It must be noted that the variables of the meta-model are proposed in their *coded* format: $\frac{x_i - \overline{x_i}}{\Delta_{x_i}}$. In which $\overline{x_i}$ is the mean value of the factor, and D_i^{max} is its absolute deviation. In this manner, regardless the dimensions of the factor, its variability inside the meta-model will always be limited between -1 an +1.

As a final note, in case the factor i is of qualitative nature, then the argument $\beta_i \left(\frac{x_i - \overline{x_i}}{D_i^{max}} \right)$ becomes a constant K_i that depends on the level of the variable.

At the end, after performing the regression for the six output variables over the generic meta-model of (4.3), six different meta-models that predict the output voltages with an acceptable level of incertitude are going to be obtained.

With the factors and the responses described, the DM can be constructed.

4.3.3 The Design Matrix for the problem of LIV in IM cables

With the input factors as described in table 4.2, and the generic response model of expression (4.3), the I-optimization algorithm [9] results in table 4.3. It must be stated that the I-optimal design is a result from an optimization problem, it depends on tolerance criteria, and stops at a local minimum [6].

The above implies that, even for the same set of factors and response models, the DM obtained for a second execution of the DoE will not be the same. And, although the author has not tested if two different DM generate relative different

meta-models, it is supposed that the final conclusions of this work are not depending on the particular design points of the DM.

Design point	Cable length	Building Size	Resistivity	Bridges	Grounding Shield	Amount pipes	Amount ducts	Wall Type	Grounding
	X_1	X_2	X_3	X_4	X_5	X_6	X_7	X_8	X_9
1	100	55	820	16	CO	1	4	Plate	Ring
2	23,5	17	1000	4	CC	1	7	Plate	Ring
3	10	55	730	4	CC	7	1	Plate	Grid
4	64	23	1000	16	CO	1	1	Plate	Ring
5	37	15	100	4	CC	1	7	Grid	Grid
6	86,5	27	730	16	CC	1	7	Grid	Ring
7	100	15	415	16	CO	1	7	Plate	Grid
8	10	15	100	16	CC	1	7	Plate	Grid
9	10	27	100	2	CC	1	1	Grid	Ring
10	32,5	55	910	16	CO	4	4	Plate	Grid
11	10	15	910	16	CC	7	1	Grid	Ring
12	100	27	640	2	CC	4	4	Grid	Grid
13	59,5	53	955	4	CO	7	1	Grid	Ring
14	10	55	1000	16	CC	4	1	Plate	Ring
15	100	55	1000	2	CC	1	1	Grid	Grid
16	82	15	550	16	CO	4	1	Plate	Ring
17	10	55	1000	16	CC	1	7	Grid	Grid
18	100	15	460	8	CC	1	1	Plate	Grid
19	10	15	1000	2	CO	1	1	Plate	Grid
20	28	15	640	4	CO	1	7	Grid	Ring
21	37	29	1000	16	CC	4	1	Plate	Grid
22	91	15	100	8	CO	7	1	Grid	Ring
23	73	15	100	8	CC	4	4	Plate	Grid
24	23,5	45	100	16	CO	4	4	Plate	Ring
25	10	25	325	2	CC	7	1	Plate	Ring
26	100	19	100	4	CC	1	7	Plate	Ring
27	10	55	325	2	CC	1	7	Grid	Ring
28	100	45	100	16	CO	7	1	Plate	Grid
29	10	55	100	2	CO	4	1	Plate	Ring
30	64	33	100	2	CC	1	4	Plate	Grid
31	77,5	23	550	2	CO	1	1	Grid	Grid
32	100	15	1000	4	CC	1	4	Grid	Ring
33	46	35	730	8	CC	4	4	Grid	Grid
34	100	29	100	16	CC	4	1	Grid	Grid
35	100	19	1000	16	CO	7	1	Grid	Grid
36	86,5	55	100	8	CO	4	4	Grid	Grid
37	55	15	100	16	CO	1	1	Plate	Grid
38	100	15	1000	16	CC	7	1	Plate	Ring
39	10	47	100	16	CO	4	1	Grid	Grid
40	10	37	145	4	CO	4	4	Plate	Grid
41	19	55	280	16	CC	1	1	Plate	Grid
42	55	15	1000	2	CC	4	1	Grid	Grid
43	95,5	55	595	8	CC	1	7	Plate	Grid
44	100	55	100	4	CC	4	1	Grid	Ring
45	23,5	15	775	16	CC	1	1	Grid	Grid
46	95,5	39	1000	8	CO	4	4	Plate	Ring
47	50,5	55	190	16	CC	7	1	Grid	Ring
48	91	49	325	16	CO	1	1	Grid	Ring
49	19	17	370	8	CO	1	4	Plate	Ring
50	23,5	41	820	8	CO	1	4	Grid	Grid
51	100	51	1000	4	CO	4	1	Plate	Grid
52	73	49	775	2	CC	1	1	Plate	Ring
53	10	15	1000	2	CO	4	4	Grid	Grid
54	95,5	55	955	2	CO	1	7	Grid	Grid
55	41,5	15	865	4	CO	7	1	Plate	Grid

Table 4.3: Design points conceived with an I-optimal criterion.

4.3.4 Procedure to fit the model

The design points of table 4.3 are conceived to estimate the generic model depicted in expression (4.3). Nevertheless, the estimation of all the effect of the factors carries an

intrinsic error, this is, the coefficients of the predicted model are within an amount of uncertainty.

To decrease the amount of uncertainty more points can be added to the original DM, or the base meta-model can be adapted to better fit the results of the FDTD simulations. The latter approach is adopted in this work.

In order to fit a confident model, some criteria must be followed to discard unacceptable coefficient estimations. In this work the False Discovery Rate (FDR) of the parameters estimation t-test is used.

The t-test of the estimation of a parameter assumes that all the factors have a standard t-distribution [11], and defines the t-ratio of a factor estimate as the relation between its estimation and its standard error.

The aim of this test is to evaluate the probability of the actual parameter being zero, this is; obtain the p-value of the t-ratio. Usually, it is considered that a parameter is well estimated if its probability of being null falls beyond a lower value: $p_{(i)} < 0.01$.

Nevertheless, in recent years, an additional strategy is used to complement the traditional p-value significance test when a lot of experiences are executed: the False Discovery Rate, which is an algorithm useful for identifying the important few effects from the trivial ones. [12].

Here the FDR is going to be used through its LogWorth scale, since it allows one to better illustrate and discriminate highly significant p-values$_{FDR}$ from nonsignificant p-values$_{FDR}$. The LogWorth scale is obtained transforming each factor p-value$_{(i),FDR}$ using expression (4.4).

In a manner that, an effect with a significance of 0.01 or less, has a LogWorth value superior to 2. If this criterion is not satisfied, the effect is discarded and the model re-adjusted. This loop is repeated until all the effects have a LogWorth value superior to 2. The figure 4.2 summarizes the procedure of finding a meta-model with meaningful estimations.

$$LogWorthFDR_{(i)} = -\log_{10}\left(p_{(i),FDR}\right) \tag{4.4}$$

It shall be noted that, the procedure in 4.2 can be executed for higher values of significance levels, obtained perhaps from a simpler meta-model, with significant effects at the cost of a more imprecise prediction of the response. This, although possible, is not a strategy suited to the objectives of this work.

In this section it was described how the problem of lightning induced voltages was adapted to the Design of Experiments technique. In the next section the developed meta-model is going to be presented, alongside with the description of the influence of the parameters.

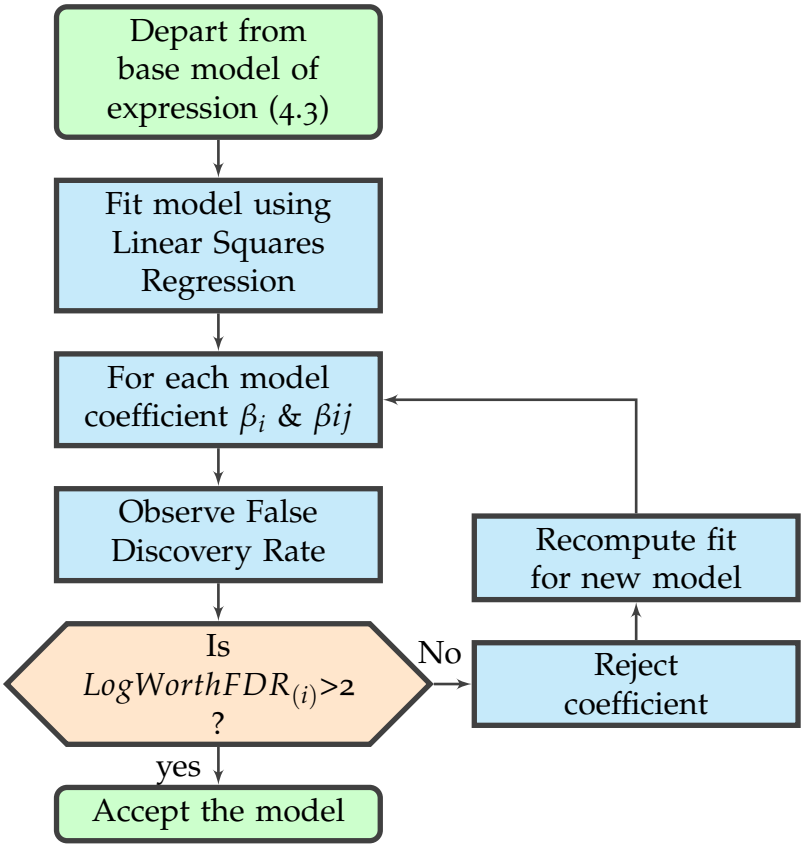

Figure 4.2: Work-flow to find a model for each output variable.

4.4 A meta-model for the LIV of IM cables

In this section the developed meta-models described by expression (4.3), are going to be presented, mainly by depicting their coefficients of principal effects and interactions.

Afterwards, the influence of each parameter is going to be discussed, and finally, some comments on the errors associated to the parameter estimation are going to be reviewed.

4.4.1 Coefficients of the models

The coefficients β_i and constants K_i of the single effects of the six meta-models are depicted in table 4.4. While the crossed coefficients β_{ij} and K_{ij} are depicted in tables 4.5, 4.6, 4.8 and 4.6.

The values indicated in the tables for the qualitative factors are only for their low level value, this is: The cable shield is connected at the remote termination (code:"CC"), the building is modeled with a grid of steel conductors (code:"Grid"), and the external grounding of the building is modeled with a grid of copper conductors (code:"Grid"). If another level of the factor is required, it is enough to change the sign of the coefficient.

It is important to note that, interaction coefficients that are not reported, were discarded effects, since they did not fulfill the criterion of the FDR.

	Inside a duct			Inside a pipe		
Factor	**Neg. S.S.**	**Neg. F.S.**	**Pos. F.S.**	**Neg. S.S.**	**Neg. F.S.**	**Pos. F.S.**
Constant	1049,284	643,818	[2]**	9926,703	7522,657	3085,445
Cable length	903,944	[2]**	171.042	[2]**	5669,528	2219.195
Building Size	[2]**	-105,970	0	-4256,518	[2]**	-215.478
Resistivity	237,568	85,131	-14.382	2834,771	1884,722	[2]**
Bridges	-110,936	-56,221	-25.008	215,126	-251,818	-264.393
Grounding Shield	-118,246	[2]**	87.304	525,932	874,777	1312.484
Amount pipes	-258,311	-106,072	11.066	-692,036	[2]**	774.847
Amount ducts	-267,810	-50,960	32.747	[2]**	-1370,785	298.992
Wall Type	44,345	-17,031	[2]**	-584,131	-487,979	[2]**
Grounding	[2]**	-32,645	-26.881	-845,118	-1222,983	-713.064

Table 4.4: Single parameters β_i and K_i for the maximum voltages in a cable.

_	Cable length	Building size	Resistivity	Bridges	Grounding shield	Amount pipes	Amount ducts	Wall Type
Cable length	-177,198							
Building Size	[2]**	233,82						
Resistivity	325,128	-168,51	-193,562					
Bridges	-148,157	122,324	-12,935	47,955				
Grounding Shield	-10,419	28,146	22,095	–	–			
Amount pipes	58,733	86,267	[2]**	-40,01	20,925	–	-88,297	
Amount ducts	-116,956	126,819	-66,288	23,661	-91,793	-256,024	-67,913	
Wall Type	28,554	-48,368	64,069	–	-15,868	[2]**	–	–
Grounding	-66,024	–	-64,692	-11,347	-23,14165	102,662	134,742	10,762

Table 4.5: Crossed parameters β_{ij} and K_{ij} for the maximum voltages in a cable inside a duct. For a negative subsequent stroke excitation.

_	Cable length	Building size	Resistivity	Bridges	Grounding shield	Amount pipes	Amount ducts	Wall Type
Cable length	-85,934							
Building Size	-103,020	51,518						
Resistivity	180,786	-24,423	-105,763					
Bridges	[2]**	33,646	-38,292	77,536				
Grounding Shield	-28,018	-29,924	47,699	[2]**	–			
Amount pipes	75,789	41,920	-12,174	69,465	52,346	-54,331		
Amount ducts	-82,359	71,105	-36,891	34,357	-92,298	-50,780	-45,968	
Wall Type	-11,211	[2]**	34,608	48,205	-19,736	-20,274	9,108	
Grounding	-104,409	-19,539	-15,500	-11,363	-20,667	49,439	37,973	44,945

Table 4.6: Crossed parameters β_{ij} and K_{ij} for the maximum voltages in a cable inside a duct. For a negative first stroke excitation.

[2]Non-communicated value

_	Cable length	Building size	Resistivity	Bridges	Grounding shield	Amount pipes	Amount ducts	Wall Type
Cable length	-62,3918							
Building Size	-19,1727	43,0387						
Resistivity	2**	-18,2652	-21,5471					
Bridges	-45,9162	-16,7224	-55,3220	65,6290				
Grounding Shield	86,6402	-22,6119	44,8320	0,0000				
Amount pipes	43,6598	-5,8238	2**	0,0000	14,5330	57,5515		
Amount ducts	-23,3632	25,6688	-34,6997	54,7846	-84,3137	26,6184	-46,8276	
Wall Type	-22,5157	-31,9662	-15,8267	40,7255	-5,2836	17,0727	48,6942	
Grounding	-80,3352	-35,4234	-24,6725	43,3687	-40,8514	54,0207	2**	28,3707

Table 4.7: Crossed parameters β_{ij} and K_{ij} for the maximum voltages in a cable inside a duct. For a positive first stroke excitation.

_	Cable length	Building size	Resistivity	Bridges	Grounding shield	Amount pipes	Amount ducts	Wall Type
Cable length	-1853,082							
Building Size	-3111,181	2625,529						
Resistivity	2458,733	-1533,635	-2632,433					
Bridges	121,150	166,996	–	–				
Grounding Shield	450,069	2**	502,580	2**	–			
Amount pipes	1570,894	455,960	155,657	-239,821	-454,327	-1645,255		
Amount ducts	-810,123	1385,963	-249,180	152,757	-623,169	-1087,804	558,761	
Wall Type	-98,676	529,465	345,197	-74,849	-145,939	-505,539	-122,473	
Grounding	2**	776,485	-832,848	-872,078	-205,629	557,498	1112,279	278,323

Table 4.8: Crossed parameters β_{ij} and K_{ij} for the maximum voltages in a cable inside a pipe. For a negative subsequent stroke excitation.

_	Cable length	Building size	Resistivity	Bridges	Grounding shield	Amount pipes	Amount ducts	Wall Type
Cable length	2**							
Building Size	-1413,613	949,219						
Resistivity	1830,83	-814,75	-1177,717					
Bridges	385,596	-187,328	-511,731	2**				
Grounding Shield	-95,478	-503,586	606,826	-69,324				
Amount pipes	1018,933	301,497	-223,306	-296,675	-237,77	-1035,36		
Amount ducts	-675,504	2**	-459,61	-172,84	-552,86	-191,37	-135,965	
Wall Type	-503,715	176,939	-89,827	140,753	-173,423	-78,154	104,366	
Grounding	-1334,5	289,542	-777,22	-350,75	-144,62	185,796	1095,51	294,292

Table 4.9: Crossed parameters β_{ij} and K_{ij} for the maximum voltages in a cable inside a pipe. For a negative first stroke excitation.

_	Cable length	Building size	Resistivity	Bridges	Grounding shield	Amount pipes	Amount ducts	Wall Type
Cable length	-1737,7730							
Building Size	-166,7691	330,4329						
Resistivity	-177,6829	-88,4512	-844,1976					
Bridges	-469,1033	-844,3390	-859,0413	2**				
Grounding Shield	1240,4488	-276,4635	788,2189	-219,5331				
Amount pipes	1409,6748	-284,6087	2**	0	34,1143	441,8670		
Amount ducts	-825,2814	378,0566	-210,2651	697,7365	-1063,0970	1068,9108	923,3399	
Wall Type	-272,3441	-585,9936	-336,0442	514,0037	-389,2503	239,1204	686,4247	
Grounding	2**	-219,7378	-136,8299	283,0662	-988,6932	2**	1466,5426	279,0175

Table 4.10: Crossed parameters β_{ij} and K_{ij} for the maximum voltages in a cable inside a pipe. For a positive first stroke excitation.

4.4.2 Adjustment of the prediction to the simulation data

The results of the relation between the adjusted models and the results obtained with the FDTD simulations are depicted in figures 4.3, 4.4 and 4.5. As it can be seen, the models fit with a coefficient of multiple determination R^2 superior 0.99, which among other things, declares a well adjustment between the prediction model and the results of the FDTD simulations.

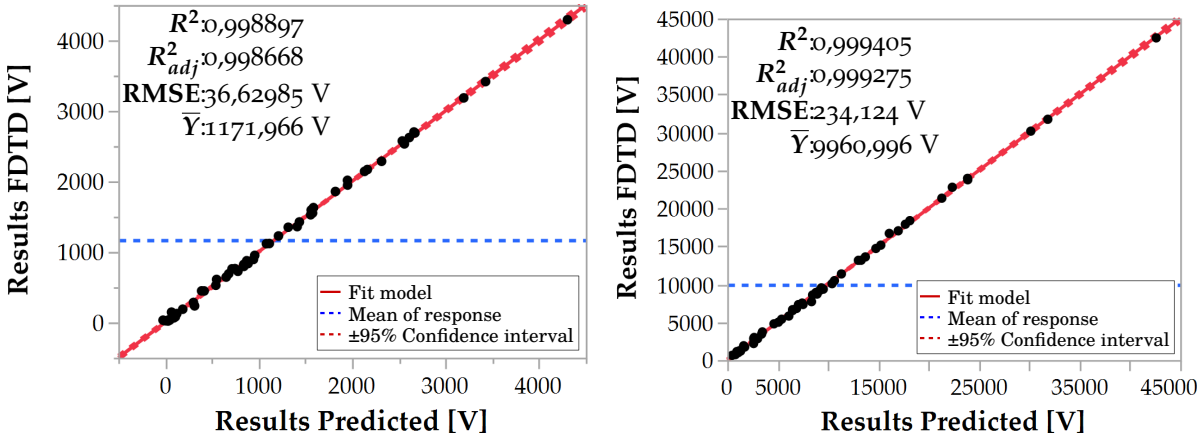

(a) Cable inside a duct. **(b) Cable inside a pipe.**

Figure 4.3: Fit between simulated and predicted values. For a negative subsequent stroke excitation.

The value indicated in the figures as R^2_{adj} is an adjustment to the classical conception of R^2 [13], to the number of parameters used in the model relative to the number of design points, in a manner that helps to compare one model to another. This is specially useful to keep track of the quality of the fit between the different models considered in the process depicted in figure 4.2; the effect discretization following the FDR.

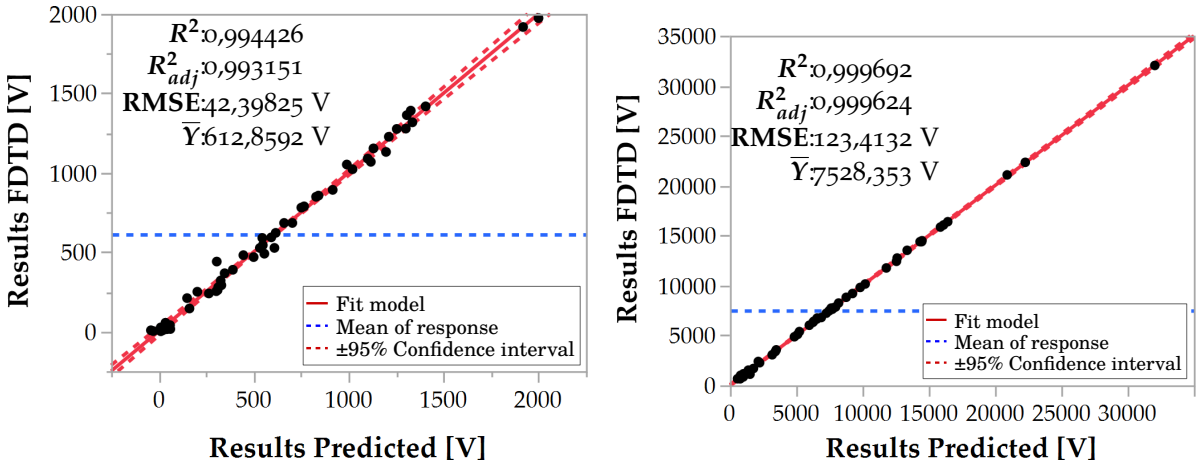

(a) Cable inside a duct. **(b) Cable inside a pipe.**

Figure 4.4: Fit between simulated and predicted values. For a negative first stroke excitation.

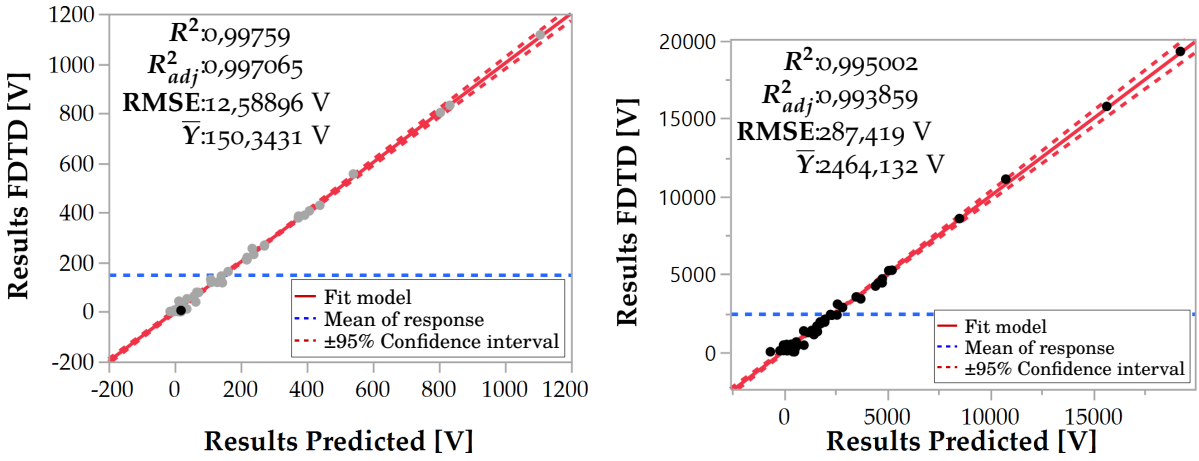

(a) Cable inside a duct. **(b) Cable inside a pipe.**

Figure 4.5: Fit between simulated and predicted values. For a positive first stroke excitation.

Expression (4.5) is used to compute the R^2, with e_i being the residual error for each experience i, and $\sum_{i=1}{}^{N}(y_i - \overline{y})^2$ is the total sum of squares, which is proportional to the variance.

$$R^2 = 1 - \frac{\sum_{i=1}^{N}(e_i)^2}{\sum_{i=1}^{N}(y_i - \overline{y})^2} \tag{4.5}$$

Expression (4.6) is used to compute the R^2_{adj}, with p being the number of coefficients in the model, excluding the constant term, and N the number of design points. As expected, the values of R^2_{adj} are always inferior or equal to R^2.

$$R^2_{adj} = R^2 - \left(1 - R^2\right)\frac{p}{N - p - 1} \tag{4.6}$$

The figures also include the Root Mean Square Error (RMSE) for each model, alongside with the mean value of the response $\overline{Y}$. At first sight, it is interesting to note that, the mean value for a negative subsequent stroke excitation is higher than for a negative first stroke.

This was also observed in the reference cases of the previous chapter, but now, comparing the models and the available data, it can be suggested as a general rule that the peak voltages of cables running inside cable duct tend to be higher when the excitation considered is an standardized negative subsequent stroke of 50kA - $^{0.25}/_{100}\,\mu s$.

The same behavior is observed for a cable running inside a dielectric pipeline, but with less notorious difference between the mean values.

In general, observing the 95 % confidence interval, and the values of the RMSE it can be concluded that the developed metamodels predict within an acceptable accuracy the simulation results, at the cost of a relatively large amount of coefficients.

Precisely, since the metamodels include in general more than 50 effects, it is advisable to examine their actual influence and importance inside the model. In the next section, this subject is going to be assessed.

4.4.3 Parameter's relevance

The model described in the previous section has more than 50 coefficients to estimate, and as it can be deduced from the previous chapter: there are some effects that have more influence on the response than others, and some factors perhaps interact in a way that cannot be expected from the previous observations. Among other reasons, because the parameter variations were performed one parameter at the time.

To evaluate the influence of the factors and their interactions, it is going to be assumed that the Pareto Principle applies, this is; only a set of effects influence most of the variations in the response of a system [14]. To do that, the value of each of the orthogonalized and standardized coefficient estimate is going to be related to the total sum of their absolute value.

The cumulative distribution of the effects is described in the Pareto curves of figures 4.6 and 4.7. They represent the influence percentile of a factor or interaction-of-factors, has over the response.

The Pareto curves include all the factors and interactions of each model, within a mark at 95 % limit, indicating that all the effects under that limit contribute with less than 5 % of the actual model response. As it can be seen, in general around 15 effects falls below this limit, therefore can be considered with no relevance to the response of the model.

In theory, this criteria can help to simplify the model and eliminate insignificant effects, nevertheless; this would increase the error of the prediction of the model. This is a non-desirable situation to the objectives of this work, since; the simplicity of the

model is not as important as the predictions being able to adapt well to the FDTD simulations.

Also, the Pareto curves help to observe the most significant effects. To do that, consider table 4.11, in which are indicated the parameters that contribute up to 60 % of the response of all the six cases. Here three aspects can be drawn:

- The cable length is the most relevant contributing factor for all the responses, with a starting point of 20 % of influence.
- In general; the cable length, the building side and the soil resistivity are the leading factors of influence.
  - Moreover, these parameters appear to be more influent on the response of a cable running inside a cable duct.
  - It was denoted in the previous chapter that a cable inside a duct is shielded from external perturbations, therefore susceptible only to high variations in the induction phenomena. As a consequence; factors affecting the rise-time of the current in the shield will have more influence in the response of the peak voltage.
- Factors identified in the previous chapter as influent at low frequency excitations: amount of conductors, grounding configurations and number of bridges, appear under lower frequencies excitations as the negative and positive first stroke.

Finally, to close the evaluation of the metamodels, a discussion about the errors of the predictions is going to be presented in the next section.

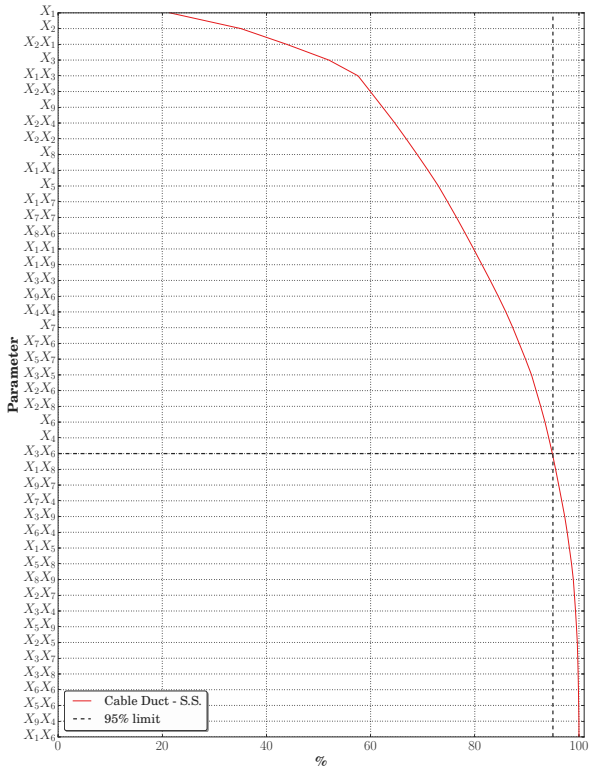

(a) Negative subsequent stroke.

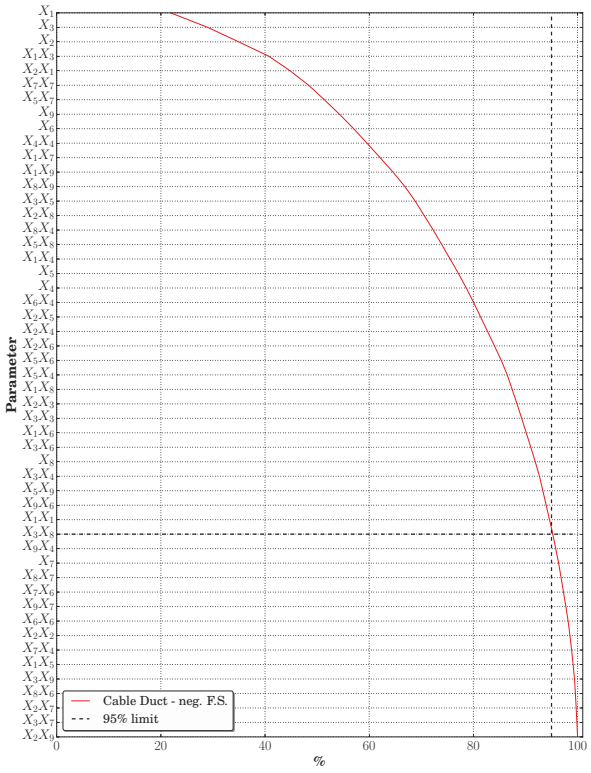

(b) Negative first stroke.

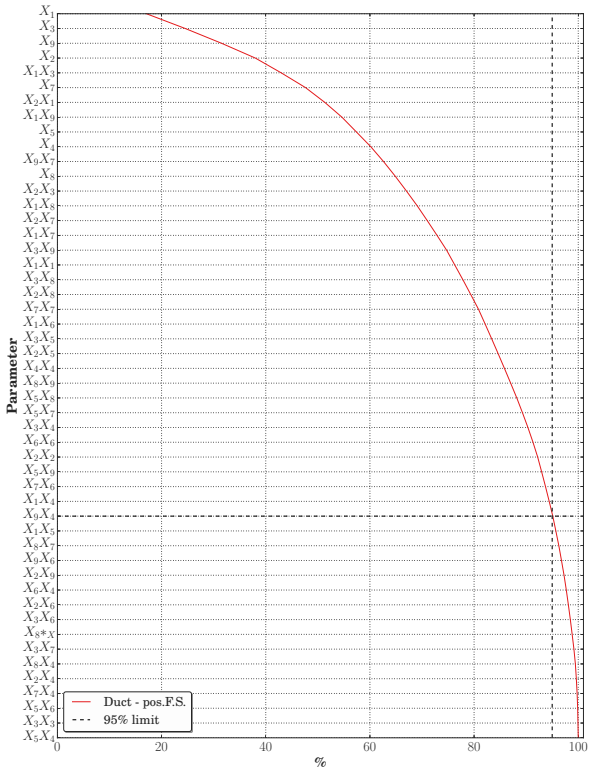

(c) Positive first stroke.

Figure 4.6: Pareto diagram for parameters estimates of cables inside a duct.

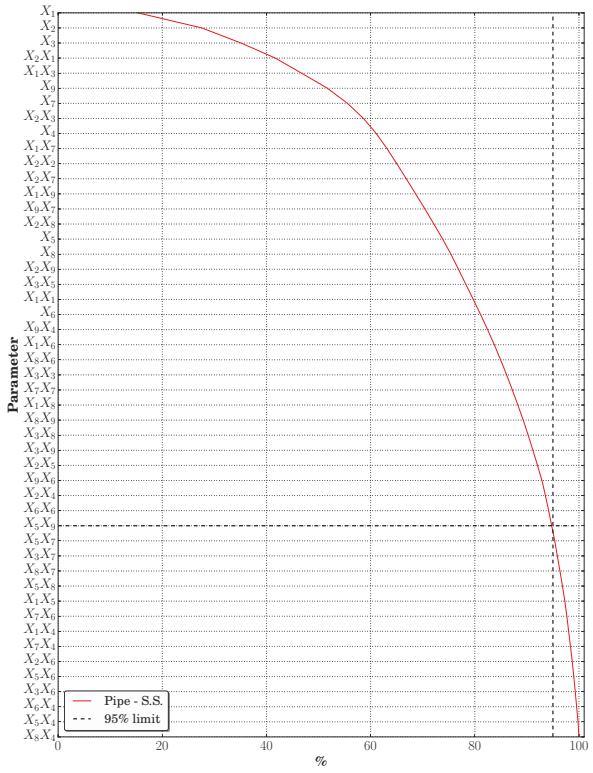

(a) Negative subsequent stroke.

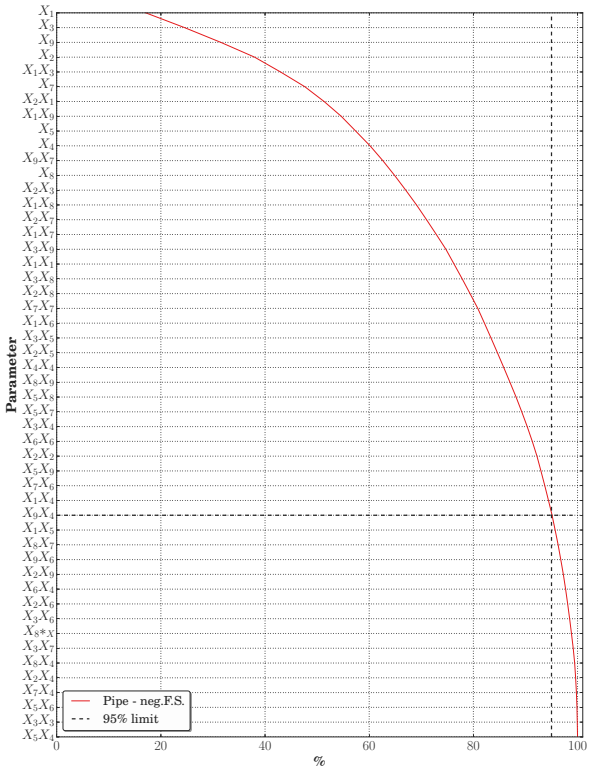

(b) Negative first stroke.

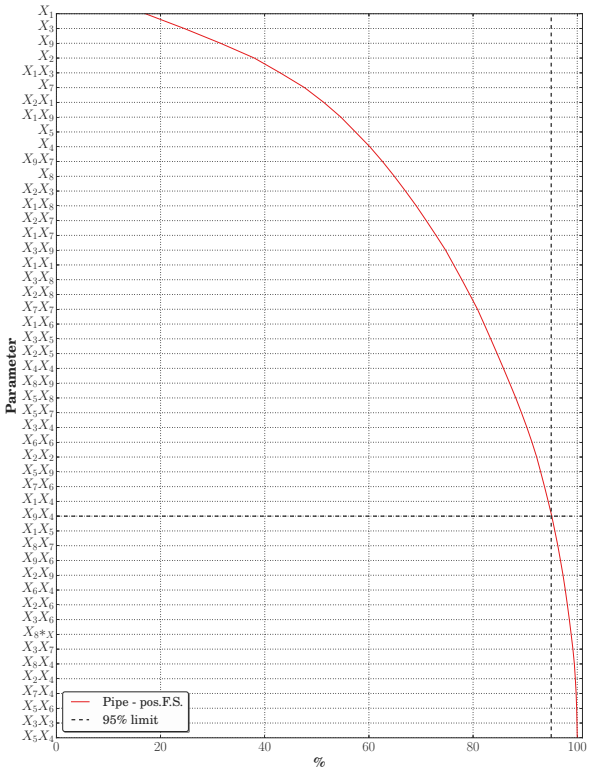

(c) Positive first stroke.

Figure 4.7: Pareto diagram for parameters estimates of cables in a dielectric pipe.

Factor	Description	Neg. S.S. Duct	Neg. S.S. Pipe	Neg. F.S. Duct	Neg. F.S. Pipe	Pos. F.S. Duct	Pos. F.S. Pipe
X_1	Cable length	✓	✓	✓	✓	✓	✓
X_2	Building Size	✓	✓	✓	✓	✓	
X_3	Resistivity	✓	✓	✓	✓	✓	✓
X_1X_2	Cable length & Building Size	✓	✓	✓	✓	✓	✓
X_1X_3	Cable length & Resistivity	✓	✓	✓	✓	✓	✓
X_2X_3	Building Size & Resistivity	✓	✓				
X_7	Amount of ducts		✓		✓	✓	✓
X_9	External Grounding		✓	✓	✓	✓	✓
X_7X_7	Amount of ducts^2			✓			
X_5X_7	Shield grounding & Amount ducts			✓			
X_6	Amount of pipes			✓			
X_4X_4	Bridges^2			✓			
X_1X_9	Cable length & Ext. grounding				✓	✓	✓
X_5	Shield grounding				✓	✓	✓
X_4	Bridges				✓	✓	✓

Table 4.11: Factors with a cumulative influence under 60 % according to the Pareto curves.

4.4.4 Errors of the models

When fitting a model, it is important to observe the nature of the behavior of the error. Two quick indications of this behavior are:

- The residual errors of the model predictions should have a normal distribution around a null value. This suggest that neither the input data or the procedure to estimate the model coefficients, were manipulated.
- The smaller the size of the deviation of the input data (the results of the FDTD simulations) from the predictions of the model, the better is.

Both of this characteristics can be appreciated in figures 4.8, 4.9,and 4.10, in which the difference between the input data and the model prediction; the residual error, is described as a dispersion for all the predicted values.

The average error deviations are depicted in table 4.12. As it can be seen, in general the average error deviates less than 20 %. Nevertheless, figures 4.8, 4.9, and 4.10 show; that some design points give a prediction with an important deviation from the simulated results. Excluding those few exaggerate points, the average error estimations reduces up to 8 % (adjusted error value in 4.12), which in general is an indication of the good quality of the models.

A special interest can be drawn from those design points that give a prediction with a relative large deviation, particularly in the cases of a cable inside a duct. Take for example the scenarios and outputs of those design points indicated in tables 4.13, 4.14, and 4.15, and some observations can be made:

- The big deviations occurs at low voltage predictions, mainly in cases with short cables. From the previous chapter, we have seen that this condition favors reduced peak voltages, and from figures 4.6 and 4.7, we see that this factor is the most influent in the output.
- The big deviations occur for voltages inferior to 500 V, which in practical terms does not poses a problem, since protection measures are usually taken for higher peak voltages. In practice, there is a minimum voltage criterion in order to determine if an equipment needs additional protection. Therefore, if a prediction suggests a low voltage value, even within an error, in general, it will not lead to an implementation of an additional protection measure.
- Big percentile residual deviations loss significance if the absolute value of the peak voltage is relatively small.

Regardless of the incertitudes inherent to the models, the nature of the error suggest that the metamodels can be used to determine the peak LIV of an IM cable in a fast and reliable way.

In the next section, this metamodels are going to be used on a realistic test case, and compared to results obtained following the procedure of the KTA standard.

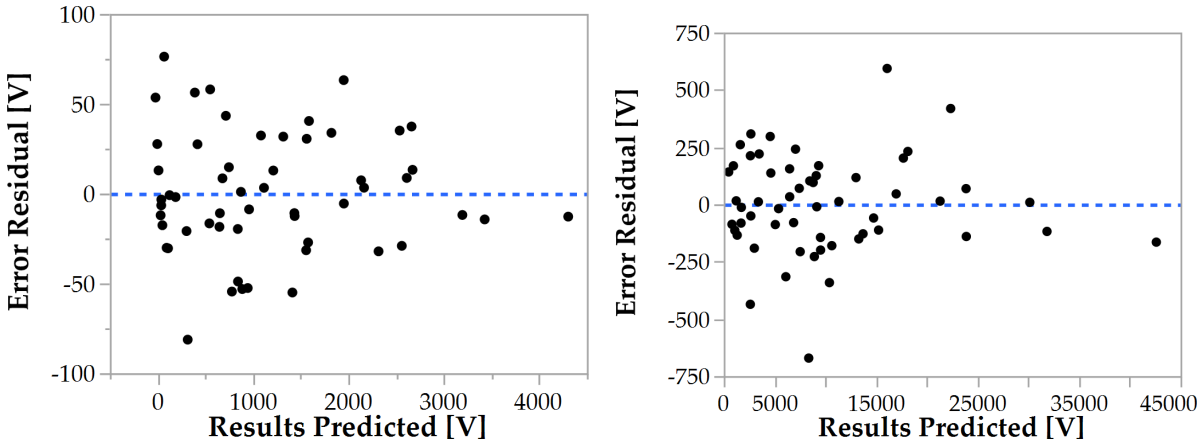

(a) Cable inside a duct. (b) Cable inside a pipe.

Figure 4.8: Residual error of simulated values for each prediction. For a negative subsequent stroke excitation.

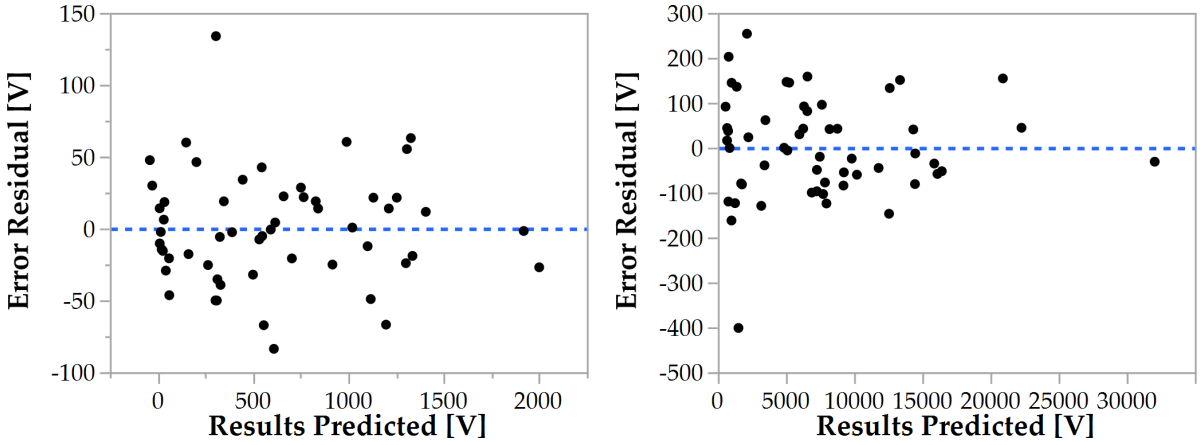

(a) Cable inside a duct. (b) Cable inside a pipe.

Figure 4.9: Residual error of simulated values for each prediction. For a negative first stroke excitation.

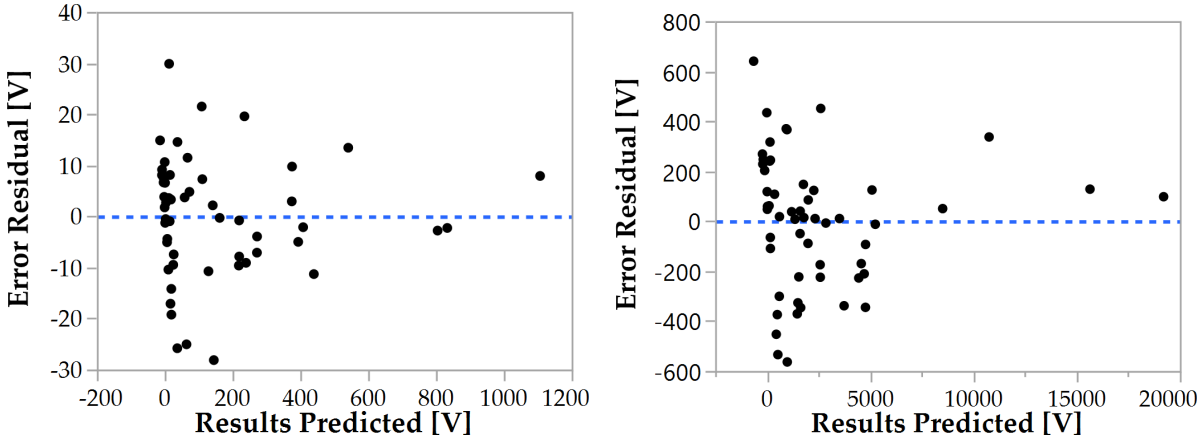

(a) Cable inside a duct. (b) Cable inside a pipe.

Figure 4.10: Residual error of simulated values for each prediction. For a positive first stroke excitation.

Error[%]	Neg. S.S. Duct	Neg. S.S. Pipe	Neg. F.S. Duct	Neg. F.S. Pipe	Pos. F.S. Duct	Pos. F.S. Pipe
Average	20.41	3.98	10.07	3.77	>100	>100
Adjusted**	7.93	—	5.89	—	10.21	10.38
Maximum	126.59	29.23	974	26.5	206	202

** This value does not includes the points deviating more than 50 % from the original data input.

Table 4.12: Average error of the models.

Design point	**8**	**14**	**24**	**29**
Cable length [m]	10	10	23,5	10
Building Size [m]	15	55	45	55
Resistivity[ρm]	100	1000	100	100
Bridges	16	16	16	2
Grounding Shield	CC	CC	CO	CO
Amount pipes	1	4	4	4
Amount ducts	7	1	4	1
Wall Type	Plate	Plate	Plate	Plate
External Grounding	Grid	Ring	Ring	Ring
FDTD Results [V]	145,502	24,745	234,908	32,226
Model prediction [V]	69,286	-2,829	316,215	-21,215
Error Residual [V]	76,216	27,574	-81,307	53,440
Error Residual [%]	110,001	-974,759	-25,713	-251,902

Table 4.13: Design points with interesting errors for the maximum voltage of a cable inside a duct. Type of excitation: negative subsequent stroke.

Design point	**9**	**14**	**25**	**27**	**29**	**39**
Cable length [m]	10	10	10	10	10	10
Building Size [m]	25	55	25	55	55	45
Resistivity[ρm]	100	1000	325	325	100	100
Bridges	2	16	2	2	2	16
Shield grounding	CC	CC	CC	CC	CO	CO
Amount pipes	1	4	7	1	4	4
Amount ducts	1	1	1	7	1	1
Wall Type	Grid	Plate	Plate	Grid	Plate	Grid
External Grounding	Ring	Ring	Ring	Ring	Ring	Grid
FDTD Results [V]	15,298	12,285	25,142	7,134	1,148	2,151
Model prediction [V]	61,725	27,853	11,096	-40,425	11,539	-27,703
Error Residual [V]	-46,426	-15,569	14,046	47,559	-10,390	29,854
Error Residual [%]	-75,215	-55,895	126,592	-117,648	-90,047	-107,764

Table 4.14: Design points with interesting errors for the maximum voltage of a cable inside a duct. Type of excitation: negative first stroke.

Design point	3	**17**	**27**	**35**	**49**
Cable length [m]	10	10	10	100	19
Building Size [m]	55	55	55	19	17
Resistivity$[\rho m]$	730	1000	325	1000	370
Bridges	4	16	2	16	8
Grounding Shield	CC	CC	CC	CO	CO
Amount pipes	7	1	1	7	1
Amount ducts	1	7	7	1	4
Wall Type	Plate	Grid	Grid	Grid	Plate
External Grounding	Grid	Grid	Ring	Grid	Ring
FDTD Results [V]	4,489	3,407	7,642	2,335	42,957
Model prediction [V]	-2,964	-3,213	1,094	-1,459	13,115
Error Residual [V]	7,453	6,62	6,548	3,794	29,842
Error Residual [%]	-251,446	-206,023	598,574	-260,037	227,541

Table 4.15: Design points with interesting errors for the maximum voltage of a cable inside a duct. Type of excitation: positive first stroke.

4.5 Comparison with the KTA procedure

It is also of interest to compare the predictions of the meta-model, to the equivalent response obtained following the procedure suggested by the KTA standard. To do so, in this section the KTA procedure to estimate the peak induced voltage is going to be applied to the 55 design points of table 4.3.

To correspond each case study to the methodology of the KTA, some considerations not treated in the standard must be assessed:

- The building size is not an input parameter, the only KTA variable that has a small relation to the size of the building is the current division factor, which is susceptible to the amount of external grounding conductors. In a manner that, in our cases:
  - If a big building has an external grounding grid, it also has more conductors intervening in the current division.
  - If the building is instead connected to an external grounding ring, the lightning current will divide only to the cable ducts around the building.
- Neighbor conductors inside a dielectric pipe does not intervene in the current division factor, this is; the amount of conductors inside pipes, is irrelevant to this procedure.
- The grounding connections of the shield is not relevant at any point of the calculation.

The peak induced voltage obtained with the KTA procedure for all the DoE design points is shown in figure 4.11. The results are described as a function of the predicted values of the meta-model, and are compared to the voltages obtained with the Finite Differences Time Domain (FDTD) simulations. Only the meta-model corresponding to cables inside metallic ducts, excited by a negative subsequent stroke is evaluated.

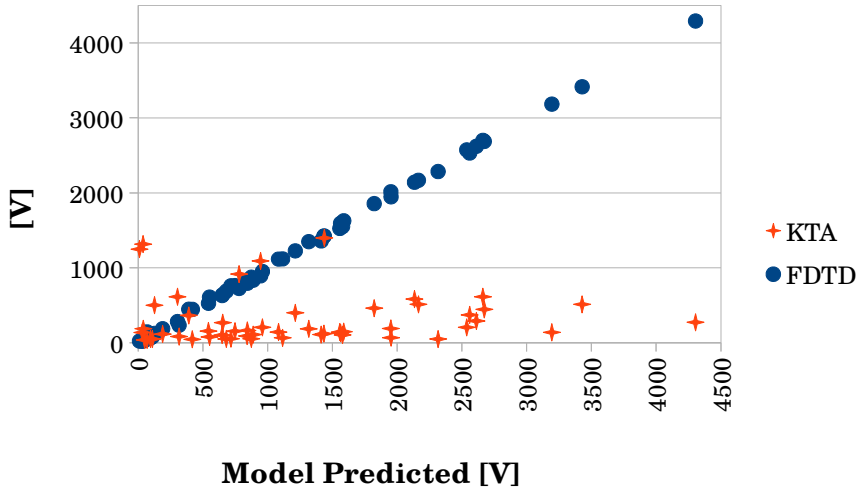

Figure 4.11: Peak induced voltages for all the scenarios in 4.3. For a cable inside a duct, and an excitation of a negative subsequent stroke.

As it can be seen, the KTA procedure, maintains a relative lower value than the FDTD simulations, and by extension, than the meta-model predictions. Only a few voltages are above 1 kV, and are observed for cases complying these two conditions:

- Only one cable duct is present, therefore, the fraction of the lightning current that it is supposed to divide to several conductors, propagates entirely through the cable duct.
- The amount of bridges of the expansion joints is 2. Which introduces the highest contribution to the fictive distance, increasing the coupling impedance.

As it can be seen, at least for all the 55 test cases, the KTA procedure results are not in agreement with the FDTD simulations. This is though mainly because of the difference in the consideration of the input parameters for each method, that does not make them entirely equivalent for the set of study cases.

As it is proposed, the meta-model is based on more concrete configuration parameters, which offers more flexibility assessing the induced voltages, in a coherent and logical manner. It is an alternative to the procedure suggested by the KTA standard, validated, accurate and computationally efficient and allows for the prediction for the peak LIV:

- For a wide range of variation for building sizes, cable lengths and soil resistivities.

- With the shield of the cable opened or grounded.
- When the cable running inside a cable duct or a dielectric pipeline.
- With simple external grounding systems, or gridded.
- For several conductors distributed uniformly around the building.
- For cable ducts including practical amounts of expansion joints bridges.

These conditions have the potential to emulate a wide variety of cases. Nonetheless, the methodology here proposed can always be extended to a more complex set of input parameters, with more constraints between them, such as:

- The inclusion of a parameter that regulates the cable distribution around the building
- A restriction imposing individual characteristics of cables, such as the length and the shield connection.
- An extended model of building geometry, allowing for the adjustment of the three dimensions of the building.
- An inclusion of metallic structures running nearby the cables of interest.

In addition; also the response variables can be modified, not to account only for the peak voltages, but to extract other interesting variables from the transient response, such as the energy at the terminal load, the maximum steepness of the voltage, the rise and tail times. In this extended case, the output variables could be correlated and be useful to extract more information about the behavior of the transients.

In general it has been shown that an expression to model a complex phenomena is a powerful, and at the same time simple alternative, to perform a computation heavily demanding in resources. Helping not only to emulate the desired response in an accurate way, but to understand the behavior, interactions and influence between the parameters characterizing the whole phenomenon.

4.6 Conclusions

- The Design of experiments technique (DoE) was used to generate an optimal set of scenarios for FDTD simulations of lightning induced voltages on IM cables of Power Generation Centers.
  - Optimal DoE techniques are required to consider the parameter variations of complex electromagnetic phenomena depending of several parameters of diverse nature.

  - If the objective is to emulate the response of an FDTD simulation with more precise tunning of the parameters, an I-optimal DoE shall be used.
  - Otherwise, if the objective is to determine the influence of the input parameters on the global response of the problem, D-optimal DoE shall be used.

- The DoE technique is useful to confirm observations about the nature of the phenomenon identified in the previous chapter. Particularly regarding the influence of the parameters:

  - The parameters that influence the most the peak LIV are the cable length, the building size and the soil resistivity, regardless of the frequency content of the excitation
  - Some parameters affect only slow excitations as the positive first stroke: the external grounding, the connections of the shield and the amount of bridges.

- Six meta-models to compute the peak transient LIV on IM in a fast an efficient way were developed

  - In order to make the meta-models useful, they allow one to use a wide set of input parameters within a practical range of variation.
  - One meta-model for each different type of cable canalization: duct or dielectric pipe, and type of lightning channel base current was developed: negative subsequent stroke, and negative and positive first stroke.

- The response of problem of LIV on IM cables of PGC can be accurately modeled with 2^{nd} polynomial expression that considers parameters interactions.

  - The prediction errors of the developed meta-models are in average less than 10 % of the expected values of the FDTD simulation.
  - The biggest deviation between the prediction and the FDTD simulations occurs at lower values of expected voltages.
  - The above is tolerable, since a minimal voltage criterion is used as a general rule to evaluate the protection at the terminations of a IM cable.

- The KTA procedure was tested against the 55 scenarios used to generate the meta-models.

  - The maximum voltage was compare for the KTA procedure, the FDTD method, and the meta-models predictions.

  - The results differ in a significant manner, this is though to be because the premises for the KTA procedure are not entirely adapted to the simulation scenarios. This is, the input parameters for both methodologies are not considered equivalently.

- The newly developed metamodels are meant to be an alternative, accurate and efficient tool to compute the peak induced voltages in IM cables, within its own limitations, and assumptions, but always expandable to better model the complex phenomenon of interest.

References

[1] Douglas C Montgomery. *Design and Analysis of Experiments*. Vol. 2. 2012, p. 757. ISBN: 0471316490. DOI: 10.1198/tech.2006.s372. URL: http://cataleg.uab.cat/record=b1764873%7B~%7DS1*cat.

[2] Averill M. Law. "A tutorial on design of experiments for simulation modeling". In: *Proc. Winter Simul. Conf. 2014* (2014), pp. 66–80. DOI: 10.1109/WSC.2014.7019878. URL: http://ieeexplore.ieee.org/lpdocs/epic03/wrapper.htm?arnumber=7019878.

[3] Susan M. Sanchez and Hong Wan. "Work smarter, not harder: A tutorial on designing and conducting simulation experiments". In: *Proc. - Winter Simul. Conf.* 2016-Febru (2016), pp. 1795–1809. ISSN: 08917736. DOI: 10.1109/WSC.2015.7408296. arXiv: arXiv:1011.1669v3.

[4] R. L. Rechtschaffner. "Saturated Fractions of 2 n and 3 n Factorial Designs". In: *Technometrics* 9.4 (1967), pp. 569–575. DOI: 10.1080/00401706.1967.10490505. eprint: http://dx.doi.org/10.1080/00401706.1967.10490505. URL: http://dx.doi.org/10.1080/00401706.1967.10490505.

[5] Russell R. Barton. "Tutorial: Simulation Metamodeling". In: *Proceedings of the 2015 Winter Simulation Conference*. WSC '15. Huntington Beach, California: IEEE Press, 2015, pp. 1765–1779. ISBN: 978-1-4673-9741-4.

[6] Mark J Anderson and Patrick J Whitcomb. "Practical Aspects for Designing Statistically Optimal Experiments". In: *J. Stat. Sci. Appl.* 2 (2014), pp. 85–92.

[7] Norman R. Draper and Irwin Guttman. *Rationalization of the 'alphabetic-optimal' and 'variance plus bias' approaches to experimental design*. Tech. rep. Madison, Wisconsin: University of Wisconsin. Department of Statistics, 1988, p. 32.

[8] Utami Syafitri, Bagus Sartono, and Peter Goos. *D- and I-optimal design of mixture experiments in the presence of ingredient availability constraints*. Working Papers 2015003. University of Antwerp, Faculty of Applied Economics, Jan. 2015. URL: https://ideas.repec.org/p/ant/wpaper/2015003.html.

[9] SAS Institute Inc. *JMP®, Version Macintosh*. Cary, NC,

[10] T. Bdour et al. "Emulation of an Expensive FDTD Code With Mixed Quantitative and Qualitative Factors for Analysis of Lightning-Induced Transient Responses". In: *IEEE Transactions on Electromagnetic Compatibility* 58.5 (Oct. 2016), pp. 1678–1681. ISSN: 0018-9375. DOI: 10.1109/TEMC.2016.2576559.

[11] Student. "The Probable Error of a Mean". In: *Biometrika* 6.1 (1908), pp. 1–25. ISSN: 00063444. URL: http://www.jstor.org/stable/2331554.

[12] Testing Author et al. *Controlling the False Discovery Rate: A Practical and Powerful Approach to Multiple Controlling the False Discovery Rate: a Practical and Powerful Approach to Multiple Testing*. 1995. DOI: 10.2307/2346101. arXiv: 95/57289 [0035-9246].

[13] Henri Theil. *Economic forecasts and policy*. English. 2nd rev. ed. Includes bibliographical references. Amsterdam : North-Holland Pub. Co, 1961.

[14] B.C. Arnold. *Pareto Distributions Second Edition*. Chapman & Hall/CRC Monographs on Statistics & Applied Probability. CRC Press, 2015. ISBN: 9781466584853.

Chapter 5

Conclusions and perspectives

5.1 Conclusions

Lightning surges over Instrumentation & Measurement (IM) cables of a Power Generation Center, are a complex phenomena often approached with full wave electromagnetic numerical methods. In this work the FDTD algorithm has been used taking advantage of a fast and accurate method to model wire structures, and of a parallel computing numerical solution.

With this strategy, with a combination of bare, isolated, and coaxial conductors, a wide diversity of actual industrial structures with realistic dimensions can be modeled: The building steel grid of the concrete walls, the cable duct and dielectric pipe canalizations, the buried copper grounding grid, and the coaxial IM cable.

A validation for each one of components of a complex industrial center was performed. Multiple sets of study cases were taken from acknowledged references, and equivalent ElectroMagnetic (EM) models were implemented and tested. It was confirmed an agreement between previously reported results and the implementations of this work, this justified the integration of all the models into a full case scenario of a lightning surges propagating through the industrial site.

A general realistic case, integrating all the validated components was also compared and validated against another numerical method, the Method of Moments (MoM). Showing good agreement on the frequency response of the current along the cable shield.

The problem of lightning surges in IM cables is known as being complex because of the multiple dimensions of structures implicated, the couplings between them, and the wide variety of parameters that simultaneously affect the propagations of currents. Here, those parameters were discretized and studied separately.

It was observed that for fast excitations, the most influential parameters were associated to distance dimensions: building size and cable lengths, alongside with the soil resistivity. Meanwhile for slower excitations, parameters relative to connections and geometries where in addition influential: grounding system configuration, cable

shield connection, and cable duct expansion joints.

For a complex EM problem, performing a sensitive analysis can be a heavy task to organize, specially considering the amount of parameters involved in the response, alongside with all their different natures: cable lengths and soil resistivity are continuous variables, while shield connections and grounding systems are nominal variables.

The technique of Design of Experiments (DoE) was used with two objectives: to completely understand and finely control the parameters influences and interactions in the peak induced voltage. As well as, to develop metamodels that are easy to implement, and correlated all the input parameters with the desired response of the system.

One meta-model was developed for each different type of lightning surge excitation: negative subsequent stroke, negative first stroke, and positive firs stroke. Considering that the cables might be inside metallic ducts or dielectric pipes. Totalizing six meta-models able to perform an evaluation of the peak induced voltage of a IM cable leaving a building hit by lightning.

The meta-models predict accurately the results expected from the FDTD simulations, within an average error inferior to 10 %. It was found that the biggest estimation errors were obtained for expected results of low peak voltages, this can be tolerable, considering that for small peak voltages, in reality, no additional protection measured is required.

The KTA procedure was applied to the 55 study cases used to construct the meta-models, the results of both methodologies were compared, resulting in an important difference. It was observed that variables that severely affect the peak voltage such as the building size, or the conductor length, used to construct the simulation scenarios, are not considered in an equivalent manner in the standard procedure.

The metamodels represent a validated, accurate and computationally efficient way to predict the response of complex electromagnetic problems. They are a tool at the service of the lightning protection engineers that are adapted to a wide variety of real case scenarios.

5.2 Perspectives

The implementations of the meta-models could be extended if some input parameters are re-restructured:

- The lightning current source is treated through the inclusion of two new input parameters: The front time constant, and the semi-amplitude time constant. Leaving the peak as the unity, and assuming a response linearly dependent and proportional.

- The building size is decomposed into its three dimensions, to adapt with more versatility to a real case scenario.
- Some parameters that evaluate the cable ducts distribution around the building shall be evaluated.
- Discretization between conductor parameters shall be made regarding each individual case: the length, the shielding connections, and the distance between expansion joints. Similar to the case of the case of the type of canalizations used in this work. These restrictions might compromise the implementation of the DoE technique.
- Instead of using a qualitative variable to describe the EM model of the building wall, a continuous variable based on the surface impedance can be used instead. This implies further validation of the model, but the works of [1] present a valid starting point.

In an equivalent manner, the outputs of the meta-models could be also extended, an even more correlated, in order to consider a bigger dimension of the transient phenomena. Parameters such as energy at the terminal load, maximum voltage steepness, rise time and semi-amplitude time could be considered simultaneously.

Nevertheless, this demands among other things more experiences to perform, more simulation time, and specially, a technique to uniformly evaluate all the different transient behaviors. Since the faster the excitations are, the more oscillatory is the response, which makes difficult the determination of the output parameters, especially the rise and semi-amplitude time.

Also, the objective function of the meta-model can be re-structured, instead of predicting the the response of the FDTD simulations, it can aim for maximizing the response, in a manner that, all the FDTD simulation results be inferior to the meta-model predictions.

References

[1] E. Bachelier et al. "Protection against lightning of reinforced concrete buildings". In: *Lightning Protection (ICLP), 2014 International Conference o*. Oct. 2014, pp. 735–740. DOI: 10.1109/ICLP.2014.6973220.

Communications

The following is the list of related articles presented and published during the realization of this work:

- **Accepted for publication - 2016**. *Lightning Transient Voltages in Cables of a Large Industrial site using a FDTD Thin Wire Model*. Luis Diaz, Céline Miry, Philippe Baraton, Christophe Guiffaut and Alain Reineix. Electric Power Systems Research Journal.

- **July 2016**. *Assessment Of The Potential Rise Of A Thin Wire In The Fdtd Modelled With The Formalism Of Holland*. L. Diaz, C. Miry, P. Baraton, C. Guiffaut, A. Reineix.18th International Symposium on ElectroMagnetic Compatibility. Rennes. France.

- **March 2016**. *Emulation of an expensive FDTD Code with Mixed Quantitative and Qualitative Factors for Analysis of Lightning-Induced Transient Responses*. Tarek Bdour, Luis Diaz, Christophe Guiffaut, Alain Reineix, Céline Miry, and Philippe Baraton. IEEE Transactions On Electromagnetic Compatibility

- **September 2015**. *Calculation of Lightning Transient Voltages in Cables considering a Large Industrial site using a FDTD Thin Wire Model*. Diaz, L., Miry, C., Guiffaut, C., Ticaud, N. and Reineix, A. International Symposium on Lightning Protection (XIII SIPDA). Brazil.

- **August 2015.** *FDTD transient analysis of grounding grids. A comparison of two different thin wire models*. Diaz, L., Miry, C., Guiffaut, C., and Reineix, A., and Tatematsu, A. IEEE International Symposium on EMC.

Lightning Induced Voltages in Cables of Power Production Centers

Abstract: When lightning strikes a building in a Power Generation Center, dangerous currents propagates through all the components connected to the building structure: The walls, the grounding grid, and the cables leaving the building. It is the interest of this work to study the transient voltages at the terminations of these cables external to the building. Particularly, the Instrumentation and Measure (IM) cables, since they are connected to electronic equipment susceptible of damage or malfunctioning due to lightning ElectroMagnetic perturbations. A full wave approach based on the numerical solution of Maxwell's equations through the FDTD algorithm is adopted. Notably, the formalism of Holland and Simpson is used to model all the structures composed of thin wires: the building steel structure, the grounding copper grid, the concrete cable ducts and the coaxial IM cables. A validation of the model developed for each component is presented. A sensitivity analysis is performed in order to the determine the main parameters that configure the problem. Also, the Design of Experiments (DoE) technique is used to generate a meta-model that predicts the peak induced voltages in the cable terminations, as a function of the main parameters that configure the industrial site. This represents an accurate, and computationally efficient tool to assess lightning performance of IM cables.

Keywords: Lightning induced voltages, cables, power generation centers, FDTD, thin wire, design of experiments, meta-models.

Tensions induites par la foudre en câbles des Centres de Génération d'Énergie.

Résumé:

Lorsqu'un bâtiment d'un centre de production d'électricité est frappé par la foudre, il se produit une dangereuse circulation de courants dans tous les composants connectés au bâtiment: les murs, le réseau de terre, et les câbles sortant du bâtiment. L'intérêt du présent travail est d'étudier les tensions transitoires aux extrémités de ces câbles, en particulier des câbles contrôle mesure, dans la mesure où ces câbles sont connectés à des équipements électroniques susceptibles d'être endommagés par des perturbations électromagnétiques engendrées par la foudre. Une approche basée sur la résolution numérique des équations de Maxwell via une méthode FDTD est adoptée. Notamment le formalisme de Holland et Simpson est utilisé pour modéliser toutes les structures constituées d'un réseau de fils minces: l'armature métallique du bâtiment, la grille en cuivre du réseau de terre, la galerie de béton et le câble coaxial de contrôle mesure. Une validation des modèles électromagnétiques développés pour chaque composant du site industriel est présentée. Une analyse de sensibilité est conduite pour déterminer l'influence des paramètres du système. En outre, la technique des plans d'expérience est utilisée pour générer un méta-modèle qui prédit la tension maximale induite aux extrémités du câble en fonction des paramètres les plus influents. Cela représentent un outil de calcul précis et computationnellement efficace pour évaluer la performance foudre des câbles de contrôle et de mesure.

Mots clés: Tensions induites, foudre, centre de production d'électricité, FDTD, fil mince, plans d'expérience, meta-models.